UNIVERSITY OF OXFORD
Department of Physics and Wadham College

TOWARDS QUANTUM SUPERPOSITIONS OF A MIRROR

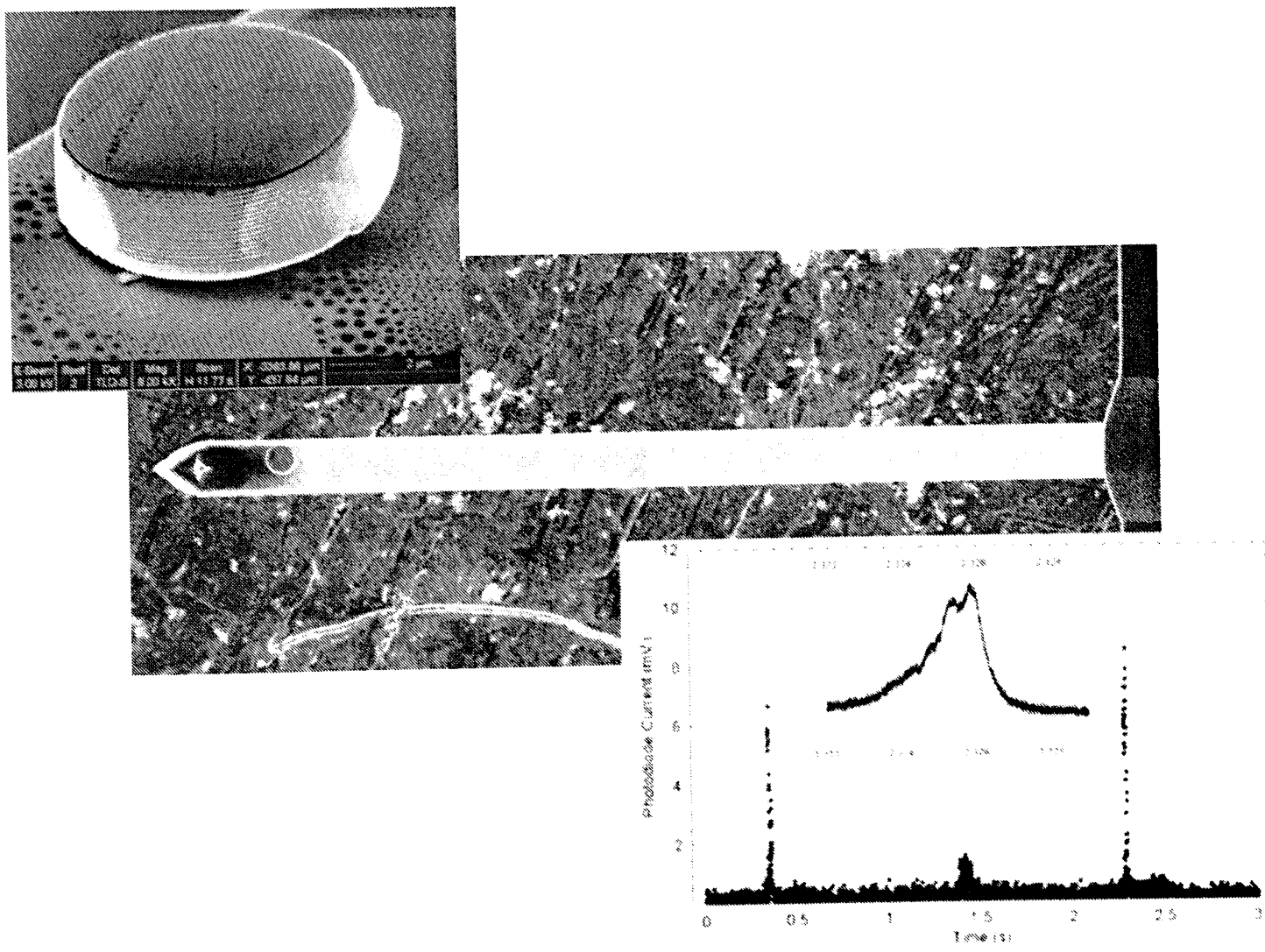

by
William Marshall

Phd.
2004.

UNIVERSITY OF OXFORD
Department of Physics and Wadham College

TOWARDS QUANTUM SUPERPOSITIONS OF A MIRROR

by

William Marshall

Department of Physics, University of Oxford
Oxford OX1 3PU, United Kingdom

wsm@physics.ox.ac.uk

Supervisors: Prof. Dik Bouwmeester & Prof. Sir Roger Penrose

Internal Examiner: Prof. Keith Burnetts

External Examiner: Prof. John Pethica

SUBMITTED IN PARTIAL FULFILLMENT OF THE
REQUIREMENTS FOR THE DEGREE OF DOCTOR OF PHILOSOPHY

Submitted June 2004

Contents

Towards Quantum Superpositions of a Mirror

William Marshall
Wadham College, University of Oxford, wsm@physics.ox.ac.uk
D.Phil. (Physics), Trinity 2004

Abstract

In principle Quantum Mechanics allows the creation of macroscopic mass superposition states – so called "Schrödinger Cat States". This has not been confirmed experimentally largely due to the difficulty of isolating such states from environmental decoherence. It is of interest to create massive superpositions both in order to test Quantum Mechanics and to shed light on the elusive 'measurement problem'. This thesis presents the theoretical analysis of, and the initial experimental steps towards, an ambitious proposal to test the superposition principle of Quantum Mechanics at the 10^{-12}kg–scale, approximately nine orders of magnitude more massive than any superposition observed to date.

The experimental principle is that a small mirror mounted on a micro-mechanical oscillator (cantilever) forms one end of a high-finesse cavity in one arm of a Michelson interferometer and is coupled to a single photon by radiation pressure. The photon, in a superposition of each arm, and the cantilever evolve into a superposition involving two distinct locations of the cantilever. By observing the interference of the photon only, one can study the creation and decoherence of the combined state.

Firstly, a detailed analysis of the experimental requirements is given based on (1) the need for sufficient momentum transfer from the photon to displace the micro-mirror/cantilever to a distinguishable degree, (2) the need to isolate the cantilever to avoid significant environmental decoherence, and (3) the need to have sufficient interferometric stability to perform the measurement. An iterative analysis was performed to optimise these to a set that is feasible with current technology. This demands: (1) cavity mirrors with a reflectivity of $R \geq 0.9999998$ at visible wavelength, (2) a system temperature of ≤ 3mK, (3) a cantilever mechanical quality $Q \geq 10^5$, (4) a vacuum with gas particle density of $10^{12}/\mathrm{m}^3$, (5) a relative position stability of the cavity mirrors of $\leq 10^{-13}\mathrm{m/min}$, and (6) optical mirror switching to 50% for $\leq 1\mu$s. Whilst extremely demanding, all of these goals appear to be within reach of current technology.

Secondly, initial experimental results are described: (1) the fabrication of a 10μm radius dielectric mirror designed for peak reflectivity $R > 0.99997$ and the attaching of this to an AFM-type cantilever of mechanical quality $Q > 4 \times 10^4$; (2) the alignment of a cavity of length 2.5cm involving this micro-mirror/cantilever at one end and the demonstration of a finesse of $F > 1000$ using two independent measurement techniques. The diffraction losses for the cavity are calculated numerically to be $< 10^{-6}$. Other mechanisms limiting the finesse are investigated and the dominant one is determined to be accoustic noise which can be alleviated by placing the cavity into a vacuum. In addition, results demonstrating ultra-fast optical switching of high reflectivity mirrors are shown.

Acknowledgments

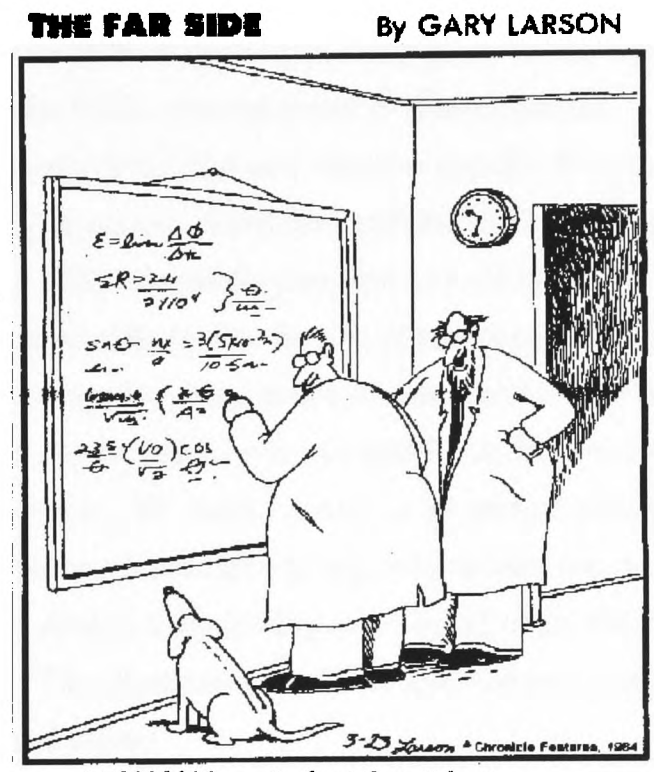

"Ohhhhhhh . . . Look at that, Schuster . . .
Dogs are so cute when they try to comprehend
quantum mechanics."

I have found my PhD experience to be very enjoyable and rewarding. I have been fortunate on many counts: a stimulating and varied research project, great supervisors, an excellent intellectual environment in my research group and some wonderful friends. It is the people with whom you interact that dictate the merits of an experience and I think it is a fair assessment to make that I have been surrounded by some of the most talented people in the world, all of whom I seek to acknowledge here for their contributions to my personal progress.

First and foremost I have enjoyed the support of two advisors which have together been everything that a PhD student could ask for in such a role. I thank Dik for his insight and spirit of adventure on the project, his patience, problem solving skills in the lab and for being a friend. Thanks to Roger for catalyzing the project, for fascinating discussions, for his Saturday meetings which never ceased to amaze and for being an inspiration throughout.

Thanks to Christoph Simon for his tremendous support for me and for being a vital component to the progress of the project at large. His ability to answer every question off the cuff and his rigour will both be missed. Thanks also for infrequent but very enlightening philosophical discussions: you have to keep us Anglo-Saxons on the straight and narrow. I benefitted greatly from a second post-doc Michiel de Dood who I would like to thank for all his help in the lab and in particular whose skills in micro-fabrication have been essential to my progress. Thanks to Hagai Eisenberg for a myriad of useful suggestions in the alignment of the cavity.

Thanks to Keith Burnett for supporting the continuation of my PhD during the move to UCSB. To Sugato Bose, John Pethica and Ramin Lalezari for useful discussions.

I would like to thank all those in the quantum optics group which has been a great environment consisting of bright, interesting and even sociable people from many parts of the world – exactly ten people and ten nationalities at one point – despite Dik's cunning email avoidance tactics.

To all those in Oxford: for their delightful and varied company. For teaching me a myriad of academia survival skills and for explaining in arduous detail the multitude of British imperfections including the general state of cuisine, the weather, the NHS, the public transport as well as several inexplicable items including the Oxford lawn rules and, most importantly by far, the use of two separate taps for hot and cold water. Roll on UN Citizenship! To Andrey Bychkov for great games of tennis and for his friendship. To Gabriel Durkin for being the most hilariously frank person I have ever met and for dedicating some time, often in the wee hours, to helping with my theory problems. To Antia Lamas for keeping a relaxed atmosphere and for staging a challenging act to follow. To William Irvine for his help with Mathematica, the occasional fun flight and for varied conversations. To Simon Anders for knowing every detail about this world imaginable, for organising the lab and for helping to label 'The Quantum'. To Christophe Couteau for being so fantastically French and reminding us what being civilised means.

To all those I have met in Santa Barbara: Sara for helping to introduce us to the California lifestyle by hosting many parties, organising the football and not least for dragging us kicking and screaming to Disneyland. To George for proving convincingly that Americans can be sarcastic. To Juan and Matt for being so amicable and for putting up with us strange Europeans. To Nima for patiently learning cavity alignment details and for recommending the Mongolian restaurant.

I have had the support of a number of friends without whom all would be less worthwhile. In Oxford, André for regular stimulating debates, for teaching me about politics and for helping to shape my view of the world. To Evangelina for many crazy times. For my house-mates Martin, Alex and Ruth for keeping the debates varied. To Alex King for his wise words and for always being on the same wavelength. In California, to George and Loretta for being the principle force enabling me to keep my sanity in the sea of ignorance that is perpetuated by the shortcomings of the American education system and media. To Kelly, Andrew, Kevin, Stephanie, Robbie and Jessy for occasional but important gatherings which kept me inspired. To Vivian for

her hugs.

To my Mother for always encouraging my continued education and for forgiving the inadequacy of my visit frequency. To Gary Larson for his insight into the natural world and lateral thinking. To Eric Weinstein's World of Physics for providing much general physics at the click of a button.

I would like to thank Dik, Roger, Christoph, Michiel, Matt, William and Alex for their time in reviewing this thesis.

Preface

My original interest in this project sprang from a lecture I attended by Roger Penrose entitled "A Proposed Space Experiment: is quantum state reduction a gravitational phenomenon?". This seemed to be a project combining two major interests of mine: fundamental physics and space science. The principle proposed to test a gravitational state reduction model by using an X-ray photon in a superposition of two distinct locations to interact with a tiny crystal. Through coupling, the combined system would evolve into a superposition involving two distinct locations of the crystal – a massive superposition. The system would be in space to allow a long delay line with which to keep an X-ray photon coherent. I enquired about the possibility of researching on this as a PhD. Roger linked up with Dik Bouwmeester and together arrangements were made.

During the research I have spent approximately equal time on the theoretical analysis of the experimental feasibility as on the implementation of initial experimental steps. A sizeable fraction of the work was performed in collaboration with others and so below I detail the contributors to the main results described in this thesis.

Before that I would like to make a note on the scope of the thesis: it does not by any means provide a complete analysis of all methods for creating massive superposition states nor does it review in detail the theory of environmental induced decoherence or the various wavefunction collapse models. These are considered beyond the scope of this study. The work focuses on one principle for making massive superposition states whose feasibility with current technology, our analysis suggests, is promising: this analysis is given and our experimental steps shown.

Initially the project involved considering ways to implement the basic principle that Roger had proposed in his lecture, and whose roots can be traced to discussions involving J. Schmidmeir, Roger Penrose, Dik Bouwmeester, J. Dapprich, H. Weinfurter and A. Zeilinger in 1997. Christoph Simon, Roger, Dik and I discussed a myriad technical options which could be employed to perform the experiment involving atom interferometry, SQUIDs, X-rays, cavity QED as well as all optical techniques. This was enjoyable and very varied since there were always new challenges and problems to solve, in an order of magnitude fashion. Much of the motivation came from wishing to test a novel wavefunction collapse scheme involving gravity proposed by Roger, as well as to test Quantum Mechanics in a previously quite untested regime.

Most routes failed by a very wide margin, to stay within the realm of current technology. Eventually a

technical root was identified which seemed not entirely unfeasible. The task then became to conduct a more thorough feasibility study. The first substantive new contribution described here is thus a thorough analysis of the above proposal to find a set of parameters which fulfil the experimental requirements and which are all within the capacity of current technology. This study was conducted principally by Christoph Simon, Dik and myself. It is largely contained in Chapter 2.

The other major contribution herein is the results of initial experiments towards the implementation of the above proposal. In particular, I describe the first demonstration of a macroscopic cavity involving a microscopic mirror. This involved two key stages: (1) the fabricating of a high-reflectivity mirror of radius 10μm attached to a micro-mechanical cantilever, and (2) the integration of this into a cavity with one large and one small mirror with appropriate incoupling optics. The former of these was performed by Michiel de Dood and myself; in particular, Michiel operated the focussed ion beam (FIB) used for two of the three methods outlined in Chapter 4 for fabricating the micro-mirror/cantilever. The latter stage, involving design of the incoupling optics, design of the cavity mount, integration of the micro-mirror/cantilever in to a macroscopic cavity, performing cavity ring down and Fabry-Perot measurements, as well as the analysis of the diffraction losses and other limiting factors, were performed principally by myself. The fabrication of the cavity mount was performed by the UCSB Physics Department machine shop. Recently work is being undertaken to place the cavity into a vacuum chamber: the vacuum chamber was designed by Michiel de Dood and built by the UCSB Physics Department machine shop and Nima Dinyari has worked on the integration of the cavity.

In addition, early in the project, ultra-fast switching of high reflectivity mirrors was investigated due to its potential to ease the stability requirement of the above proposal. Distributed Bragg reflector samples containing non-linear materials were designed by myself and fabricated by the EPSRC III-IV Semiconductor facility at the University of Sheffield. Recently, switching measurements have been performed on these samples: all of the measurements of which were conducted by Sara Hastings and Michiel de Dood.

Finally, and to a large extent unrelated to the core work, I have for some years been interested in the social responsibility of scientists and the use of technology for military purposes. During my PhD I was able to dedicate some time to write two research papers on an issue of particular concern to me relating to the deployment of weapons in space. I have included these in Appendix D. This work was done independently of my supervisors but I would like to thank Dik for being especially supportive of my exploring this research. In fact this work has led me to accept a post-doctoral position to research these issues further. The main contributors to the work presented here other than myself are from George Whitesides, Robbie Schingler, Jessy Cowan, Andre Nilsen, Gen. Pete Worden and Bob Lawson.

Summary for Non-Specialists

Quantum Mechanics (QM) allows for the creation of situations where a single object is simultaneously in two or more distinctly different conditions (or 'states'), e.g. two different energies or, more dramatically, two different locations. This has been confirmed experimentally for photons, electrons, atoms and molecules, but not for large mass objects. In short, this thesis presents the theoretical analysis of and initial steps towards the realisation of an ambitious experiment to test this fundamental superposition principle of Quantum Mechanics on an object containing approximately 10^{14} atoms – an object about a thousand million times more massive than any superposition experiment to date.

Background

The theory of Quantum Mechanics describes very well the nature of small objects (e.g. atoms, molecules, particles of light). It was developed in the 1920s by Heisenberg, Schrödinger, Dirac and others during a revolutionary period for physics. Since its inception it has been verified experimentally to a great degree

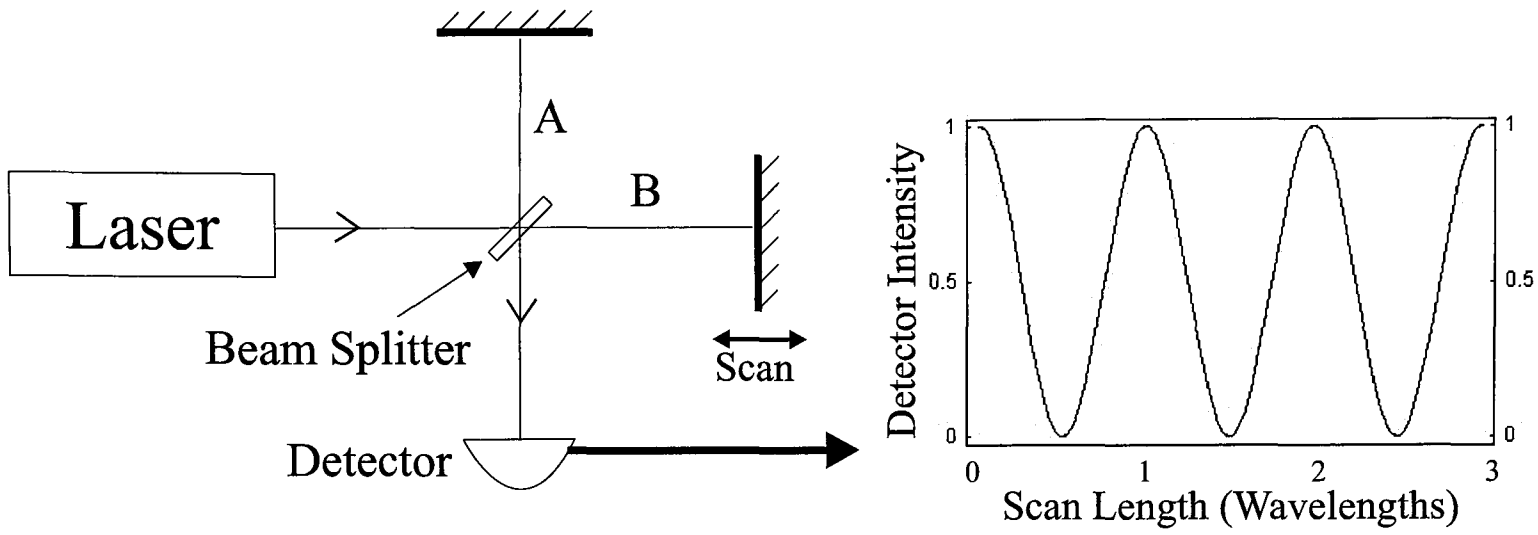

Figure 1: The Michelson interferometer. A particle of light (photon) from a laser passes through the beam-splitter and evolves into a quantum superposition state of going in either arm A or arm B. Following reflection by the mirrors, the photon interferes with itself at the beamsplitter and for appropriate settings of the arm lengths is detected all exits to the detector.

of accuracy. One of its core principles is the ability to create quantum superpositions: these are situations that are quite non-intuitive, since they are not apparent in the "macroscopic" world in which we live. To describe the idea of a superposition let us consider a case of particular relevance for this experiment: an optical interferometer as shown in Fig. 1. Light from the laser passes through a half-silvered mirror, called a beamsplitter, and travels into arms A and B. Light on either path is reflected back to the beamsplitter by a plane mirror. If one of the arms is varied in length by just a few wavelengths of light then one observes a sinusoidal pattern as shown at the detector as a function of scan distance (with one wave corresponding to a arm length change of half of a wavelength of light in one arm length). This is because the two components interfere at the beamsplitter, just as two waves on a pond interfere, resulting in constructive and destructive interference – that is extra high and extra low regions. An important point to mention is that should a detector be placed in either arm which can in principle indicate whether or not the photon went in that arm, then the photon does go one way only and the interference pattern disappears!

One might expect that if a single particle of light — called a photon, which for the sake of this discussion can be said to be indivisible — is sent into the interferometer then it would go in either arm A or it would go into arm B and one would see no interference. Remarkably, however, even if only a single particle of light is in the interferometer at any one time, the same interference pattern is seen to build up after repeating the experiment many times. The crucial point here is that this cannot be understood in terms of the photon being in one path only — the pattern necessitates some interaction between components from two arms (if we were to remove one of the mirrors the pattern is found to disappear) and this forces us to consider that the photon to some extent goes in *both* arms! This is one of the central and rather bizarre features of QM. (Note the pattern can also not be due to the photon splitting into two photons of half the energy each, since mirrors can

be used that are reflective only around the photon energy/wavelength sent in, and as such any photons at a different energy would transmit through.)

Quantum Mechanics embodies an explanation for the above phenomena, which is powerful if un-intuitive. In the theory every system (e.g. a particle) is represented by a complex wavefunction, which is a function with imaginary and real parts. In the case of the photon the wavefunction evolves at the beamsplitter into having two componants – one in each of the arm. Each componant travels along its path, and they meet back at the beamsplitter to cause the interference. The situation following the beamsplitter is called a superposition, which represents the fact that the photon is not on one path but in some sense in both. This behaviour has been observed for photons, electrons, atoms and molecules and is predicted to within experimental (which is very small in some cases) error by Quantum Mechanics.

Two Problems for Physics

Schödinger first pointed out that there is no reason *a priori* why it should not be possible to create super-position states of large objects. He illustrated this with a thought experiment in which a radioactive atom, a container of poison and a cat are placed in a box in a way such that if the atom radioactively decays then the poison will be released resulting in the death of the cat. If the atom does not decay, then the cat remains alive. Since an observer external to the box does not know whether the atom has decayed, then, according to quantum mechanics, the atom becomes a superposition of having decayed and having not decayed. But, in this case, this necessarily results in a superposition of the cat being both alive and dead simultaneously!

It was first proposed that the measurement process might circumvent the problem: when a measurement occurs, QM states that the situation of a superposition 'jumps' to one of the options, e.g. if one opens the box and measures (looks at) the cat then one finds it to be either dead *or* alive. However the idea of having two separate processes in QM — one for the free evolution before measurement and one for the jump on measurement — is an uncomfortable situation for many physicists. This is called the 'measurement problem' and it remains central to resolving which interpretation(s) of QM are correct. In turn, these connect to philosophical questions regarding the nature of reality.

The second and perhaps more fundamental problem in physics related to the superposition principle is that superpositions seem to expose a conflict between QM and General Relativity (GR), the other great pillar of physics. GR tells us that space-time is curved by the presence of mass-energy. For example the Sun bends space-time, which has been observed experimentally by looking at the distortion of constellations which are almost directly behind the Sun during an eclipse caused by the bending of the light by the curved space-time region near the Sun. If the position of a massive object is moved, space-time is necessarily different – e.g. if the Sun were to be moved to a different location naturally the space-time would be shaped around its new position. Thus, if one considers a superposition of two spatially displaced masses, and wishes to treat it consistently with GR, then one must treat two distinct but correlated space-times in a single Schrödinger

Equation – the main equation of Quantum Mechanics. However, as Roger Penrose has pointed out, this would be inconsistent with GR, which doesn't allow you to show how a point on one space-time corresponds to a point on a separate space-time. Thus, it seems one cannot consistently consider both the evolution of a superposed quantum system in QM together with the appropriate curved space-times of GR.

What can be done about these problems?

One way to shed light on the problem is by exploring how systems evolve when we attempt to place them into a superposition as the masses are raised towards those of the macroscopic world, such as Schrödinger's Cat. Creating more massive superpositions is exactly the aim of the experiment discussed in this thesis.

The motivation for the experiment herein is important so let us explain it more precisely: it is the scientific philosophy that a theory can not be proved, only disproved. Progress thus depends upon continually testing a theory to its limits. The first and principle motivation of the experiment proposed in this thesis is in this spirit: to test the superposition principle of quantum mechanics in an as yet untested regime. Physicists by and large expect QM to hold, and that Newtonian mechanics emerge from QM. However, it should then be possible to isolate large states in order to see them exhibit superpositons. Secondly, the experiment would allow the testing of theories which scientists have proposed about interaction of a quantum system with the environment which surrounds it, which embodies a proposed resolution to the measurement problem (the first problem above). Thirdly, motivated by the second problem, of the conflict between GR and QM, Roger Penrose and others have postulated that the gravitational self energy of the difference in mass distribution of an object in a superposition of two locations will cause such states to have a finite lifetime and thus QM has to be modified to include this effect. In the longer term, such models might be testable by this experiment.

The Experiment

The proposal on which this thesis focusses aims to create a superposition involving two distinct positions of a tiny cantilever that is like a microscopic diving board – similar to the cantilevers in atomic force microscopes. The setup is shown in Fig. 2. It consists of an interferometer where a cavity is placed in both arms. One of the cavities has one large mirror and one microscopic mirror mounted on the end of the cantilever. The other cavity is constructed of two large mirrors and serves to balance the arm lengths. The experiment starts by sending in a single photon. If the photon goes in the bottom arm then the microscopic mirror will be kicked by the momentum of the photon reflecting from it many times as it bounces back and forth in the cavity. If it goes in the other (left) arm, then naturally it does not affect the cantilever. However, the photon is initially in a superposition of the two arms, as discussed above: thus the microscopic-mirror/cantilever and photon evolve into a superposition involving both the cantilever having moved and not moved from its initial position – two distinct locations of the cantilever. The photon leaks out of the cavity and ends at the detectors. The interference effects of the photon allows one to study the superposition of the cantilever.

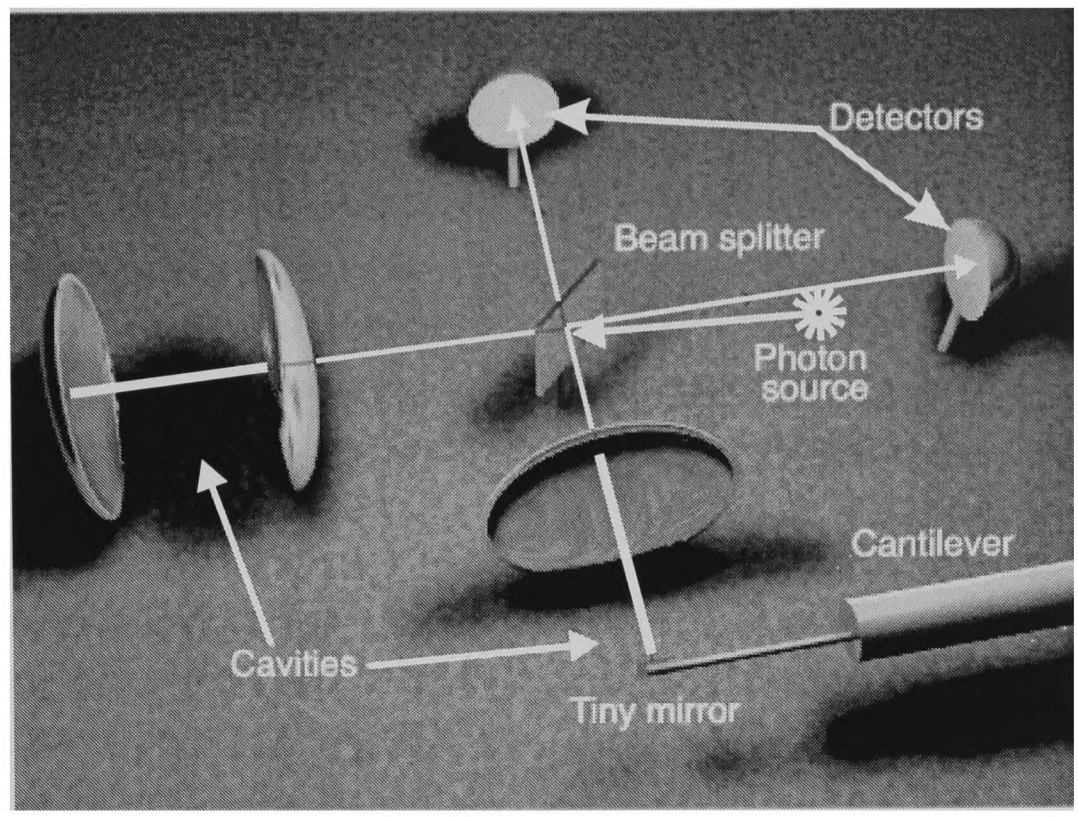

Figure 2: The proposed setup: an interferometer with a high-finesse cavity in each arm. The cavity in one arm has a very small end mirror mounted on a micro-mechanical oscillator whilst the one in the other arm has two large mirrors. A single photon enters the interferometer from the source. A photon in the first arm effects the motion of the small mirror due to radiation pressure. A photon in the other has no effect on the micro-mirror. The photon later leaks out of either cavity and is detected at the detectors. Multiple trials allow one to discern the interference pattern.

Is the experiment feasible?

The first contribution of this thesis is providing a detailed analysis of the experimental requirements to carry out the experiment under discussion. This part of the study was carried out by Christoph Simon, Dik Bouwmeester, Roger Penrose and me. There are three key physical requirements of the experiment: (1) Momentum: the photon has to reflect from the micro-mirror/cantilever enough times to kick it sufficiently to be able to distinguish the two cases, (2) Environment coupling: one must isolate the micro-mirror/cantilever sufficiently such that the environment (rest of the Universe) is not aware whether the cantilever is kicked (this is like ensuring that there is no detector placed in either arm of the interferometer in Fig. 1 which, as already discussed results in the interference pattern disappearing), and (3) Measurement: there should be sufficient stability in the setup in order to perform the measurement. This results in 6 key experimental requirements:

1. Mirror reflectivity: the cavity mirrors must have a $> 99.99998\%$ reflectivity (for visible light)

2. Cooling: the setup must be cooled to temperature of 0.003 degrees above absolute zero (i.e. close to -273 degrees Celcius).

3. Damping: the cantilever must have very little damping, such that, if set swinging, it can make 100,000 oscillations before coming to rest.

4. Vacuum: a gas particle density of just a million atoms per cubic cm is needed in the vicinity of the cantilever.

5. Stability: a relative position stability of the cavity mirrors of about the width of a nucleus of an atom is required over the timescale to get sufficient data. This turns out to be approximately 1 minute.

6. Ultra-fast switching: optical mirror switching techniques must be developed such that the high reflectivity mirror can be made much less reflective for short periods.

Whilst extremely demanding, each of these goals appear to be within reach of current technology: all but the last have been achieved in separate experiments and thus the main challenge is to implement them together.

Results to date

Encouraged by the results of the feasibility study a serious experimental effort has begun. The second contribution of this thesis is in presenting results from initial experiments made towards the final experiment. It should be emphasised that the end experiment is very demanding and the results presented are far from the regime needed in a number of important respects. Having said that, significant progress has been made specifically:

1. The fabrication of a mirror just 0.01mm in radius, but very high reflectivity (over 99.997%) attached to a micro-mechanical cantilever (like a micro diving board) made of silicon and which is a little smaller in dimension than the end of a human hair. This device lies at the centre of the experiment. Examples of microscopic cantilevers with microscopic mirrors are shown in Fig. 3. This research was conducted by Michiel de Dood and myself.

2. The alignment of an optical cavity of length 2.5cm involving the micro-mirror/cantilever at one end. A parameter for measuring how good the cavity is, called the finesse, is defined as the number of round-trips that light will make on average in the cavity, multiplied by 2π. We demonstrated a cavity finesse of $F > 1000$. This is measured by sending into the cavity a pulse of light (many photons) and observing the energy decay. If there are more round-trips of light on average then the decay time is longer. The decay of the field against time is shown in Fig. 4. The moderately high finesse is despite the very unusual geometry: if one were to scale up the cavity, it is equivalent to a mirror of radius 1cm being held 25 meters from a mirror of radius 3m and wavelength being 0.8mm. To get the light to bounce back and forth from the 0.01mm radius mirror to the large mirror and back many hundreds of

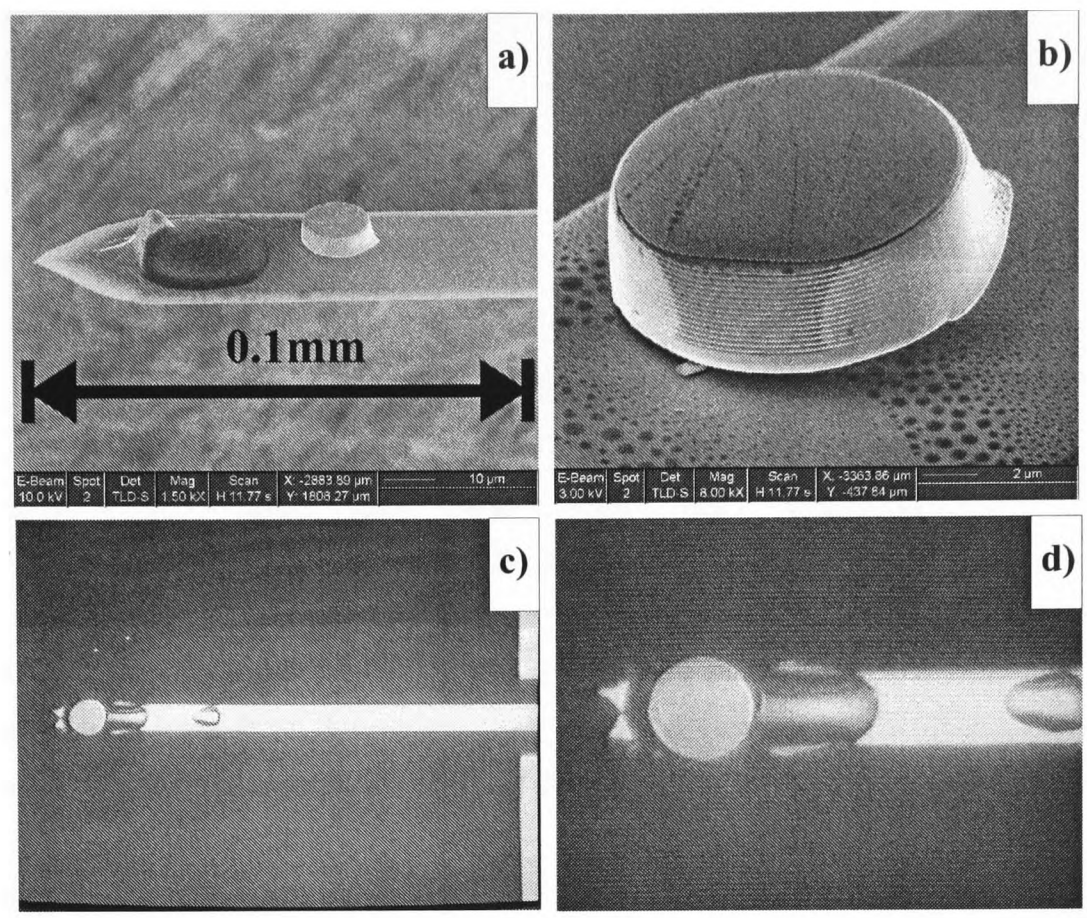

Figure 3: (a) SEM image of full cantilever with a 0.01mm radius mirror. There is a drop of glue next to the mirror. (b) Close up Scanning Electron Microscope image of the mirror showing the mirror layers and the mirror surface which has is slightly scratched. (c) & (d) Microscope photograph of Cantilever with 0.03mm diameter mirror and droplets of epoxy.

times without leaking from the edge of the tiny mirror is difficult. The major loss mechanisms of the cavity are analysed. The dominant one is determined to be acoustic noise which vibrates the cantilever and knocks it out of alignment. This can be alleviated by placing the cavity into a vacuum, which is the next major step for the experiment.

In addition, high-reflectivity switchable mirrors were designed and fabricated and results demonstrating ultra-fast optical switching of high reflectivity mirrors are shown. By shining an intense but short (100 femto-second) pulse on to a high reflectivity mirror it can be made to be much worse reflectivity. Such a mirror is shown to change in transmission from 0.0024% to 0.065% – a factor of 27 increase. The switching measurements were performed by Sara Hastings and Michiel de Dood.

Outlook

The results presented are just the first steps and there are a great deal of experimental hurdles left to overcome in order to make superposition states of a tiny mirror: not only are each of the 6 experimental requirements

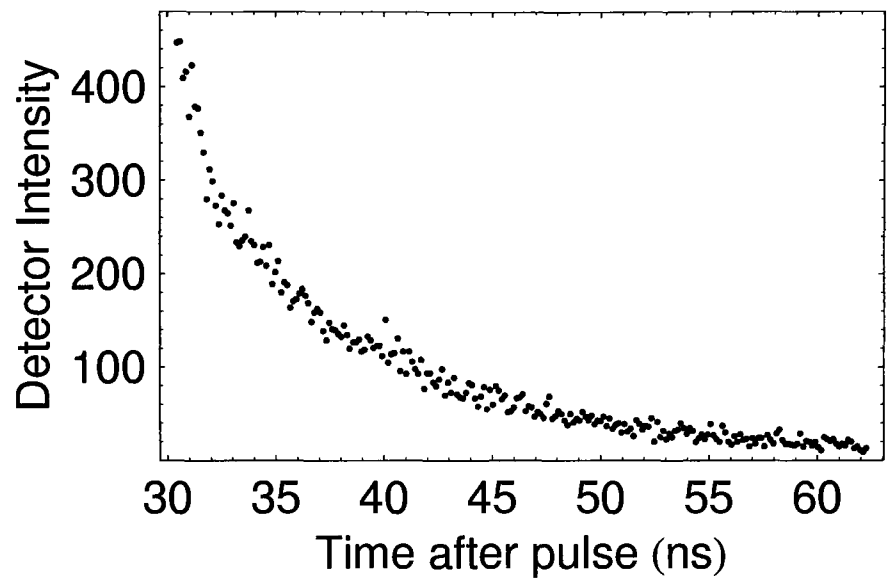

Figure 4: The intensity of the field exiting the cavity is measured versus time after the pulse. The field decays exponentially as the light leaks from the cavity. The time of the decay is in proportion to the cavity finesse: 1ns corresponds to 6 round-trips of light in the cavity and so the curve shows a finesse of over 1000.

tough but the integration of them into one setup will be harder still. As a result, it is expected to take several more years to complete the full experiment. The initial experimental results are promising and, moreover, it is remarkable that there is a technological niche where it seems to be possible to test quantum mechanics in a mass regime a thousand million times more massive than tested to date!

Although the main motive is to probe fundamental physics there may be some spin-off technology in the progress made to date and the experiments that are planned. Steps on the way are of importance for other applications in high precision measurements, optical communications, cavity quantum electro-dynamics and quantum state preparation of micro/nano mechanical systems. The uses of a massive superposition, if ever made, are purely speculation although it would be unwise to think that there would be none.

Further Reading

1. P. Ball, *Schrödinger's cat comes closer* Nature Online, October 2003 Link: http: //www.nature.com
2. C. Seife, *Quantum Experiment Asks 'How Big Is Big?'* Science, Vol.**298** p.342, October 2002 [Link: http: //www.sciencemag.org/cgi/reprint/298/5592/342.pdf]
3. C. Choi *Scaled-Up Superposition – Supersizing Schödinger's cat by a billion times* Scientific American, February 2003
4. *Goodbye Schrödinger's Cat* Cover Article, New Scientist, Vol. **2333**, p. 26, March 2002

Chapter 1

Introduction and Motivation

Motivation

Quantum Mechanics (QM) is in full agreement with all definite physics experiments to date yet it remains puzzling how the macroscopic world emerges from it: so far physicists have been unable to perform strict, detailed quantum calculations of macroscopic objects, therefore it is not possible to discern whether classical behavior is physically contradicting the rather different basic rules of QM or whether our observations merely display the complex nature of entangled quantum states. It is of interest to embark on a programme to study superpositions of larger and larger systems in order to test QM in massive domains and in the hope of shedding light on some of the philosophical conundrums surrounding the nature of our macroscopic world. More precisely, the motivation is four-fold. Firstly, it is the scientific philosophy to continue to test a theory in all ways possible to see how able it is to describe nature: whilst decades of experiments have shown that QM accurately describes microscopic system, separated out by macroscopic distances (now up to km scales) it has not been tested for superpositions involving macroscopic mass system (even if displaced by small spatial distances). Secondly, and more fundamentally, many are troubled by the measurement problem: a quantum state evolves in a deterministic fashion until the measurement, whereupon it jumps probabilistically to an eigenstate of the observable. Reconciling this apparent jump in modality (ontology) is a big problem of contemporary physics with no generally accepted conclusion. Creating and studying larger mass superpositions should shed light on this.

A third motivation for creating more massive superposition states comes from wanting to study the behaviour of these states due to interaction with the environment and thus enable a better understanding of Environment Induced Decoherence (EID), the most widely accepted view of how the macroscopic world appears to exist without such superposition states. To test EID models and verify their nature would be of great interest. A fourth and related motivation in the longer-term is to search for unconventional decoherence processes which suggest a modification to QM: EID is expected to dominate over most other

proposed decoherence mechanisms for states involving small mass and thus current superpositions experiments do not test these models but larger mass superpositions would. Examples of these models include the Ghirardi, Rimini, Weber (GRW) spontaneous wavefunction collapse model whereby a new term added into the Schrödinger equation multiplies the wavefunction by a Gaussian of a certain width and repetition rate to force the state to spontaneously collapse approximately to a Gaussian wavepacket in position space [Ghirardi et al., 1986, Ghirardi et al., 1990], or the Penrose gravitational decoherence model whereby gravitational self-energy of the difference of mass distributions of the multiple parts of a superposed state would cause the collapse of the wavefunction [Penrose, 1996].

One may ask why, given the above motivation, have large mass superposition states not been observed experimentally to date? The reason is that more massive superposition states have more coupling to the environment and as such are expected to become entangled with the environmental very quickly. Once entangled with all the unknowns of the environment then there are no clear quantum predictions, even if we measure the system only, since it is entangled with the environment and so one cannot verify the quantum state. Superposition states have been verified experimentally for single and small groups of photons and atoms. In terms of mass, the limits of experiments to date are captured by demonstrations of superposition states of superconducting quantum interference devices (SQUIDs) where of order 10^9 electrons are placed in a superposition of alternative current directions [van der Wal et al., 2000] and atom interferometry where large molecules (e.g. C_{60} and C_{70}) have been placed in a spatial superposition [Arndt et al., 1999].

To avoid EID the system must be well isolated and herein lies the challenge for those wanting to study macroscopic mass states. Despite the EID hurdles there have nevertheless been proposals on how to create and observe macroscopic mass superpositions in various systems including in Bose-Einstein condensates (BEC) [Ruostekoski et al., 1998, Cirac et al., 1998], in optical interaction with a tiny movable mirror [Bouwmeester et al., 1998, Bose et al., 1999, Penrose, 2000, Marshall et al., 2003a], and by coupling a superconducting island or Josephson Junction to a cantilever [Armour et al., 2002, A. Cleland, 2003]. In the latter three recipes a small quantum system (e.g. a photon [Bouwmeester et al., 1998, Penrose, 2000, Bose et al., 1999, Marshall et al., 2003a], a superconducting island [Armour et al., 2002] or a phase qubit [A. Cleland, 2003]) is reversibly coupled to a large system (e.g. a cantilever [Armour et al., 2002, A. Cleland, 2003] or a moveable mirror [Bouwmeester et al., 1998, Penrose, 2000, Bose et al., 1999, Marshall et al., 2003a]) – similar in principle to Schrödinger's *gedanken* experiment. It makes use of states that physicists have experience in creating, manipulating and measuring. In this case, the existence of the quantum superposition of the large system is verified by observing the disappearance and reappearance of interference for the small system, as the large system is driven into a superposition and then returns to its initial state. The challenge is to find a feasible implementation of this basic idea.

The proposed experiment

In this thesis the experiment under investigation involves the creation of relatively massive superposition states, involving of order 10^{14} atoms – an object approximately 10 μm in linear dimension. It follows Schrödinger's experimental principle above where, in this case, the small system is a photon that is in a superposition of two spatially distinct paths, having been reflected or transmitted at the beamsplitter. The large system is a circular mirror of 10μm radius and 6μm depth mounted on a tiny cantilever, similar to those used in atomic force microscopy, which acts as a harmonic oscillator. Interaction of the small and large parts of the system is achieved by reflecting the photon, in one arm of a Michelson interferometer, off the micro-mirror. The setup is shown in Fig. 1.1. The superposition of the photon being in arm A or arm B and the mirror at rest ($|M\rangle_r$) evolves into a superposition of the photon being in arm A and pushing the cantilever and mirror into a moving state ($|M\rangle_m$), or the photon being in the arm B and the mirror remaining at rest ($|M\rangle_r$). In Dirac notation this is written as

$$\frac{1}{\sqrt{2}}(|0\rangle_A|1\rangle_B + |1\rangle_A|0\rangle_B)|M\rangle_r \tag{1.1}$$

$$\Downarrow$$

$$\frac{1}{\sqrt{2}}(|0\rangle_A|1\rangle_B|M\rangle_r + |1\rangle_A|0\rangle_B|M\rangle_m). \tag{1.2}$$

Therefore, the cantilever is forced into a superposition of two momentum states. Being mounted on a harmonic oscillator, the two different motion states of the mirror $|M\rangle_r$ an $|M\rangle_m$ correspond to two different oscillator excitation states, ideally the ground state and the first excited state. For realistic micro-mirror/cantilever masses, to achieve distinct oscillator states a single reflection of an optical photon is not sufficient and the interaction must be enhanced which is the function of the cavity in arm A. The cavity has a micro-mirror on a cantilever as one of the two cavity mirrors and a large curved mirror: momentum transfer of approximately a million photon reflections at optical wavelengths places the micro-mirror into a superposition of two distinguishable spatial locations, different quantum excitation states of the harmonic oscillator. A cavity is needed in the other arm to ensure each arm holds the light for the same time.

Given certain experimental conditions, a superposition of the combined photon-mirror state can be observed by the disappearance and reappearance of the interference pattern with the oscillations of the mirror. This can be understood by considering the following two cases: firstly, if the photon leaks from the cavity at a time of half the cantilever oscillation, then the oscillator is left in a superposition of two physically distinguishable states at the time when the photon is detected. By studying whether or not the cantilever moved or not at a later time, one has the potential to know which way the photon went, thus the photon has been effectively measured by the cantilever. Just as for the well known case when a detector is placed in either arm of the interferometer, which path information destroys the coherence of the photon and no interference pattern is seen. Conversely, if the photon leaks out of the cavity after an integer number of oscillations of the mirror,

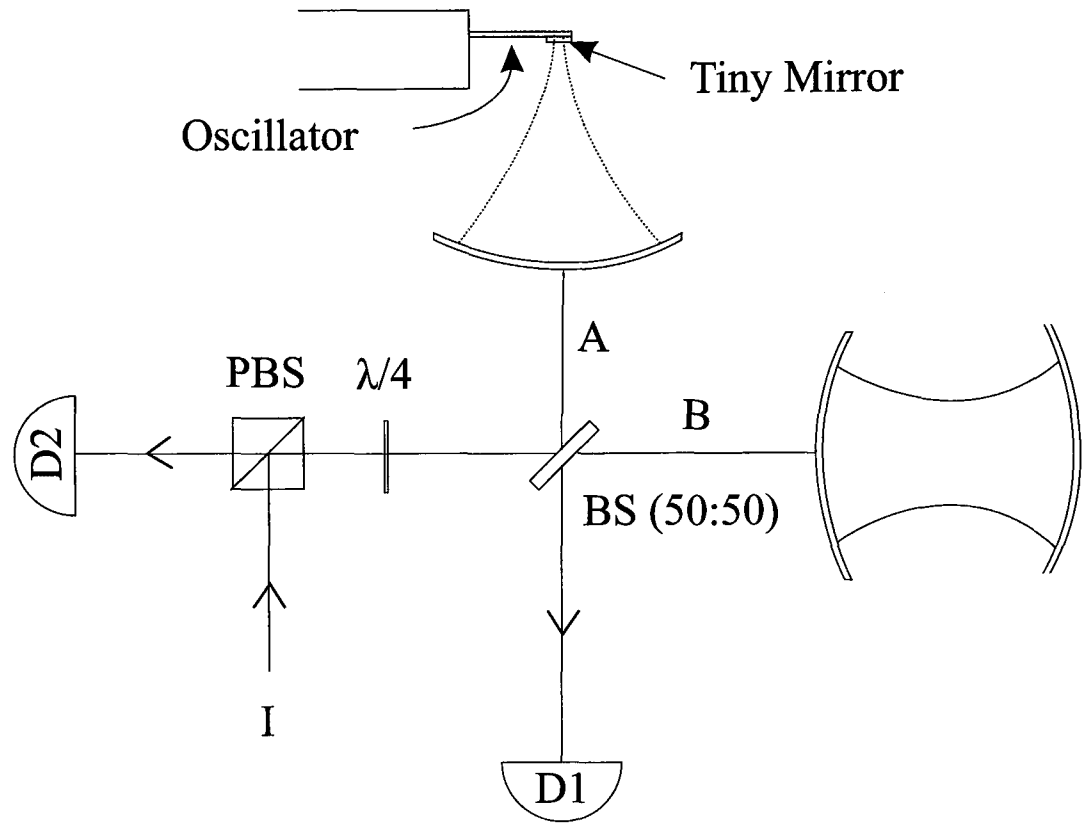

Figure 1.1: The proposed setup: a Michelson interferometer with a high-finesse cavity in each arm. The cavity in arm A has a very small end mirror mounted on a micro-mechanical oscillator whilst the one in B has two macroscopic mirrors. A single photon enters at I. A photon in arm A effects the motion of the small mirror due to radiation pressure. A photon in arm B has no effect on the micro-mirror. The photon later leaks out of either cavity and is detected at $D1$ or $D2$. Multiple trials allow one to discern the interference visibility of the interferometer.

then the cantilever is back in its original state and there is no information left in the system to determine which way the photon went. The cantilever oscillates around a new equilibrium position displaced from the rest state when undergoing forced motion and the rest position marks the extremity of the cantilever swing. Thus after one full period the cantilever is back at its rest position both in position and velocity. In this case the superposition would not collapse and standard interference patterns of a Michelson interferometer should be visible. From the decay of the interference and its revival at one oscillation one can infer the presence of a superposition at intermediate times.

In practice, there are three physical requirements leading to six key experimental requirements for the above to occur.

1. The photon must impart sufficient momentum. This requires a momentum kick greater than the spread of the momentum wavepacket of the cantilever in order to put it in an orthogonal momentum state. This necessitates

    - of order 5×10^6 reflections of an optical photon and thus a cavity finesse of 1.5×10^7, and hence

mirrors that have a reflectivity 99.99998%.

2. The environmental decoherence timescale must be long enough such that the environment cannot 'detect' the state on the experimental timescale. The requirements calculated from standard models of EID show that:

   - the temperature of the system should be $\leq$ 3mK,
   - the cantilever should have a mechanical quality $\geq 10^5$, and
   - the pressure needs to be sufficiently low to ensure that no atom hits the cantilever on the experimental timescale, which demands a vacuum gas particle density of $10^{12}/\mathrm{m}^3$.

3. The stability of the interferometer has to be high enough to maintain the arm lengths to within the wavelength.

   - The cavity mirrors should maintain their separation to within 6×10^{-15}m over a period of 10s.
   - Optical switching of the cavity mirror from $R = 0.9999998$ to $R = 0.5$ for a duration of < 100ps or up to 1μs.

Individually, each of these has been achieved in experiments with the exception of the last. However, several are near the state of the art, and collectively they amount to a tremendous hurdle requiring a serious experimental effort over a period of several years. That being said, it must be emphasised that what is remarkable is that it seems possible with current technology to create a superposition of an object 10^9 more massive than any other experiment to date – which takes us into an entirely untested regime.

Results of our experiments to date show the successful fabrication of a high reflectivity (16 pair dielectric stack) 10μm radius micro-mirror attached to a high-mechanical quality silicon cantilever and the demonstration of a moderate finesse hemispherical cavity of length 2.5cm involving the micro-mirror at the focus. These represent steps toward the final experiment and thus far the efforts have not come across a fundamental limitation on doing so.

Considering the above requirements, it is worth noting that the amalgamation of new technologies *en-route* shows promise in conceiving new optical devices with more general application – which provide great motivation in their own right. For example, ultra-fast all-optical switchable high-reflectivity mirrors have been demonstrated, and this could have a wide variety of optical applications such as optical communication. The setup and results achieved and described in §4.4 satisfy the essential ingredients for optical cooling: the cantilever motion can be sensitively monitored by observing the interference pattern formed by the light exiting the cavity with respect to the light exiting from a reference cavity. A second laser beam reflecting on the back of the cantilever can provide a force proportional to the velocity of the cantilever (a damping force) and hence the cantilever centre of mass motion can be cooled [Mancini et al., 1998]. Due to the heating effects of

absorbed light which overwhelm such a process for this mass scale, it is probably not useful for this proposal, in terms of cooling to meet EID and stability requirements, but it could be of use for other applications.

In Chapter 2, environmental induced decoherence is introduced, along with some non-conventional decoherence models. In Chapter 3, the experimental principle is developed and a thorough examination of the technical feasibility given current day technology is conducted. In Chapter 4, results of initial experiments are discussed. In Chapter 5, the conclusions of the study and the ways forward are summarised.

Chapter 2

Theory of Decoherence

2.1 The Measurement Problem

Despite the success of Quantum Mechanics (QM) in predicting a myriad of physical phenomena and experiments (e.g. spectral lines, atomic stability, black body radiation, the laser, single photon interference effects, Bose-Einstein condensates, etc.), there continues to be an active debate on how to interpret it. This centres on the apparent difference between the predictions of its formal rules when applied to measurements of quantum systems using macroscopic apparatus and the reality we experience: the rules of QM suggest that coupling of a microscopic quantum state that is prepared in a superposition to a macroscopic measuring device will lead to a superposition involving two or more outcomes of the macroscopic device. However, real experimental devices are always observed in a definite state. The paradox was first espoused in 1935 by Schrödinger in a now famous *gedanken* experiment involving the fate of a cat [Schrödinger, 1935].

Physicists are by and large content with the linear and deterministic evolution of a quantum system as given by the Schrödinger equation, but a non-negligible fraction are troubled by the measurement process where the quantum state reduces irreversibly to an eigenstate of the observable. A measurement is a procedure whereby a control device correlates a microscopic state, e.g. a spin $|\uparrow\rangle$ or $|\downarrow\rangle$, to macroscopically distinct states of the apparatus that can be read by an observer. In the case below, the apparatus to be measured is a cat whose two distinct states are that of 'alive', $|C_{alive}\rangle$, and 'dead', $|C_{dead}\rangle$. This can be imagined to be made so by coupling of the spin system to the cat by way of a lethal device, e.g. a poison vessel, whose opening is triggered by the spin state. Formally, such an action is encapsulated in a Hamiltonian term that determines the operator U, which acts on the initial measuring device state $|C_{alive}\rangle$ as

$$\begin{aligned} U|\uparrow\rangle|C_{alive}\rangle &\Rightarrow |\uparrow\rangle|C_{alive}\rangle \\ U|\downarrow\rangle|C_{alive}\rangle &\Rightarrow |\downarrow\rangle|C_{dead}\rangle. \end{aligned} \tag{2.1}$$

However, if our spin state is initially is in a superposition $\alpha|\uparrow\rangle + \beta|\downarrow\rangle$ then, by the normal rules of quantum mechanics when such an operator is applied one expects the system to evolve into a superposition of two distinct macroscopic states

$$U(\alpha|\uparrow\rangle + \beta|\downarrow\rangle)|C_{alive}\rangle \Rightarrow \alpha|\uparrow\rangle|C_{alive}\rangle + \beta|\downarrow\rangle|C_{dead}\rangle = |\psi_{SC}\rangle, \tag{2.2}$$

a superposition of the cat being simultaneously dead and alive! Such states seem to be an absurdity to us since macroscopic measuring devices are only ever in one definite state, according to our perception.

Some theorists have proposed that one or both of the dynamics are simply an approximation to an underlying framework with a single, determinate dynamics – 'hidden variable theories' – however, the famous proof by John Bell [Bell, 2004] showed that the predictions of QM are inconsistent with any possible *local* dynamics involving hidden variables and subsequent experiments demonstrating the violation of Bell's inequalities have shown convincingly that QM is correct and necessarily that no such local hidden variable theory can be true.

There are several other interpretations of quantum mechanics that each have a proposed resolution to the measurement problem [Joos et al., 1996, Zurek, 1991, Penrose, 1996, Leggett, 2002]. An heuristic overview of these is given below. It should be emphasised at the outset that there is no solution to the problem that could be said to enjoy anywhere close to universal acceptance in the physics community: it remains one of the greatest unresolved problems in physics.

The Copenhagen Interpretation

First espoused by Bohr [Eisberg and Resnick, 1985], this proposes a resolution based on having a distinct division between the quantum (small) and classical (large) worlds. Here it is said that no greater meaning should be afforded to the quantum formalism that is applied to the microscopic state than to generate the amplitudes that are interpreted as classical probabilities when the state is measured using classical apparatus. One has two processes: evolution, which is deterministic, and measurement, which is probabilistic. Quantum state evolution is governed by the Schrödinger equation

$$i\frac{\partial}{\partial t}|\psi_{SC}\rangle = H|\psi_{SC}\rangle. \tag{2.3}$$

where $|\psi_{SC}\rangle$ is the state of the system S (spin) and control device C (cat). The measurement, von Neumann's "Process 1", is radically different: as Dirac explains, "A measurement always causes the system to jump into an eigenstate of the dynamical variable being measured". The probability of the various outcomes is determined by the square of the modulus of the amplitude of each component (presuming that the state has been normalised). For comparison with the other interpretations, let us write this out in density matrix

formalism: one starts with the state given by Eq. 2.2 whose density matrix is

$$\begin{aligned}\rho_{SC} &= |\psi_{SC}\rangle\langle\psi_{SC}| \\ &= \begin{pmatrix} |\alpha|^2|\uparrow\rangle|C_{alive}\rangle\langle\uparrow|\langle C_{alive}| & \alpha\beta^*|\downarrow\rangle|C_{dead}\rangle\langle\uparrow|\langle C_{alive}| \\ \alpha^*\beta|\uparrow\rangle|C_{alive}\rangle\langle\downarrow|\langle C_{dead}| & |\beta|^2|\downarrow\rangle|C_{dead}\rangle\langle\downarrow|\langle C_{dead}| \end{pmatrix}.\end{aligned}$$

The collapsing to an eigenstate of the observable is equivalent to cancelling the off-diagonal terms of the density matrix in the appropriate basis [Zurek, 1991] to produce a density matrix

$$\rho_r = \begin{pmatrix} |\alpha|^2|\uparrow\rangle|C_{alive}\rangle\langle\uparrow|\langle C_{alive}| & 0 \\ 0 & |\beta|^2|\downarrow\rangle|C_{dead}\rangle\langle\downarrow|\langle C_{dead}| \end{pmatrix}.$$

This is a mixed state with coefficients that can be interpreted as the (correctly predicted) classical probabilities of the measurement.

Some questions that arise are as follows. It is assumed that the quantum rules should not be applied to any measurement apparatus. How does one determine what is "classical"? There is a need for a precise criterion here. Also, as alluded to already, the measurement process described above is a discontinuous change to the state vector as well as being indeterminate, exactly at odds with the standard continuous and determinate quantum evolution. Is it satisfactory to have two quite different processes in a theory?

Environmental Induced Decoherence

Perhaps the most standard contemporary proposed alleviation of the measurement problem is based on the unavoidable connection of a quantum state to the surrounding (quantum) environment, an approach first explored by Zeh [Zeh, 1970] and followed up by Zurek [Unruh and Zurek, 1989, Zurek, 1991] and others. All quantum systems interact with the environment to some degree. Thus, in a quantum experiment one has a system S, control device C and environment E. The environment represents any interaction that is unwanted, which is, in general, largely constituted by interaction with the external environment through photons, phonons etc, but can also be internal degrees of freedom of the system or control that the experimenter cannot know or control.

Any real quantum system will evolve from Eq. 2.2 into an entangled state of system + environment (which is also a quantum system):

$$(\alpha|\uparrow\rangle|C_{alive}\rangle + \beta|\downarrow\rangle|C_{alive}\rangle)|E_0\rangle \Rightarrow \alpha|\uparrow\rangle|C_{alive}\rangle|E_\uparrow\rangle + \beta|\downarrow\rangle|C_{dead}\rangle|E_\downarrow\rangle = |\psi_{SCE}\rangle. \qquad (2.4)$$

where $|E_\uparrow\rangle$ and $|E_\downarrow\rangle$ are the states of the environment, initially in a state $|E_0\rangle$, corresponding to the two spin states. This entanglement can be understood as information transfer to the environment. This gives a density

matrix

$$\begin{aligned}\rho_{SCE} &= |\psi_{SCE}\rangle\langle\psi_{SCE}| \\ &= \begin{pmatrix} |\alpha|^2|\uparrow\rangle|C_{alive}\rangle|E_\uparrow\rangle\langle\uparrow|\langle C_{alive}|\langle E_\uparrow| & \alpha\beta^*|\downarrow\rangle|C_{dead}\rangle|E_\downarrow\rangle\langle\uparrow|\langle C_{alive}|\langle E_\uparrow| \\ \alpha^*\beta|\uparrow\rangle|C_{alive}\rangle|E_\uparrow\rangle\langle\downarrow|\langle C_{dead}\langle E_\downarrow| & |\beta|^2|\downarrow\rangle|C_{dead}\rangle|E_\downarrow\rangle\langle\downarrow|\langle C_{dead}|\langle E_\downarrow| \end{pmatrix}.\end{aligned}$$

Now the density matrix for the system-detector (spin and cat), which one aims to measure, is found by tracing over the environment

$$\begin{aligned}\rho_{SC} &= Tr_E|\psi_{SCE}\rangle\langle\psi_{SCE}| \\ &= \sum_i \langle E_i|\psi_{SCE}\rangle\langle\psi_{SCE}|E_i\rangle \\ &= \sum_i \langle E_i|\rho_{SCE}|E_i\rangle. \end{aligned} \tag{2.5}$$

For cases where the states of the environment corresponding to $|C_{alive}\rangle$ and $|C_{dead}\rangle$ are orthogonal $\langle E_i|E_j\rangle = \delta_{ij}$ (i.e. the state changes the environment), then one has

$$\rho_{SC} = \begin{pmatrix} |\alpha|^2|\uparrow\rangle|C_{alive}\rangle\langle\uparrow|\langle C_{alive}| & 0 \\ 0 & |\beta|^2|\downarrow\rangle|C_{dead}\rangle\langle\downarrow|\langle C_{dead}| \end{pmatrix}. \tag{2.6}$$

This is a mixture of states $|C_{alive}\rangle$ and $|C_{dead}\rangle$, with probabilities $|\alpha|^2$ and $|\beta|^2$ respectively. Thus, if the states of the environment corresponding to the two or more outcomes of the measurement are mutually orthogonal, then the density matrix of the detector-system (tracing over the environment) is placed into a mixture in the alive/dead cat basis. The key feature of this density matrix is that it is identical to that found by the *ad hoc* "Process 1" of cancelling the off-diagonal terms. Thus, the collapse to an eigenstate of the observable is achieved by environmental coupling: coherence has been lost to the environment and the cat is now found to be either dead or alive and never in a superposition of the two.

But in order to circumvent the measurement problem, an additional step is required to the entanglement/diagonalisation process described above: one must *interpret* that because the results of measurement on the pure state are mixed when tracing over the unknown degrees of freedom (the environment), almost identical to a classical mixture, that therefore the state *is* in one or the other state. There is an important, albeit subtle, ontological shift here because the density matrix is diagonal in one basis, ($|C_{alive}\rangle$, $|C_{dead}\rangle$) *transforms* to a probability mixture: as Penrose summarises, "To obtain a probability-weighted mixture of alternatives, rather than a single state involving complex-number-weighted alternatives, something other than unitary evolution has to be invoked". To make clear the distinction, it can be remarked that appropriate coupling of the system-device to the environment could re-create the coherence of the system as the information remains in the environment. In fact, this is a consequence made use of in the proposal presented in Chapter 3, where the coherence of the photon is lost and then recovered with the oscillation of the cantilever. This reversibility leaves it unclear whether this fully resolves the measurement problem.

It is pertinent to note that the reason why the control does not decohere in the myriad of successful quantum experiments that have been performed is that the degree of entanglement between the system and control is low: the control changes in a negligible way despite being able to manipulate the system and can be treated as a classical effect. For example, a photon in an optical cavitywith large mirrors interacts with the mirrors but the resulting difference in the mirrors, having interacted with the photon or otherwise, is so minimal that it does not lead to distinguishable states.

A different but also environmental approach is constituted by the fact that a system of particles subject to a sequence of scattering events leads to *relative* position localisation of the particles [Rau et al., 2003].

Many Worlds

In the opposite spirit of the Copenhagen Interpretation, Everett proposed [Everett, 1973] to avoid the measurement problem by taking quantum evolution as absolute reality and suggesting that there is no such thing as measurement at all. In this case macroscopic measuring devices *do* evolve into superpositions of the form shown in Eq. 2.2. At each suitable interaction/decision point (e.g. a photon encountering a beamsplitter) the Universe splits into two or more branches, each equally real – hence "many worlds". Reduction of the off-diagonal elements according to EID is needed in the model to account for the observation that the different branches do not seem to interfere. However, how it is inferred that the probabilities are associated with the future perception of an observer is unclear: "I *still* need a rule to translate this density operator into probabilities assigned to the alternatives,", Preskill [Preskill, 1998].

A consequence is that one must accept the existence of an almost infinite number of "parallel Universes", which leads some to complain about their meaning, e.g. Leggett states, "If someone could explain to me what these words [equally real parallel Universes], ostensibly English, actually mean, I might know whether or not I believed this interpretation." [Leggett, 2002].

Modifications to Quantum Mechanics

Some physicists have suggested that modifications to QM are needed to resolve the measurement problem. In such schemes, QM is expanded to include a physical process that forces the state to collapse into one of the possibilities, allowing reduction to take place *prior* to ("objective reduction") or during measurement. Some models are also motivated by the larger problem of the incompatibility of General Relativity and Quantum Mechanics. Since the idea of testing these models has played an important role in motivating the experiment on which this thesis focuses, an overview of some proposed ideas are given in §2.3. The interest is that the experiment of the kind presented in Chapter 3 has the ability, in the long run, to test the validity of these theories involving modifications to QM.

Regardless of the interpretation believed, the fact that a quantum state will change due to interaction with

its environment is not disputed. This interaction must be taken into account for any real experiment. As such, an overview of the standard EID model is given below for the purpose of being able to calculate its effect on our experiment in Chapter 3. The essential requirement is that EID must remain small on the experimental timescale if it is to be possible to demonstrate massive quantum superposition states.

2.2 The Environment as a Bath of Harmonic Oscillators

A model of the EID process was developed by considering the environment as an (Ohmic) bath of simple harmonic oscillators — an idea traceable to Feynman [Feynman and Vernon, 1963] — on the basis that most systems can be treated quantum mechanically as a set of harmonic oscillators coupled together by some interaction. The interaction depends on the physical characteristics of the system. One should imagine in our case that the bath is the phonons of the cantilever and its substrate and the system is the cantilever centre of mass motion. It is unclear how well the approach will work in real cases where less simple phenomena, for example surface defects, become important. But it is partly the motivation of this experiment to probe the effects of the environment since they are not clearly understood.

As an example, for the system in the experiment of Chapter 3 (and outlined in Chapter 1) there are several physical mechanisms likely to cause decoherence: it is intuitive that any natural damping that the cantilever has means that there is a certain energy loss to the environment, causing the environment to become entangled with the state that will lead to loss of coherence of the state. Thus a high mechanical quality is required. That this energy flow might scale with the system temperature also seems likely. The decoherence rate is also related to the displacement, which can be understood intuitively from the fact that larger separations are distinguishable by larger wavelength, and thus lower energy, particles. For the photon, decoherence can occur due to dissipation in the non-perfect mirrors.

A quantum system's time evolution is determined by the Hamiltonian of the system and the Schrödinger Equation. The Hamiltonian of the situation involves terms for the system, H_{sys} (for the case in Chapter 3, this is a harmonic oscillator of mass m, frequency ω_m), the term for the reservoir that constitute the environment, H_{res}, made up of the bath of harmonic oscillators with masses M_i and frequencies w_i and the interaction between the two H_{int} involving a coupling parameter, g_i, between the i-th oscillator and the system. Given in terms of position and momentum, X and P, these can be written:

$$\begin{aligned} H &= H_{sys} + H_{res} + H_{int} \\ &= \frac{P^2}{2m} + \frac{1}{2}m\omega_m^2 X^2 + \sum_{i=1}^{N}\left(\frac{P_i^2}{2M} + \frac{1}{2}M\omega_i^2 X_i^2\right) + X\sum_{i=1}^{N} g_i X_i \end{aligned} \tag{2.7}$$

Such a model was used to find the dynamics of the reduced density matrix ρ(x,x') of the system-control

(after tracing over the environment). This is given by a master equation independently derived by Caldeira and Leggett [Caldeira and Leggett, 1983, Leggett, 2002] and Zurek and Unruh [Unruh and Zurek, 1989] and others, see [Joos et al., 1996, Zurek, 1991, Venugopalan, 1999]

$$\frac{\partial \rho}{\partial t} = \frac{i}{\hbar}[H, \rho] - \gamma(x - x')(\frac{\partial \rho}{\partial x} - \frac{\partial \rho}{\partial x'}) - \frac{2m\gamma k_B T(x - x')^2}{\hbar^2} \tag{2.8}$$

where γ is the mechanical damping rate, T is the temperature of the bath, k_B is Boltsman's constant, $\hbar$ is the Planck constant over 2π, and m is the oscillator mass. This assumes that the thermal excitations of the field dominate the interaction process and that the decoherence rate is much less than the system (cantilever) frequency (weak coupling). The first term has the form of the usual unitary evolution for a system with Hamiltonian H (the usual Schrödinger term), the others account for transitions that the system may undergo due to interaction with the reservoir. The second term is dissipation of energy. The last term leads to decoherence in the position basis. For pieces of the wavepacket that are spatially separated, the coherence is destroyed. This can be seen because, for diagonal terms of the density matrix, the second and third terms of the master equation are negligible as $(x - x') \sim 0$, whereas, for the off-diagonal terms, $(x - x') \sim \Delta x$. Thus, for a superposition of two Gaussian wavepackets separated by a distance Δx, the off-diagonal terms decay with respect to the diagonal terms at a rate

$$\tau = \frac{\hbar^2}{2m\gamma k_B T \Delta x^2}. \tag{2.9}$$

The main features of this and related EID schemes explored are that, (1) for macroscopic mass objects decoherence takes place on a timescale much faster than the thermal relaxation timescale and (2) the decoherence time is inversely proportional to the square of the separation of the two superposition components. The master equation has been derived for different relative system timescales by Strunz, Haake and Braun [Strunz et al., 2003, Strunz and Haake, 2003].

There are many EID models, but most have the same two basic features described above. Naturally the model most able to describe nature can only be determined by experimentation, which is in part the aim of the developments described here. To date, decoherence has been observed by some microscopic mass systems including (1) a macroscopic electromagnetic field placed in a superposition of two classically distinct phases by means of coupling to an atomic transition [Brune et al., 1996, Raimond and Haroche, 1999] and where models relevant for the quantum optics domain, e.g. [Walls and Milburn, 1985], are being tested, (2) motional states of ions in a trap [Monroe et al., 1996], and (3) C_{70} molecules in interferometry experiments [Hackermüller et al., 2004]. These experiments have confirmed the two basic features predicted by EID schemes given above. In addition EID schemes also show that the decoherence rate increases with temperature and this has been tested in the latter experiment, where heating of the molecules has a sharp effect on the coherence, as seen by the interference visibility. This is caused by increased photon emission by the molecules on the experimental timescale. The temperature dependance has also been verified by looking at the influence of a heat bath on a superposition of light states in a cavity [Kim, 1992].

Other proposals have been made to investigate decoherence [Leggett, 1984, Anglin and Zurek, 1996, D.Home and R.Chattopadhyaya, 1996], but to date there have been no tests of decoherence of spatially separated states of a macroscopic mass object as no one has yet created such a state.

2.3 Gravitational and Spontaneous Localisation Decoherence

A basic conflict between quantum mechanics and General Relativity

The superposition principle of QM and the definition of a space-time metric in General Relativity (GR) seem incompatible and yet are both fundamental principles in their theory. This can be viewed from two perspectives: on the one hand, according to QM one has the uncertainty relation

$$\Delta x \Delta p \geq \frac{\hbar}{2} \tag{2.10}$$

thus the position and velocity of any system is subject to quantum fluctuations which are in contradiction with the exactly defined metric $g_{\mu\nu}$ at each position x that is fundamental to GR. On the other hand, GR tells us that the curvature of space-time is dictated by the presence of mass-energy. If the position of a massive object is moved, the manifold is necessarily different. Thus, if one considers a superposition of two spatially displaced masses, and wish to treat it consistently with GR, then one must treat two distinct space-time manifolds. This would require replacing the $\partial/\partial t$ in the Schrödinger equation (that is, flat space-time) by the time-like vector field which expresses the stationary, curved nature of the space-time of each component of the superposition. However, the Principle of General Covariance – which lies at the heart of GR – doesn't allow the point-wise identification of two separate space-time manifolds [Kenyon, 1990] required to have a single Schrödinger Equation involving two space-time manifolds. Thus, one cannot consistently consider both the evolution of a superposed quantum system in QM together with the appropriate curved space-time of GR.

The Penrose Objective Reduction (OR) Model

Károlyházy [Károlyházy et al., 1982, Károlyházy et al., 1986] and Penrose [Penrose, 1996, Penrose, 1999, Penrose, 2000, Penrose, 2004] have postulated the possible connection between the above fundamental conflict of GR and QM by providing an objective basis for the resolution of the measurement problem. Károlyházy, Frenkel and Lukács [Károlyházy et al., 1982, Károlyházy et al., 1986] developed a model for collapse based on estimates of the effects of "smearing" of space-time, needed for GR, on the coherence of a quantum object and showed that the coherence can be seen to be lost for massive objects in superpositions. This model was further formalised by Diòsi [Diòsi, 1989] whose main result of the decay of the coherence is identical to that of the Penrose model. Penrose motivates the dynamics by postulating that the "error" in identifying the two

space-times in the Schrödinger equation is an energy uncertainty that is subject to the uncertainty principle and thus has a finite lifetime.

In the Penrose model, wavefunction reduction is an objective effect of gravity due to an energy uncertainty in identifying the (two) different space-time manifolds of a quantum system superposed in two distinguishable locations. The essential suggestion is a modification to QM to accommodate gravity, resulting in a gravity-induced decoherence within a quantum framework. The focus of the theoretical predictions of this and other gravity-related reduction models [Károlyházy et al., 1982, Károlyházy et al., 1986, Ghirardi et al., 1990, Pearle, 1999] have been on quantum superpositions of an object in the intermediate "mesoscopic" mass range $10^{-10} - 10^{-15}$ kg (not much less than the Planck mass) which lies in a range in between where it is known that QM works to a good approximation and where classical mechanics works well. For such masses the reduction timescales are calculated to be $10^{-3} - 10^{2}$s given certain approximations on the mass distribution. The experiment proposed in this thesis is expected to result in a superposition involving an object in this range of mass scales and so in principle able to test these models.

There is an error made if one wishes to take a single time derivative $\partial/\partial t$ in the Schrödinger Equation over the space-time region that includes a massive object in a superposition of two locations. The error can readily be expressed as energy error and Penrose proposes that such an energy error might be subject to the uncertainty relation, in an analogous way to radioactive decay,

$$\Delta E \Delta T \geq \frac{\hbar}{2}. \tag{2.11}$$

Thus, Penrose proposes, the superposition has a finite lifetime inversely proportional to the energy uncertainty.

Two space-times may be considered identified if free fall is the same in both: the error in identifying the two as one can be expressed with units of energy which Penrose estimates as the error which is subject to the uncertainty relation. Penrose shows [Penrose, 1999] that for the case of a superposition of separation similar to the size of the object a simple estimate can be given by the Newtonian gravitational self-energy of the difference between the mass distributions. Equivalently, in this simple case, this is the potential energy of the mass in one location in the gravitational field of it in the other location. The energy uncertainty is then given by

$$E_g \simeq 20 G \rho^2 \Delta x^5, \tag{2.12}$$

where G is the Gravitational constant, and ρ is the quantum objects density, assumed to be given by the expectation value of the mass density distribution, and Δx is the mass radius (position uncertainty). Point particles yield an infinite energy, so one has to treat the matter in its true granular nature – being made of atoms – then one expects the principle effect to be from the superposition of each nucleus. Nuclei have a mass distribution as described by the wavefunction. Now ρ becomes the nuclear density and, to get the energy for the whole object of N_{nuc} nuclei, one multiplies by a factor of the number of N_{nuc} to obtain the total energy

[Penrose, 1999]

$$E_g \simeq 20G\rho^2\Delta x^5 N_{nuc}. \tag{2.13}$$

Substituting this into the uncertainty relation Eq. 2.11, one obtains the formula for the collapse timescale t_g:

$$t_g = \frac{}{20G\rho^2\Delta x^5 N_{nuc}}. \tag{2.14}$$

The timescale reduces quadratically with increased mass of the object. One intriguing feature of the model is that for distances less than the nuclear spatial extent, the gravitational self energy E_G rises quadratically with superposition displacement, while the displacement caused by a kick from the photon decreases linearly with the mass (or equivalently number of nuclei) – as such, at small displacements, the reduction time *increases* with mass for a given momentum kick.

Diòsi arrives at the same result for the decoherence rate of the off-diagonal terms of the density matrix when introducing a term to the Schrödinger equation that is derived from considerations of space-time smearing. Ghiradi, Remini and Weber [Ghirardi et al., 1986, Ghirardi, 1990] extended the Diòsi scheme for collapse by the addition of a fundamental length scale in order to overcome some difficulties.

In summary, the Penrose model addresses the two theoretical concerns of the measurement problem and the difference in the treatment of time of QM and GR by proposing that the mechanism for collapse is provided by gravity (the gravitational self-interaction of a quantum state) and that the timescale for the collapse is that given by the error (energy uncertainty) in the treatment of time when a quantum system with non-negligible mass is treated with the Schrödinger Equation. The reduction is objective, i.e. not dependent on observer/measurement, and consequently is dubbed objective reduction (OR). It is not a theory establishing full dynamics for collapse, rather it is a first-approximation minimalist scheme that uses known physics to make predictions which are testable. It is a proposal for what might be a classical limit (in a specific regime) to a full quantum-gravity theory. This, together with the potential testability (see below) adds motivation for experimenters to probe the regime. Theoretical issues that are outstanding include (a) the exact geometric factor in the formulation, and (b) whether the nucleus is the size at which the effect is greatest.

Testable predictions

According to the Penrose model, the decay time for macroscopic objects of mass 10^{-7}kg (e.g. a grain of salt/flea) superposed by 10^{-12}m, is $t_g \sim 10^{-4}$s – so the model is consistent with classical observations. The timescale for microscopic objects of mass 10^{-24} kg (e.g. a bucky ball) superposed by a similar distance, is $t \sim 10^{13}$s so the model is consistent with the results of known quantum experiments. Putting an object the size of Schrödinger's cat into a superposition would yield a timescale so small it would be hard to observe (as well as being something hard to isolate!). It is clear that if one shall ever be able to test OR schemes, one needs to aim for a compromise regime – a "meso-scopic" object – for example an object of mass 10^{-12}

kg ($N_{nuc} \sim 10^{14}$), equating to a sphere of approximate linear dimension 10μm, more like one *cell* of Schrödinger's cat, the anticipated collapse timescale for which is 10s.

In order to test models of gravitational reduction of our micro-mirror in the setup shown in Fig. 1.1, the reduction due to this effect must be distinguishable over the environmental decoherence. Ideally, the timescale of the EID, t_E must be greater than the timescale of the gravitational collapse:

$$t_E > t_g = \frac{}{20G\rho^2\Delta x^5 N_{nuc}}, \tag{2.15}$$

where

$$\rho \sim \frac{3m_p Z_C}{4\pi\Delta x^3}, \tag{2.16}$$

m_p = proton mass and Z_C = atomic number. In order to probe the gravitational collapse scheme, the displacement of the micro-mirror should be greater than the coherent wavepacket (as in the optical setup proposed in the next chapter) in order to create orthogonal superposed states. The separation must also be greater than the radius within which the nucleus oscillates – the 'nuclear blur width' Δx_{nuc} of nuclei in the micro-mirror for an appreciable gravitational reduction effect. This must also be known in order to get an estimate of ρ in equation 2.14. One can estimate Δx_{nuc} using the Debye-Waller model of atomic motion [Blakemore, 1985, Grosso and Parravicini, 2000],

$$\Delta x_{nuc} = \sqrt{\frac{3}{4m_p Z_c k_B T_D}} \tag{2.17}$$

where T_D = Debye temperature. The blur width is of order $\Delta x_{nuc} \sim 3\times10^{-12}$m for the micro-mirror/cantilever proposed in Chapter 3 at a temperature of 4mK. This is just one order of magnitude greater than the displacement required to verify coherent superpositions of mesoscopic objects. This does not mean that there is no gravitational collapse for displacements of less distance than this, it is simply that a calculation of the models predictions here has not been performed.

Substituting t_D from Eq. 2.15 with Eqs. 2.16, 2.17 one finds:

$$\frac{N_{nuc}Z_C^2}{m\gamma_{osc}\theta\Delta x^3}\ \frac{16\pi^2 k_B}{90Gm_p^2}. \tag{2.18}$$

To illustrate the difficulty in reaching this regime, for $N_{nuc} = 6 \times 10^{13}$, $Z_C = 50$, $m = 5 \times 10^{-12}$kg, $T_D = 645$K, $\Delta x = 3 \times 10^{-12}$m one requires $Q/T_E \geq 4.10^{12}$ (i.e. an extremely cold undamped mirror). The requirement on Q/T_E is 5 orders of magnitude harder to reach than verifying mesoscopic superpositions (§3). However, the collapse model may take effect at displacements of order the coherent state wavepacket in which case the experimental requirements drop to $Q/T > 7 \times 10^9$ – a factor 200 harder than verifying mesoscopic superpositions.

The timescale of each run of the experiment is much larger than for creating the superposition state — minutes compared to ms — if it is the intention to observe a 1/e reduction of the interference visibility. One

has to wait for of order 10^4 oscillations of the cantilever. It is possible to detect the visibility change earlier if one has sufficient interferometric contrast ratio which measures the sensitivity of the interferometer to changes in fringe pattern: one can measure it after one oscillations (the same timescale as before) given a contrast ration of 10^6. However, necessarily then the number of trials has to increase by the same factor and thus it is not clear that this reduces the feasibility.

In summary, the Penrose Model has distinct predictions for the collapse which are in principle distinguishable from EID since for superpositions with displacement tending to the atomic separation the model predicts that the collapse time will rise again (if the micro-mirror is a reasonably uniform crystal), since the two space-time manifolds will be nearly identical. If it becomes feasible to probe the collapse of mesoscopic objects then one can distinguish many different collapse models by the exact scaling of predicted collapse timescale with mass and atomic structure of the micro-mirror. In order to test the Penrose OR model one requires a reduction in Q/T_E by 5 orders of magnitude further than that required to verify mesoscopic superpositions. On top of that increases in stability are required to accommodate the longer experimental timescale. However, developments here are possible for example cantilever quality factors are known to increase with decreasing temperature and an increase in achievable N or reduction in λ would have a knock on effect easing the other parameters.

Continuous Spontaneous Localisation (CSL)

Ghiradi, Remini and Weber [Ghirardi et al., 1986, Ghirardi, 1990] and later with Pearle [Ghirardi et al., 1990], proposed a modification to the Schrödinger equation in order to exclude macroscopic masses being subject to linear superpositions of two or more locations separated by large distances. In so doing, the model accounts for the quantum behaviour for the microscopic and classical behaviour for the macroscopic. Their phenomenological method is to create a formulation that leaves the dynamics of microscopic objects essentially unaltered and recovers classical trajectories of macroscopic objects by modification to the quantum dynamics of their microscopic constituents.

Essentially the state is multiplied by a Gaussian of width α. The spontaneous localisation distance, α determines the size that the process localises a state to and hence the size above which states shall be localised, and at a repetition rate λ. Thus there are two free parameters in the model. The key feature is that for the state's density matrix the off-diagonal terms with separation $|x' - x''| > 1/\sqrt{\alpha}$ have an amplitude which decays as $e^{-\lambda t}$ whereas the diagonal terms do not decay. Hence the state is transformed from a pure state into a statistical mixture.

The additional term acts to "localise" a quantum system. The localisation acts on individual particles of a macroscopic system. If the macroscopic system is in a superposition of two distinct spatial locations then localisation of one of the constituent microscopic particles leads to localisation of the whole. If the spontaneous localisation is at a frequency λ, then for a macroscopic object with N particles localisation

occurs with a frequency λN.

For $\lambda = 10^{-16}\mathrm{s}^{-1}$ and $\alpha = 10^{-7}\mathrm{m}$ then quantum and classical mechanics seem to be recovered in their respective domains: microscopic systems are localised on very long timescales ($10^8 - 10^9$ years), whilst for an object of order 1g in mass, the localisation is extremely fast (10^{-7}s). There has been an investigation of an experimental constraint of this variety of model [Collett et al., 1994]. An analysis of the predictions of the CSL model on the experiment presented in Chapter 3 was made in Ref. [Bassi et al., 2004]. It was concluded that the experiment discussed herein, in the form presented in [Marshall et al., 2003a], is not able to be a decisive test of CSL theory but could help put bounds on λ.

A complaint with such a model might be that it is purely phenomenological: the additional term in the Schrödinger equation has no physical drive in and of itself and thus appears rather *ad hoc*. The two free parameters are unknown. On the other hand many an advance in physics has been made in this manner!

An important point touched on in the paper by Bose et al. [Bose et al., 1999] is whether the OR schemes have different variable dependence from the EID schemes. This is a topic for further investigation but certainly the model can in principle be distinguished from that predicted by Penrose's OR scheme due to the difference scaling with superposition displacement.

To summarise, only EID considerations are of direct relevance for what follows. The primary aim is to progress towards the creation of macroscopic superposition states. To study the specific non-QM decoherence models is of secondary consideration at this stage of the project and is not developed further. However, in principle the set up can be used to test Penrose's OR model, although this would require 5-order of magnitude improvement in Q/T_E, and other collapse models.

Chapter 3

Experimental Principle and Requirements

In this chapter the feasibility analysis of the experiment under consideration is given. It is based on the results presented in [Marshall et al., 2003a]. This begins with the theoretical study of the evolution of the experiment in §3.1. In §3.2 the experimental requirements are analysed. In §3.3, §3.4. and §3.5. an overview of Gaussian cavity mode matching, high reflectivity mirrors and optical cooling of a cantilever are given, respectively. The final section §3.6, discusses related experimental avenues that are being taken.

3.1 Experimental Principle, Hamiltonian and State Evolution

Consider the Michelson interferometer shown in Fig. 1(p.XV). Each photon entering the interferometer is represented by a wavefunction that evolves into a mathematical probability mixture of being both reflected (into arm A) and transmitted (into arm B): a quantum superposition. The different components of the wave-function travel along both paths and meet back at the beamsplitter to cause the interference. By adjusting the arm lengths around the point of equal length, whilst keeping the length difference less than the coherence length of the source, the light can be made to exit either at the detector, or reflected back into the laser. To improve efficiency one can use a polarising beamsplitter (PBS) in conjunction with a quarter waveplate to detect the output from both arms as shown in Fig. 1.1(p.4). Here, vertically polarised light from the laser is reflected into the interferometer by the PBS then converted into right handed circularly polarised light by the wave-plate mounted at 45 degrees to the polarisation. All the light is left handed circularly polarised after reflection from the mirror. The light exiting the interferometer in the input arm is converted to horizontally polarised light by a second pass through the wave-plate and thus largely transmitted to $D2$ (and not back into the laser).

The proposal of reference [Bouwmeester et al., 1998, Penrose, 2000] on which this study focusses, and the setup for which is shown in Fig. 1.1, essentially places a high finesse cavity in each arm of the Michelson Interferometer. One cavity has a micro-mirror attached to a micro-mechanical oscillator, similar to the cantilevers in atomic force microscopes, as one of the end mirrors. It is a near-hemispherical cavity where the (flat) micro-mirror is near the centre of curvature of the large curved mirror. A single run of the experiment starts by sending a weak pulse into the interferometer: to probabilistically prepare a single-photon state as required to a good approximation. The cavity is used to enhance the radiation-pressure interaction between the photon and the mirror through multiple reflections. The other cavity made from two large mirrors serves to balance the arm lengths. In principle, the micro-mirror will be displaced by the momentum transfer upon the photon reflection in that cavity. One can imagine the field as a constant force on the cantilever. The photon will be red-shifted as the micro-mirror/cantilever is pushed backwards and blue-shifted as the mirror swings back, returning to its original frequency after a full period. Provided the cavity lengths are identical, one would still expect an interference pattern. In this case, one does not know from which cavity the photon escaped. After a time, the photon leaks out of the cavity and returns along the interferometer arm. Knowledge of the interference visibility is determined by repeating the experiment many times to build up the interference pattern.

It will be shown that the initial superposition of the photon being in either arm A or B causes the system of mirror and photon to evolve into a superposition of states corresponding to two distinct locations of the mirror. The observed interference of the photon allows one to study the creation of coherent superposition states of the mirror.

The Hamiltonian

The Hamiltonian for a cavity with a moveable mirror system (but neglecting coupling to the environment) was first studied in Ref [Mancini and Tombesi, 1994], whose analysis I shall follow. It has three components: the field, the oscillator/mirror and the interaction:

$$H = H_c + H_m + H_{int}. \tag{3.1}$$

Firstly, the field energy, which ignoring the vacuum contribution, since it does not effect the dynamics, is the number operator $N_c = a^\dagger a$ multiplied by the photon energy, which for a photon frequency ω_c is

$$H_c = \omega_c a^\dagger a. \tag{3.2}$$

Secondly for the oscillator of frequency ω_m and mass m, one has

$$H_m = \frac{p^2}{2m} + \frac{m\omega_m^2 x^2}{2}, \tag{3.3}$$

where p is momentum and x is the position operator. This can be re-written in terms of two non-Hermitian operators, the phonon creation and annihilation operators for the oscillator,

$$b = \sqrt{\frac{m\omega_m}{2}}(x + \frac{ip}{m\omega_m}), b^\dagger = \sqrt{\frac{m\omega_m}{2}}(x - \frac{ip}{m\omega_m}) \tag{3.4}$$

such that, ignoring the vacuum contribution one obtains

$$H_m = h\omega_m b^\dagger b. \tag{3.5}$$

Thirdly, the Hamiltonian component for the interaction between the cavity field and the oscillator must be considered. The cavity length changes due to radiation pressure. The energy of the interaction is understood as the work done by the radiation force,

$$F = \frac{h}{\lambda}\frac{c}{L}a^\dagger a = \frac{\omega_c}{L}a^\dagger a, \tag{3.6}$$

in causing the displacement Δx:

$$H_{int} = \omega_c a^\dagger a \frac{\Delta x}{L}, \tag{3.7}$$

assuming perfect mirror reflectivity. Three conditions for this interaction term are that: (1) the mirror motion is slow compared to the round-trip time of light in the cavity; (2) the correction to the radiation force due to the Doppler frequency shift of the field is negligible; and (3) the Casimir force is negligible. The term can also be understood to be the change in energy of the field due to the change in length of the cavity[1]. From our phonon creation and annihilation operators one can see that

$$\Delta x = \sqrt{\frac{}{2m\omega_m}}(b + b^\dagger) \tag{3.8}$$

and thus

$$H_{int} = Ga^\dagger a(b + b^\dagger), \tag{3.9}$$

where G is a coupling constant given by

$$G = \frac{\omega_c}{L}\sqrt{\frac{}{2m\omega_m}}. \tag{3.10}$$

Above, it is assumed that the field is only ever in one mode, whereas Law [Law, 1993, Law, 1994] gives a full analysis of the coupling between modes and takes into consideration the Casimir force. In doing so, the above interaction term is shown to be the limiting case for slow mirror motion compared to the cavity round-trip time.

[1]The photon will be red-shifted as the mirror is pushed backwards and blue-shifted as the mirror swings back, returning to its original frequency after a full period. To calculate the energy shift, it is noted that for a cavity of length L the resonances are given by $\omega_c = \frac{\pi n c}{L}$. Thus for a change Δx ($\ll L$) in the cavity length, the change in frequency of the field is $\delta\omega_c = \frac{\omega_c \Delta x}{L}$, and hence the change in energy is $H_{int} = a^\dagger a \delta\omega_c = \omega_c a^\dagger a \frac{\Delta x}{L}$.

Finally, the system can be described by a Hamiltonian [Mancini and Tombesi, 1994, Law, 1993, Law, 1994]

$$H = \omega_c a^\dagger a + \omega_m b^\dagger b - G a^\dagger a (b + b^\dagger). \tag{3.11}$$

An order of magnitude comparison of the sizes of the Hamiltonian terms, for λ, L, ω_m and m under consideration in this proposal, and for a single photon in the cavity such that $a^\dagger a = 1$, is $10^{15} : 10^3 : 10^4$. The energy of the interaction is much smaller than that of the field but comparable to the oscillator. The system would only be in a regime where the interaction energy is similar to the field energy if the displacement of the mirror became of order the cavity length. In most cases, and certainly in our case as will be seen in the experimental requirements section, this can not be so as the displacement of the mirror is much smaller than the wavelength.

It is interesting to note that the effect of the interaction term makes the cavity behave like a non-linear medium since the length of the cavity depends upon the intensity of the field in an analogous way to the optical length of a nonlinear material. Because of this analogy with optical nonlinearity it has been called a mechanical Kerr effect [Mancini and Tombesi, 1994].

3.1.1 The Evolution for the Mirror in the Ground State

The evolution of the mirror coupled to the field of the cavity is determined by the time evolution operator which satisfies the Schrödinger equation for that operator,

$$i\frac{\partial U(t, t_0)}{\partial t} = H U(t, t_0). \tag{3.12}$$

For a time independent Hamiltonian, the solution is

$$U(t, t_0) = e^{-iH(t-t_0)/}. \tag{3.13}$$

For the Hamiltonian given in 3.11 the time evolution operator is given by

$$U(t) = e^{-i\omega_c t} e^{-i\omega_m t b^\dagger b + i\kappa(b+b^\dagger)t}. \tag{3.14}$$

where

$$\kappa = G/\omega_m. \tag{3.15}$$

κ quantifies the displacement of the mirror in units of the size of the ground state wavepacket – it can be thought of as the kick of the photon on the cantilever. The size of the ground state wavepacket is the minimum position uncertainty of the mirror according to Heisenberg's Uncertainty Principle. It is the limit on the precision of continuous position measurements, and for an oscillator ground state wavepacket is given by [Bradinsky et al., 1995]

$$\Delta x = \sqrt{\frac{}{m\omega_m}}. \tag{3.16}$$

Since the cantilever is in its ground state, it is convenient to rearrange Eq. 3.14 in the following way such that the first two exponential factors to operate return the ground state and the overall phase is last to operate. Utilising a unitary transform operator

$$T = e^{-\kappa(b^\dagger - b)} \tag{3.17}$$

and the Baker-Cambell-Hausdorf expansion, the time evolution operator can be rearranged [Bose et al., 1999, Mancini et al., 1997] to give

$$U(t) = e^{-i\omega_c a^\dagger a t} e^{i\kappa^2(\omega_m t - sin\omega_m t)(a^\dagger a)^2} e^{\kappa a^\dagger a(\eta b^\dagger + \eta^* b)} e^{-ib^\dagger b\omega_m t}, \tag{3.18}$$

where

$$\eta = 1 - e^{-i\omega_m t}. \tag{3.19}$$

This can be applied factor by factor to the initial mirror state [Sakurai, 1994]. Assuming that the mirror/oscillator is initially in its ground state $|0\rangle_m$ (the thermal case will be discussed later), one has

$$\begin{aligned}
|\psi(t)\rangle &= U(t)|\psi(t_0)\rangle \\
&= U(t)|0\rangle \\
&= e^{-i\omega_c a^\dagger a t} e^{i\kappa^2(\omega_m t - sin\omega_m t)(a^\dagger a)^2} e^{\kappa a^\dagger a(\eta b^\dagger + \eta^* b)} e^{-ib^\dagger b\omega_m t}|0\rangle \\
&= e^{-i\omega_c t} e^{i\kappa^2(\omega_m t - sin\omega_m t)} e^{\kappa(\eta b^\dagger + \eta^* b)} e^{-ib^\dagger b\omega_m t}|0\rangle.
\end{aligned} \tag{3.20}$$

In the last line $a^\dagger a$ is set to 1 as there shall be a single photon in the cavity. The fourth exponential factor gives back the same state to which it is applied, since it involves the number operator of the ground state ($= 0$) (easily understood by considering the expansion of the exponent).

$$|\psi(t)\rangle = e^{-i\omega_c t} e^{i\kappa^2(\omega_m t - sin\omega_m t)} e^{\kappa(\eta b^\dagger + \eta^* b)}|0\rangle. \tag{3.21}$$

Re-writing the third exponential term by noting the general relation

$$e^{\alpha_1 a + \alpha_2 a^\dagger} = e^{\alpha_1 a} e^{\alpha_2 a^\dagger} e^{-\alpha_1\alpha_2/2}, \tag{3.22}$$

one sees that the third exponential factor acting on the state is

$$\begin{aligned}
|\psi(t)\rangle &= e^{-i\omega_c t} e^{i\kappa^2(\omega_m t - sin\omega_m t)} e^{-\kappa^2\eta\eta^*/2} e^{\kappa\eta b^\dagger} e^{-\kappa\eta^* b}|0\rangle \\
&= e^{-i\omega_c t} e^{i\kappa^2(\omega_m t - sin\omega_m t)} e^{-\kappa^2\eta\eta^*/2} e^{\kappa\eta b^\dagger}|0\rangle \\
&= e^{-i\omega_c t} e^{i\kappa^2(\omega_m t - sin\omega_m t)} e^{-\kappa^2\eta\eta^*/2} \sum_{m=0}^{\infty} \frac{(\kappa\eta b^\dagger)^m}{m!}|0\rangle \\
&= e^{-i\omega_c t} e^{i\kappa^2(\omega_m t - sin\omega_m t)} e^{-\kappa^2\eta\eta^*/2} \sum_{n=0}^{\infty} \frac{(\kappa\eta)^n}{\sqrt{n!}}|n\rangle \\
&= e^{-i\omega_c t} e^{i\kappa^2(\omega_m t - sin\omega_m t)}|\kappa\eta\rangle,
\end{aligned} \tag{3.23}$$

where $|\kappa\eta\rangle$ is a coherent state, defined as the eigenstate of the annihilation operator, with amplitude $\kappa\eta$. The first exponential factor is equivalent to the overall phase gained by the evolution of the interferometer (since the second arm of the interferometer involves no moving parts). The second exponential factor gives a phase to the cavity state. The mirror oscillates around a new equilibrium position determined by the driving force.

Above, the evolution of the cavity and micro-mirror has been calculated. This needs to be extended to the entire interferometer. Let us suppose that initially a single photon is fed into the interferometer and thus is in a superposition of being in either arm A or B, and the mirror is in its ground state $|0\rangle_m$, then the initial state of the interferometric system is

$$|\psi(0)\rangle = \frac{1}{\sqrt{2}}(|0\rangle_A|1\rangle_B + |1\rangle_A|0\rangle_B)|0\rangle_m. \tag{3.24}$$

The photon in arm B will have the same dynamical phase as that in arm A, but there is of course no moving mirror. Hence, it can be seen that the interferometric system will evolve in a way that after a time t the state is

$$|\psi(t)\rangle = \frac{1}{\sqrt{2}}e^{-i\omega_c t}(|0\rangle_A|1\rangle_B|0\rangle_m + e^{i\kappa^2(\omega_m t - \sin\omega_m t)}|1\rangle_A|0\rangle_B|\kappa\eta\rangle_m). \tag{3.25}$$

In the second exponential factor, the mirror moves under the influence of the radiation pressure of the photon in cavity A.

Interference Visibility

The interference visibility of the interferometer is dependent on two factors. Firstly, the (internal) degree of entanglement between photon and mirror. Secondly, the degree of entanglement between the mirror/photon/interferometer system and the external environment. The latter shall be ignored presently. The former is determined by the photon's reduced density matrix. The state is given from Eq. (3.25) as

$$\begin{aligned}\rho &= |\psi\rangle\langle\psi| \\ &= \begin{pmatrix} \frac{1}{2}(|0\rangle_A|1\rangle_B|0\rangle_m\langle 0|_A\langle 1|_B\langle 0|_m & e^{i\kappa^2(\omega_m t - sin\omega_m t)}|0\rangle_A|1\rangle_B|0\rangle_m\langle 0|_A\langle 1|_B\langle\kappa\eta|_m \\ e^{i\kappa^2(\omega_m t - sin\omega_m t)}|0\rangle_A|1\rangle_B|\kappa\eta\rangle_m\langle 0|_A\langle 1|_B\langle 0|_m & |1\rangle_A|0\rangle_B|\kappa\eta\rangle_m\langle 1|_A\langle 0|_B\langle\kappa\eta|_m \end{pmatrix}.\end{aligned} \tag{3.26}$$

Interference (fringe) visibility characterises the coherence of the photon. It is defined as

$$V = \frac{I_{max} - I_{min}}{I_{max} + I_{min}} \tag{3.27}$$

where I is the power seen at one detector and the minimum and maximum of which are seen by varying the length of one arm over a distance $\lambda/2$. The maximum possible interference visibility for the photon is given

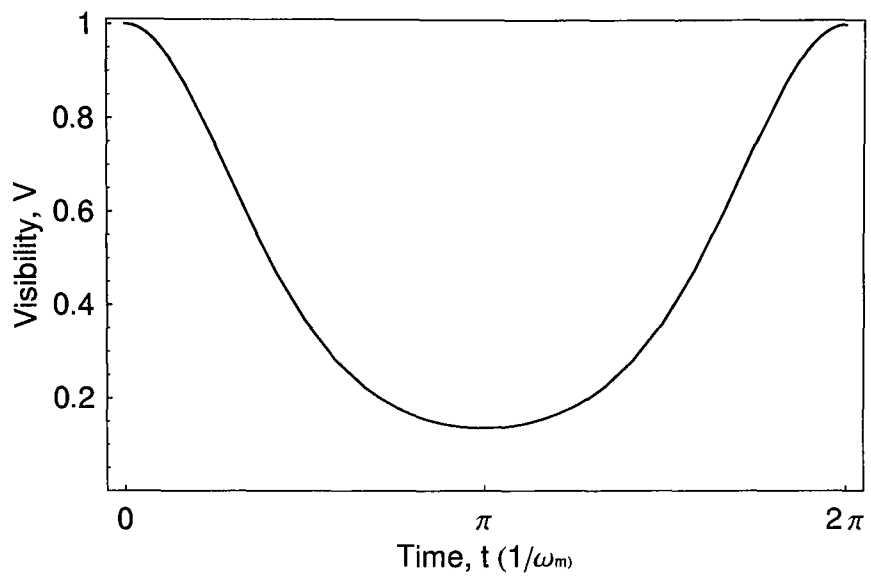

Figure 3.1: Time evolution of the interference visibility V of the photon over one period of the mirror's motion for the mirror in its ground state $|0\rangle$. Zero visibility corresponds to half the light exiting either way from the interferometer with 50% probability, regardless of path length configuration whereas unit visibility corresponds to being able to have all the light exit in one arm. The visibility decays after $t = 0$, but in the absence of decoherence there is a revival of the visibility with a maximum at an integer number of periods.

by twice the modulus of the off-diagonal element of ρ. By tracing over (ignoring) the specific state of the mirror one finds that the off-diagonal element has the form

$$\frac{1}{2}e^{-\kappa^2(1-\cos\omega_m t)}e^{i\kappa^2(\omega_m t-\sin\omega_m t)}. \tag{3.28}$$

The first factor is the modulus, which shows that the interference visibility varies with time with the exponential to the sine with its maximum at $t = 2p\pi/\omega_m$ (where p is an integer) and minimum at $t = p\pi/\omega_m$. Thus interference appears and disappears with the motion of the cantilever as shown in Fig. 3.1. The second factor gives the phase, which is identical to that obtained classically due to the varying length of the cavity. The visibility is measured by setting the interferometer such that all the light escapes from one exit since the interference is optimal (visibility $V = 1$): if the interferometer arm lengths and laser wavelength are stable then any deviation from all the light exiting there measures a reduction in the visibility, until a point where half the light exits at each detector, there is no interference, then the visibility $V = 0$.

To understand the behaviour of the interference, let us consider two cases, once again assuming absence of decoherence: firstly, if the photon leaks from the cavity after half an oscillation $t = \pi/\omega_m$ then the state given by Eq. 3.25 is clearly still entangled and the interference visibility given by Eq. 3.28 is close to zero. The cantilever, in being left in a state of motion or at rest, depending on which path photon took, has effectively measured the photon. Secondly, if the photon leaks from the cavity after exactly one full period of the oscillator $t = 2\pi/\omega_m$, the system is in the state

$$\frac{1}{\sqrt{2}}\left(|0\rangle_A|1\rangle_B + e^{i\kappa^2 2\pi}|1\rangle_A|0\rangle_B\right)|0\rangle_m, \tag{3.29}$$

such that the mirror is again disentangled from the photon. The interference visibility given in Eq. 3.28 gives unity. Thus, full interference can be observed if the photon is detected at this time. Here the cantilever is back to its initial state (at rest) whichever path the photon took and thus there is no information remaining of which path the photon took. Note that after a full period the oscillator returns to its initial state in both position and velocity since when forced it oscillates around a new equilibrium position of which the initial rest position is one extremity. Since there is no other mechanism that could lead first to loss of visibility then its revival with the cantilever oscillation as seen in Fig. 3.1, the revival demonstrates the coherence of the superposition state that exists at intermediate times.

For $(\kappa)^2 \gg 1$, which physically means that the photon momentum kick must be larger than the initial uncertainty of the mirror's momentum, the superposition involves two distinguishable mirror positions. Photons leaking from the cavity around the time of the predicted revival peak will be of most interest. The key is to understand the experimental requirements for achieving a superposition of distinct mirror positions and for observing the revival at $t = 2\pi/\omega_m$.

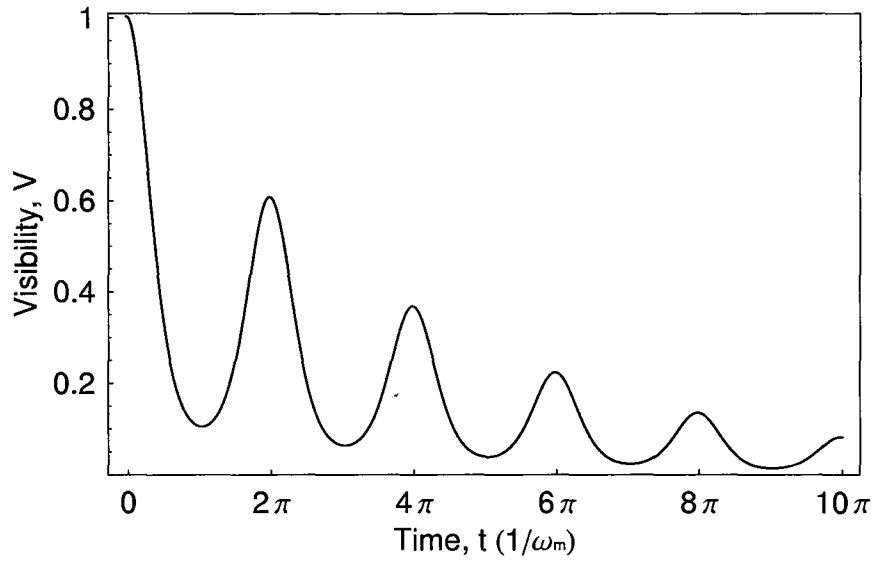

Figure 3.2: Time evolution of the interference visibility V over 5 periods of the mirror's motion for the mirror in its ground state $|0\rangle$ but subject to a decoherence process. The revival peak height decays as e^{-t/t_E}, where $t_E = \omega_m/2$

The second effect on the interference visibility seen comes from the environmental induced decoherence. If the environment of the mirror interacts sufficiently with the mirror on the experimental timescale then the system is effectively "measured" and the wavefunction collapses leaving no interference visibility. In other words, if the environment "remembers" that the mirror has moved, then, even after a full period, the photon will still be entangled with the mirror's environment, and thus the revival will not be complete. Therefore, the setup can be used to measure the decoherence of the mirror.

In Fig. 3.2, the visibility is shown as a function of time for a system subject to decoherence mechanism which has a timescale of $t_E = \omega_m/2$. This acts to reduce the peak visibility. This decoherence could be

caused by standard environmental induced decoherence (EID), which is outlined in §2. It may be possible to distinguish different decoherence mechanisms by their different scalings with various parameters such as superposition mass, displacement and so forth.

3.1.2 The Evolution for a Mirror in a Thermal State

Above, it has been assumed that the mirror starts out in its ground state which is extremely difficult for such a massive object as is being considering here. Notwithstanding this, in Ref. [Bose et al., 1999] it is shown that the revival can nevertheless be observed: this is because the thermal state can be understood as a mixture of pure states, all of which arrive with identical phase over a period of the oscillator (the phases collected are different but have fixed intervals and consequently are all the same multiple of 2π after one oscillator period) and thus the state will return exactly to its initial state, whether or not the initial state was the ground state or thermal. This allows a revival of the interference visibility regardless of the initial state. Note that in the thermal case the state at $t = \pi/\omega_m$ would not be a true Schrödinger Cat state but instead a mixture of Schrödinger Cat states. This can be illustrated as before by applying the evolution operator to a coherent mirror state $|\beta\rangle$, which can later be averaged over a Gaussian distribution to obtain a thermal state. The cantilever is modelled as a linear harmonic oscillator which seems valid since we are considering tiny displacements.

First, the coherent mirror state is written in the number state basis.

$$|\beta\rangle = e^{-|\beta|^2/2} \sum_{m=0}^{\infty} \frac{\beta^n}{\sqrt{n!}} |n\rangle. \tag{3.30}$$

Applying the evolution operator Eq. 3.20 factor by factor, one obtains

$$\begin{aligned}
|\psi(t)\rangle &= U(t)|\beta\rangle \\
&= e^{-i\omega_c t} e^{i\kappa^2(\omega_m t - sin\omega_m t)} e^{\kappa(\eta b^\dagger + \eta^* b)} e^{-ib^\dagger b\omega_m t} |\beta\rangle \\
&= e^{-i\omega_c t} e^{i\kappa^2(\omega_m t - sin\omega_m t)} e^{\kappa(\eta b^\dagger + \eta^* b)} e^{-ib^\dagger b\omega_m t} e^{-|\beta|^2/2} \sum_{m=0}^{\infty} \frac{\beta^n}{\sqrt{n!}} |n\rangle \\
&= e^{-i\omega_c t} e^{i\kappa^2(\omega_m t - sin\omega_m t)} e^{\kappa(\eta b^\dagger + \eta^* b)} e^{-|\beta|^2/2} \sum_{m=0}^{\infty} \frac{\beta^n}{\sqrt{n!}} e^{-iN\omega_m t} |n\rangle \\
&= e^{-i\omega_c t} e^{i\kappa^2(\omega_m t - sin\omega_m t)} e^{\kappa(\eta b^\dagger + \eta^* b)} e^{-|\beta|^2/2} \sum_{m=0}^{\infty} \frac{\beta^n}{\sqrt{n!}} (e^{-i\omega_m t})^n |n\rangle \\
&= e^{-i\omega_c t} e^{i\kappa^2(\omega_m t - sin\omega_m t)} e^{\kappa(\eta b^\dagger + \eta^* b)} |\beta e^{-i\omega_m t}\rangle \\
&= e^{-i\omega_c t} e^{i\kappa^2(\omega_m t - sin\omega_m t)} |\beta e^{-i\omega_m t} + \kappa n\eta\rangle,
\end{aligned} \tag{3.31}$$

where the fourth step uses the relation

$$e^{iG\lambda} A e^{-iG\lambda} = A + i\lambda[G, A] + (i\lambda)^2[G, [G, A]] + ...+ \tag{3.32}$$

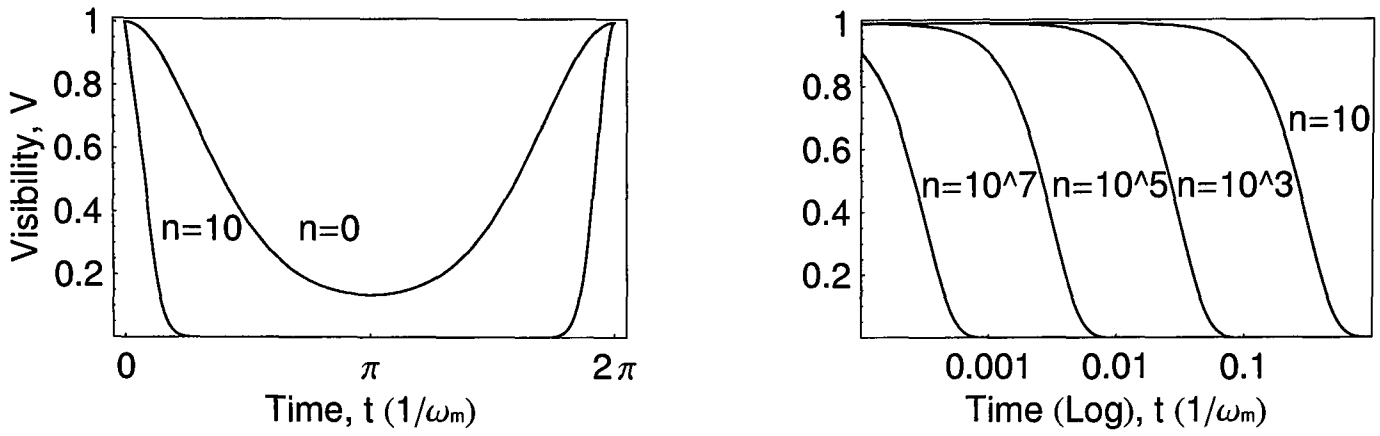

Figure 3.3: Time evolution of the interference visibility V of the photon over one period of the mirror's motion for the mirror in a thermal state $|\beta\rangle$. The visibility decays after $t = 0$, but in the absence of decoherence there is a revival of the visibility after a full period. The visibility is shown for different thermal states characterised by phonon numbers $\bar{n} = 0, 10, 10^3, 10^5 \& 10^7$ corresponding to temperatures of the ground state, $T = 0.2\mu$K, $T = 20\mu$K, $T = 2$mK and $T = 200$mK. The graph on the right shows the decay of coherence on a log plot and demonstrates that the width of the revival peak scales like $1/\sqrt{\bar{n}}$.

and

$$bb^\dagger + b^\dagger b = 1. \tag{3.33}$$

Thus, in the absence of decoherence, after a time t the mirror state will be

$$|\psi(t)\rangle_m = |\beta e^{-i\omega_m t} + \kappa n(1 - e^{-i\omega_m t})\rangle_m. \tag{3.34}$$

Applying the evolution operator to the initial interferometric system one finds

$$|\psi(t)\rangle = \frac{1}{\sqrt{2}} e^{-i\omega_c t}(|0\rangle_A|1\rangle_B|\beta\rangle_m + e^{i\kappa^2(\omega_m t - \sin\omega_m t)}|1\rangle_A|0\rangle_B|\beta e^{-i\omega_m t} + n\kappa\eta\rangle_m). \tag{3.35}$$

To calculate the visibility, one again calculates the amplitude of the off-diagonal elements of the density matrix of this state

$$\frac{1}{2} e^{i\kappa^2(\omega_m t - \sin\omega_m t)}|\beta\rangle\langle\beta e^{-i\omega_m t} + n\kappa\eta|. \tag{3.36}$$

It can be seen then from the evolution of the coherent mirror state that at a time $t = 2\pi/\omega$ the mirror is back to its initial state as $|\beta\rangle$. The result of averaging over a Gaussian distribution of coherent states

$$\int e^{-|\bar{\beta}|^2/\bar{n}} e^{n\kappa\eta} d^2\beta \tag{3.37}$$

was shown in Ref. [Armour and Blencowe, 2001] to be

$$\frac{1}{2} e^{-\kappa^2(1-\cos\omega_m t)(1+2\bar{n})} e^{i\kappa^2(\omega_m t - \sin\omega_m t)}, \tag{3.38}$$

where $\bar{n}$ is the thermal occupation number

$$\bar{n} = 1/(e^{\omega_m/kT} - 1). \tag{3.39}$$

This differs from the evolution found for the case with the cantilever initially in its ground state by a factor $(1+2\bar{n})$ in the exponential. In Fig. 3.3 it is shown how this effects the interference visibility. It can be seen that the new exponential factor reduces the width of the revival peak by a factor $\sim 1/\sqrt{\bar{n}}$. In Fig. 3.3 the revival peak is shown for different temperatures of interest of $T = 0.2\mu$K, 20μK, 2mK and 200μK. The narrowing of the peak leads to stricter requirements on the vacuum (§3.2.3) and stability (§3.2.4) by increasing the time needed to get sufficient events in the revival interval in order to verify it. The development of ultra-fast switchable mirrors would help considerably to reduce the stability needs, as discussed in §3.2.4.

3.2 Experimental Requirements

The experimental scenario is as follows: a single run of the experiment starts by sending a weak pulse into the interferometer, such that on average 0.1 photons go into either cavity. This necessitates the photon number in the pulse to be of order 10^6 due to the back reflection of the cavity mirror. This probabilistically prepares a single-photon state, as required, to a good approximation, whilst keeping the two-photon contribution low, which is necessary as it causes noise in the interferometer. Detection of the revival happens by measuring photons which leak out of the cavity around the time of one oscillation (the width of the interval depends on the temperature, see Fig. 3.3): by adjusting one interferometer arm length by a range $\lambda/2$, one can determine the maximum and minimum intensity of the detector and thus the interference visibility. The experiment is repeated many times since detecting the second revival peak is very unlikely and since multiple data points are needed to demonstrate the revival. For every run of the experiment we have to prepare the initial state.

3.2.1 Momentum

The conditions for displacement of the mirror such that the oscillator, initially in a ground state, is placed in its first excitation state (one phonon) is equivalent to demanding that the momentum kick imparted by the photon has to be larger than the initial quantum uncertainty of the mirror's momentum (Eq. 3.16). In the above notation, this requires $\kappa^2 \gg 1$. To see the revival of interference, one needs the photon to remain in the cavity for one or more periods p of the cantilever. If N denotes the number of roundtrips of the photon in the cavity during one period of the mirror's motion, then one obtains

$$\frac{NL}{c} = \frac{\pi p}{\omega_m}. \tag{3.40}$$

Wavelength λ	Microwave, 1mm	Visible, 780nm	X-rays, 1.5A^o
Reflectivity R	99.9999994%[1]	99.9998%[2]	18%
N^3/λ^4	10^{38}	10^{43}	10^{11}

Table 3.1: Comparison of mirror reflectivities at different wavelength regimes. [1] see Ref. [Brune et al., 1996]. [2] see Ref. [Hood et al., 2001]. The best mirrors for 8keV ($\lambda = 1.5A^o$) X-rays photons provide a reflectivity of 32% at 5 degrees incidence [Y. Stockman, 1997] thus assuming a series of 18 mirrors together giving normal incidence, then $N = 10^{-9}$.

From Eqs. 3.10, 3.15, 3.40 condition κ^2 1 can be written

$$\frac{2}{\pi c}\frac{N^3 L}{pm\lambda^2} \quad 1, \tag{3.41}$$

where λ is the wavelength of the light. This is easiest to satisfy if $p = 1$, a single oscillation of the cantilever. The factors entering Eq. (3.41) are not all independent. The achievable N, which is determined by the reflective quality of the mirrors, and the mirror size (and hence m) both depend strongly on λ.

The mirror's lateral dimensions must be larger than the beam focus by a factor of 2-3 to ensure that the diffraction losses are minimal (see §4.5). The beam focus size is proportional to the wavelength, and thus for any given loss the minimum lateral dimensions of the mirror must scale with wavelength. The thickness of the micro-mirror required in order to achieve sufficiently high reflectivity depends on λ as well: the best optical mirrors are made by a series of layers of dielectric materials of high and low refractive index each $\lambda/4n$ (see §4.2). Thus $m \propto \lambda^3$. The cavity length L for a given loss is also proportional to wavelength since larger L requires larger curved mirror lateral dimensions, the ease of which to make is approximately in proportion to wavelength.

Considering the above scaling, Eq. (3.41) allows one to compare the viability of different wavelength ranges. Since $m \propto \lambda^3$, and $L \propto \lambda$ to find the optimal wavelength one must maximise N^3/λ^4. While the highest values for N are achievable for microwaves using superconducting mirrors (up to 10^{10}), this is counteracted by their longer wavelengths. On the other hand, there are no good mirrors for highly energetic photons. In Table 3.2.1 the best available mirror reflectivities in 3 different wavelength regimes are given. The visible regime is the optimal of them given current mirror technology.

Here it is proposed that the experiment use λ around 630nm, although for practical reasons the initial experiments of §4 shall be conducted at 780nm. High reflectivity mirrors at optical wavelengths with width 3mm and radius of curvature about 3cm have been manufactured [Hood et al., 2001] and cavity of finesse 2×10^6 demonstrated [Rempe et al., 1992]. Here it is proposed that a cavity length of 5cm, and a small mirror of radius 10 microns and thickness 6 microns, are used, the latter two leading to a mass 5×10^{-12} kg. Such a small mirror on a mechanical oscillator can be fabricated according to steps outlined in §4.1.

For the above dimensions the condition Eq. (3.41) is satisfied with $\lambda = 630$nm if $N = 5.5 \times 10^6$.

If one aims for a finesse of 1.5×10^7 and cavity length $L = 5$cm then 1% of the photons are still left in the cavity after a full period of the mirror. This finesse is a factor of 7 above the best reported values and requires a maximum loss of 3×10^{-7} per reflection, a factor 4 below best values for a Fabry-Perot cavity [Rempe et al., 1992, Hood et al., 2001] and transmission 10^{-7} per reflection, consistent with a 6μm mirror thickness (see Eqs. 3.67, 3.69). There is a trade off here with the stability requirement (§3.2.4): the finesse can be lowered only if one has the stability to afford more trials and vice versa.

The values of N and L constrain the oscillator frequency by Eq. 3.40 to $\omega_m = 2\pi \times 500$ Hz. This frequency is achievable with a cantilever of a size that allows the holding of the mirror but which allows a mass smaller or of the same order as that of the mirror. For the above values, the spread of the ground state wavepacket, given by Eq. 3.16 is 4×10^{-13} m — which is thus the distance of displacement required by the photon momentum pressure in order to take the oscillator from the ground to first excited state.

One might also consider the use of whispering gallery modes of silicon micro-spheres which have been shown to have high finesse, the best values being almost identical to that of the optical Fabry-Perot cavity at 2.2×10^6 but there are no obvious ways to couple the field to a momentum state of the cantilever (or the micro-sphere) and long timescales are not possible due to the small dimensions.

The momentum requirement for placing a thermal cantilever into a quantum superposition is the same as for doing so with a cantilever in its ground state as discussed in §3.1.2..

3.2.2 Environmental Induced Decoherence

The requirement of observing the revival puts a boundary on the acceptable environmental decoherence. The revival of the interference visibility of the Michelson Interferometer must be detectable above the noise after a full period of the cantilever. If Environmental Induced Decoherence (EID) has caused total loss of coherence of the state, then naturally there will be no interference visible. The main effects of EID will be from phonon interaction in the cantilever itself. Recall that it is proposed that the experiment be conducted with the cantilever in a thermal state, since the revival of the interference is observable even if that is so (§3.1.2.), which means that the phonon occupation number will be very large.

The effect of the environment can be approximately described by the model of environmental induced decoherence described in §2.2. This gives a decoherence rate of

$$\gamma_D = \frac{\gamma_m k T_E m (\Delta x)^2}{2} \tag{3.42}$$

governing the decay of off-diagonal elements between different mirror positions [Joos et al., 1996, Zurek, 1991]. Here γ_m is the damping rate for the mechanical oscillator, T_E is the temperature of the environment, which is constituted mainly by the internal degrees of freedom of the mirror and cantilever, and Δx is the separation of two coherent states that are originally in a superposition. This approximation is derived under two

assumptions that experiment time scales are longer than $2\pi/\omega_m$ and for Δx that is large compared to the width of the individual wavepackets. Here it is assumed that the order of magnitude of the decoherence is well captured by γ_D, even though these two assumptions are not strictly met in our case, in order to establish the approximate parameters to first find whether the experiment is technically feasible. One of the purposes of the experiment is, after all, to investigate which, if any, of the models of EID is most able to describe nature. A topic of further research would be a detailed analysis of the decoherence rate for the conditions here, especially considering the role of surface defects that may not behave as harmonic oscillators and this may not fit the standard EID models.

If the experiment achieves $\kappa^2 \quad 1$, i.e. a separation by the size of a coherent state wavepacket, $\Delta x \sim \sqrt{\frac{}{m\omega_m}}$, the condition $\gamma_D \quad \omega_m$ can be cast in the simpler form of

$$Q \quad \frac{kT_E}{\omega_m}, \tag{3.43}$$

where $Q = \omega_m/\gamma_m$ is the quality factor of the mechanical oscillator. It is worth noting that Eq. 3.43 can be obtained from the simple consideration of criteria for observing quantum behaviour of objects using continuous position measurements [Bradinsky and Khalili, 1996]. For the cantilever frequency in §3.2 then $Q/T > 4 \times 10^7$. For $Q \quad 10^5$, which has been exceeded for silicon cantilevers of approximately the right dimensions and frequency [Mamin and Rugar, 2001, Yang et al., 2000], this implies that the temperature of the environment has to be ≤ 2.5 mK. Cooling a macroscopic object to this temperature is achievable with dilution refrigerators and can be improved further with adiabatic demagnetisation cooling (§2.3.4.). Improvements in Q seem feasible (see immediately below) and an increase of a factor of 4 on best reported values to 10^6 would ease the system temperature required to 25mK.

From Eq. 3.16 it is seen that Δx depends on m and ω_m, which were constrained in §3.2. In fact, m and ω_m in §3.2., were optimised iteratively in conjunction with the environmental induced decoherence constraints of Q and T. In order to have a realisable T and Q one would like ω_m to be large. The joint constraints from momentum and EID considerations can be obtained from Eqs. 3.43, 3.40 and 3.41 as

$$\frac{k_B T}{Q} < \omega_m < \frac{2N^2}{m\lambda^2} \tag{3.44}$$

from which it is clear that the EID and momentum considerations have competing wishes for the oscillator frequency, but which both are just satisfied by all of the above figures. Improving the quality factor and decreasing the cantilever frequency (and thus force constant) would ease the constraints on N (and m) that currently seems likely to be the most difficult to obtain.

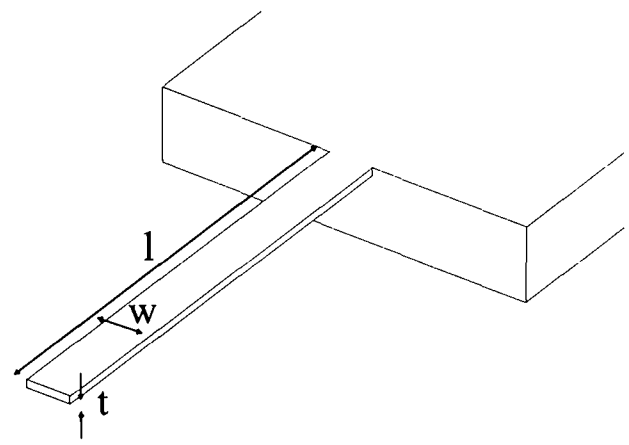

Figure 3.4: Schematic of a Cantilever

Basic Cantilever Mechanics

The natural frequency ω_0 of a cantilever of dimensions $t \times w \times L$, as shown in Fig. 3.4, and with density ρ and Young's modulus Y, is given by [Harris et al., 1999, ?]

$$\omega_0 = \frac{0.562\pi t}{l^2}\sqrt{\frac{Y}{12\rho}}. \tag{3.45}$$

For Si, $Y = 179$ GPa whether bulk or small [Virwani et al., 2003] and $\rho = 2330\text{kg m}^{-3}$, therefore in order to achieve a frequency of 500Hz one needs a ratio of $t : L^2 = 1 : 2.83$. For the case of the cantilevers in use in §4.1 and §4.3, these are of length 400μm, and from this one would demand a thickness 56nm, which is a factor 20 thinner than our samples which are designed for 10kHz frequency. It was fortunate that for the frequency range of interest there have been cantilevers developed with high quality factors, mostly for use in Atomic Force Microscopes. The force constant k is given by

$$k = \frac{Ywt^3}{2l^3}, \tag{3.46}$$

giving ~ 0.1N/m for the cantilever used in §4.

It has been assumed that the cantilever has one oscillation mode. In reality, there are a very large number of degrees of freedom and the equation of motion should be derived from elastic theory. The amplitude of a mode is dominated by lower order flexural modes, starting with a single bend in the cantilever and rising. It has been found that the energy stored in higher order modes is such that their ratio for the first few modes is approximately $1 : 1/50 : 1/500 : 1/1200$, which means that the higher order modes can, to first approximation, be neglected [Sidles et al., 1995, Harris et al., 1999, ?].

The mechanical quality of μm-thick resonators is in the range $1 - 100$ at room temperature, $10^4 - 10^5$ in a vacuum (see §4.4 and [Mamin and Rugar, 2001]) and an increase of an order of magnitude when annealed (see below). Although dissipation mechanisms are not well understood for micro-structures, quality factors are known to decrease with decreasing thickness [Yasumara et al., 2000, Huang et al., 2003] for cantilevers of

relevant dimensions for our study, cantilevers with thickness 0.3μm have been shown to exhibit $Q = 1.5 \times 10^5$ [Mamin and Rugar, 2001]. Limitations here are probably due to losses from surface mechanisms, such as dissipation enhancement due to surface contamination, which dominate for sub-micron thick cantilevers. This is known partly because of the success of the flash heat treatment described below that affects only the surface of the cantilevers. Thus limitations on Q are less likely to be due to bulk internal friction losses due to lattice defects, thermo-elastic dissipation, phonon-phonon scattering, etc., or from clamping losses, which all are likely to be low for our cantilevers. It is partly fortunate that the mass and frequency requirements are met at a size just larger than this thickness threshold.

Heat treatment in nitrogen to 700^oC for 1 hour was shown to improve the quality factor of silicon cantilevers by a factor of 3-5 for 0.7μm thick cantilevers [Yasumara et al., 2000]. Flash heating by a laser beam to 1000^oC for 30s in a vacuum improved the quality of silicon cantilevers of similar dimension to the ones used here by an order of magnitude to 2.5×10^5 [Yang et al., 2000]. In cooling a silicon cantilever from room temperature to cryogenic temperatures, the quality factor is known to first decrease to a minimum at about 135K and then increase past the room temperature quality factor until a peak a factor 2.5 larger than that of the room temperature quality at a temperature of 4K [Yasumara et al., 2000]. It continues to grow at lower temperatures [Mamin and Rugar, 2001] which could be useful to our experiment.

3.2.3 Vacuum

The experiment requires ultra-high vacuum conditions in order to ensure that events where an atom hits the cantilever are sufficiently rare not to cause significant errors. The momentum of a light atom (e.g. Hydrogen) at 3mK is of order 10^{-5} that of the momentum required to place the cantilever into a superposition therefore we can not afford greater than 10^5 collisions of atoms with the cantilever on the experimental timescale. Taking Scenario 2 of §3.2.4., this requires a maximum collision rate of about 10^3/s. This requires a particle density less than 10^{12}/m^3, equating to a pressure of 10^{-13} Pa, which has been exceeded for vacuums at a temperature of 4K [Gabrielse et al., 1990]. The low temperatures (which are demanded in this experiment in order to keep EID low, §3.2.2) are a significant help in achieving ultra-high vacuum as particles are captured by the cold walls of the cryostat and do not have sufficient momentum to escape.

3.2.4 Stability

In order for the interference effects to remain, the distance between the large cavity end mirror and the equilibrium position of the small mirror has to be stable to of order $\lambda/20N = 6 \times 10^{-15}$m over the whole measurement time.

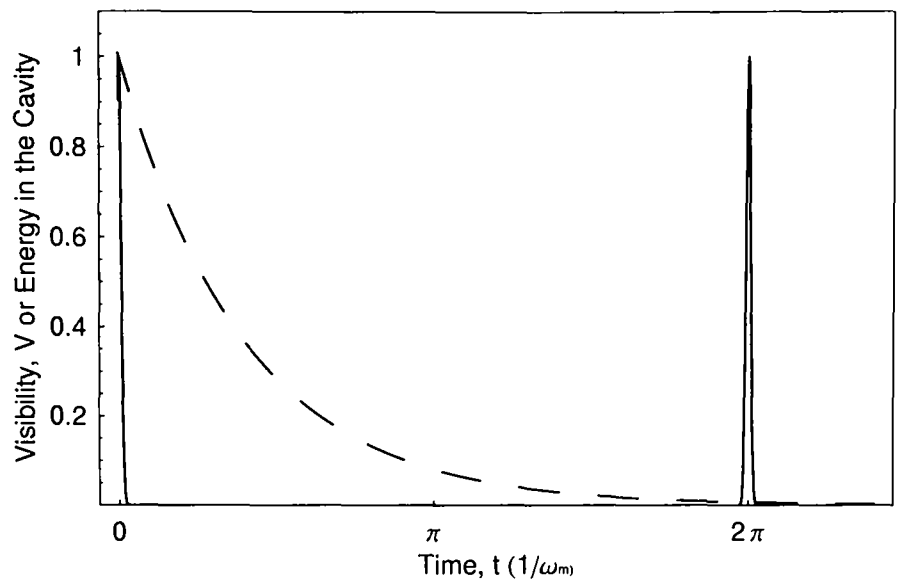

Figure 3.5: Solid line: time evolution of the interference visibility V of the photon over one period of the mirror's motion for the micro-mirror/cantilever at 20μK. The revival peak width is a factor of 10 wider than for a temperature of 2mK for illustrative purposes. Dashed line: the exponential decay of the cavity field, for a cavity of finesse 1.5×10^7. The probability of the photon randomly leaking during the revival peak at $t = 2\pi$ is very low for high temperatures.

To calculate the timescale of the experiment required to collect sufficient data, one has to consider the experimental scenario, as discussed at the start of §3.2 approximately 1% of the photons remain after a full period for the assumed cavity loss, this implies a detection rate of approximately 0.5Hz. To calculate the time needed to detect the revival peak, one must calculate the probability for the photon to leak out during the revival peak. Ones ability to detect the revival depends upon the probability a photon has to leak out in the revival peak, whose width scales as $1/\sqrt{T}$ (see Fig. 3.3). In Fig. 3.5 the decay of the field for $F = 1.5 \times 10^7$ as required in §3.2.1 is shown. Only 1% of the photons remain in the cavity at the revival time and even less will leak out by chance in the revival window. The peak shown is for $n = 1000$, $T = 20\mu$K, with a revival peak a factor 10 wider than that for $T = 2$mK for illustrative purposes. In practice the counting depends also on measuring the revival above any detector noise and on having sufficient interferometric contrast ratio (which is a measure of the sensitivity to detect deviations in visibility). Given a resonator contrast ratio of 10 (the maximum possible due to two photon contributions) then essentially the height of the decay at mid-revival peak multiplied by the peak full width at half maximum gives the probability of a photon leaking and being a point on the revival peak. It will be assumed that 20 points are needed to verify the peak with good statistics. Detector noise can be minimised by using light from a down converted source, the use of an optical delay line and coincidence counting. With coincidence windows of 3ns, which is approximately the width in time of the revival peak for $T = 2$mK, and the electronics for which are readily available, detector noise could be reduced significantly since counts outside the revival time would be neglected.

Consider three scenarios, each starting from the point that there is a photon in the cavity at the time of the

revival peak at a rate 0.5Hz.

1. Scenario 1: the system is at 2mK as prescribed above to meet the EID requirement, then only 3×10^{-3} of the photons remaining in the cavity at one period of the oscillator will actually leak out in the revival time. This means a detection rate in the revival window of once per 500s. Such a rate is detectable above dark counts (typically 100/s) if a down converted source and coincidence detection is used that can cut the dark counts to once per 1000s or greater: one photon from the down-conversion is sent into the interferometer and the other is used for timing purposes with a separate detector, then coincidence counts of the two detectors are made. To get 20 points, one needs 10^4s, the full time over which the cavity must remain stable. Resulting stability requirement: 6×10^{-15}m/10^4s.

2. Scenario 2: optical switching of 50% over 100ps timescale or as long as 1ms for mirrors (see section below). In this case the detection rate is constituted by all photons left in the cavity after one period and the timescale to collect sufficient data to verify the revival peak is 40s. Resulting stability requirement: 6×10^{-15}m/40s.

3. Scenario 3: cooling of the cantilever using adiabatic demagnetisation cooling (see section below): cooling to 60μK increases the probability of random leaking during the revival interval by a factor 6 compared to starting at 2mK, thus the timescale is approximately 2×10^3s. Resulting stability requirement: 6×10^{-15}m/2×10^3s.

Clearly Scenario 2 is preferable from a stability perspective. Achieving this stability requirement can best be done by placing the system of resonant frequency ω_m onto a suspension stack of resonant frequency ω_{stack}, where vibrations are reduced in amplitude by $\frac{\omega_m}{\omega_{stack}}$ per layer, and consequently isolate the setup. Such a suspension proposed in [Chan et al., 1999] calculates a possible 250dB reduction in noise at 1kHz. Stability of order 10^{-13}m/min for an STM at 8 K was achieved with a rather simple suspension [Stipe et al., 1999] and 8.8×10^{-14}m/min, in Ref. [Hood, 2000]. Gravitational wave observatories using interferometers also require very high stability in order to have a length sensitivity of 10^{-19}m over timescales of $\sim$ms for arm lengths of order 1 km [Rowan and Hough, 2000], although they can allow for a large field with which to improve the length measurement for active control.

Note that a technical constraint here for current needs is thermal contact to the system which is needed to cool it, which to some extent goes against the drive for keeping the system vibrationally isolated since one risks that the cooling system introduces vibrations. A solution is to use a moveable cold finger which could temporarily touch with the system, but is removed for the experiment. Alternatively, thicker thermally-conducting springs could be used on the suspension system stack and thus cooling through it. However, the thermal conductivity of silicon cantilevers decreases as T^3 at sub-K temperatures [Harris et al., 1999, **?**](ch.2), [Asheghi et al., 2004] and so the cooling power needs to be fairly large despite the cantilever's minute mass.

In summary, thermal initial states remove the need for cooling while making more demanding stability requirements, nuclear demagnatisation could cool to sufficiently low temperatures, and ultra-fast switching reduces the stability requirements but all introduce new technological challenges. It is not clear which contributions provide the most near-term possibility of implementation of the mirror quantum superposition state.

3.2.5 Ultra-fast Optical Switching

If one were to be able to switch out the photon from the cavity at a specific time then one could switch out and detect it at $t = 2\pi/\omega_m$. A photon will then be detected in 0.1% of cases and the timescale over which the cavity must remain stable will be as in Scenario 2 above — considerably technologically easier than the other scenarios. The requirements are that the switching has a rise time and duration greater than a round trip time of approximately 100ps and less than the interferometer visibility revival time ($\sim \mu$s for the cantilever at mK), and that the switching elements do not reduce the cavity finesse when the switch is in the off state. The speed requirement is easily met by Acousto-Optic Modulators (AOM) or Pockell's Cell but they would have to be placed inside the cavity and both have associated absorption and scattering that would reduce the finesse by orders of magnitude. The motivation then for developing ultra-fast all-optical switching is that it has the potential to be fast whilst not affecting the finesse since no elements are placed into the cavity. A separate benefit of optical switching, although not required in the experiment under investigation, is that optical switching has the potential to switch on timescales as short as the pulse length as low as the 100fs regime, which is considerably faster than the AOM or Pockell's Cell whose switch timescale is $>$ 10ns.

Distributed Bragg Reflectors (DBR), as described in §3.4, are of high reflectivity over a wavelength region $\Delta\lambda$ whose width is dependent on the difference in refractive index between the two layer types. The principle of optical switching is as follows: a DBR is constructed where there is a difference in nonlinearity between the two materials — such as due to one layer being much more nonlinear than the other. A non-linear material is one where the refractive index is given by [Dmitriev et al., 1999, Günter, 1997]

$$n = n_0 + n_2 I \tag{3.47}$$

where I is the field intensity, n_0 is the refractive index at zero field and the nonlinear refractive index is related to the χ_3 nonlinearity by $n_2 = \frac{3\chi_3}{4c\epsilon_0 n_0}$. Physically the nonlinearity of a semiconductor is due both to the direct Kerr effect, which only exists during the time of the E-field, and the creation of electron-hole pairs which change the refractive index for timescales which can be longer. By changing the field strength with a pump laser (at a wavelength far from the band gap), it is possible to change the refractive index of the non-linear material and thus the difference in refractive indices. This changes the quality (i.e. reflectivity) and width of the band-gap. By selecting the high n material with a with a negative n_2, or the low n material positive n_2 then the band gap reduces with I, and a probe laser frequency, particularly if located near the edge of the band gap, will see a highly reflecting mirror for a low field (pump laser off) and a partially transmitting

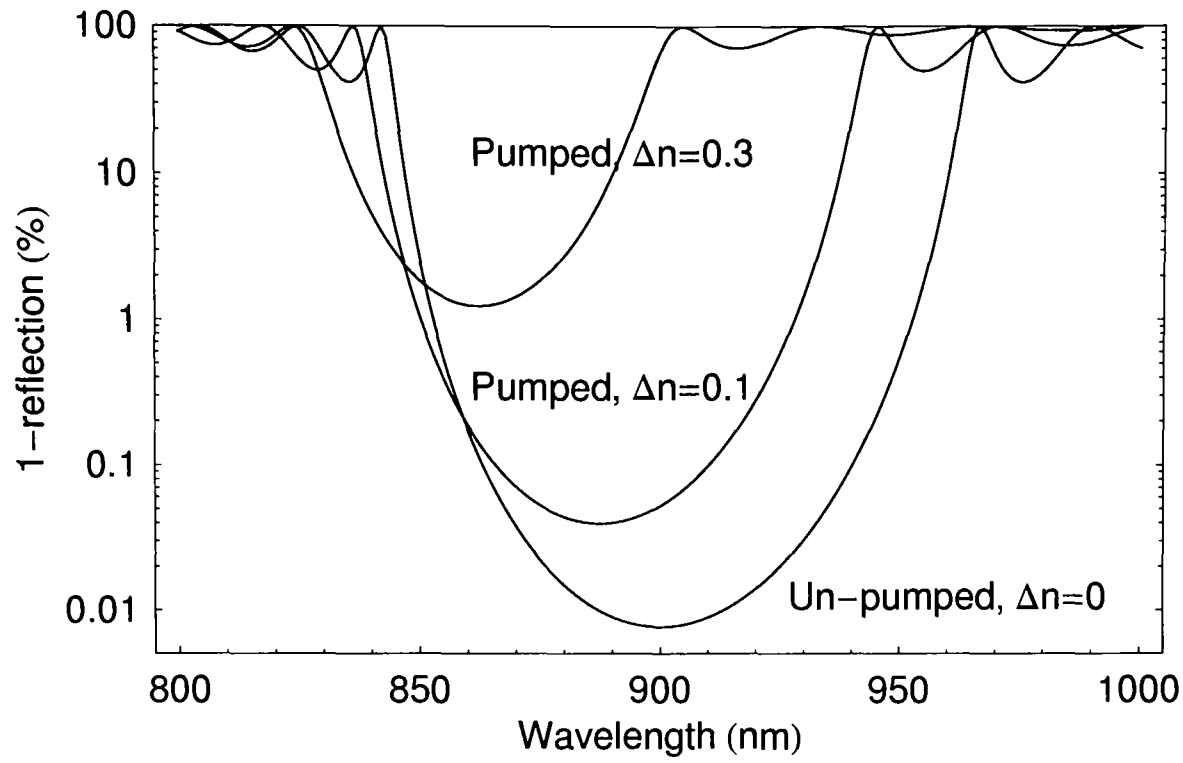

Figure 3.6: 1-reflection of a non-linear DBR mirror reflectivity for 3 cases: unpumped (highest reflectivity mirror), pumped such that $\Delta n = 0.1$ (somewhat worse mirror) and $\Delta n = 0.3$ the low reflectivity mirror shown. For a probe wavelength of 900nm the former corresponds to a switching by a factor of 5 from $< 0.01\%$ to 0.05% and the latter by a factor 10^4 from $< 0.01\%$ to 70% at 933nm.

device for a high field (pump laser on) [Scalora et al., 1994]. The lifetime of the field dictates the field and electron-hole pairs dictate the switching lifetime.

The key feature is that this switching of the device from high reflectivity to partially transmitting can be done on very short timescales since the effect is present, ideally, only when the field is on and has no elements in the cavity. High powered sources with switching on $<$ 100fs timescales are available, which is less than the cavity round-trip time, and so this allows us to be able to switch light out of the cavity after a known number of cavity round-trips. This would allow one to release any photon remaining in the cavity from there at a given time. Opening the cavity (reducing the mirror reflectivity) at the time of the revival peak would considerably increase the data acquisition rate and hence reduce the stability difficulty by 2-3 orders of magnitude (see Scenario 2 above). The pump laser wavelength is chosen to be far from the probe wavelength such that the cavity has a low finesse at that wavelength and scattered light does not ruin the main experiment occurring with the probe.

In order to make a switchable mirror with high reflectivity the materials used must have low absorption at the desired operation wavelength, a large indices of refraction contrast between the materials and in addition at least one material must exhibit a large nonlinear index of refraction. GaAs/AlAs meet these criteria with GaAs known to be nonlinear and also has large free carrier nonlinearity in index of refraction [Huang et al., 1998]

and AlAs being less nonlinear.

The reflectivity of a mirror made of a 30-pair DBR structure of GaAs/GaAs with a design peak reflectivity wavelength of 900nm was calculated as a function of wavelength and is shown in Fig. 3.6. The equivalent reflectivity curves for the same mirror except where the refractive index of GaAs is modified by $\Delta n = 0.1$ and $\Delta n = 0.3$ is shown. If one were able to switch by $\Delta n = 0.1$ and if operating the probe at a wavelength of 900nm then one could achieve a switching by a factor of 5 from $< 0.01\%$ transmission to 0.05%. If one were able to switch by $\Delta n = 0.3$ then one could achieve a switching by a factor of 10^4 from $< 0.01\%$ transmission to 70%. In fact if one were to switch by $\Delta n = 0.61$ then the refractive index of GaAs and AlAs would match and low reflectivity is expected. Increasing the number of layers would lead to a greater initial reflectivity so long as the absorption remains low enough at the probe wavelength. DBRs with sharper band-gap edges might also be designed to get switching at lower pump powers.

The conclusion of that calculation is that a change in refractive index of $\Delta n = 0.3$ is required for switching to a $\sim 50\%$ level required for a reasonable switching out probability. Whether this is possible depends on the nonlinearity of GaAs and AlAs. Bulk GaAs has $n_2 = 3 \times 10^{-16} m^2/W$ [Said et al., 1992] and considerably higher for GaAs/AlAs quantum well structures [Miller and Mlynek, 1982]. In the cantilever superposition experiment such switching would be applied to the large mirror of the micro-mirror/cantilever cavity given the configuration of Fig. 1.1. The need for the photon to return into the interferometer, and since high intensities would cause instability in the cantilever if applied at the large mirror. The switching would also have to be applied to one of the mirrors in the cavity in the other arm. Switching of the large mirror would require at least an area to be switched of 0.3mm diameter. In order to get this change in refractive index of $\Delta n = 0.3$, one requires 10^{15} W/m^2 intensity. This is possible over that area for a Ti:Sapphire with regenerative amplifier with pulse length 100fs and repetition rate 40kHz and whose average power is 400mW. The change in mirror reflectivity is only expected to last for the 100fs pulse length due to the Kerr effect nonlinearity and thus would have to be timed accurately enough to coincide with the arrival photon in the cavity at that mirror. One may also consider a faster repetition rate system such that more than one pulse arrives during the $\sim 1\mu s$ revival time e.g. a Ti:Sapphire 80MHz 100fs system would have approximately 150 pulses in the revival window and thus would only have to switch to $0.5^{1/150} = 99.6\%$ for each pulse than many less intense ones. However, this would still require $\Delta n = 0.1$ and so it is preferable to use a single more intense pulse. One may also consider pumping at an energy near the band-gap edge of GaAs so as to excite free carriers in the semiconductor which would alter the refractive index and would have a longer switching duration which would be of advantage in this case.

A significant hurdle is that mirrors with reflectivity $> 99.999\%$ have not been developed for GaAs/AlAs and it is not clear that the absorption is low enough to do so. Another foreseeable problem with this scheme is that the pump laser could swamp the cavity with a large number of scattered photons. However, any ultra fast switching to a lower finesse cavity at the frequency of the pump would ease the stability requirements.

Switching of the kind described here has been studied recently in two and three dimensional photonic crystals in refs. [Hache and Bourgeois, 2000, Leonard et al., 2002, Bristow et al., 2003, Mazurenko et al., 2003, Huang et al., 1998]. The goal here is to switch by large percentages, rather than by large factors of transmission from a very high reflectivity mirror. Samples of high-reflectivity mirrors were fabricated and tested and the results are shown in §4.6.

3.2.6 Adiabatic Demagnetisation Cooling

Another method to help the stability requirements is adiabatic demagnetisation cooling. This involves 2 steps: (1) a ferrous material in contact with a cryogenic bath is subject to a high B-field which aligns the atomic magnetic dipoles; (2) the contact with the cryogenic bath is removed and the B-field is turned off adiabatically. No heat can flow back to the bath, and the sample will cool due to random re-orientation of the atomic spins which can only do so by absorbing phonons and thus reducing the lattice temperature. This can allow the cooling of samples from liquid Helium temperatures to 1.5mK. Much lower temperatures can be attained by an analogous means called adiabatic nuclear demagnetization in which the nuclear dipoles are used. Such methods have demonstrated cooling of kg size masses of Copper from dilution refrigerator temperatures (mK) to 60μK [Tuoriniemi and Knuuttila, 2000, Knuuttila, 2000]. See [Oja and Lounasmaa, 1997] for a good review article.

By mounting the cantilever onto a ferrous substrate (e.g. a Copper block) then cooling of the micro-mirror/cantilever may be achieved through conduction with the ferrous block which would be subject to the above procedure. In theory the only additional experimental requirement is a high-B field in the setup however in practice thermal isolation is very involved and only a few laboratories worldwide make use of the technique to cool to sub-mK temperatures. A test of nuclear demagnetisation of such a cantilever is scheduled for spring 2005 in a 10 Tesla cryostat.

3.2.7 Summary of Experimental Feasibility

3.3 Cavity Modes and Mode-Matching

ABCD matrices and solutions to periodic sequences

The method of ray transfer matrices can be used to propagate a beam through any series of optical elements. Consider first a ray defined by a distance r_1 from an optical axis, which is defined as the z-axis, and a gradient

	State of the Art	Required
Cavity finesse	2×10^6 [1]	1.5×10^7
Cantilever Q, m, ω, k	2.5×10^5 [2], 7×10^{-11}kg, $2\pi \times 10$kHz, 0.1N.m^{-1} [3]	10^5, $< 5 \times 10^{-12}$kg, $2\pi \times 500$Hz, 10^{-8}N.m^{-1}[4]
Bath Temperature, T	60μK [4]	3mK
Mirror Mass, m	5×10^{-12}kg [5]	5×10^{-12}kg
Stability	10^{-13}m/min [6]	10^{-15}m/min
Vacuum	10^8atoms/m^3 [7]	10^{12}atoms/m^3
Switching	$99.998 \rightarrow 99.94\%$ /10ps [8]	$99.99998 \rightarrow 50\%$ /100ps

Table 3.2: Summary of the experimental demands versus those achieved experimentally to date. [1] see Ref. [Rempe et al., 1992]. [2] see Ref. [Yang et al., 2000]. [3] see Ref. [Nanodevices,]. [4] see Ref. [Oja and Lounasmaa, 1997, Tuoriniemi and Knuuttila, 2000]. [5] see §4.1. [6] see Ref. [Stipe et al., 1999, Hood, 2000]. [7] see Ref. [Gabrielse et al., 1990]. [8] see §4.6. Note that the laarge difference in cantilever force constant needed compared to state of the art is mostly due to the change in size of the cantilever used and is perfectly feasible with a much smaller and thinner cantilever.

$r' = dr/dz$ from that axis as shown schematically in Fig. 3.7. The beam at a later time will be given by

$$\begin{pmatrix} r_2 \\ r_2' \end{pmatrix} = \begin{pmatrix} A & B \\ C & D \end{pmatrix} \begin{pmatrix} r_1 \\ r_1' \end{pmatrix} \tag{3.48}$$

or in a more compact notation where **M**=$ABCD$ matrix, $\mathbf{r}_2 = \mathbf{M}\,\mathbf{r}_1$. The $ABCD$ matrix is determined by the elements through which the ray propagates. Its determinant should be unity. For multiple elements $ABCD$ are determined by the multiplication of the individual optical element matrices in the reverse order of how the beam encounters those elements $\mathbf{r}_2 = \mathbf{M}_n\mathbf{M}_{n-1}....\mathbf{M}_1\mathbf{r}_1$. The curvature of a beam, R_2, after an optical system represented by an $ABCD$ matrix is then determined from the curvature before the $ABCD$ system, R_1 using the transformation

$$R_2 = \frac{AR_1 + B}{CR_1 + D}. \tag{3.49}$$

Given a periodic sequence of elements, or resonator, the solution such that the ray returns to itself after one period is

$$\mathbf{Mr} = \lambda\mathbf{r}, \tag{3.50}$$

which only has non-zero solutions if

$$\begin{pmatrix} A-\lambda & B \\ C & D-\lambda \end{pmatrix} \begin{pmatrix} r \\ r' \end{pmatrix} = 0. \tag{3.51}$$

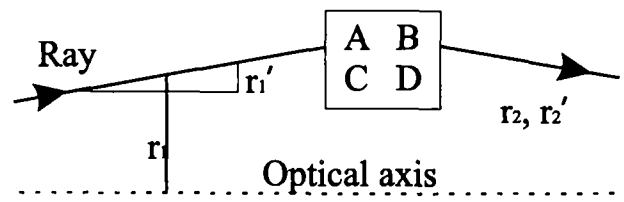

Figure 3.7: The basics of ABCD matrices: a ray defined by a slope r_1' and distance r_1 from the optical axis is translated by a general system $ABCD$ to a new ray r_2, r_2'

This has quadratic solutions

$$\lambda_a, \lambda_b = m \pm \sqrt{m^2 - 1} \tag{3.52}$$

where

$$m \equiv \frac{A + D}{2}. \tag{3.53}$$

There are two eigen-rays such that $\mathbf{M}\mathbf{r}_a = \lambda_a \, \mathbf{r}_a$, $\mathbf{M}\mathbf{r}_b = \lambda_b \, \mathbf{r}_b$. Any periodic system with $|m| < 1$ is stable. The stable and unstable conditions for a two-mirror resonator are usually written in terms of two parameters $g_1 = 1 - L/r_1$ and $g_2 = 1 - L/r_2$ where r_1 and r_2 are the radius of curvature of the two mirrors and L is their separation. The stability condition is then

$$0 << g_1 g_2 << 1. \tag{3.54}$$

A plot of the stability regions are shown in Fig. 3.8. The cavity geometry of interest to the experiment is the hemispherical one: it lies on the stable/unstable boundary.

Gaussian Beams and Cavity Modes

The spatial and time evolution of a field component u must satisfy the scalar wave equation. Assuming that the field changes slowly along the z-axis, such that terms in $d^2\psi/dz$ are assumed to be negligible, then one obtains the paraxial wave equation:

$$\frac{d^2\psi}{dx^2} + \frac{d^2\psi}{dy^2} - 2ik\frac{d\psi}{dz} = 0. \tag{3.55}$$

One solution to this is, which has a Gaussian intensity profile as required, called the fundamental mode is

$$\psi = e^{-i(\phi + \frac{kr^2}{2q})}, \tag{3.56}$$

where q is the complex beam parameter which can be expressed in terms of two real beam parameters which describe the beam completely, that is the beam radius (defined as the distance from the peak amplitude to the 1/e amplitude) w and radius of curvature R, as

$$\frac{1}{q} = \frac{1}{R} - \frac{i\lambda}{\pi w^2} \tag{3.57}$$

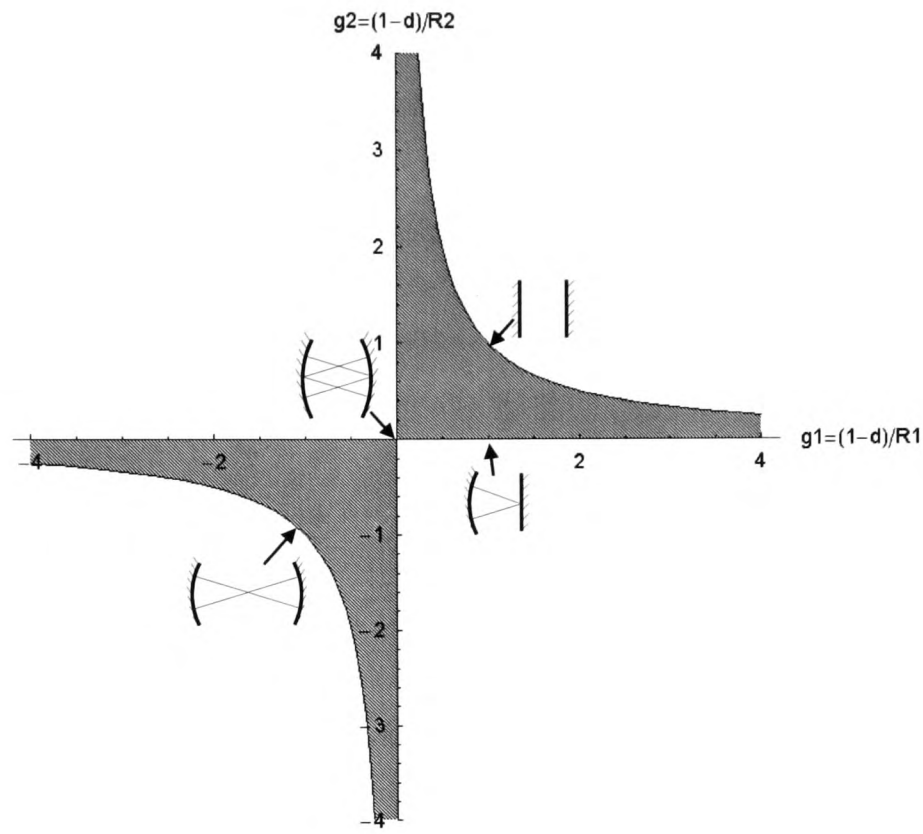

Figure 3.8: Cavity stability graph: the shaded are stable. Various cavity geometries are shown schematically.

and where the phase ϕ is given by

$$\phi = tan^{-1}(\frac{\lambda z}{\pi w^2}). \tag{3.58}$$

The wave equation has other solutions which constitute high order modes. In particular for beams with symmetry in cartesian coordinates have the Hermite-Gaussian solutions of the form

$$\psi = g(\frac{x}{w}).h(\frac{y}{w})e^{-i(\frac{\phi+kr^2}{2q})}, \tag{3.59}$$

where

$$g.h = H_m(\sqrt{2}\frac{x}{w})H_n(\sqrt{2}\frac{x}{w}) \tag{3.60}$$

where H_m are the Hermite polynomials

$$\begin{aligned} H_0 &= 1 \\ H_1 &= 2x \\ H_2 &= 4x^2 - 2 \\ H_3 &= 8x^3 - 12x \\ H_4 &= 12 - 48x^2 + 16x^4 etc. \end{aligned} \tag{3.61}$$

Examples of these are shown experimentally in §4.2.1. For beams with cylindrical symmetry there are solutions to the paraxial wave equation called Laguerre-Gaussian modes. Real beams often have astigmatism between the x and y axes which means that in practice beams opt to operate in the Hermite-Gaussian mode see Ref. [Siegman, 1966](p. 647).

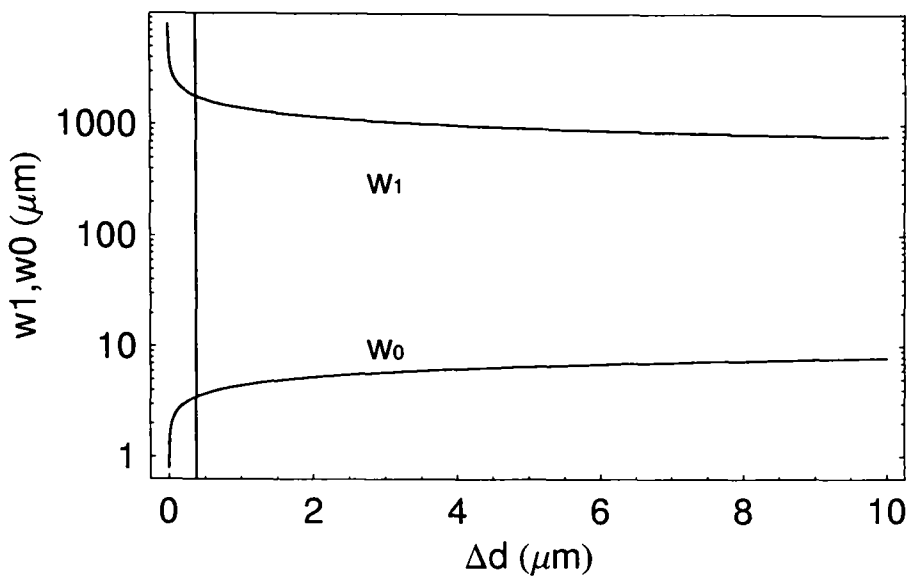

Figure 3.9: The spot size on either end mirror shown as a function of $\Delta L = R - L$. The vertical line shows the optimum cavity length given mirrors of radii of 10μm and 3mm respectively.

The complex beam parameter q can be manipulated by $ABCD$ matrices, just as for ray optics, from an initial beam q_1 to a final beam q_2 using the transformation

$$q_2 = \frac{Aq_1 + B}{Cq_1 + D}. \tag{3.62}$$

For a planar concave cavity the single round-trip $ABCD$ matrix is

$$\begin{pmatrix} A & B \\ C & D \end{pmatrix} = \begin{pmatrix} 1 & 2L \\ -2/R & 1 - 4L/R \end{pmatrix}. \tag{3.63}$$

The solution such that the beam matches back on itself after one round-trip, $q_1 = q_2$, is given by

$$q = -L \pm L\sqrt{1 - R/L}. \tag{3.64}$$

where R is the radius of curvature of the concave mirror and d is the mirror separation. The solution giving a real beam width shows that the beam width at the small mirror is

$$w_0^2 = \frac{\lambda}{2\pi}\sqrt{L(R - L)} \tag{3.65}$$

and that the beam width at the other mirror is inversely proportional to that being given by

$$w_1 = \frac{\lambda R}{\pi w_0}. \tag{3.66}$$

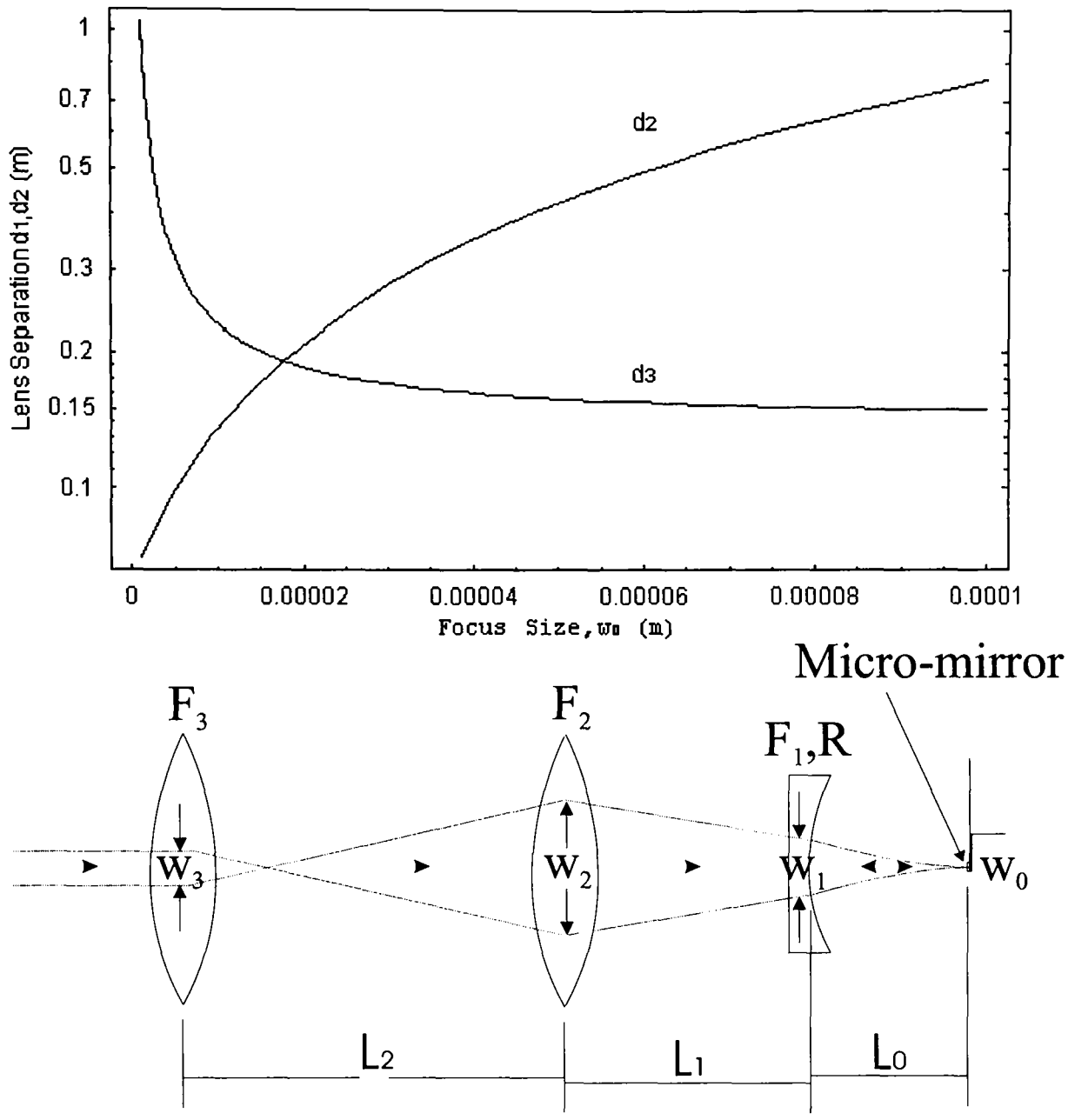

Figure 3.10: Graph showing the optimum distances L_1 and L_2, as defined in the bottom figure, as a function of spot size on the micro-mirror w_0.

Fig. 3.9 shows how w_0 and w_1 behave with $R - L$. The vertical line indicates the optimum cavity length for the mirrors used in the experimental setup of §4.2.. Both are determined by the cavity length to which they are very sensitive as $L \to R$. Such a cavity is stable so long as $L \leq R$.

One has to match the input beam to this cavity mode using lenses. In our case 2 lenses of focal length were used. For a given small spot size the optimum distances of the two incoupling lenses can be calculated. This calculation must take into account the lensing effect of the back mirror. Given w_0, w_1, L_0 from above and given fixed lens focal lengths F_z, F_L, F_1, F_2 and the incoming beam width w_3, as shown in Fig. 3.10, one can determine L_1 and L_2. $F_z = 1.25$cm and $F_L = 5$cm are determined by the curvature and substrate of the large mirror. The other lenses used were $F_1 = 8$cm, $F_2 = 6$cm and the incident beam width is $w_3 = 2$mm. Fig. 3.10 shows how the spot size vary as the cavity length (shown in units of $R - L$) and Table 3.3 shows

some key incoupling configurations used.

w_0 (μm)	L_0 (mm)	L_1 (cm)	L_2 (cm)
50	21.8	40.4	15.9
10	24.9941	13.1	23.4
4.55	24.99972	9.6	33.6
3	24.99995	8.4	45.3

Table 3.3: Summary of mode matching parameters (optics separations L_1,L_2 and L_3) for incoupling lenses of focal length 6 and 8cm onto a cavity with curved mirror $R = 25$mm. The lowest loss mode is that with a beam waist 4.55μm for the cavity of §4.2.

There are higher order modes solutions to the wave equation also which for cavities in linear media always have lower finesse [Fox and Li, 1968]. In fact the Fox and Li method is employed to analyse the diffraction losses from the finite sized mirrors in §4.5.

3.4 High Reflectivity Mirrors

Highly reflective surfaces are achieved through the use of multiple layers of dielectric materials of alternately high n_H and low n_L refractive indices [Elshabini-Riad and Barlow, 1997]. Each layer is $\lambda/4n$ thick such that the reflection from each boundary layer adds up constructively, and transmitted wave destructively. One must consider that reflection from a boundary where the incident refractive index is lower than the transmitted receives a π phase shift whereas reflection from a boundary going from high to low refractive index gives no phase shift. This type of mirror is called a dielectric mirror or Distributed Bragg Reflector (DBR).

More layers and greater contrast of refractive index both allow a greater reflectivity up to the point where losses become dominant. If there are x layers of each type (x pairs) then the peak reflectivity is given by [Elshabini-Riad and Barlow, 1997]

$$r = \left(\frac{n_0 - \frac{n_H^{2x}}{n_L^{2(x-1)} n_{sub}}}{n_0 + \frac{n_H^{2x}}{n_L^{2(x-1)} n_{sub}}} \right)^2, \tag{3.67}$$

where the complex refractive index $n = \eta + i\kappa$, where η is the classical refractive index. For r close to 1, the reflectivity is related to the maximum number of reflections in a cavity N, introduced earlier, by:

$$N = (\frac{1}{1 - r^2}). \tag{3.68}$$

Reflectivity is limited by two things, firstly fabrication constraints and secondly losses. Fabrication constraints include:

1. The difference in refractive indices.
2. The number of layers.
3. The divergence of the layers from the optimum thickness $\lambda/4n$ both in average thickness and in uniformity.

Loss constraints are:

1. Absorption inherent in the layers.
2. Scattering from impurities and crystal imperfections and crystalline defects.

In practice the best such mirrors at optical wavelengths are made through sputtering deposition of layers of SiO_2 ($n = 1.455, \rho = 2200\text{kg.m}^{-3}$) and Ta_2O_5 ($n = 2.0411, \rho = 8200\text{kg.m}^{-3}$) onto a SiO_2 substrate. These two materials are chosen because they are both extremely low absorbers ($\alpha < 1\text{m}^{-1}$[Palik, 1997]) and scatterers, [Tittonen et al., 1999, Rempe et al., 1992, Hood et al., 2001] at optical wavelengths and the difference in refractive indices is substantial. In addition the layers match well after annealing, causing little inter-layer stress which can otherwise deform the mirror and, lastly, sputter deposition techniques for these materials are accurate to <nm layer thickness. The dominant constraint on reflectivity is the absorption and scattering losses contributions of which are at a similar order [Rempe et al., 1992, Hood, 2000, Hood et al., 2001] being at the the 1 part per million level — consistent with α given the mirror thickness of order a few microns. Mirrors with reflectivities of 99.9998% at 850nm wavelength given $x = 20$ pairs of layers have been fabricated [Rempe et al., 1992].

The number of layers required for the reflectivity desired dictates the minimum thickness of the micro-mirror. Thickness, T is given by:

$$T = \frac{x\lambda}{4}\left(\frac{1}{n_h} + \frac{1}{n_L}\right). \tag{3.69}$$

Accordingly one requires $x = 16$ pairs of layers to get a reflectivity of 0.99997, or 23 pairs, to get our required $F = 1.5 \times 10^7$ ($N = 2.4 \times 10^6$ reflections).

3.5 Optical Cooling of a Micro-Mechanical Cantilever

Optical cooling of a moveable mirror's centre of mass motion via force feedback was first proposed by Mancini et al Ref. [Mancini et al., 1998]. By monitoring the position of the movable mirror to high precision a feedback mechanism can be implemented to dampen the motion and thus cool the micro-mirror/cantilever's centre of mass motion far below the temperature of its environment. The cooling factors possible for such small objects as the micro-mirror/cantilever are in principle very large with moderate feedback laser powers.

Hence one might use the method to cool the cantilever to near the ground state centre of mass motion. This would have the effect of reducing the phonon number in that mode to of order 1 and hence, from §3.1.2 & §3.2.4 the stability factor can be greatly reduced. Initial calculations and indications from reported experiments suggest that heating due to the absorption of photons is likely to mean that the process of cooling of the centre of mass motion cannot be done on cantilevers of our dimensions if the lattice temperature is to remain below a few mK, required in order to keep environmental decoherence low (§3.2.2). However, there is a large uncertainty in the thermal conductivity of silicon at very low temperatures and so the matter is not settled. Moreover, the scheme applied to cooling of a cantilever's centre of mass motion is of independent interest for applications not concerned with the lattice temperature or if starting from a much higher temperature cantilever (e.g. room temperature) where cooling factors can be large.

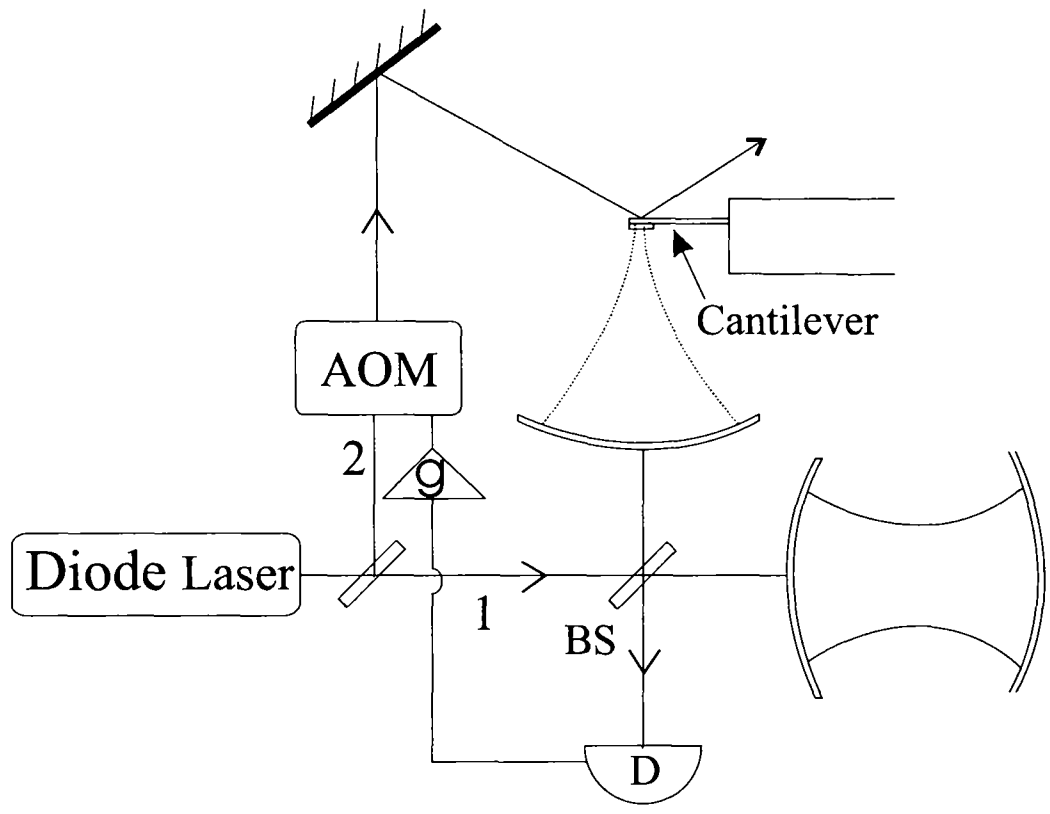

Figure 3.11: A schematic of the setup proposed to cool the centre of mass motion of a cantilever. Beam 1 is used to monitor the position of the cantilever by use of a high finesse cavity whose output phase is compared to a reference cavity. Beam 2 is used to provide a modulated force on the moveable mirror.

A variation of the original scheme [Cohadon et al., 1999] has a feedback force proportional to the natural damping force, but larger by a gain factor g. The size of g determines the achievable final temperature for a given environment temperature T_E as

$$g \sim \frac{T_E}{T_0}. \tag{3.70}$$

A possible setup for optical cooling of a moveable mirror is shown in Fig. 3.11 whereby the mirror on an oscillator to be cooled is placed in a cavity, whose length can be monitored with high precision by observing

the phase of the output field compared to a reference cavity. A second modulated beam is reflected from the back of the oscillator. One can design a feedback loop such that the radiation pressure from the second beam on the mirror is proportional to the velocity and hence corresponds to a viscous force on the cantilever. Thus the second beam's intensity is adjusted in real time in order to damp the mirror/oscillator motion below the temperature of its environment.

Starting from the Hamiltonian of the setup, and taking into account the fact that measurement and feedback introduce shot noise, the system dynamics have been derived in Ref. [Courty et al., 2001, Vitali et al., 2002], and give the result that the final energy of the cooled mirror is given by

$$E_c = \frac{\omega_m}{2}\frac{1}{2(1+g)}\left[\frac{4k_B T_E}{\omega_m} + \zeta + \frac{g^2}{\eta\zeta}\right], \tag{3.71}$$

where

$$\zeta = \frac{64\pi c P}{m\gamma_m\omega_m\lambda\gamma_c^2 L^2} = \frac{16PQF^2}{\pi m\omega_m^2\lambda c}, \tag{3.72}$$

with P the light intensity incidently, in the cavity, γ_c the cavity decay rate, and η the detection efficiency. The first term in Eq. (3.71) comes from the original thermal fluctuations, which are suppressed by the feedback. The second term is the back action noise from the measurement and feedback light. The third term is the feedback noise due to imperfect measurement. For the cantilever under discussion in §3.1 and §3.2 the back action noise and feedback noise are small compared to the original thermal fluctuations and so the first term dominates. In this case the minimum temperature realisable is determined by the gain in the same way as a rather more simple classical analysis [Cohadon et al., 1999]. The full quantum analysis leading to Eq. 3.71 revealing that there is an optimal power and thus a maximum cooling ratio of T_E/T dependent on the physical properties of the mirror/oscillator.

This scheme has been experimentally implemented in Ref. [Cohadon et al., 1999, Pinard et al., 2000] where a large (mm-sized) mirror's temperature was reduced by a factor of 40 (and also increased by reversing the feedback gain).

Here it is of interest to implement such a scheme for a micro-mechanical cantilever. This would involve a setup as in Fig. 3.11, where the only difference from Ref [Cohadon et al., 1999] is the tight focus cavity field. The feedback force would also require such a focus. Conveniently, this setup fits entirely with the setup elaborated for the mirror superposition experiment §3.2. The only change needed is that a lower finesse cavity is required (longer γ_c) than that required in §3.2.1 in order to have sufficient power in the cavity to equalise the feedback power whilst maintaining a reasonable gain. Incidentally, the finesse required is approximately that achieved experimentally to date §4.3.4.

The minimum energy given by Eq. 3.71 is when $g = \zeta$. For such a small object large gain values are realistic using the radiation pressure of a moderate second laser beam providing the feedback force. In fact the energy of the mirror can be made very close to its ground state energy ($E_c \sim \omega_m$) choosing the following parameter values; $g = 6 \times 10^5$, $T_E = 2$ mK, $P = 1$nW, $\gamma_c = 3 \times 10^7 \mathrm{s}^{-1}$ (a cavity finesse $F = 3600$ for

$L = 5$cm), $\lambda = 800$ nm, $\eta = 0.8$, $\gamma_m = 0.03\ \mathrm{s}^{-1}$, and m, ω_m, L as in §3.2. The necessary feedback force for such a high value of g can be determined by

$$\begin{aligned} gF_{damp} &= F_{fb} \\ gbv &= \frac{P_{fb}r}{c} \\ \frac{g\omega_m}{Q}\sqrt{mk_BT_E} &= \frac{P_{fb}r}{c} \end{aligned} \tag{3.73}$$

where r is the reflectivity of the cantilever at the feedback laser wavelength, v is the cantilever velocity, $b = \omega_m/Q$ is the drag coefficient given from the oscillator equation of motion (Eq. 4.10). The final step makes use of the equipartition theorem which for a one-dimensional case is

$$\frac{1}{2}k_bT_E = \frac{1}{2}mv^2. \tag{3.74}$$

For the above values and Q= 10^5 a feedback laser intensity modulation of $\Delta P_{fb} = 2 \times 10^{-6}$W is required. For our proposed experiment the constant component of the feedback laser has to balance the force from the measurement field, since otherwise the mirror would start to oscillate when the light is turned off thus the feedback laser should be $\bar{P}_{fb} = 4 \times 10^{-6}$W.

However, heating due to absorption of light was neglected in 3.71 and is likely to be significant for a tiny oscillator. If such heating would increase the lattice temperature over that allowed by environmental decoherence (3mK) then any advantages of the mechanical stability may be outweighed by costs in a faster decoherence rate. The power threshold at which the cantilever is maintained at a temperature under that imposed by the EID requirement is given from the thermal conductivity of silicon and the cantilever dimensions. The maximum power which if incident on the cantilever would heat it at most to a temperature T_{cant} compared to the environment temperature T_E, given cantilever width w, and length l, absorption α ($<$ 1/m for silicon below the band-gap, $\lambda > 1300$nm, [Palik, 1997]) and a thermal conductivity C is

$$P_{fbmax} = \frac{wC(T_{cant} - T_E)}{\alpha l}. \tag{3.75}$$

Let us calculate the heating expected in a few scenarios:

Scenario 1: consider the cantilever discussed in §3.2 and presume a system temperature maintained by a dilution refrigerator of $T_E = 2$mK. The thermal conductivity is not known for silicon at mK temperatures but for bulk scales approximately with T^3 at low ($<$ 100K) temperatures down to the lowest measured at 1K of $C = 6$W/m/K [Asheghi et al., 2004]. Extrapolation of this trend would suggest a thermal conductivity of approximately 2×10^{-7} at 3mK. Using these numbers would mean $P_{fbmax} = 2 \times 10^{-12}$W which is much less than that required for the large gain factor envisioned. In fact no damping gain above 1 would be possible at all if the cantilever is to remain below the EID required lattice temperature. Heating effects of a laser on a silicon cantilever approximately an order of magnitude less massive than the one proposed for use here were studied experimentally in Ref. [Mamin and Rugar, 2001] and back up results of the heating effects: an

incident power at 1500nm (below the band-gap) of 10nW caused a cantilever noise temperature of 300mK from an initial temperature of 100mK which would suggest that $C = 3 \times 10^{-5}$ at 400mK, even less than that obtained the above extrapolation. However, the extrapolation may not be valid in few mK regime and/or with very thin layer cantilevers.

Scenario 2: for the cantilever in use in §4.3 and attempting cooling from room temperature, where the conductivity of silicon is known eperimentally to be $C = 148$W/m/K whilst not wishing to heat the cantilever above 350K then $P_{fbmax} = 600$W. Using Eq. 3.71 gain factors of 10^5 are possible with this cantilever using powers of 10^{-6}W therefore large damping gains of the cantilever centre of mass motion should be possible without undue heating.

Scenario 3: for the same cantilever as §4.3 but cooling from mK temperatures and not wanting the lattice to exceed mK temperatures then $P_{fbmax} = 7 \times 10^{-12}$W and again no gain is possible without too much heating. The sharp contrast with Scenario 2 can be attributed to the fact that the C factors scales with T^3. Since $T_{cant} - T_E$ scales with T also, the maximum gain scales with T^4.

Clearly, either a more in depth study of the nature of the thermal conductivity of silicon at mK temperatures is needed and/or this must be determined experimentally if it is to be possible to calculate whether or not the optical cooling is a useful technique to help the superposition experiment outlined in §3.1 & 3.2. Schemes where one measures the position without cooling could be as useful and could reduce the restrictions from heating and should be explored further. If it is possible to reduce the centre of mass temperature below mK then it would enable reduction of the experimental timescale and thus the stability and vacuum criteria.

If it were to be used then before every run of the experiment the cooling procedure would have to be performed so as to prepare the mirror in its rest state. The cooling timescale is of order $1/(\gamma_m g)$ [Pinard et al., 2000]. Once cooled the measurement and feedback laser fields should be turned off simultaneously to avoid the cantilever being left in motion. Then the experiment proceeds as described in §3.2. Reheating of the mirror happens at a timescale of $1/\gamma_m$ [Pinard et al., 2000] and thus is not a problem for a high-Q oscillator.

3.6 Related Schemes

Superposition of a Cantilever by coupling to a Cooper box

Armour et al. [Armour et al., 2002] proposed a scheme similar in principle to the optical scheme presented in this Chapter except where the cantilever is coupled to a Cooper box rather than a photon. A Cooper box is a superconducting island in which a large number of electrons all form Cooper pairs. The island is connected to a reservoir via a Josephson Junction. The island has difference charge states due to different

occupation numbers of electron pairs. It has been shown to be possible to form an artificial solid state based two-level system consisting of two different charge states differing by one electron pair. Applying a potential enables control of the evolution of the state and can be made into a superposition of the two levels [Nakamura et al., 1999]. Armour et al. propose that such a superposition charge state of the box can be coupled to the motional state of a micro-mechanical oscillator via electrostatic interaction by applying a potential different between the Box and cantilever which are placed close together. With sufficiently strong coupling the two cantilever states associated with the two occupation states of the Box can have a separation greater than the quantum position uncertainty. In this case, then just as for the optical scheme above, the coherence of the microscopic system – the Cooper pair (replacing the photon in the proposal outlined in this section) – varies with the period of the oscillator: after exactly integer number of periods it returns to its rest state and consequently (in the case of no decoherence) disentangles from the Box. The charge state can be read out, after different wait times, by a radio frequency single electron transistor (SET).

The scheme has several advantages over the optical scheme: it is relatively less demanding to obtain sufficient coupling of the microscopic state to the cantilever at realistic separation of box and cantilever (0.1μm) and realistic capacitance and potential between the box and cantilever. The Cooper box scheme is readily able to cause separation of greater than the quantum position uncertainty on much shorter timescales and with higher cantilever force constants (which in general rise with cantilever frequency see Eqs. 3.45, 3.46). Thus faster experimental timescales are feasible. This has several benefits: (1) This allows one to have stronger environmental coupling (3.43) allowing for lower cantilever quality factors and/or higher environment temperature; (2) higher frequency resonators are placed into the ground state at higher temperatures which thus enable larger revival intervals; finally, (3) at such frequencies there is very little non-intrinsic mechanical noise which is more problematic at lower frequencies. Given the above coupling the main requirements are then to have the coherence lifetime of the Cooper pair box longer than one cantilever oscillation and to have sufficient position sensitivity with the SET to resolve displacements of a size about that of the ground state wavepacket (a factor n below the standard quantum limit for an oscillator with thermal occupation n) [Bradinsky et al., 1995].

Recently, considerable progress has been made towards implementation of this scheme. Firstly, Nakamura et al. showed a coherence time of 2ns for the superposed Cooper Box, and avenues for keeping the Cooper box coherent for about an order of magnitude longer, sufficiently long for the experiment, seem feasible [Nakamura et al., 1999]. Secondly, resonators in the GHz range have been fabricated [Huang et al., 2003] which are in their ground state already at dilution refrigerator temperatures. Thirdly, a SET displacement sensitivity of $2 \times 10^{-15}\mathrm{mHz}^{-1/2}$ for a 116MHz oscillator, a sensitivity a factor 100 greater than the standard quantum limit has been achieved [Knobel and Cleland, 2003] and similar sensitivity was shown more recently for a lower frequency (19.7MHz) resonator, a factor 4.3 above the standard quantum limit [LaHaye et al., 2004]. In the former experiment cooling further to 1mK or using a 1GHz resonator would place the oscillator in the

ground state. In the latter, improved SET sensitivity by a factor 4.3 would enable measurement with resolution of the ground state wavepacket and thus sensitivity to occupation number and the ability to resolve quantum zero point fluctuations of the cantilever. Interaction with the superconducting island would then enable demonstration of quantum superpositions.

The main task is in integrating the Cooper Box, cantilever and SET and achieving the same results simultaneously. A potential hurdle, for example, is that the SET is likely to reduce the coherence time [Cleland, 2004].

Superposition of a Cantilever by coupling to a Josephson Junction

A Josephson Junction phase has the dynamics of a particle in a potential with a meta stable minima. The lowest two energies form a phase qubit. This can be controlled using a radio frequency field and Rabi oscillations have been seen [Nakamura et al., 1999]. Cleland and Geller [A. Cleland, 2003] propose coupling such a Josephson Junction phase qubit to a piezo-electric resonator. The voltage across the cantilever is proportional to the phase of the phase qubit and hence a phase qubit prepared in a superposition evolves to a cantilever in a motional superposition state. The Hamiltonian for the combined Junction/cantilever system is very similar to that for the photon/cantilever. As for the Cooper pair case, sufficient coupling can be achieved with relative technological ease compared to the optical scheme. All requirements for the setup have been achieved individually: sufficiently high quality cantilevers of the right dimensions and frequencies, cold enough setup, sensitive enough read out, preparation of the phase qubit superposition. Combining these achievements in the same setup is the major hurdle.

From the progress to date it seems that the above two elegant approaches using superconducting devices are the most promising avenue in the near term for creating the first truly macroscopic mass superposition. It might be mentioned that the different timescales involved in coupling a cantilever to a photon (ms) compared to coupling to a Cooper pair box (ns) may allow more scope to test EID models in the longer run in the optical scheme. Also, the mass involved in the superposition in the optical scheme is 3-4 orders of magnitude larger and this is a significant advantage for testing gravitational collapse models which is a longer term motivation of the scheme.

Other

Bose et al. [Bose et al., 1999] in their proposal of coupling a photon to a cantilever, largely along the lines of the present optical scheme, but deviate from it in suggesting the use of an atom in a superposition of two different excitation states passed through the cavity rather than our interferometric scheme, to prepare the photon superposition. This aspect of the proposal causes technical difficulties due to its demand for a shorter cavity (to enhance atom-field interaction) – this opposes the drive for a large L which is helpful because, as

seen from Eq. 3.41, for a given N, it allows one to use a lower frequency ω_m, and thus a more weakly bound mirror that is easier to displace by the photon.

Superpositions involving two macroscopically distinct current flows in a Superconducting Quantum Interference Device have been demonstrated [Friedman, 2000]. A SQUID is a superconducting loop broken by a Josephson Junction, around which a current can flow without dissipation. A superposition of two different flux states has been shown where the flux states correspond to two different directions of a current involving of order 10^9 electron pairs, differing in current by $2 - 3\mu$A. The mass involved is small but the system is still of great interest in testing EID models and it is conceivable that schemes could be though of where this state is coupled to a more massive object.

Proposals exist for creating a superposition state by interacting two Bose-Einstein Condensates (BEC) of different internal states [Ruostekoski et al., 1998, Cirac et al., 1998]. BECs involving involve of order 10^6 atoms have been created and so implementation of such a scheme would yield a macroscopic superposition albeit considerably less massive than the cantilever approaches.

Progress on atom interferometers [Godun et al., 2001] opens possibilities to couple superposed atoms to larger objects.

Chapter 4

Experimental Results

In this Chapter the experimental progress towards the realisation of the proposal outlined in Chapter 3 is given. Since the experimental requirements are extremely demanding it is important to converge stepwise to the desired setup. Necessarily then several experimental parameters deviate from the designed values given in §3 due to practical considerations.

In Section §4.1 the fabrication of the micro-mirror/cantilever is presented. In §4.2 the techniques used to measure the finesse of a cavity are discussed and illustrated with results from a planar-concave cavity constructed of two large mirrors. In §4.3. the finesse measurements of a cavity involving that micro-mirror are shown. In §4.4. the cantilever mechanical quality factor measurements are given and the integration of the system into a vacuum chamber discussed. In §4.5. calculations of diffraction losses and other loss mechanisms are given, and finally, in §4.6 results from experiments demonstrating ultra-fast all-optical switching are presented.

4.1 Mirror-Cantilever Fabrication

The ultimate goal is to fabricate a mirror of diameter $\sim 10\mu$m and with a reflectivity 99.99998% and have this attached to a micro-mechanical cantilever whose mass is less than the mirror mass, of kHz frequency and which has a mechanical quality factor $Q > 10^5$. Three methods were investigated for fabricating this:

1. Sputtering of a high-reflectivity mirror coating onto a cantilever.
2. Cutting a micro-mirror from a large high-reflectivity mirror and attaching to a cantilever
3. Cutting both micro-mirror and cantilever from a large high-reflectivity mirror.

All three methods are described below. The first leads to bending of the cantilevers while the third is extremely time consuming. The second of these was the most successful and was used to fabricate the samples that were used to produce the results in §4.4.

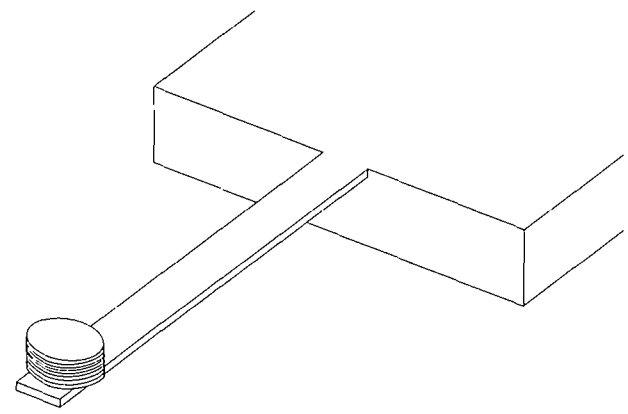

Figure 4.1: Schematic of a Mirror on a Cantilever

The basic configuration desired is a DBR on the end of a cantilever as illustrated in Fig. 4.1. Cantilevers with micron-sized distributed Bragg reflector (DBR) §3.4 mirrors have been constructed for the purpose of variable wavelength Vertical-Cavity Surface-Emitting Lasers (VCSELs) [Vail et al., 1996, Li et al., 1998] but have low finesse, here the whole cantilever is made of a DBR stack resulting in a higher frequency and higher force constant. Also oscillating cavity mirrors of larger dimensions (mm) have been constructed and high finesse achieved ($F \sim 1.5 \times 10^4$) [Tittonen et al., 1999]. None to date come close to combining the reflectivity required for the purpose of the experiment with a cantilever of the specified mass, frequency and quality.

4.1.1 Sputtering of a DBR Mirror onto a Cantilever

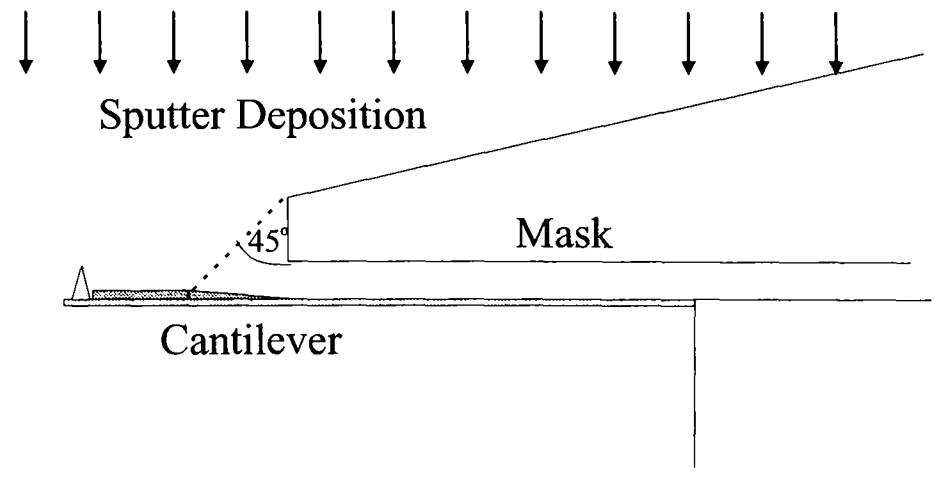

Figure 4.2: A schematic of setup for sputtering the DBR onto the masked cantilever.

One method of fabricating a high-reflectivity mirror of 10μm dimension on a mechanical oscillator is

by coating the end of a silicon cantilever with the distributed Bragg reflector layers (of the type described above). Since the requirements demand a high quality factor, low frequency and low mass, it would be best to coat only the end of the cantilever. This requires the cantilever to be masked such that all but the end of the cantilever (taking into account that sputtering process is not perfect anywhere within a 45 degree shadow of the mask edge), as shown in Fig. 4.2. A larger (mm-sized) silicon oscillator has been coated with SiO_2/Ta_2O_5 and used as part of a high-finesse cavity in Ref. [Tittonen et al., 1999].

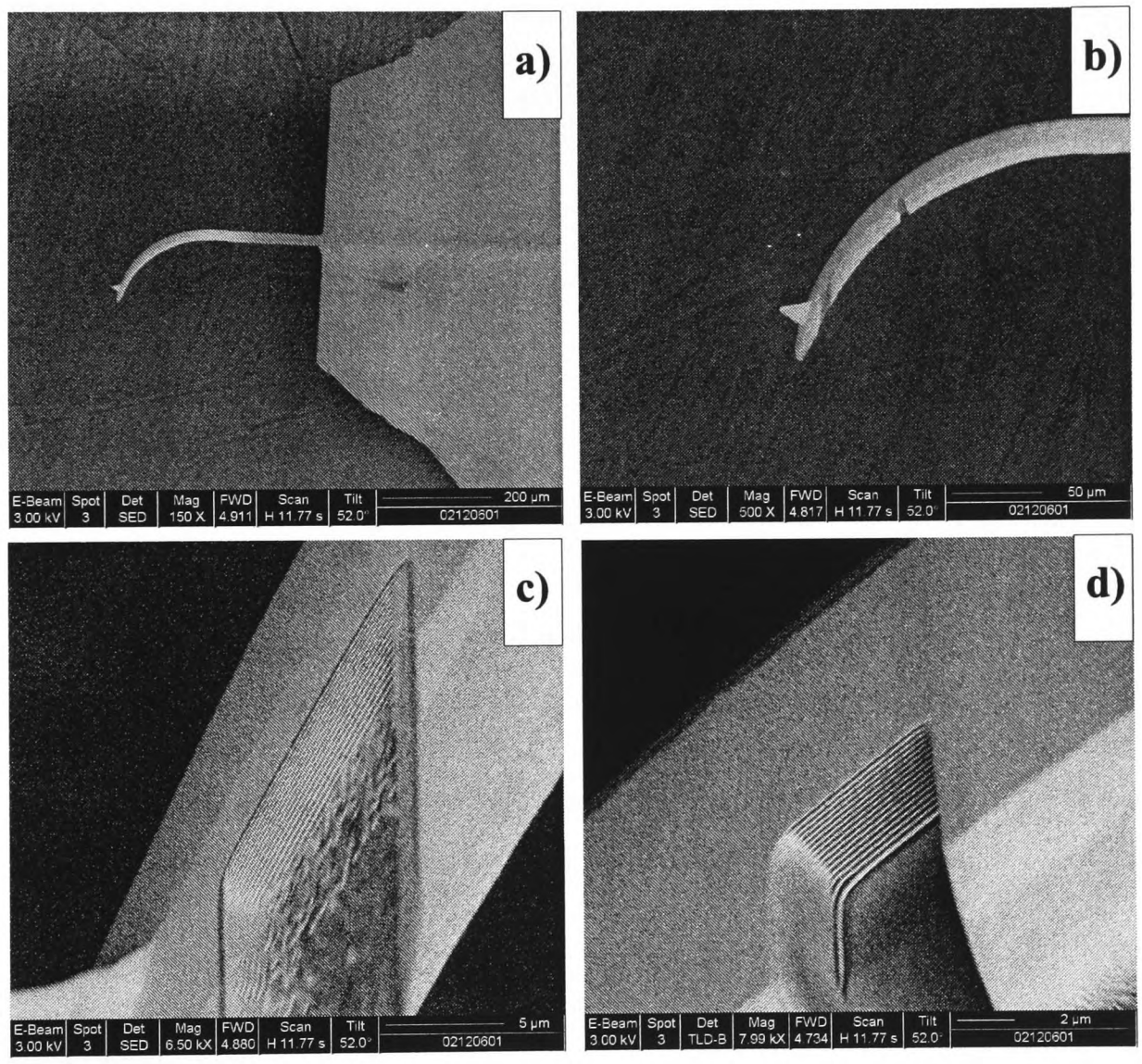

Figure 4.3: SEM images of a coated cantilever. (a) the full, bent cantilever following coating. (b) The cuts made by the focussed ion beam. (c) Layers in the cut nearer the end of the cantilever are shown. The layers get thinner towards the top. The thickness of the 16 pairs is 2.5μm. (d) The layers in the cut nearer the base of the cantilever. The thickness of the 16 pairs is 2.9μm.

Four cantilevers were masked with the $\sim 100\mu$m edges of steel blades and were sent on a special coating run of the commercial coating facility Advanced Thin Films. The coating consisted of a 16-pair SiO_2/Ta_2O_5 distributed Bragg reflector designed for peak reflectance of $R > 99.997\%$ [Advanced Thin Films, 2002] for light of wavelength 780nm at normal incidence.

The cantilevers used were "Contact 10" single crystal silicon Atomic Force Microscope cantilevers of dimension $450 \pm 10 \times 35 \pm 5 \times 2 \pm 1 \mu$m, resonance frequency 10 ± 5kHz, spring constant 0.1N/m and typical quality factor in air of 300 [Nanodevices,], which are known to have high quality factors once annealed and in vacuum [Mamin and Rugar, 2001].

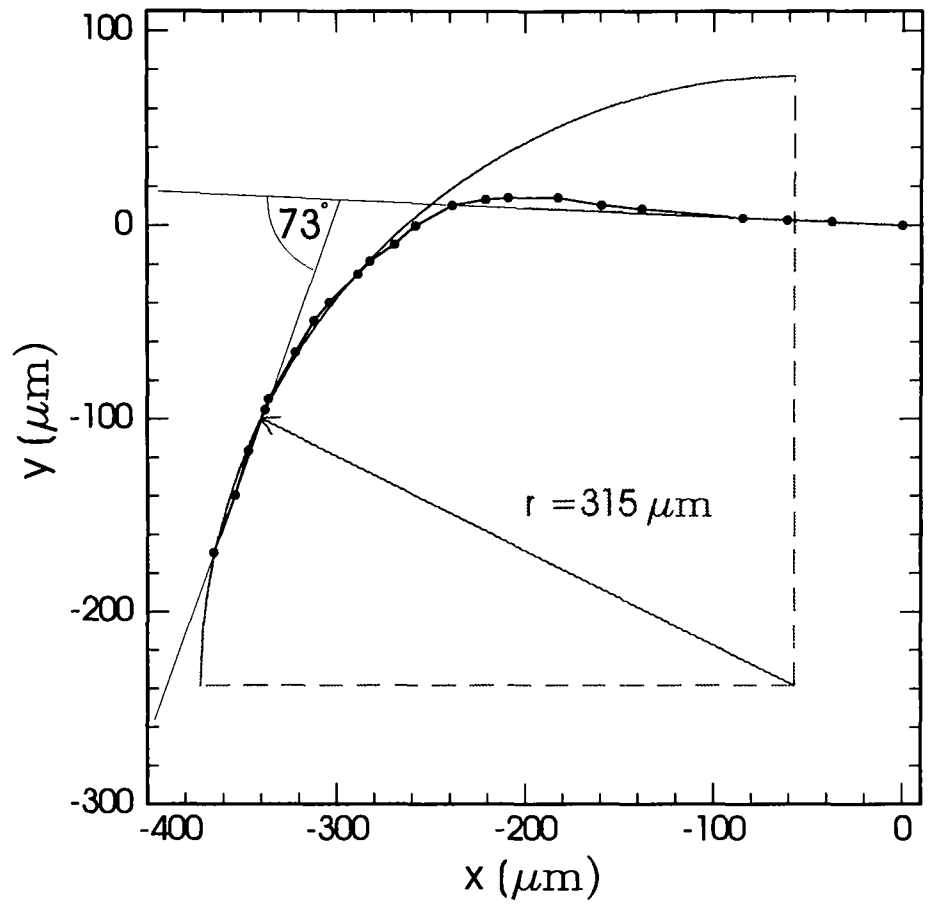

Figure 4.4: The side profile of one of the bent cantilever is shown along with the angle of bending.

A joint scanning electron microscope image of the cantilever samples is shown Fig. 4.3. Unfortunately, the stress in the layers caused the cantilevers to bend, as can clearly be seen. The bending can be attributed to compressive stress of the coatings which is in the range of 10^9 Pa for such material layers [Advanced Thin Films, 2002].

A Focussed Ion Beam (described further in §4.2.2.) was used to cut through the thickness of one of the sample cantilevers in two places – once near the start of the coated (and curved) region and once near the end of the cantilever. This helped us to diagnose the situation: the layers at the end were thinner than in the middle, and that the layers at the top of the DBR were thinner than the bottom – both indicating that the cantilever bent during the coating process. Fig. 4.4 shows the side profile of one of the bent cantilevers showing a bending angle of 73 degrees. One cantilever remained straight because the DBR layers had become detached from the cantilever.

To circumvent these stress problems a more careful masking procedure such as putting a resist layer on the cantilever that allows a much smaller mirror area. Alternatively, the annealing temperature could be

increased or the sample rotated along the cantilever axis during coating.

4.1.2 Cutting a Tiny Mirror from a High-Reflectivity Mirror and Attaching it to a Cantilever

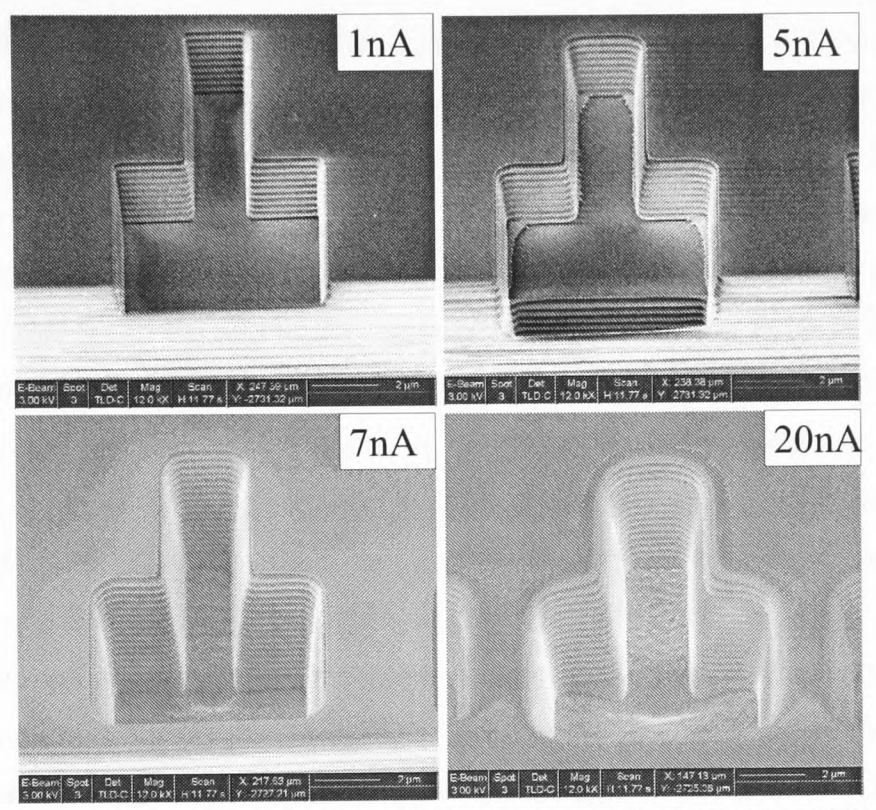

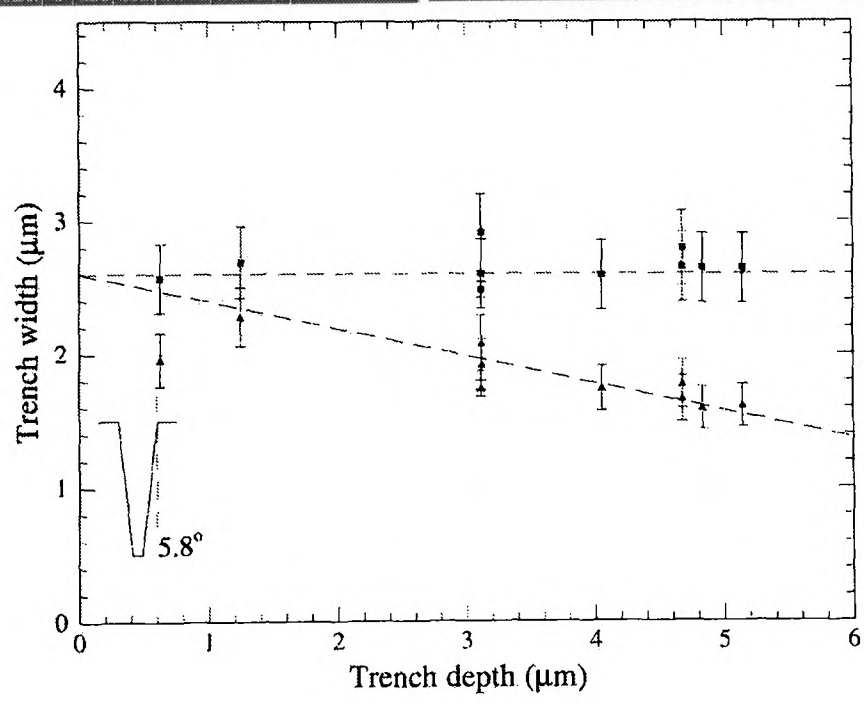

Figure 4.5: SEM images of T-shape cuts by the FIB using beam currents of 1,5,7 and 20nA. The depth of the cut is 10μm for the first two and 20μm for the latter two. The cuts clearly show that lower currents have more vertical edges the mirror's layered structure is clearly visible. Bottom: analysis of the T cut at 7nA.

The experiments in §4.3. make use of the micro-mirror/cantilevers that were made in the way described below.

A silicon substrate was coated by Advanced Thin Films with a 16-pair SiO_2/Ta_2O_5 distributed Bragg reflector designed for peak reflectance of $R > 99.997\%$ [Advanced Thin Films, 2002] for light of wavelength 780nm at normal incidence (the cantilevers used in §4.2.1. were coated in this run also). In the same coating run a SiO_2 substrate was also coated in which the peak reflectance was of the same order. The next step made use of a focused ion beam (FIB) which, situated in a vacuum, accelerates Ga^+ ions with a potential of 30keV. These displace individual or a few atoms of the sample per collision, thus cutting it, with a sub-micron beam diameter. The cutting rate is approximately $\pi/20\mu m^3/s/nA$ which puts our operation near the upper limit of feasibility for the device for reasonable cutting times. The whole operation is carried out under vacuum of 10^{-4}Pa ($= 7.5 \times 10^{-7}$ Torr) and the machine is equipped with an electron column that is used to do in-situ scanning electron microscopy (SEM).

The mirror on the SiO_2 substrate caused the beam to deviate from alignment due to localised charging of the mirror, which did not occur for the mirror on the silicon substrate and so the silicon substrate mirror was used for all cutting described below. T-shaped trenches were cut in to the mirror on the silicon substrate in order to analyse the particle beam profile at different currents 1, 5, 7 and 20nA, as shown in Fig. 4.5. The trench gets narrower at the bottom the deeper the cut. The bottom image of Fig. 4.5 shows the width of the trench measured as function of the trench depth for a 7nA current. The linear fit to the data for a 7nA current the beam cone angle is 6^o as shown in Fig. 4.5. From the images it can also be seen that the 20 nA beam damages the surface up to 500 nm away from the actual trench.

Fabricating the micro-mirror involved two cuts, both illustrated in Fig. 4.6:

1. Normal to the mirror surface, and at its edge, a cut is made in the shape of a ring of inner diameter that of the intended mirror diameter and outer diameter $2 - 4\mu$m larger. The cut depth has to be greater than the mirror layer thickness. The cut is shown schematically in Fig. 4.6(a) and SEM image of the realisation on a mirror is shown in Fig. 4.6(b).

2. Having rotated the sample by 90 degrees, a manoeuver which necessitated the fabrication of a special mount for the FIB, a rectangular cut of width and depth both slightly larger than the mirror diameter is made parallel to and just below the mirror surface such that the mirror is cut almost completely free (Fig. 4.6(c)). It was important that the second cut take into account the beam 6 degree cone angle in order to ensure a parallel cut with respect to the mirror surface. The cut is shown schematically in Fig. 4.6(c) and SEM image of the realisation on a mirror is shown in Fig. 4.6(d).

Following the above cutting the mirror often remains attached to the substrate by a small uncut region and in some cases re-deposited material. The re-deposition occurs more for higher beam currents and currently limits our ability to cut mirrors larger than 35μm. Small mirror cutting times were easier to determine since

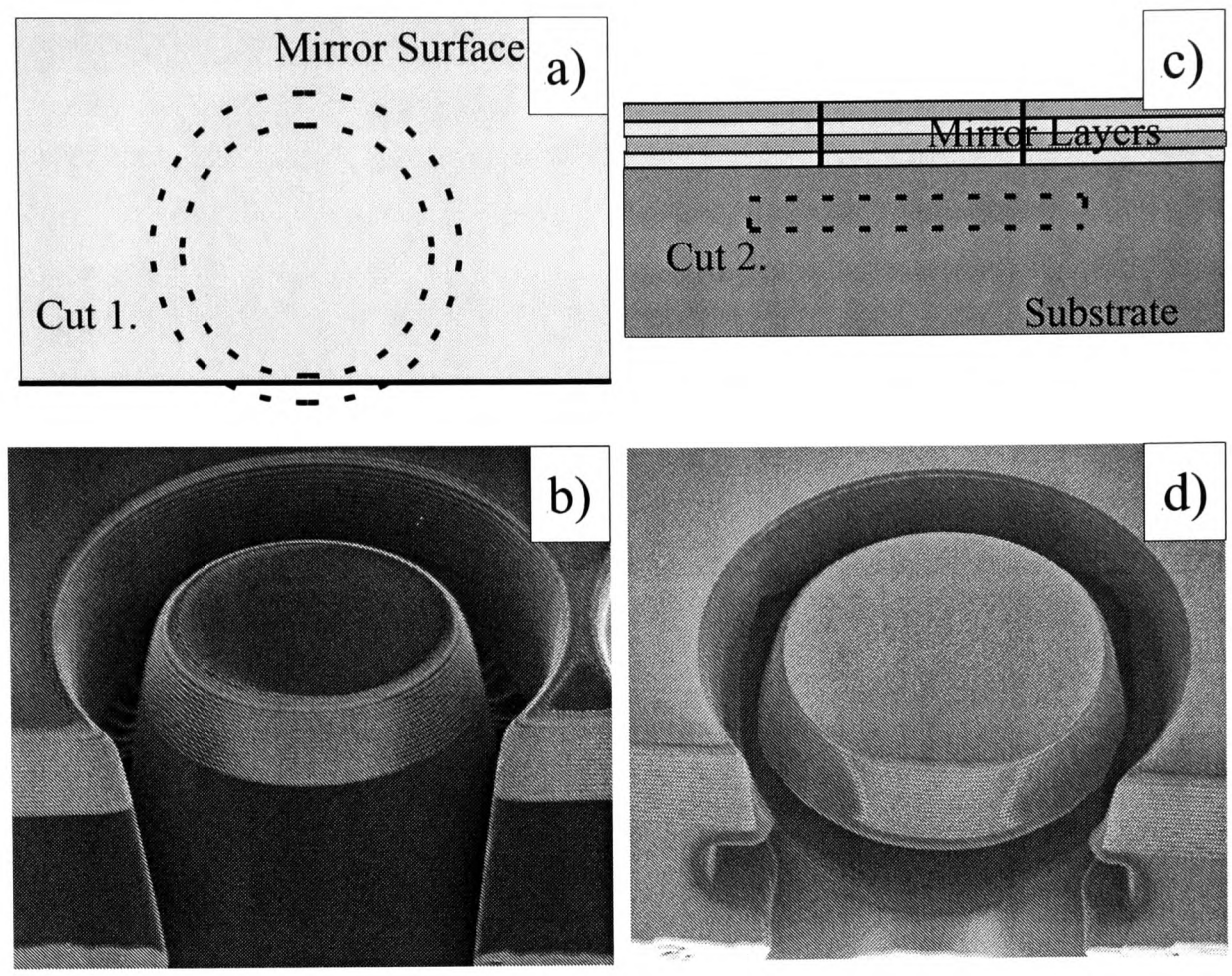

Figure 4.6: Schematic of the two-cut process. The mirror is first cut normal to the mirror surface and in the shape of a ring, (a) then the second cut is parallel and just beneath the mirror surface (b). SEM images of the a mirror after the first and second cuts are shown in (c) and (d).

more trials could be made. A cutting current of 7nA was found to be the optimal balance between cutting speed and re-deposition and cutting angle. The total cutting times for a 7μm diameter mirror using a 7nA beam was 8 minutes and for a 10μm diameter mirror was 10 minutes at the same current. It is critical how much connection is left between the mirror and the substrate since if it is too little then the mirrors are swept away by air either in the venting of the FIB chamber or in moving them from the FIB to the microscope, but if too much is left then a great deal of force needs to be applied for the mirrors release in the 'picking' process outlined below.

In Fig. 4.7 a selection of images of cut mirrors are displayed. The top rectangular mirror was the very first attempt and the cross pattern on the surface is due to the ion beam being dragged across the mirror surface in between cuts, which was later avoided by doing cuts in series. Several 10μm mirrors are shown as well as a single 35μm mirror.

The next step is to detach the mirror from the substrate and attach it to a cantilever. Manipulating the mirror onto the cantilever is done in three steps, as illustrated in Fig. 4.8 largely based on the procedure known for the making of Transmission Electron Microscopy (TEM) samples [Hansma, 2003, Digital Instruments,].

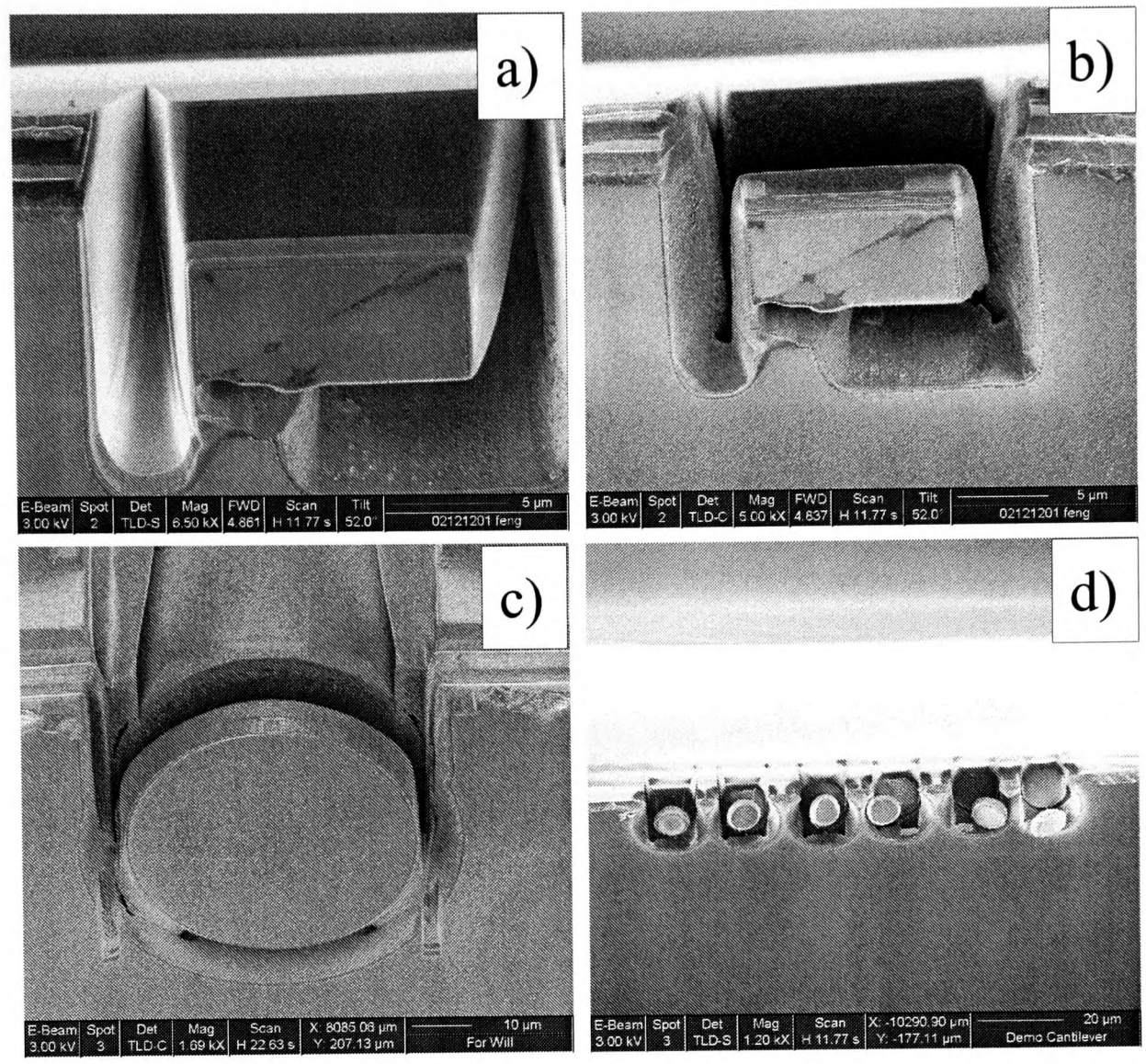

Figure 4.7: SEM images of FIB cut mirrors. The first mirror fabricated, with a rectangular geometry is shown in (a) after the first cut and (b) after the second. The largest mirror made with a diameter of 35μm is shown in (c) and a series of small (10μm diameter) mirrors cut out (in various states of attachment) are shown in (d).

1. Under a microscope, a sharp glass rod with a tip diameter of $3-5\mu$m mounted on a 3-axis micrometer translation stage, is manoeuvered to touch the mirror and snap it from its substrate. Using the rod at a shallow angle to the mirror and a region of the rod about the mirror diameter is lowered onto the mirror. After some bending of the rod the mirror snaps which is seen as a visual jolt. Then the rod is slowly raised.

2. Electrostatic forces allow the mirror to be held to the glass rod for it to be manoeuvered on to an AFM cantilever.

3. A droplet of transparent epoxy glue of diameter $1-5\mu$m is placed on the cantilever directly adjacent to and touching the mirror.

Four cantilevers with mirrors were made in this way with mirror diameters varying in the range 10, 20,

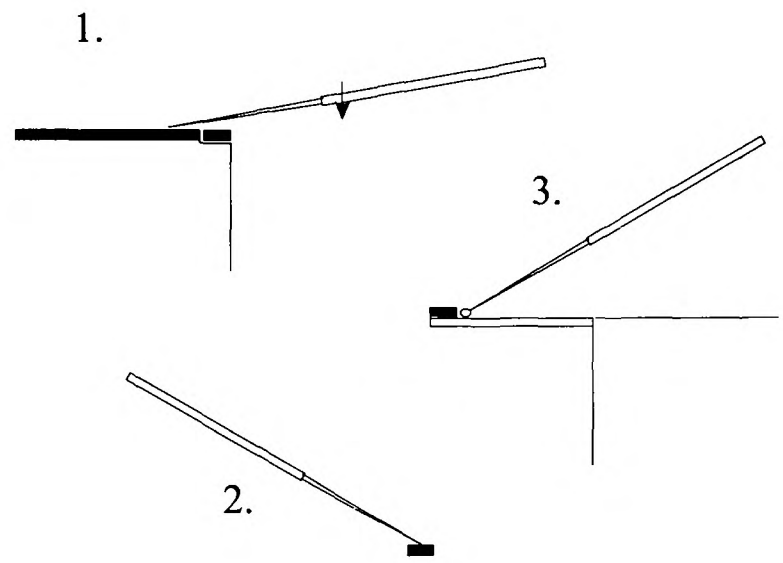

Figure 4.8: Schematic of the procedure, performed using a 3-axis translation stage under a microscope, to detach the mirror from the substrate (1), move to the cantilever (2) and attach to the cantilever (3).

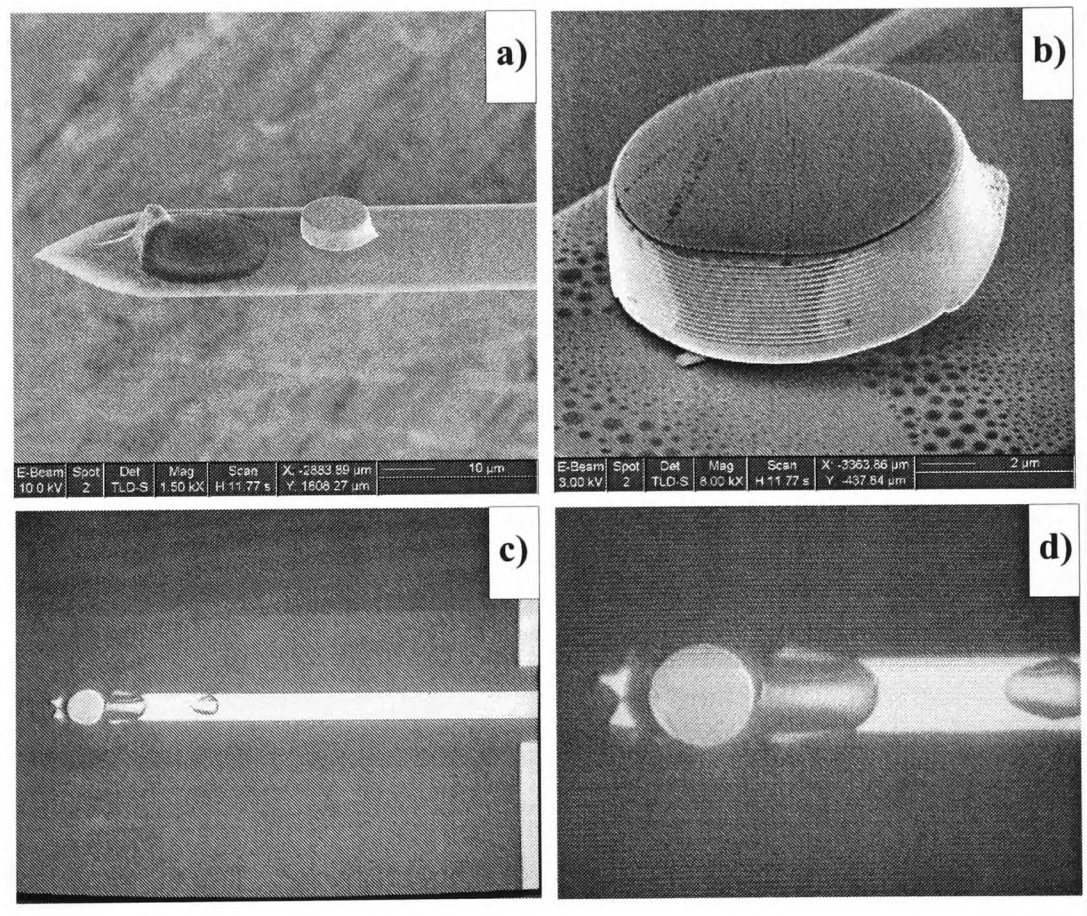

Figure 4.9: (a) SEM image of full cantilever with 10μm diameter mirror. There is a drop of glue next to the (blunted) AFM tip. (b) Close up SEM image of the 10μm diameter mirror showing the mirror layers and the mirror surface which has is slightly scratched. (c) & (d) Microscope photograph of Cantilever with 30μm diameter mirror and droplets of epoxy.

30 and 35μm. In the experiments in §4.3. the cantilever with a 20μm diameter mirror was used. Results of the 10μm ((a) and (b))and 35μm ((c) and (d)) mirrors attachment to cantilevers are shown in Fig. 4.9.

There were several complications to this simple procedure. Firstly, the applied current which is varied in the range $1 - 20$nA to change the speed of cutting, has the side effect of increasing the beam thickness and cone angle, which has to be corrected for. Secondly, cutting the mirror free on the second cut is left largely to trial and error since there is no reliable gauge for the depth of the cut. This is made particularly troublesome by the fact that the second cut, under the mirror, often leads to some re-deposition that connects the sides of the cut mirror back to the substrate, especially for larger mirrors where higher currents are often needed to give reasonable cutting times. This often resulted in the mirrors not snapping free readily in the above procedure. A third cut, similar to the first, may be necessary in order to cut mirrors $> 30\mu$m. Thirdly, in the process of removing the mirror from the substrate onto the glass rod or from the glass rod onto the cantilever, it was sometimes pinged off the rod. Performing the procedure on a clean glass slide allowed it to be recovered by scanning the slide over an area approximately 1mm in radius from the drop point. Finally, the cutting process does not ensure that the mirror surface is parallel to the cantilever surface, both due to the undercutting not being precisely parallel and due to the possibility of the mirror being raised by the epoxy glue. This is clearly seen in Fig. 4.9(b). Despite these hurdles 4 micro-mirrors were cut, detached from the substrate and attached to the cantilever using this methodology.

4.1.3 Cutting a Tiny Mirror and Cantilever from a High-Reflectivity Mirror

A third method to fabricate a micro-mirror/cantilever is to cut it as one unit from a large high reflectivity mirror on a substrate. This is done by having a similar procedure to cut out the mirror, except using a not quite full circle cut from the top, and then using a consecutive set of rectangular cuts around a central volume to become the cantilever as shown in Fig. 4.10(a,b, c). Two cantilevers were made using this method as shown in Fig. 4.10 (c, f).

The trade off between this method and the last is that on the one hand it means that there is no need for the snapping, moving, sticking procedure. But, on the other hand the cutting times are much longer and it means that one has to cut out a cantilever with high quality and the appropriate frequency and force constant. For the latter two properties it is simple to estimate from the cantilever dimensions required to satisfy these (see §3.2.1) but ensuring the quality is more difficult since it depends on having very clean edges to the rest of the substrate (which the picture Fig. 4.10e shows is not the case for these first attempts) and no surface defects or impurities. Clean edges and high Q are already guaranteed in the off the shelf AFM single crystal silicon cantilevers.

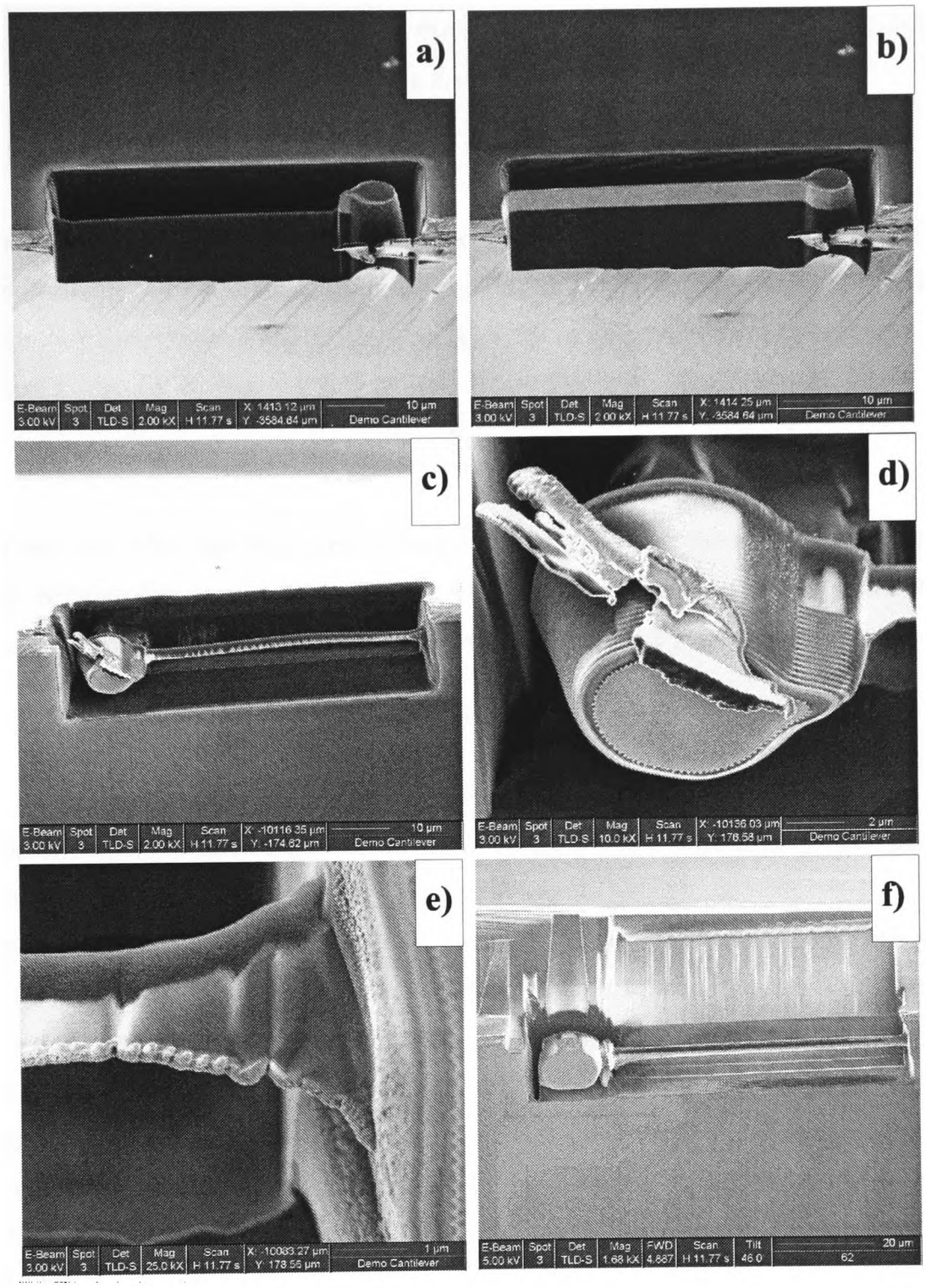

Figure 4.10: SEM imageds of the FIB cantilever and mirror cutting procedure. An outline of the cantilever and mirror is cut from with the beam normal to the mirror plane (a). The DBR layers are etched away on the arm (b). The mirror and cantilever are cut from underneath – parallel to the mirror plane (c). A zoom in of the mirror showing the DBR layers and damage to the side caused by the FIB (d). The base of cantilever (e). A second version is shown in (f).

4.2 Cavity Finesse Measurements for Large Mirror Cavity

In this section a cavity made of two large mirrors is considered. Two concepts which are useful in the following analysis are the finesse F and the quality Q of a cavity. The finesse is given by $F = 2\pi N$ where

N is the number of round-trips light takes before the energy in the cavity reduces by a factor 1/e given now incident light. It is determined from the cavity loss δ_C by

$$F = \frac{2\pi}{\delta_C}. \tag{4.1}$$

The loss is determined by the internal losses per round-trip due to absorption and scattering, and the limited reflectivity of the mirrors r_1, r_2. Considering the case of two infinite plane mirrors of reflectivity r_1 and r_2, and where internal absorption is negligible (e.g. a cavity in air), and where the mirrors are fairly highly reflective such that $1 - r << 1$, then

$$F \simeq \frac{2\pi}{1 - r_1 r_2}. \tag{4.2}$$

For real cavities one must also take into account losses from the sides of the mirrors which have finite extent, alignment losses, stability losses and incoupling losses, all of which are discussed in more detail in §4.5.

A related cavity diagnostic is the cavity quality which is defined as

$$Q = 2LF/\lambda, \tag{4.3}$$

where L is the cavity length and λ is the wavelength. Physically this is 2π times the ratio of the energy dissipated per optical cycle to the energy stored in the cavity, which is the average number of wavelengths travelled by light inside the cavity.

A central requirement from Chapter 3 was the need for a high-finesse cavity with one mirror being microscopic and attached to a cantilever. The first experimental steps taken in this project were in aligning an optical cavity of two large mirrors and measuring its finesse. Two well-known cavity finesse measurement techniques were employed which are described below: (1) Cavity Ring Down (CRD) and (2) Fabry-Perot fringe measurement.

At optical wavelengths mirrors with reflectivity in the '6-nines' region are possible and thus finesses up to 2×10^6 have been demonstrated for a Fabry-Perot resonator of length a few mm at this wavelength [Rempe et al., 1992].

4.2.1 Cavity Ring Down

A cavity with a constant incident field contains a fixed field energy, E_0 and fixed transmitted intensity I_0. If the input is switched off then the energy of the cavity field decays exponentially as

$$I = I_0 e^{-t/\tau} \tag{4.4}$$

where τ the cavity lifetime is year = 2003 given by

$$\tau = \frac{LF}{2\pi c} \tag{4.5}$$

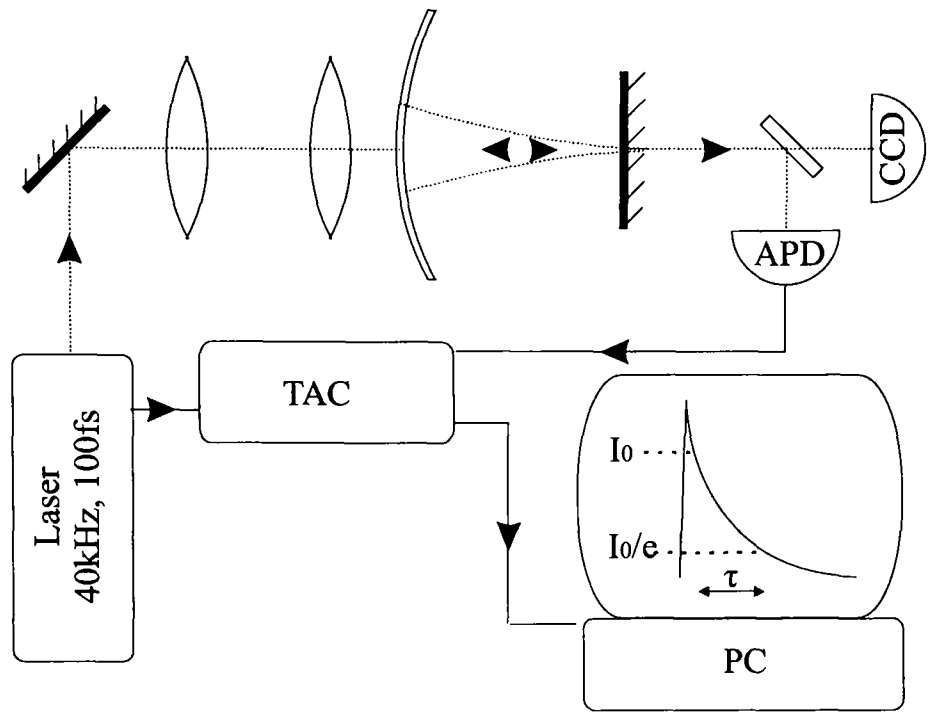

Figure 4.11: A schematic of the experimental setup for cavity ring-down measurement. A laser with repetition rate 40kHz and pulse length 100fs is incident on the cavity. An avalanche photo-diode (APD), capable of detecting individual photons and with timing information accurate to 0.5ns, detects the light transmitted through the cavity. A time-to-amplitude converter (TAC) measures the coincidence rate between the APD signal and the 40kHz trigger from the Regen. Every $= 25\mu$s, there should be a peak in coincidences corresponding to the laser pulse. After this pulse a decay curve is seen.

where c is the speed of light. By measuring the decay time the finesse of the cavity can be determined.

To measure the finesse using Cavity Ring Down (CRD) one needs a light source incident on the cavity which can be switched off in a timescale $< \tau$, a detector sufficiently sensitive to measure the transmitted light through the cavity and with a time resolution $< \tau$. Our setup to measure the decay is shown and described in Fig. 4.11. Its limitations are, firstly, that the time jitter of the avalanche photo diode (APD) of 0.5ns limits the finesses measurement to F 35 for the 2.5cm length cavity. The 40kHz repetition rate means that for a finesse greater than a million the next pulse arrives before sufficient decay has occurred in order to be detected. Thus this method allows measurements of finesse in the range $35 < F < 10^6$. Secondly, after detection of a photon the APD has a dead time of 20ns and thus for decay times $\tau \ll 20$ns, which is the regime in which the experiment operates, one typically has of order one photon per pulse and the measurement curve only results from the average of decays from many pulses over the period of integration, typically $1 - 100$s. APD count rates were 5000s^{-1}, and were always kept much less than the 40kHz repetition rate of the system so to not be flooding the detectors after each pulse obscuring the decay. A schematic of the results expected from the setup is given in the computer screen in Fig. 4.11.

For a higher finesse cavity it is possible to use a simpler technique to measure the finesse due to the fact

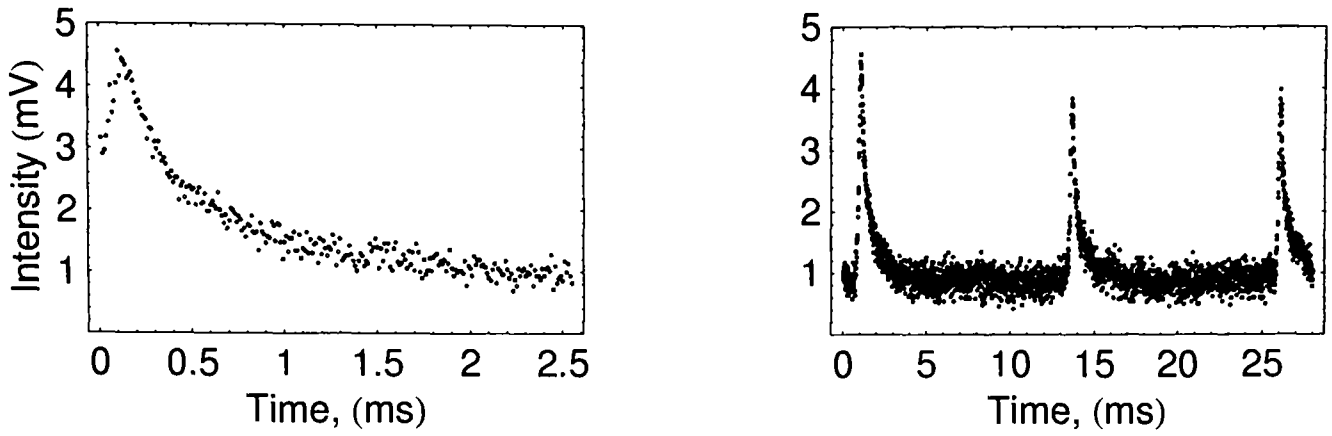

Figure 4.12: CRD measurements for a cavity made of two large mirrors. The transmission of a cavity of length L=1.62cm when illuminated by a diode laser scanning over a range 0.06nm at a frequency of 3Hz around the central wavelength of 780nm. Several Fabry-Perot peaks are seen each with a decay of the field on the right hand side. The Free Spectral Range is 12ms which corresponds to cavity length of 12.6cm and thus a mode making eight round-trips to return to itself is observed. The ring down time is $t = 0.94$ms which for this cavity length implies a finesse of $F = 1.1 \times 10^6$.

that the longer decay times allows the use of much longer cut off times. The method is to use the setup of Fig. 4.13 where a diode laser is incident on the cavity whose wavelength is scanned through several Fabry-Perot peaks (see §4.2.2.) and since the peak widths are shorter than the cavity decay time the decay of the field is observed after each peak.

A planar-concave cavity was built from two ultra-high reflectivity mirrors from Research Electro Optics Inc., one with a radius of curvature of 2.5cm and radius 3mm and one 12.5mm radius flat, both designed for a reflectivity $R > 0.999997$ at 780nm. Data was taken for these mirrors forming a cavity of length 1.6cm (well inside the stable region) using the above method. A CRD time of 0.94ms was observed, as shown in Fig. 4.12. The free spectral range can be calculated using the 12ms separation of the peaks, the scan repetition rate of 3Hz and the scan amplitude of 0.06nm to be 0.0024nm (1.2 GHz). This indicates a cavity of length 12.7cm suggesting that the mode excited in this instance is an eight round-trip mode. The finesse can then be calculated to be 1.1×10^6. This is a factor of 2 below best reported values [Rempe et al., 1992] and consistent with the designed reflectivity of the mirrors.

4.2.2 Fabry-Perot Fringes

A Fabry-Perot cavity has certain frequencies that meet the resonant condition at which the round-trip length exactly equals an integer number of wavelengths

$$\omega = \frac{mc}{2nL}, L = \frac{m\lambda}{2} \tag{4.6}$$

where n is the refractive index of the medium in the cavity (1 in the case of air) and m is the mode of the resonance frequency (a positive integer). The separation of two consecutive resonances, the Free Spectral Range (FSR), given by:

$$FSR[s^{-1}] = \frac{c}{2L}; FSR[m] = \frac{1}{\frac{1}{\lambda} + \frac{1}{2L}}. \tag{4.7}$$

If the coherence length of the laser light is greater then NL then on resonance the intensity of light transmitted through the cavity is enhanced. This can be understood by considering the phases (and therefore constructive and destructive interference effects) of transmitted and reflected beams compared to the incident beam when the cavity meets the resonance condition $L = \frac{m}{2}\lambda$ and when the cavity is off resonance, $L = \frac{m+1/2}{2}\lambda$.

The degree of the cancelling naturally depends on how well the beams are aligned. Assuming zero absorbtion, perfect alignment and high reflectivity mirrors one finds the transmitting intensity is given by [Hecht, 2002]

$$I_T = I_{max}\left(1 + \frac{4R}{(1-R)^2} sin^2(\frac{2\pi nL}{\lambda} cos\theta)\right)^{-1} \tag{4.8}$$

$$\sim I_{max}\left(1 + \frac{F^2}{\pi^2} sin^2(\frac{2\pi L}{\lambda})\right)^{-1} \tag{4.9}$$

where θ is the angle of the incidence beam with respect to the optical axis, n is the refractive index of the medium in between the mirrors, $r = r_1 \times r_2$ where r_1 and r_2 are the reflectivities of the two mirrors. Eq. 4.9 is for a cavity in air with a close to normal incidence beam, large end mirrors and F is the finesse. Plotting this shows the well known Fabry-Perot peaks seen on the right hand side of Fig. 4.13. The peaks are separated by the FSR. The finesse is then defined as the ratio between the FSR and the full width at half maximum of the peaks, which is easily measured.

By scanning the wavelength of the laser over a few times the FSR year = 2003 ($\Delta\lambda = 0.05$nm for $\lambda = 780$nm and $L = 2.5$cm, see Eq. 4.7) one can scan through multiple resonant peaks and troughs. This can be achieved experimentally with a setup shown and described in Fig. 4.13. Initially results were obtained by scanning the cavity length over a distance of a few wavelengths using a piezo-electric driven translation stage, rather than scanning the wavelength of the light, but the latter method proved optimal due to minimal vibrations.

The limitation of the technique is provided by the line-width and wavelength stability of the laser – the maximum measurable finesse is that when either the Fabry-Perot peak full width at half maximum (FWHM) equals the line width or equals the stability. As a guide, for an optical cavity of length in the cm range, FSR= 10^{10}s^{-1}. At optical frequencies $\omega = 10^{14}$s^{-1} thus $\Delta\lambda/(\lambda F) = 10^{-4}$. To measure a cavity finesse of 100, one needs stability of order $\Delta\lambda/(\lambda F) = 10^{-6}$. An external-cavity stabalised diode laser in use in the setup used is stable to typically 0.5MHz over 50ms timescales (or $<$ 2MHz over 20s timescales) [Sacher, 2003] and is thus limited to $F \sim 12000$ for our measurement system. However, with the same setup

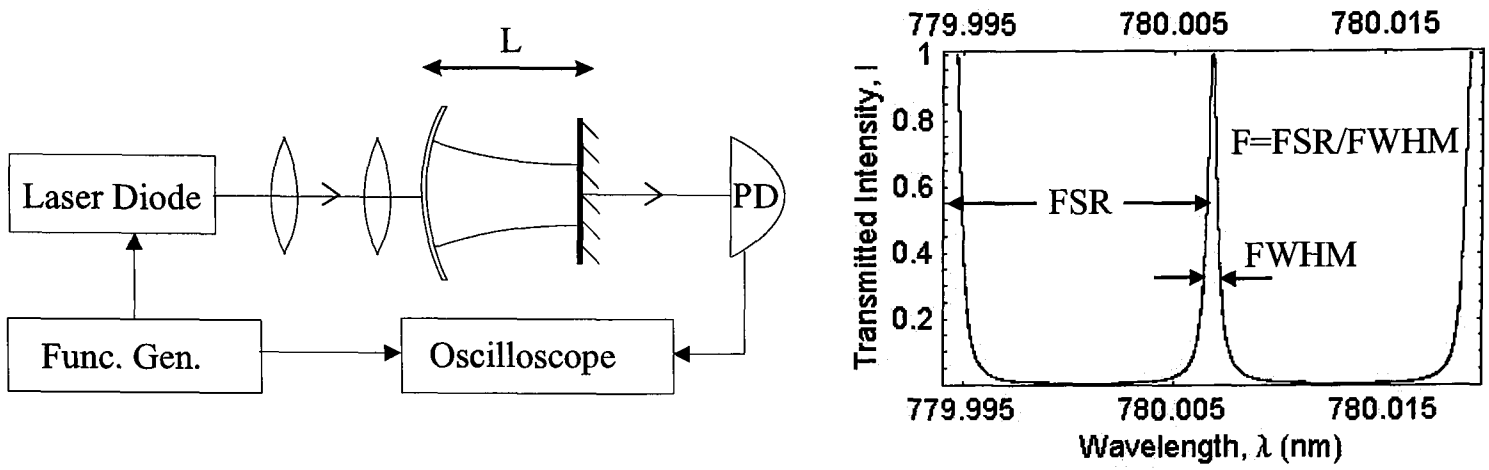

Figure 4.13: LHS: An external cavity diode laser gives continuous wave output of 20mW at 780nm. The intensity of light transmitted through the cavity is measured as the wavelength is varied over 0.02nm at a frequency of 10Hz resulting in the observation of several resonant peaks. RHS: Theoretical plot of intensity of light transmitted through a Fabry-Perot cavity as the wavelength is scanned over two $\times$ Free Spectral Ranges (at $\lambda = 780$nm) for a perfectly aligned cavity involving two mirrors of reflectivity 0.99 ($F = 100\pi$).

it is possible to do cavity ring-down by quickly scanning through resonance peaks and then watching the decay and was used for the measurements made using the large mirror cavity.

Demonstrating Higher Order Modes

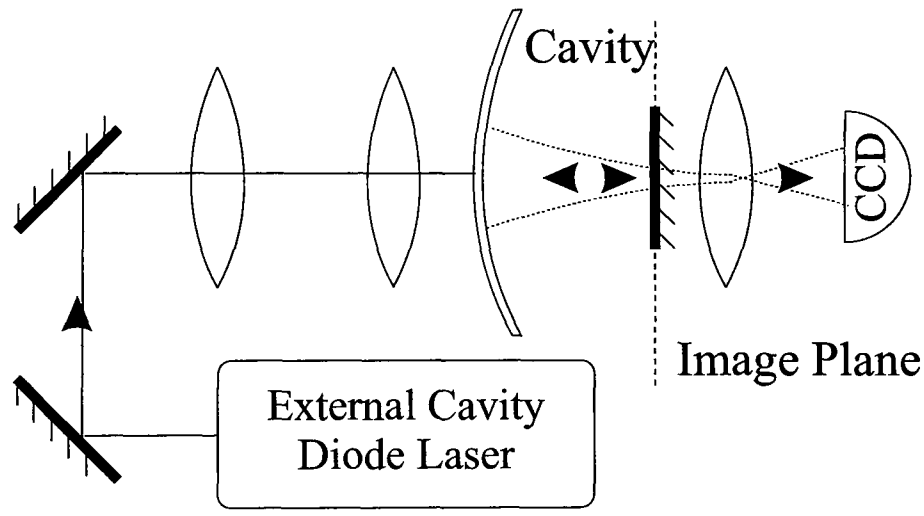

Figure 4.14: Schematic of setup used to show the Hermite-Gaussian higher-order modes using a simple planar-concave cavity.

Since the final cavity configuration is rather unusual, and very sensitive to the beam width at the tiny mirror, in order to get familiar with various cavity field configurations a planar-concave cavity was used to demonstrate several higher order Hermite-Gaussian modes. A simple setup shown in Fig. 4.14 was used. Near the edge of the stability region as $L \rightarrow R$ it was possible to generate these modes by adjusting the incoupling

optics. Figure 4.15 shows measured TEM_{10}, TEM_{11}, TEM_{30} and TEM_{32} modes along with theoretical plots based on Eqs. 3.59. The modes observed match the theoretical plots well with the exception of the last where some spots are less bright than others. This may be because of the finesse being so low that the first few reflections are considerably more prominent.

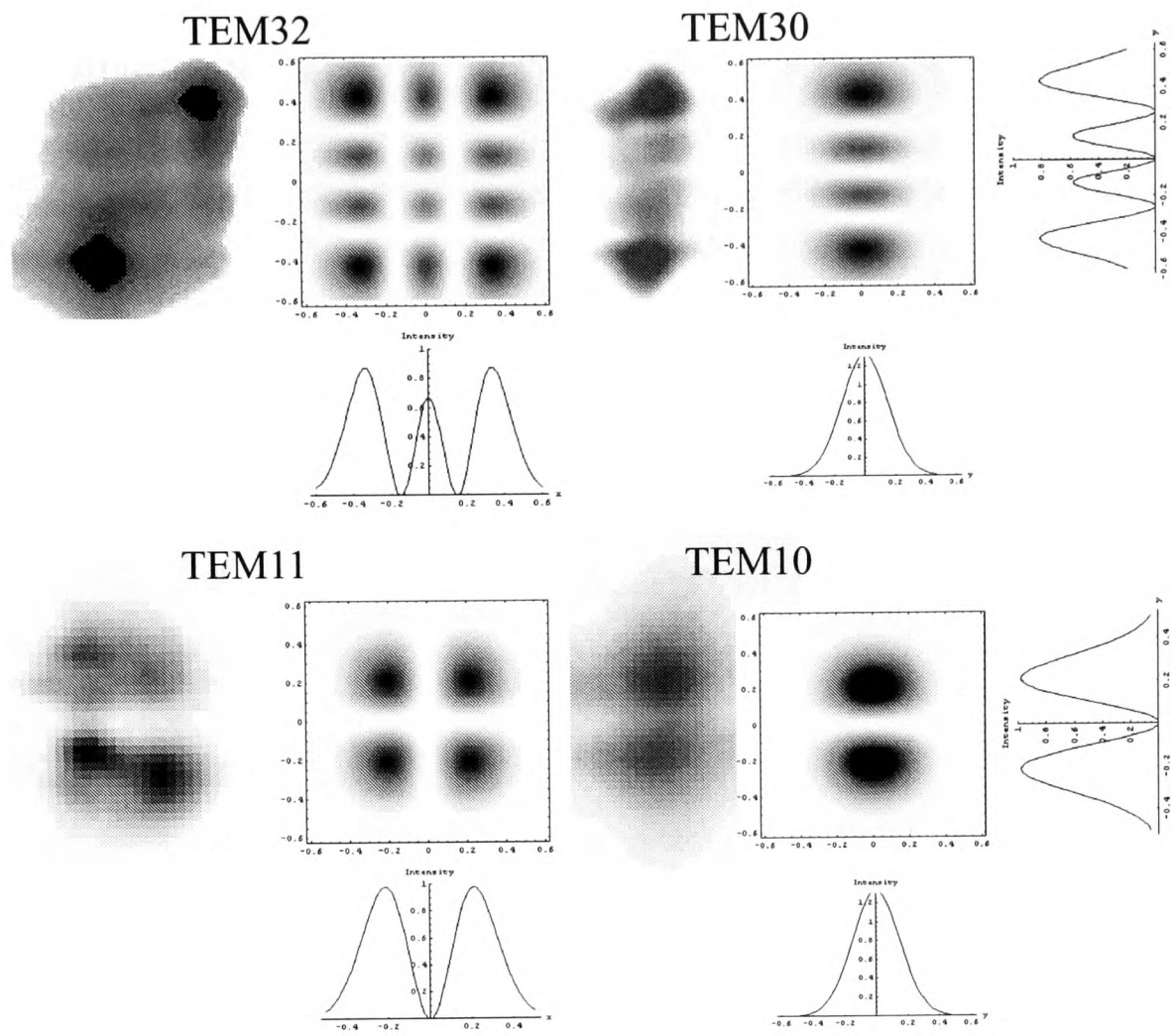

Figure 4.15: Higher order Hermite-Gaussian modes of TEM_{10}, TEM_{11}, TEM_{30} and TEM_{32}. The left hand pictures in each quadrant are the photographs taken with the CCD from setup shown in Fig. 4.14 and the right hand side pictures are those generated by the mode theory given in equations 3.59.

4.3 Cavity Involving a micro-mirror

In this section the integration of the micro-mirror/cantilever developed in §4.1 into a cavity of length 2.5cm is demonstrated and finesse measurements taken. To my knowledge the results below present the first demonstration of a macroscopic (cm) cavity with such a micron-size mirror attached to a micro-mechanical cantilever since all previous near-hemispherical cavities have involved a large flat mirror.

The cavity uses one large concave mirror, radius of curvature $R = 2.5$cm and the micro-mirror. It is evident that the geometry has to be very close to hemispherical (near to $R = L$) in order that the spot size on the small mirror is sufficiently small. This is close to the unstable region on the cavity stability graph in Fig. 3.8: relative vibrations of the mirrors in this configuration can put the cavity into an unstable geometry, especially considering that the small mirror is on a small force constant oscillator.

From §3.3 it can be seen that the spot size on either mirror are inversely related: the spot at the micro-mirror tends to 0, and the spot at the large curved mirror tends to a solid angle of 2π Steradians, as $L \rightarrow R$. The design of the incoupling optics and the cavity stability are much more critical than for finesse measurements of a large mirror cavity. The optimum cavity length is approximately given when the ratio of spot size to mirror aperture is equal at both ends since this minimizes power losses. In this section the 10μ radius mirror attached to a Contact 10 cantilever, as fabricated according to the procedure described in §4.1.2 is integrated into a cm sized cavity. The large curved mirror is a 2.5 cm radius of curvature, 3mm radius mirror manufactured by Research Electro Optics Inc. for a reflectivity $R > 0.999997$ at 780nm. For such cavity mirrors equal ratios of spot radius to mirror radius at each end is given for a focus radius at the micro-mirror of $w_0 = 4.55\mu$m, and radius $w_1 = 1.36$mm at the large mirror. This corresponds to a cavity length $L = 24.99972$mm (see Eqs. 3.65, 3.66).

4.3.1 Cavity Mount

The first step was to design and construct a cavity mount in which to house the micro-mirror/cantilever and large mirror in a way that enabled; (1) cause and fine adjustment of their relative position (x,y,z) and angle (θ_x, θ_y), and; (2) which kept the optics very rigid and stable. The design of the second iteration of such a mount is shown in Fig. 4.16 and enabled 5 degrees of freedom of the cantilever, θ_x, θ_y, x, y and z, where z is the optical axis, with respect to the other cavity mirror. The cantilever orientation and position with respect to the large mirror can be moved coarsely using the 4 outer screws seen on the left hand side of the mount, for movements in the x-y plane and 4 inner screws for movement in z, θ_x, θ_y. This coarse adjustment allows a x,y,z range of $\sim$ 1mm and resolution of 0.01mm and θ_x, θ_y range of 10 degrees and resolution 0.3 degrees. The cantilever and large cavity mirror are held together with a Piezo Electric tube, shown in Fig. 4.16. with 4 quandrant contacts on the outside and one on the inside allowing fine adjustment of z, (x, θ_x), (y, θ_y), where the brackets indicate coupling, of range 6μm, resolution 10nm, in translation and range 0.1^o and resolution 0.001^o in rotation. Pictures of the realised mount are also shown in Fig. 4.16 and the full exploded diagram of the mount is given in Appendix A.

4.3.2 Cavity Incoupling

The incoupling optics were setup for the optimal cavity mode as calculated in §3.4. Incoupling to the cavity is through the curved mirror since incoupling through the cantilever lead to considerable scattering of the beam,

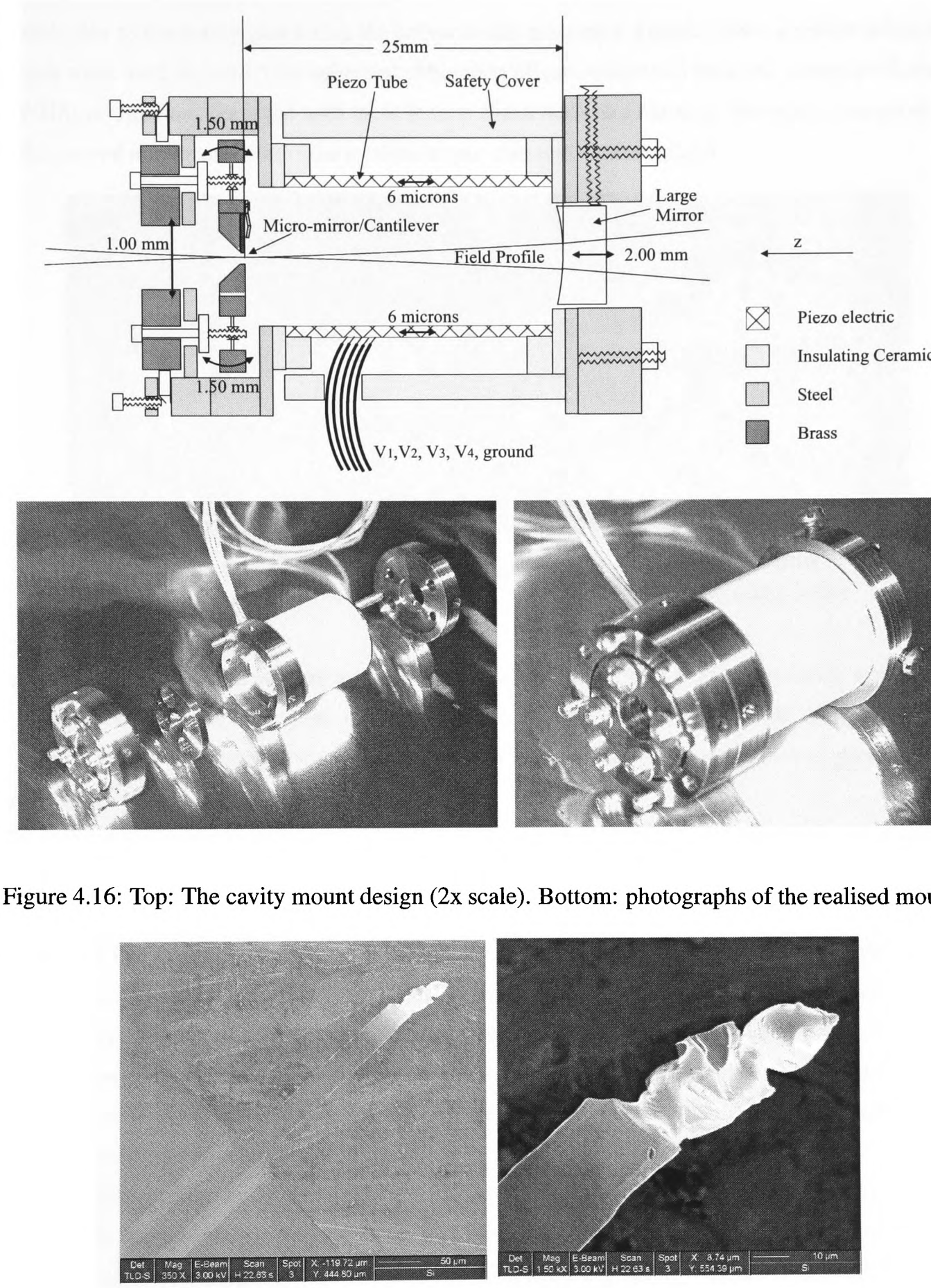

Figure 4.16: Top: The cavity mount design (2x scale). Bottom: photographs of the realised mount.

Figure 4.17: SEM image of a micro-mirror/cantilever melted due to a too intense beam.

presumably due to the epoxy glue fixing the mirror to the cantilever. Lenses with a gradient refractive index with depth were used to correct for spherical abberation effects which can limit the minimum focus size. A spot FWHM of 4μm was achieved with these lenses. Since the beam has to go through a non-gradient index lens – the curved mirror substrate – the minimum spot size was closer to 6μm.

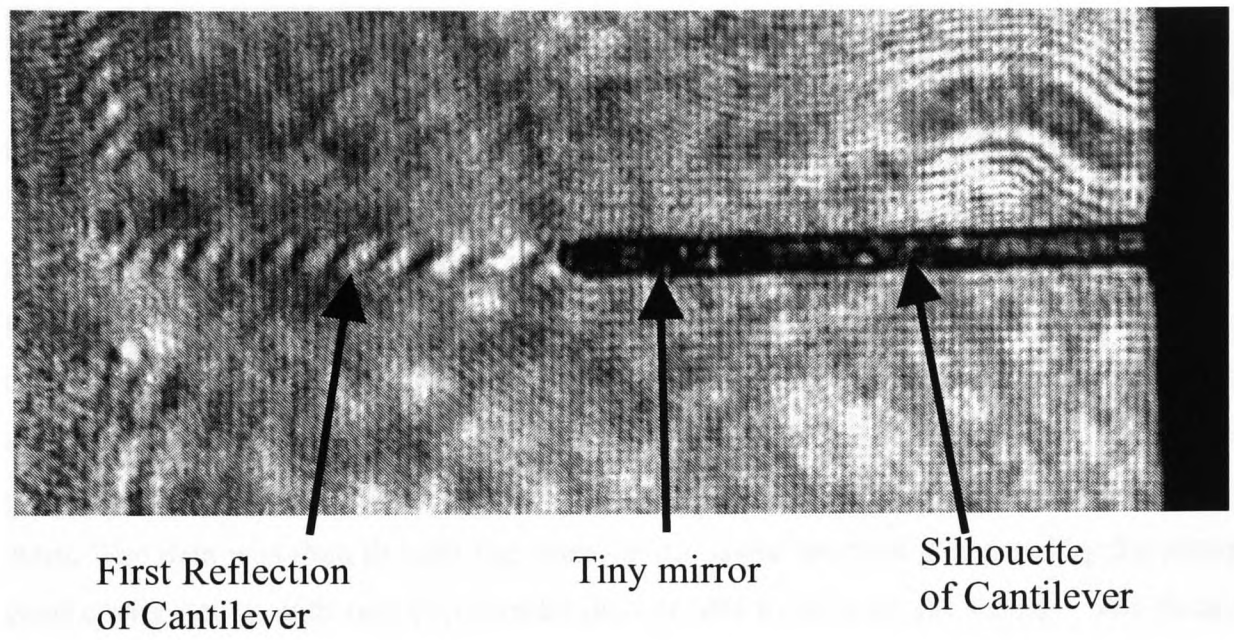

Figure 4.18: A CCD picture looking in the plane of the cantilever from behind the cavity when illuminated by a HeNe beam (with no incoupling optics) according to Fig. 4.11. The silhouette of the cantilever along with the first reflected image of the cantilever, reversed in orientation is shown. A fringe pattern can be seen on the reflected image.

One has to be careful not to shine too much light on the cantilever so as to melt it, as was discovered empirically and is shown in Fig. 4.17! This calculation was encouraged by my supervisors following me showing them this image. Considering the thermal conductivity of the cantilever ($C = 148$ J.kg^{-1}K^{-1}), silicon absorption of $\alpha = 10^5$/m at 780nm wavelengths [Palik, 1997] and assuming that the mount to the cantilever is an infinite bath at room temperature, then the maximum power incident on the cantilever so as to avoid melting (at 1710 K) is 60μW. This means that the maximum incident light on the cavity must be 60μW/F. The limit shall be an order of magnitude lower power for the cantilever anticipated for use in the final experiment due to lower mass.

Initial alignment was achieved by using a CCD camera to image the plane of the cantilever. An un-focussed HeNe laser beam (no incoupling optics in the setup) incident on the cavity according to the setup shown in Fig. 4.11. The image seen is shown in Fig. 4.18. Ensuring that the cantilever first reflected image (on the left) was in focus simultaneously with the cantilever silhouette (on the right) ensured that the cantilever was positioned close to the focus of the large curved mirror: this was adjusted using the course z adjustment of the cantilever position. Aligning the images such that the part where the micro-mirror sat were co-aligned made sure that the element optical axes were aligned: this was adjusted by altering the lateral position (x,y)

and angle (θ_x, θ_y) of the cantilever. The incoupling optics were incorporated and set to achieve a diffraction limited spot size of 3μm, and adjusted so that the spot lay on the mirror. Further alignment was made by adjusting the voltage on the piezo contacts to maximise the finesse observed in real time.

4.3.3 Cavity Ring Down Results

CRD data was taken with the cavity aligned and misaligned. Results are shown in Fig. 4.19. The data for the misaligned cavity is fit well by a Gaussian pulse of width 0.34ns, limited by time jitter of the APD. The longer decay curve associated with the aligned cavity shows a steep decay region immediately after the pulse which flattens to a shallower slope after $10 - 15$ns. This was first fit with the convolution of the pulse Gaussian with two exponential decays. The fit showed decay constants of 1.43 ± 0.3ns and 9.8 ± 1.2ns with relative power in the later exponent of $5.6 \pm 0.9\%$. The fit was seen to be inaccurate in several regions due to underlying pulse structure clearly seen in the log plot. The anomalous–looking peaks on the decay, correspond to small power leakage of the pulsed laser source, their separation in time corresponding to one cavity round-trip time for that system. The data was then fit with the convolution of the function generated by the interpolation of the misaligned cavity decay with two exponential decays (the fit seen on the graph). The decay constants were found to be 0.9 ± 0.03 and 11 ± 1ns. The longer ring down time corresponds to $F = 415 \pm 30$ and contains $6 \pm 1\%$ of the input power. This indicates that the input beam is coupling to more than one mode and not perfectly to the high finesse one. This behaviour can be expected since the solution beam profile is non-Gaussian (as will be seen in §4.5.) and this cannot be coupled to perfectly with a Gaussian beam.

4.3.4 Fabry-Perot Results

The cavity was illuminated by a continuous wave (external-cavity diode) laser whose wavelength is being scanned 0.05nm at a frequency of 1-10Hz using the setup shown in Fig. 4.13. By measuring the width and free spectral range of Fabry-Perot peaks seen the finesse was shown to be $> 1000 \pm 50$. The deviation from the CRD results can be attributed to the fact that the alignment is more precise with the Fabry-Perot method since it is easier to adjust in real time. The scan frequency was kept below the threshold at which oscillations in the cavity energy are expected to interfere with the form of the Fabry-Perot peaks [Rohde et al., 2002].

Fabry-Perot measurements were taken at different cavity lengths as the length was being optimised. These are shown in Fig. 4.27 along with the calculated limiting finesse due to diffraction effects.

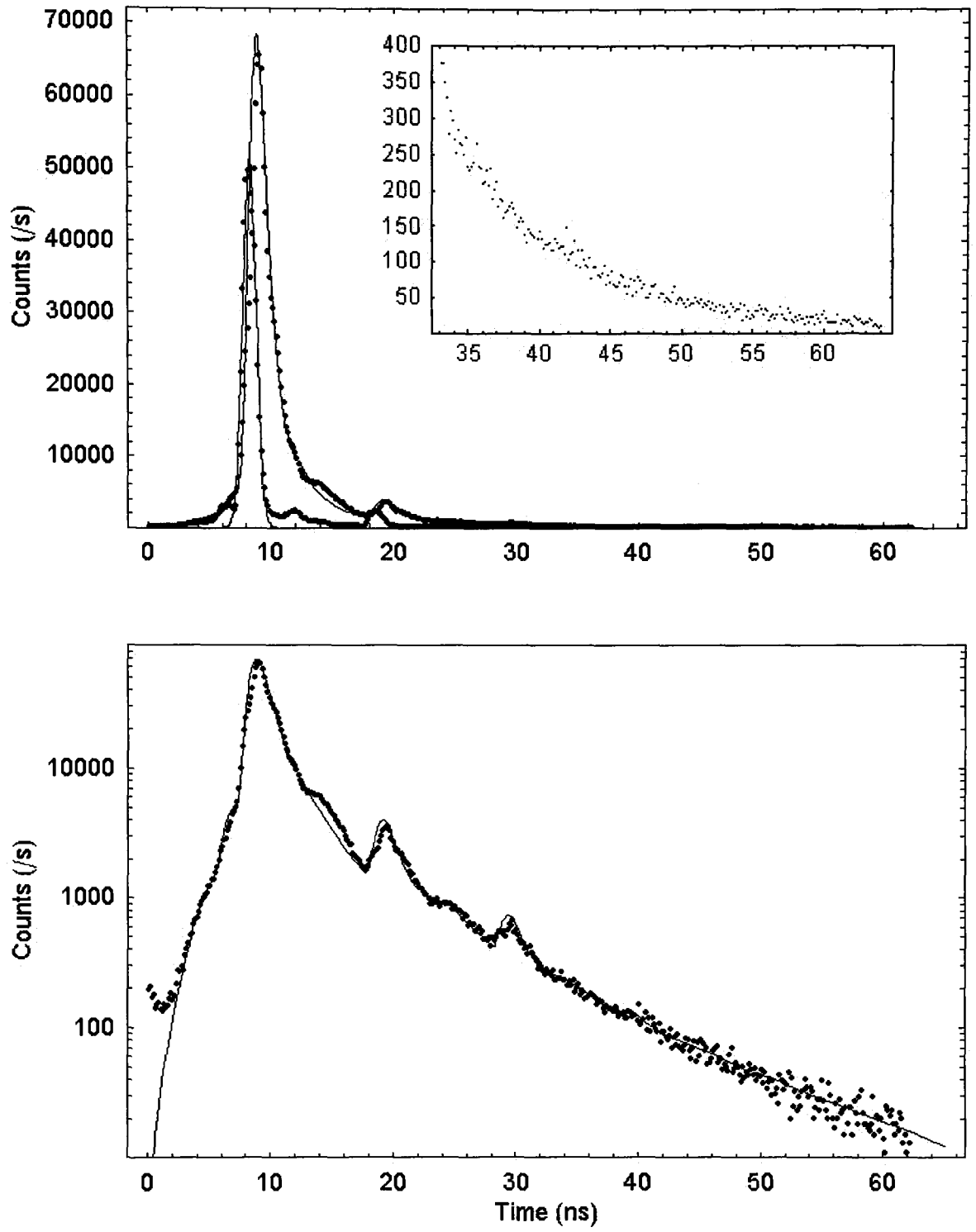

Figure 4.19: Cavity Ring Down results for the cavity with micro-mirror/cantilever: Top: the field exiting the cavity is measured versus time after the pulse. The near-Gaussian peak is a misaligned cavity. The longer decay is that of the aligned cavity showing a finesse of $F = 415 \pm 30$ at 12ns after the pulse (shown in the inset). Bottom: the same on a log plot showing a non-single exponential decay.

4.4 Integration in a Vacuum and Cantilever Quality Measurements

A vacuum chamber of inner height and diameter approximately 20cm was designed and built for the purpose of integrating the cavity into it and is shown in Fig. 4.21. Initial tests allowed a pressure of 10^{-4}Pa (=

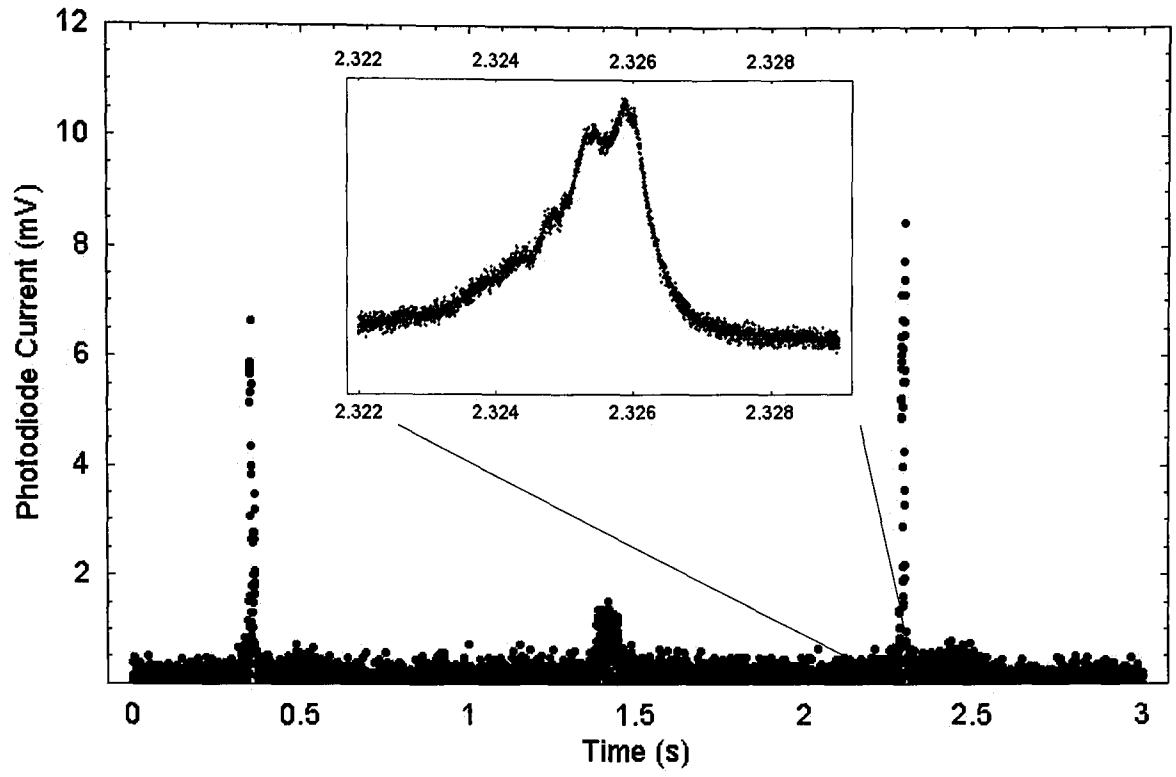

Figure 4.20: Power transmitting through the cavity onto a photodiode is measured against time whilst the wavelength is scanned 0.05nm at 0.1Hz (see setup in Fig. 4.13). The cavity Fabry-Perot peaks show a free spectral range of 2s, and a peak full width half maximum (see inset) of < 2ms.

10^{-6}Torr) at room temperature using a turbo pump. Heating the chamber to $150 - 200^{o}$C whilst being evacuated helps to reduce the pressure considerably. This will allow the turbo pump to evacuate to 10^{-6}Pa at which point the ion pump will be used to reduce the pressure further. An ion pump is of particular value to this experiment since it has no moving parts and so does not add mechanical noise. The chamber seals, ion pump and valves are set to achieve 10^{-10}Pa ($= 10^{-12}$Torr) or better. Cooling to cryogenic temperatures as in Ref. [Gabrielse et al., 1990] should then enable us to reach the regime required for the final experiment.

To measure the cantilever quality a vibrometer is used which consists of an interferometer with the cantilever at the end of one arm. The interference pattern seen is sensitive to changes in the interferometer arm length caused when the cantilever vibrates. The Fourier transform of the spatial motion gives a frequency spectrum of the cantilever motion amplitude. The width of the natural resonance of the cantilever in frequency space is determined by the quality factor.

The equation for a forced harmonic oscillator of mass m, frequency ω_m is

$$m\ddot{x} + b\dot{x} + kx = ks_0 sin(\omega_m t) \tag{4.10}$$

where the drag coefficient $b = \frac{\omega_m m}{Q}$ and s_0 is the initial strain amplitude. The solution shows that the amplitude varies with driving frequency ω as

$$x_{max} = \frac{s_0 \omega_m}{\sqrt{(\omega_m^2 - \omega^2)^2 + (\omega_m \omega / Q)^2}}. \tag{4.11}$$

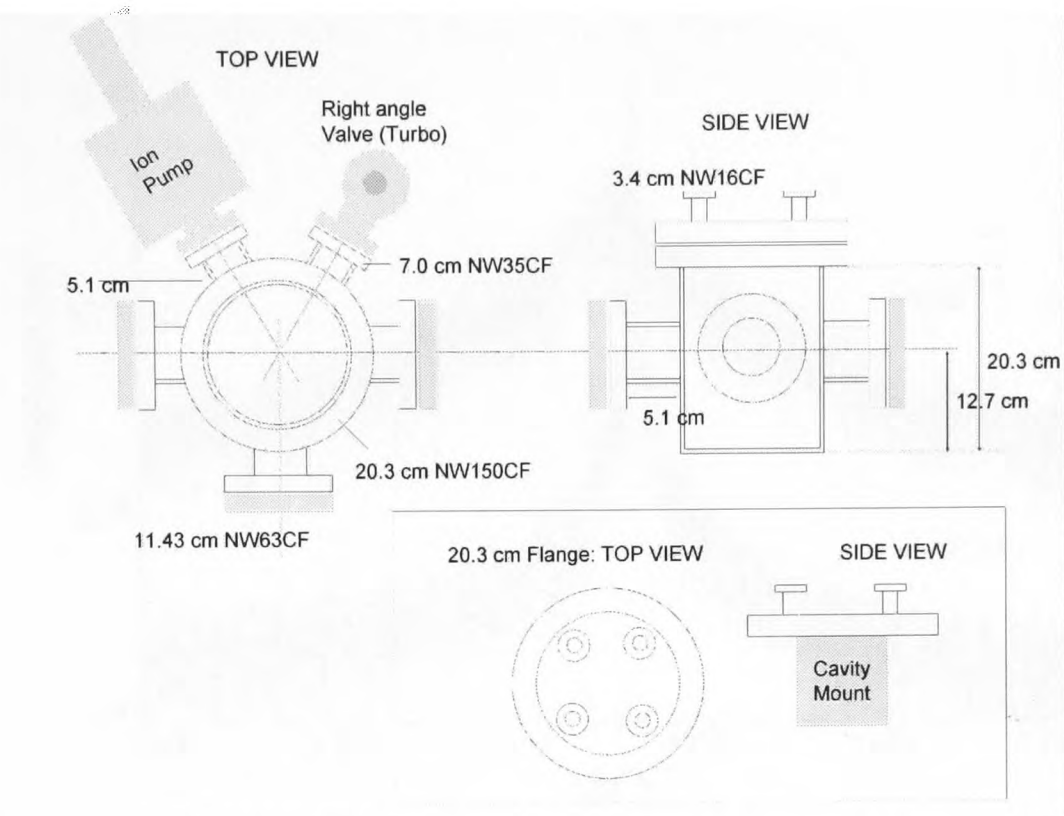

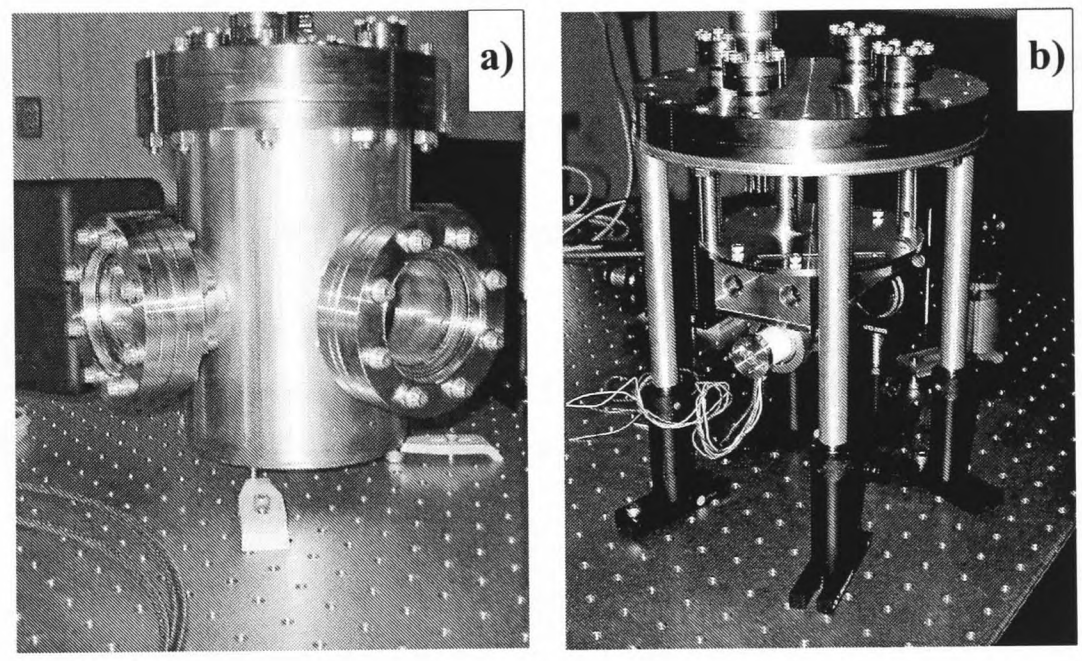

Figure 4.21: Chamber design and chamber pictures.

This can be fit to the vibrometer data to determine the quality factor Q. Measurements were made in a vacuum chamber at various pressures. Fig. 4.22 shows two measurements taken, one at atmospheric pressure and the other measurement at a pressure of 10^{-2}Pa. Fits to the data using the above theory show cantilever quality of $Q = 30$ and $Q = 22,000$ for the two pressures. At 10^{-2}Pa ($=$ 40milli-Torr) the quality was still rising with decreasing pressure suggesting that the quality is still pressure limited.

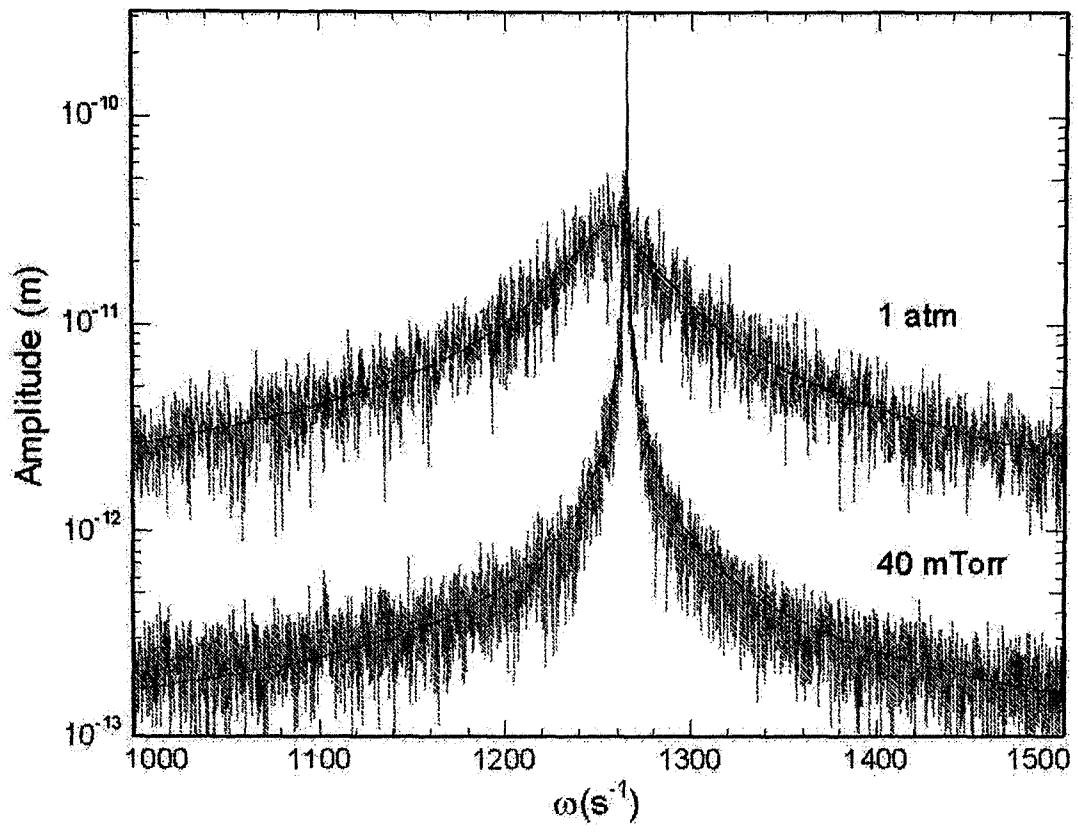

Figure 4.22: The resonance peak of a silicon Contact 10 cantilever at atmospheric pressure and 10^{-2} Pa (=10^{-4}Torr) measured using a vibrometer showing quality factors of 30 and 22000 respectively.

4.5 Limitations on the Cavity Finesse

Below five possible limitations to the cavity finesse measured in the preceding section are explored. In practice the finesse is limited by Mirror Reflectivity (F_r), Scattering and Absorption (F_s), Diffraction Losses (F_d), Geometric Losses (F_g) and Mechanical Stability (F_m), and the overall finesse is given by the following relation:

$$\frac{1}{F} = \frac{1}{F_r} + \frac{1}{F_s} + \frac{1}{F_d} + \frac{1}{F_g} + \frac{1}{F_m}. \tag{4.12}$$

Each factor is discussed below, apart from F_s which is the limit on the finesse due to internal scattering and absorption in the cavity which are assumed to be negligible ($F_s > 10^6$).

4.5.1 Limiting Finesse due to the Finite Mirror Reflectivity, F_r

For high reflectivity mirrors F_r can be approximated by

$$F_r \sim \frac{2\pi}{1 - r_1 r_2} \tag{4.13}$$

where r_1 and r_2 are the reflectivities of the two mirrors. The 16-pair DBR of use on the micro-mirror has a design reflectivity $r > 0.99997$, and the large curved mirror has a manufacturer minimum reflectivity of

$r > 0.999997$. Thus theoretically $F_r > 1.9 \times 10^5$. The large mirror is known to be this reflective from the measurements in §4.2.1. However, the cantilever mirror might not be as good as the designed DBR structure due to (a) spoiling of the mirror layers by the focussed ion beam which incorporates Gallium ions and defects in the mirror at the edges, a too high density of which would create a change in refractive index or could cause absorption and thus ruin the mirror; (b) the mirror surface may be scratched by the 'picking' process or could leave dust or epoxy glue on the mirror surface; (c) the epoxy glue used to fasten the mirror to the cantilever may cause stress on the mirror layers causing deformation from flat or inherent layer stress may do the same.

The Gallium ions only have a penetration depth of $<$ 500nm and so are not expected to damage the mirror away from that distance from the mirror edge which remains the bulk of the mirror. The scratching and deformation can be seen to be low in SEM images. Thus it seems unlikely that these are the limiting factor for the finesse of 1000 seen experimentally is §4.3.4.. A definite answer can only be determined experimentally upon elimination of the other potential finesse limiting factors.

4.5.2 Limiting Finesse due to Diffraction Losses, F_d

These are losses associated with finite sized mirrors. A first næve approach leads to the simple power loss of a Gaussian beam reflected by a finite mirror which is given by

$$\delta = \frac{2}{\pi w^2} \int_a^\infty 2\pi r e^{-2r^2/w^2} dr = e^{-2a^2/w^2}. \tag{4.14}$$

where a is the radius of the mirror and w is the beam radius at the mirror. The loss determines the finesse as

$$F_d = \frac{2\pi}{\delta}. \tag{4.15}$$

From Eq.(3.65) the losses per mirror reflection for the solution mode for the cavity with no apertures is

$$\delta^2 = e^{-\frac{2\pi a_0 a_1}{\lambda R}}. \tag{4.16}$$

For our setup the losses are 6.4×10^{-5} thus $F_r = 1.9 \times 10^5$.

However, it turns out that the real cavity losses are significantly lower than this due to the fact that the actual cavity solution modes have not got a Gaussian beam profile but adjust themselves to the finite size mirrors. Gaussian optics no longer holds here and one must calculate the beam behaviour numerically. One must use the Huygen's integral to determine the field $u_2(r_2, \phi_2)$ at a distance L from a given aperture (or in our case finite mirror) given an arbitrary input field $u_1(r_1, \phi_1)$. In cylindrical coordinates (r,ϕ) and given a circular aperture radius a the Huygen's integral is given by [Siegman, 1966]:

$$u_1(r_2, \phi_2) = \frac{i}{2\lambda} \int_{r_1=0}^{a} \int_{\phi=0}^{2\pi} u_1(r_1, \phi_1) \frac{e^{-i2\pi\rho/\lambda}}{\rho} cos\theta(r_1 r_2) r_1 d\phi_1 dr_1 \tag{4.17}$$

where θ is the angle between the element axis and ρ is the displacement between a point on the input aperture (r_1,ϕ_1) to any point on the observation plane (r_2,ϕ_2) which for spherical mirrors of curvature R_1 and R_2 is

$$\rho = \sqrt{L^2 + g_1 R_1^2 + g_2 R_2^2 - 2R_1 R_2 cos(\phi_1 - \phi_2)}, \tag{4.18}$$

where

$$\begin{aligned} g_1 &= 1 - L/R_1 \\ g_2 &= 1 - L/R_2. \end{aligned} \tag{4.19}$$

This integral is performed twice – once at each mirror aperture – to get the field profile at one round-trip, relative to the input field. In general the E-field profile at aperture 2, E_2, is given from the profile at aperture 1, E_1, and vice versa by the following relations

$$\begin{aligned} E_2 &= \gamma_1 \int_S K E_1 dS_1 \\ E_1 &= \gamma_2 \int_S K E_2 dS_2 \end{aligned} \tag{4.20}$$

where K is the round-trip propagation kernel (Huygens kernel) which operates on the initial field in a given plane to give the new field profile after one cavity length. These are eigenvalue equations for the propagation of the beam in the cavity and γ is the eigenvalue which is related to the cavity loss as $1 - |\gamma|^2 = \delta$. For a general $ABCD$ system in 1-dimension K is given by [Siegman, 1966](page 781)

$$K(x_2, x_1) = \sqrt{\frac{i}{B\lambda}} e^{\frac{i\pi}{B\lambda}(Ax_1^2 - 2x_1x_2 + Dx_2^2)}. \tag{4.21}$$

Note that K is in general not Hermitian and therefore the existence of a complete orthogonal set of eigen-solutions is not guaranteed. It has no known exact solution except in a few particular cases, e.g. the confocal and parallel-plane geometries but for the near-hemispherical resonator of interest it must be solved numerically. Fox and Li first performed such a numerical analysis using a method of successive approximations [Fox and Li, 1968]. For this one can imagine a light pulse whose length Δz (where z is the optical axis which lies along L) is much smaller than the cavity length L but much larger than the wavelength, $L >> \Delta z >> \lambda$. The Fox and Li method is equivalent to propagating this pulse of light back and forth in the cavity until the field profile is self repeating except for a reduction in power $1 - |\gamma|^2$ per round-trip. The loss is related to the finesse limitation as

$$F_d = 2\pi/(1 - |\gamma|^2). \tag{4.22}$$

Li implemented this approach for the near-hemispherical resonator [Li, 1965] and Taché et al [Taché, 1984] gave an approximate expression for some of the results of Ref. [Li, 1965] but neither studies, or any other found by the author, contain results directly relevant to our mirror sizes.

Under the Fresnel approximation a cavity with two spherical mirrors has

$$\rho \sim L + (r_1 + r_2 - 2r_1 r_2 cos(\phi_1 - \phi_2))/(2L) \tag{4.23}$$

and noting the relation

$$e^{in(\pi/2-\beta)} J_n(xy) = \frac{1}{2\pi} \int_0^{2\pi} e^{ixycos(\alpha-\beta)-n\alpha} d\alpha \tag{4.24}$$

the eigenvalue integral equations reduce to

$$\begin{aligned} F_n^{(2)}(r_2) &= \frac{\gamma_n^{(2)}}{\sqrt{r_2}} \int_0^{a_1} K_n(r_2, r_1) F_n^{(1)}(r_1) \sqrt{r_1} dr_1 \\ F_n^{(1)}(r_1) &= \frac{\gamma_n^{(1)}}{\sqrt{r_1}} \int_0^{a_2} K_n(r_2, r_1) F_n^{(2)}(r_2) \sqrt{r_2} dr_2 \end{aligned} \tag{4.25}$$

where F is the component of the field $u = F(r)e^{-i\phi}$. The Huygen's kernel K for two circular mirrors was shown by Fox and Li to be [Li, 1965]

$$K_n(r_2, r_1) = \frac{i^{n+1} 2\pi}{\lambda L} J_n(\frac{2\pi r_1 r_2}{\lambda L}) \sqrt{r_1 r_2} e^{-\frac{i2\pi(g_1 r_1^2 + g_2 r_2^2)}{\lambda L}}. \tag{4.26}$$

In our case the flat mirror ($R_1 = \infty$) has $g_1 = 1$, and the mode of interest is the TEM_{00} mode for which n= 0. In accordance with the Fox and Li approach, a method of successive approximations was used to solve Eqns. 4.25. The Mathematica routine used is given in Appendix B within which each step is briefly described. The beam profile converged to the solution mode profile in $15 - 1000$ round-trips, depending on the exact cavity parameters computed. The routine was verified against results for a hemispherical cavity performed by Li [Li, 1965] (see Appendix B). The integration step size used was $a/50$ at each mirror. Repeating a case with $a/500$ showed agreement up to an error in γ of 4×10^{-7}.

For the experimental setup of §4.3. the radius of the small flat mirror is $a_0 = 10\mu$m and the radius of the large curved mirror is $a_1 = 3$mm and has a radius of curvature $R = 25$mm. The solution where the mirror separation is such that the ratio of beam width to mirror width is identical at each ends is given by Eqs. 3.65, 3.66 as being when the beam focal radius is $w_0 = 4.55\mu$m and the beam radius at the large mirror $w_1 = 1.36$mm which dictates a cavity length of 24.99972mm. In such a configuration the beam radius of curvature matches the mirror surfaces and as such is infinite at the small mirror and 25mm at the large curved mirror. This is expected to be close to the lowest loss mode for a cavity with finite mirrors of the above dimensions. The input beam used $u_1(r_1, \phi_1)$ is Gaussian and an exact solution of this geometry assuming no edge effects which is a mode which one can couple to well using a real laser beam.

Solving Eqs. 4.25 for these parameters gives a power loss per round-trip of the solution mode due to diffraction of $1 - |\gamma|^2 = 1.5 \times 10^{-7}$. The error calculated is 4×10^{-7} and so one can only reliably state that the loss $< 4 \times 10^{-7}$. This corresponds to a finesse $F_d = 1.6 \times 10^7$, coincidentally just above the finesse required for the experiment (§3.2.1.). The shape of the solution beam that was converged to, as seen at the

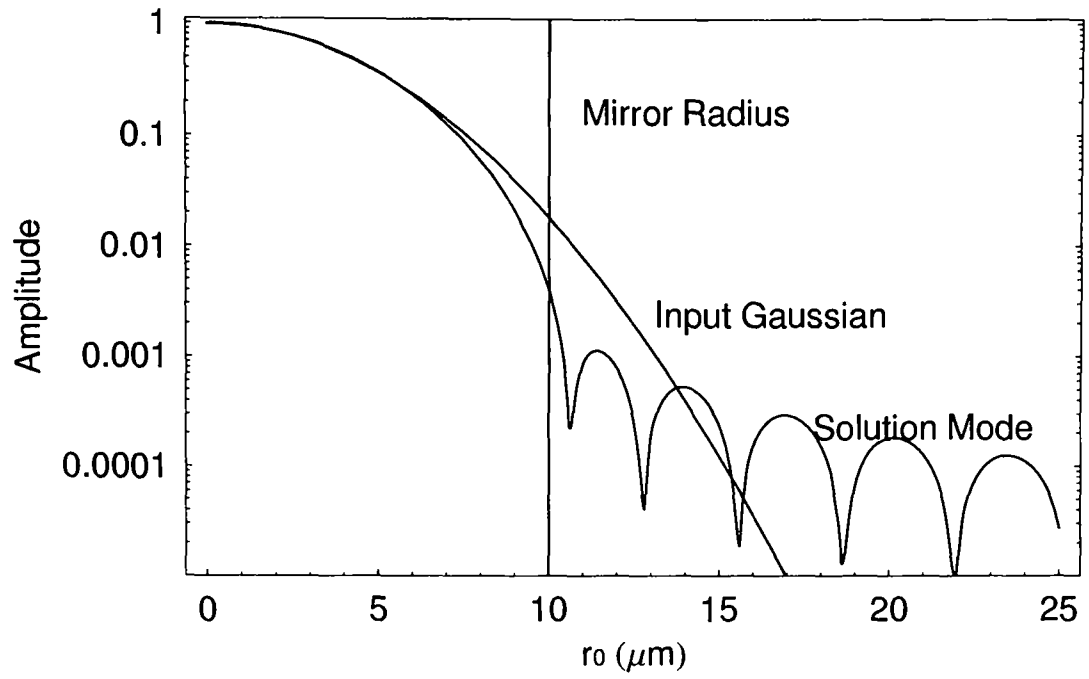

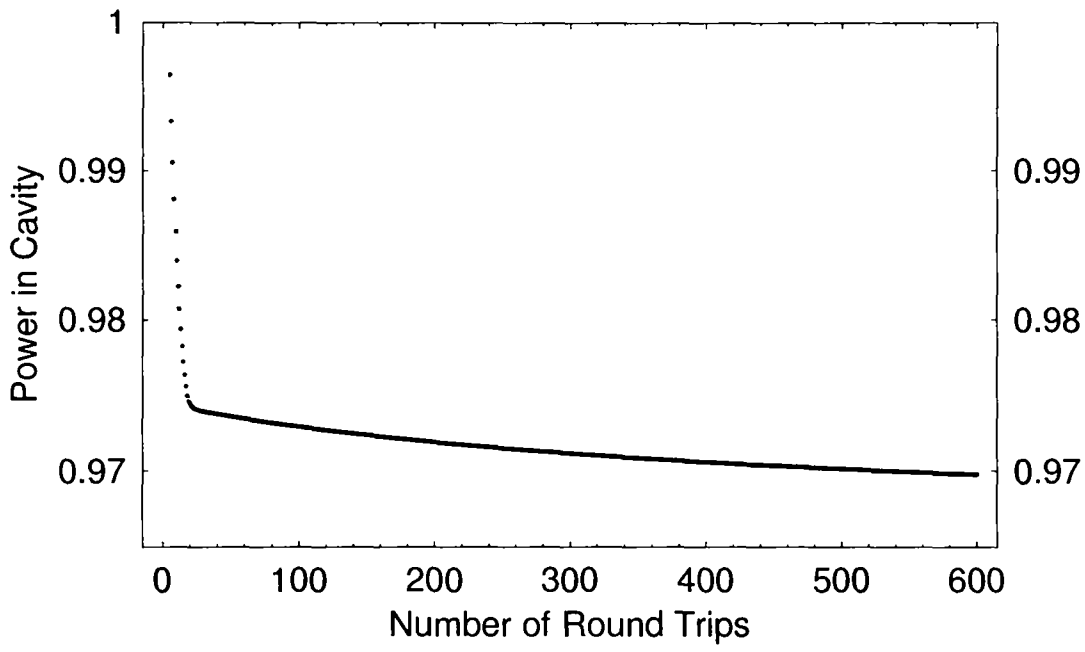

Figure 4.23: Results of diffraction loss calculation. Top: a log plot of the amplitude profile (the field amplitude versus distance from the centre of the field) at the small mirror for the solution mode for the cavity with diffraction loss. The input Gaussian profile is overlayed for comparison and the mirror size indicated with a vertical line. Bottom: the energy in the cavity as a function of number of round-trips for ideal alignment. The eigenvalue, (which represents 1-loss), starts at a rate of $|\gamma|^2 = 0.996$ per round-trip and quickly the mode adapts such that the loss is $|\gamma|^2 < 0.99998$ after 35 round-trips. It then slowly improves to $|\gamma|^2 < 0.999997$ after 500 round-trips.

small mirror, is shown in Fig. 4.23. The Gaussian input beam is shown for comparison. In addition the decay in power of the field as a function of number of round-trips is shown, where it can be seen that the loss is higher initially (steeper slope) but levels off to a constant after 38 round-trips. This can be compared to the CRD graph of Fig. 4.19 noting that 6 round-trips corresponds to 1ns: it has a similar form but lower losses. Thus this explains the need for 2 exponential decays in order to approximately fit the CRD results (§4.3.3.).

The loss of 4×10^{-7} expected from these considerations is a factor 430 less than the næve initial estimate assuming a Gaussian solution mode. This can be understood from the evolving beam profile which tends to "tuck in" the wings of the beam as seen in Fig. 4.23 where the solution mode profile sharply reduces in amplitude just before the mirror edge at 10μm. The losses are increased to 9.5×10^{4} (2.3×10^{-3}) for a 8μm (6μm) radius flat mirror.

It should be noted that the Fresnel approximation used for Eq. 4.23 requires that

$$\frac{a^2}{\lambda L} << (\frac{a}{L})^2 \tag{4.27}$$

which physically demands that the ratio of length of the cavity to the mirror diameter be large. This condition is not met in our geometry for the integral over the large mirror. However, there is an inconsistency with this limitation since there is no such equivalent near-field limit for the paraxial approximation, which is formerly equivalent to the Fresnel approximation. It turns out that the Huygen's integral in the Fresnel approximation can be applied when the above condition is not met so long as the beam is truly paraxial [Siegman, 1966](p. 634). The ratio of sizes of the terms in z to those in the x,y plane in the wave equation is given by $\theta^2/4$, where θ is the angle between the wave front and the optical axis. In our case of $\theta < 1/15$, the ratio of the terms in z to those in x and y is $1 : 10^3$ and thus the beam is paraxial to a good approximation. Given perfect alignment the diffraction losses are clearly not the limiting factor on the finesse observed in §4.3.4..

4.5.3 Limiting Finesse due to Geometric Losses, F_g

Geometric losses are effects due to non-perfect alignment of the cavity mirrors. In a near-hemispherical cavity an angular misalignment of either mirror is equivalent to simply moving the element axis away from the centre of the curved mirror – a situation that is identical to the aligned case except for where the mirror edges are with respect to the beam. This effectively reduces the mirror aperture, and thus acts to increase the diffraction losses. Losses due to length misalignments can be calculated by directly inserting that into the diffraction loss calculation. Thus by calculating changes in length and mirror sizes, geometric losses can be assessed. The diffraction calculation was thus repeated for different values of a_0, a_1 and L and the results are summarised in Table 4.5.3. The power loss 'CRD curves' for varying ΔL, a_1 and a_0 are shown in Figs. 4.24, 4.26, and 4.25 respectively. On the top of each is the mode amplitude profile at the small mirror after the loss per round-trip was at a constant (i.e. when the solution mode has been found).

The relative angle of the elements axes of the two mirrors was estimated to be < 1 degree. With a cavity

a_0 (μm)	a_1 (mm)	Δ L (mm)	Convergence	Loss, $\lvert\gamma\rvert^2$	F_g
10	**3**	**0**	~ 1000	$< 4 \times 10^{-7}$	1.7×10^7
-	4	-	> 1000	$< 3 \times 10^{-6}$	$> 2.1 \times 10^6$
-	2.5	-	20	3.7×10^{-5}	2.5×10^5
-	2	-	58	7.1×10^{-4}	8.8×10^3
14	-	-	> 168	$< 9 \times 10^{-6}$	$> 7.0 \times 10^5$
8	-	-	> 162	6.6×10^{-5}	9.5×10^4
6	-	-	42	2.3×10^{-3}	2.7×10^3
-	-	1	75	2.0×10^{-5}	3.1×10^5
-	-	3	396	9.2×10^{-5}	6.8×10^4
-	-	10	152	7.9×10^{-4}	8.0×10^3
-	-	30	12	2.1×10^{-2}	3.0×10^2
-	-	100	18	3.8×10^{-2}	1.7×10^2
-	-	300	12	0.68	9.2
-	-	1000	10	0.84	7.5
14	4	-	> 1000	$< 4 \times 10^{-7}$	$> 1.7 \times 10^6$

Table 4.1: Predicted diffraction losses and maximum finesse for the cavity with various micro-mirror radius a_0, large mirror radius a_1 and cavity length deviations ΔL from the optimal 24.99972. The cavity has one large mirror of curvature R=25mm, and $\lambda = 780$nm light is used. These together with the values in the first three columns of the first row (in bold) represent the 'standard' setup. A dash means no change from the standard setup. The calculation considers the field over a radius $5a_0$ at the small mirror end and $5a_1$ at the large mirror and with an integration step size of $a_0/50$ and $a_1/50$. The values with $>$ or $<$ used are incidences where the program failed to converge fully after 1000 iterations. Logically the finesse can only improve from the final iteration values which are given in these cases. Decreasing mirror radius at either end or deviations in cavity length all serve to reduce the maximum finesse.

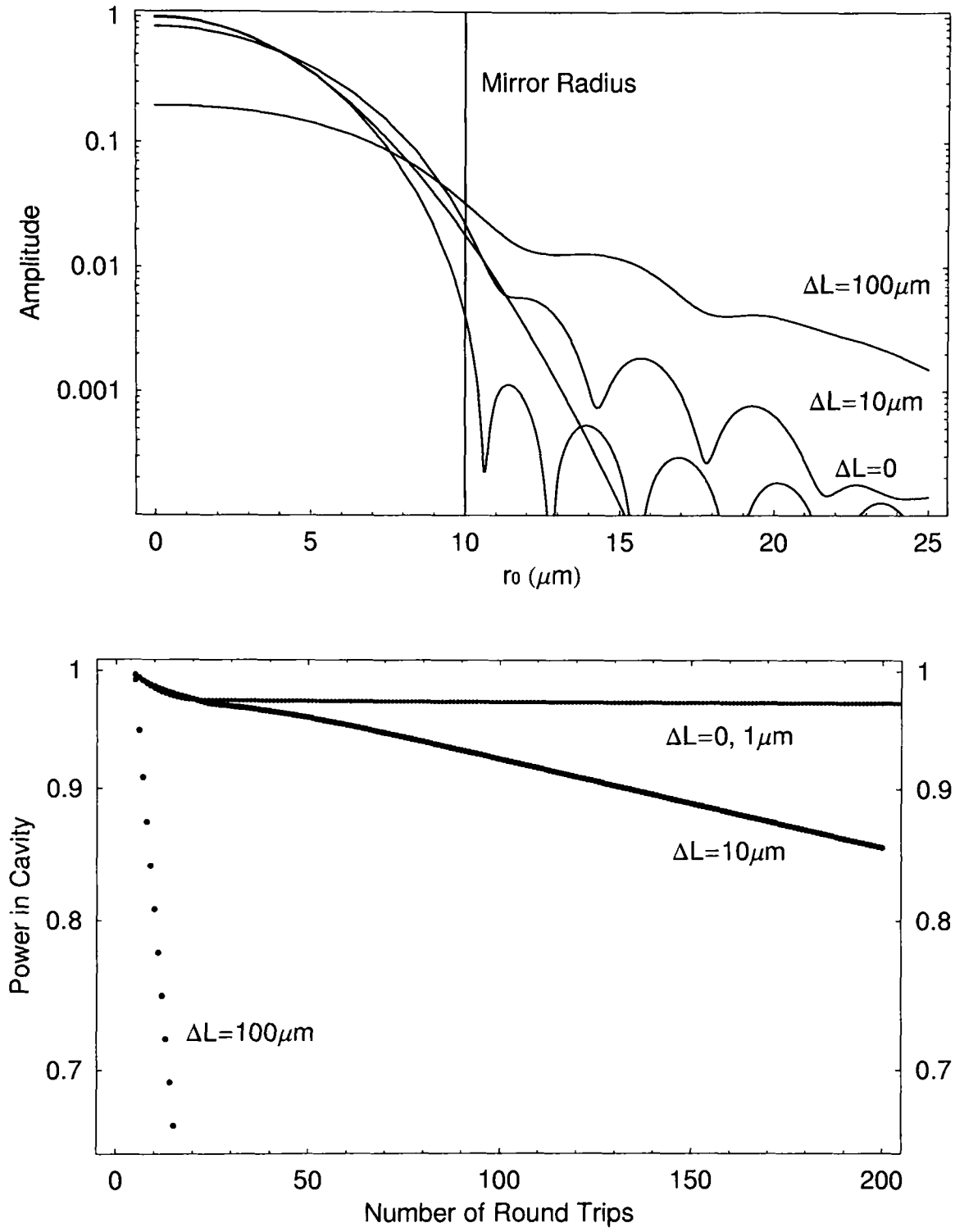

Figure 4.24: Losses as a function of cavity length $\Delta L = 24.99972 - L$ where $L = 25$mm. Top: a log plot of the solution mode amplitude profile as a function of distance r_0 from the centre of the small mirror (whose radius is shown as a vertical line) for different cavity lengths $\Delta L = 0, 10, 100\mu$m. Bottom: cavity loss as a function of number of round-trips shown for several cavity lengths $\Delta L = 0, 1, 10, 100\mu$m.

length of 25mm, this corresponds to 0.5mm offset of the beam on the large mirror. It is this large since there is no reliable method to locate the optical axis of the large mirror which diverges the beam sharply. To a first

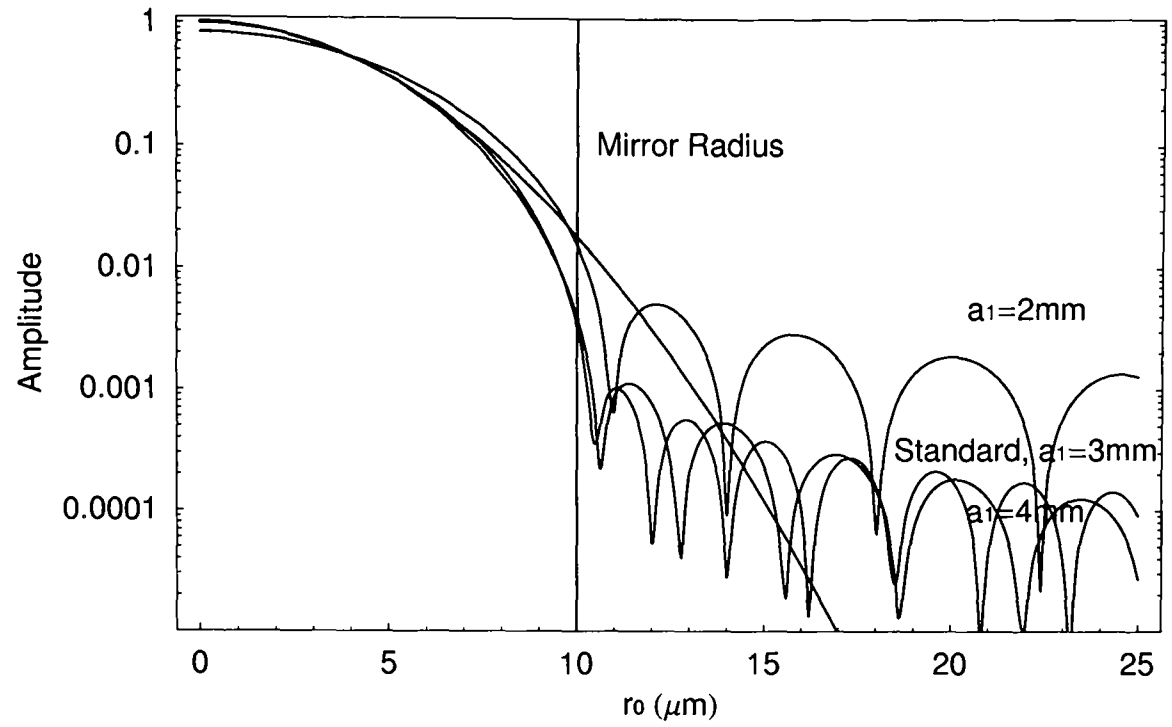

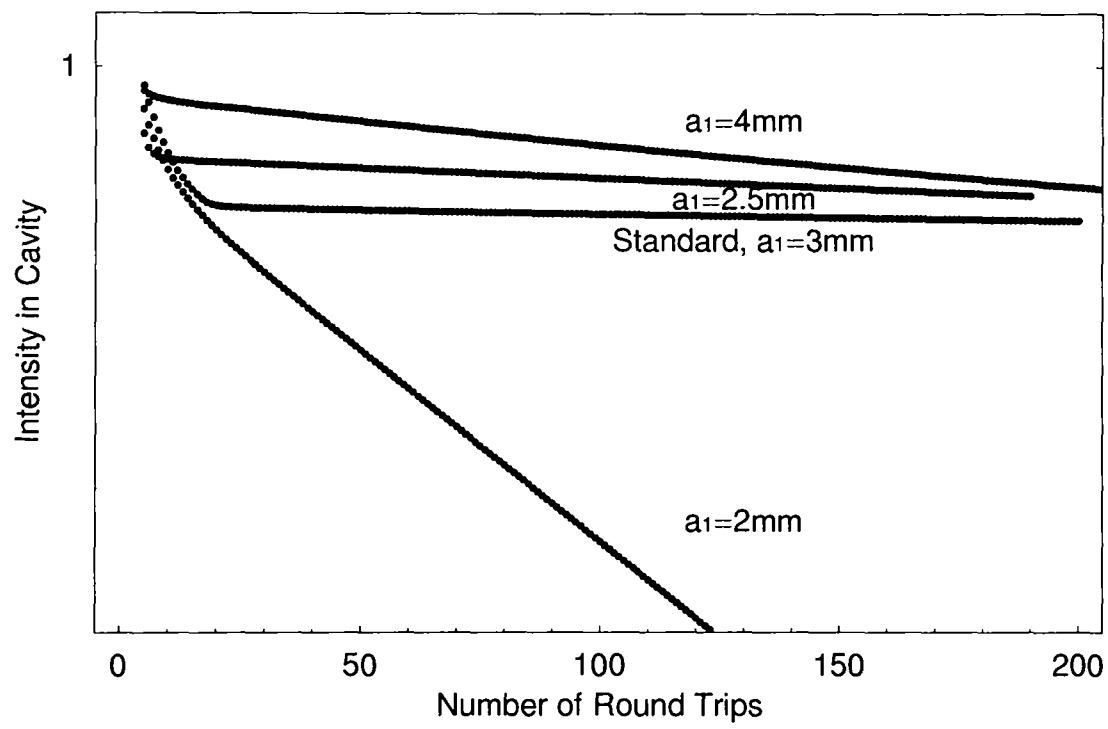

Figure 4.25: Losses as a function of large (curved) mirror radius a_1. Top: a log plot of the solution mode amplitude profile as a function of distance r_0 from the centre of the small mirror (whose radius is shown as a vertical line) for different large mirror sizes $a_1 = 2, 3, 4$mm. Bottom: cavity loss as a function of number of round-trips shown for several cavity lengths $a_1 = 2, 2.5, 3, 4$mm.

approximation the losses in such a geometry would be the same as with the case of the big mirror reducing in radius by 0.5mm which from our diffraction loss calculations show increases loss by a factor 70 keeping

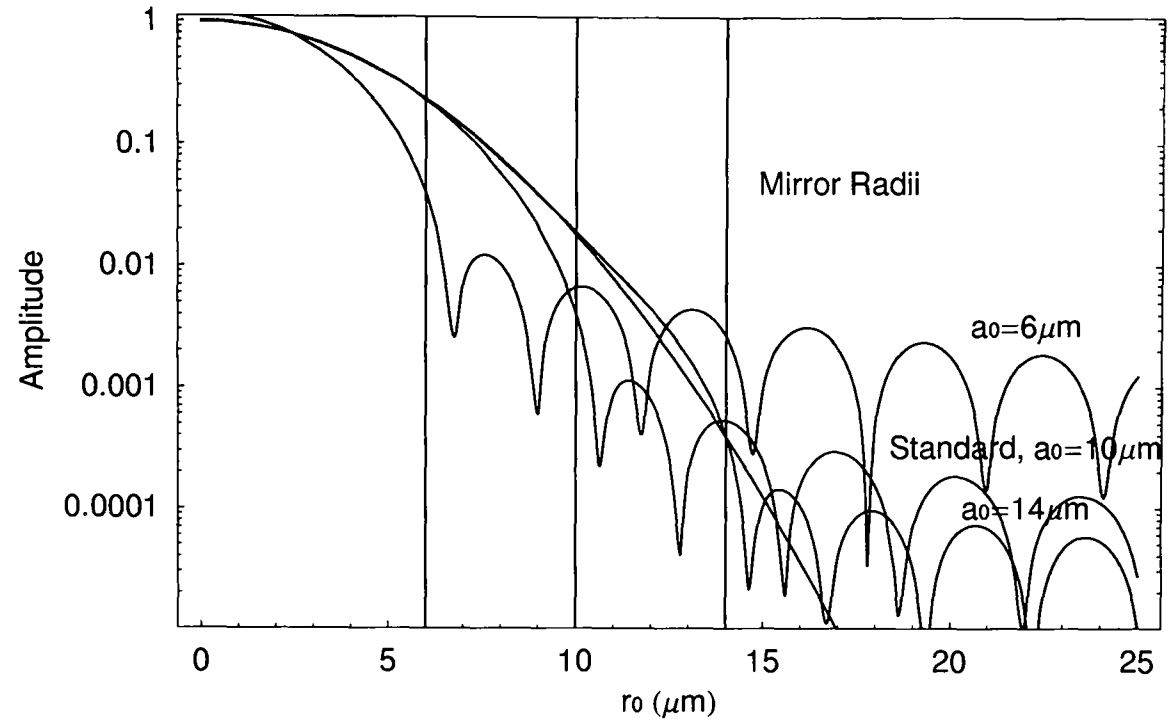

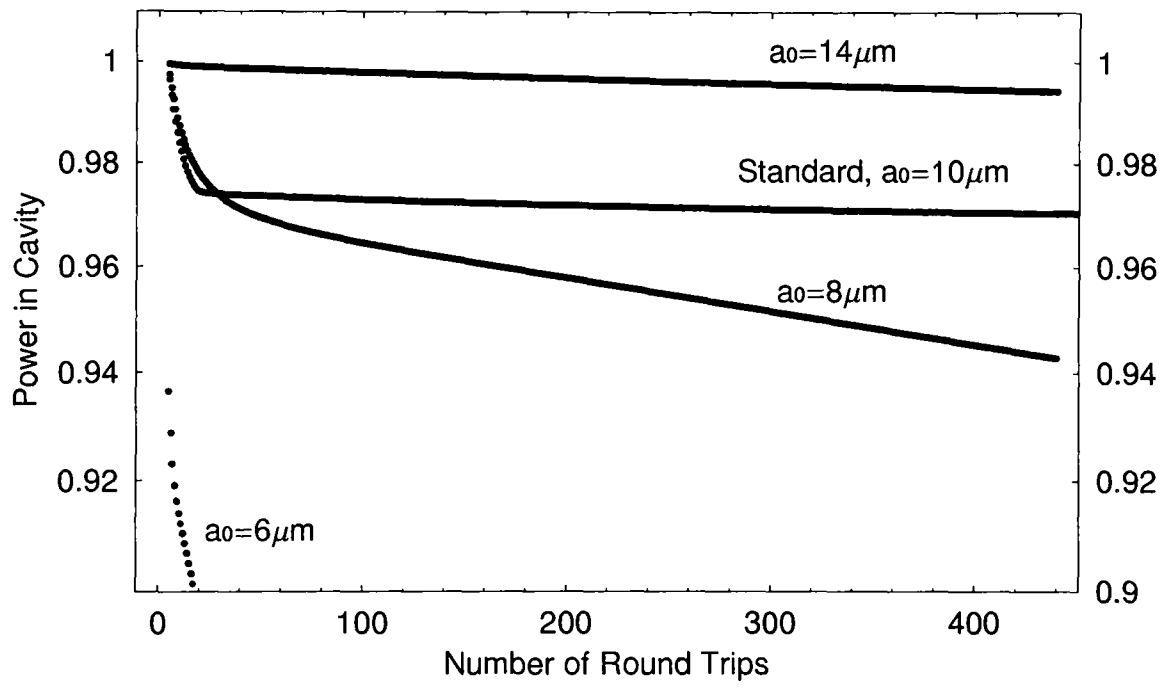

Figure 4.26: Losses as a function of small mirror radius a_0. Top: a log plot of the solution mode amplitude profile as a function of distance r_0 from the centre of the small mirror (whose radius is shown as a vertical line) for different cavity lengths in units of $a_0 = 6, 10, 14\mu$m. Bottom: cavity loss as a function of number of round-trips shown for several cavity lengths $a_0 = 6, 8, 10, 14\mu$m.

all other factors equal. Double that angle would be a factor 2000.

Losses due to length misalignments are much more critical than angular misalignments and are computed

directly by changing L in the diffraction calculation. For example a cavity length change of 1, 10 and 100μm from the optimum results in increased losses of a factor 50, 2000 and 10^5 respectively for increases and decreases in cavity length alike. Thus for optimisation in z must be done using the piezo electric positioner. One can see from Fig. 4.24(top) that the beam amplitude profile at the small mirror becomes wider as ΔL becomes larger, which is expected since the micro-mirror is further from the focus of the cavity. The difficulty in aligning the cavity length to $< 10\mu$m, given the cavity mirror mount limitations of §4.3.1., suggests that $F_g \sim F_d/2000 = 8 \times 10^3$, a finesse not that much larger than the best measured value.

The fact that length increases past $L = R$ have the same diffraction loss is the case because the diffraction losses are the limiting factor. If a cavity with a hemispherical cavity were made with a large flat then the finesse will be near constant for $L < R$ but will rapidly tail off for $L > R$ due to the unstable configuration (see Fig. 4.28).

Finally, losses as a function of small mirror size were calculated in order to determine how critical losses are on this parameter, and in particular to find what the smallest mirror size is to have the finesse required. The results are given in Fig. 4.26. The losses increase slightly faster with a reduction in small mirror size than for the same fractional reduction in large mirror size but are of the same order of magnitude. It is expected to be a similar rate since the ratio of beam width to mirror diameter at each mirror is approximately the same due to the large diffraction angle of the beam from the small mirror (which increases with decreasing spot size as shown in Eq. 3.66). Perhaps the most interesting feature can be seen on the top of Fig. 4.26: here the fact that the mode adapts to the small mirror size (6, 10 and 14μm) is very clear. On the bottom of Fig. 4.25 one can see how the solution mode is formed faster for lower finesse modes (e.g. by comparing the decays for $a_1 = 2.5$mm and $a_1 = 3$mm). Note that the $a_1 = 4$mm has yet to find the solution mode after the number of round-trips shown on the plot.

It is worth noting that several of the calculations did not converge in the 1000 round-trips, and since this calculation already took 24 hours to complete they were not extended. Time limitations also dictated the integration step size which can not distinguish losses $< 4 \times 10^{-7}$. In general the higher the losses the quicker the convergence to the optimal mode.

4.5.4 Limiting Finesse due to Mechanical Stability, F_m

Mechanical vibrations on the measurement timescale of approximately 1s can be from 3 sources:

1. Shot noise from the laser.
2. Thermal noise.
3. Acoustic noise.

The Fabry-Perot method of measuring the finesse is considerably more sensitive to vibrations than the cavity ring down since the transmission in the former method depends on the phase and hence the length. To

see a finesse F one has a maximum length variation of

$$\Delta L < 2\pi\lambda/F. \tag{4.28}$$

Given that $F = 1000$ was measured an upper limit of the vibrations is $\Delta L < 5$nm is known experimentally. This can be compared to calculated values for the aforementioned vibrations:

1. The radiation pressure of a beam with photon number N has a shot noise driving force in proportion to $\sqrt{N}$ given by

$$\sqrt{\frac{N}{\omega_m}}\frac{Fh}{2\pi\lambda} = k\Delta N = k2\pi\lambda/F \tag{4.29}$$

   where ω is the frequency of interest, F is the cavity finesse, k is the cantilever force constant and N is the number of photons per second in the beam. For a 1mW beam power and the cantilever in use in the experiment in §4.3 the maximum finesse is given by $F_m > 1.5 \times 10^7$. Thus shot noise is not the limiting factor here. However, for the cantilever planned for use in the final experiment (whose k factor and ω_m are both a great deal less) then by definition of the momentum considerations a shot noise consisting of 1 photon will cause a displacement of the ground state wavepacket for the finesse requirement. This is at the threshold of the maximum displacement due to noise which can be allowed.

2. The motion ΔL due to thermal energy in cantilever at a temperature T is given by the equipartition theorem for an object with a single degree of freedom

$$\frac{1}{2}k_BT = \frac{1}{2}k\langle\Delta L^2\rangle, \tag{4.30}$$

   where k_B is Boltzmans constant. At room temperature one expects thermal vibrations to be of order $L = 0.2$nm that corresponds to $F_m = 2.4 \times 10^4$. This is approximately an order of magnitude above the finesse seen.

3. Acoustic noise intensity I at the resonance frequency results in a vibration amplitude ΔL given by

$$\frac{2v\rho}{k}IA = \Delta x \tag{4.31}$$

   where v is the velocity of sound in air and ρ is the density of air. To interfere with the cavity finesse at the best measured value ($F_m = 1000$) an intensity of $I < 5 \times 10^{-7}$W/m^2 is required – a sound level similar to the background noise in our laboratory. This therefore seems to currently be the limiting factor on the finesse. This can be overcome by placing the cavity into a vacuum chamber. That exact task is ongoing.

4. Relaxation/drift: piezo drift or other such effects could have change the mechanical stability. A calculation of the scale of this in the case under study has yet to be performed.

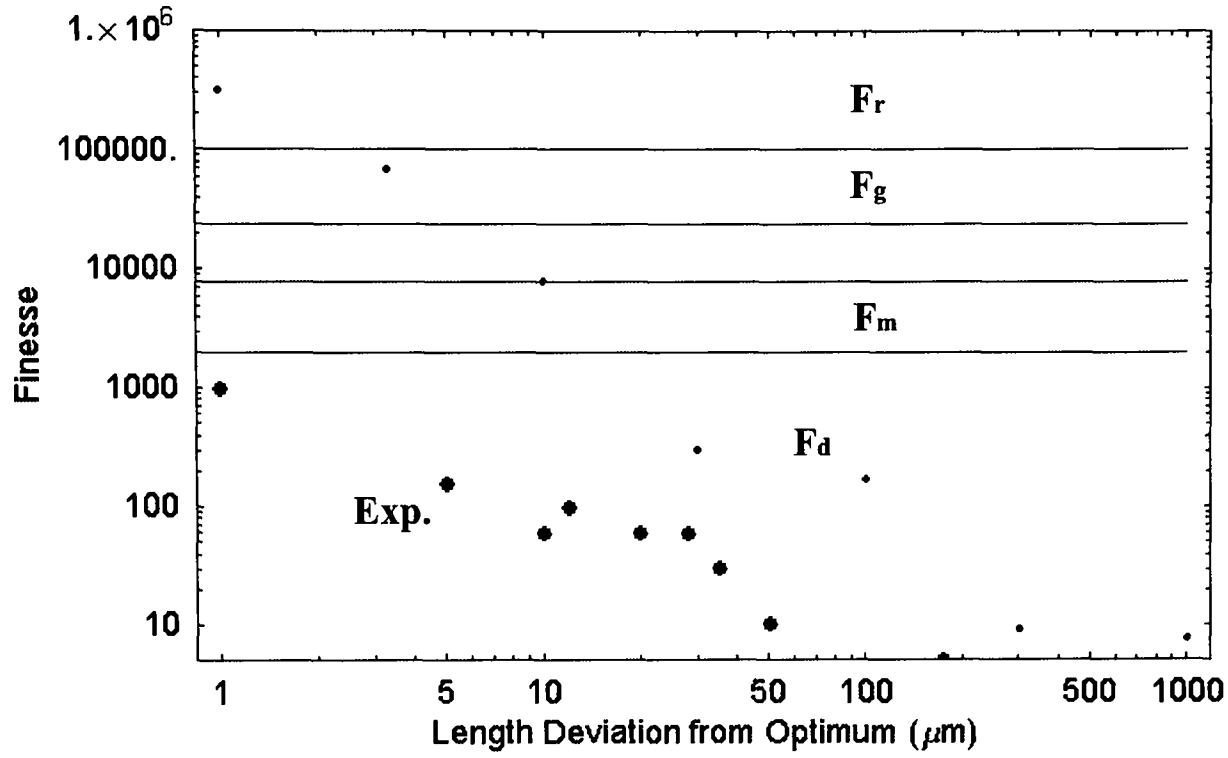

Figure 4.27: Comparison of finesse limitation factors. The finesse fall off with cavity length deviation from optimum ΔL is shown as predicted due to diffraction loss theory (small dots) and as measured experimentally (large dots). The horizontal lines represents the maximum finesse dictated by various other factors: (a) mirror reflectivity (top line), (b) thermal vibrations of the cantilever at room temperature (second to top line), (c) diffraction loss for a cavity length 10μm from optimum (second to bottom line) and (d) finesse limitation due to acoustic noise (bottom line). The measured results differ from the theory by a greater margin at smaller deviations from the optimum cavity length (and higher finesse) which would be expected if other loss mechanisms were limiting the finesse e.g. acoustic noise.

4.5.5 Summary of Limitations on the Finesse

Fig. 4.27 shows the practical limits on the finesse due to diffraction losses as a function of cavity length, which is the most sensitive alignment parameter. Clearly a great deal of improvement in the finesse has to be made in order to obtain the momentum kick required but none of the limitations above seem fundamental at present. Measurements of the maximum finesse as the cavity length was scanned in length around the optimum are shown on the plot alongside the calculated ones. The current limiting finesse of the mirror reflectivity, F_r, the thermal vibrations, F_m, the geometric losses F_g for a 10μm length deviation are overlayed. At larger cavity deviation from optimum length the measured finesse agrees better with the diffraction loss calculation (eg. at $\Delta x = 200\mu$m deviation the difference is a factor of 10) whereas as the length deviation is reduced the diffraction losses are considerably smaller than those seen experimentally (e.g. at $\Delta x = 1\mu$m the difference is a factor 2×10^4). Limitations due to acoustic noise are currently limiting our finesse but limitations due to thermal vibrations are not so much greater than those seen experimentally (a factor of 8). These two

limitations can be circumvented by placing the cavity into a vacuum and by cooling.

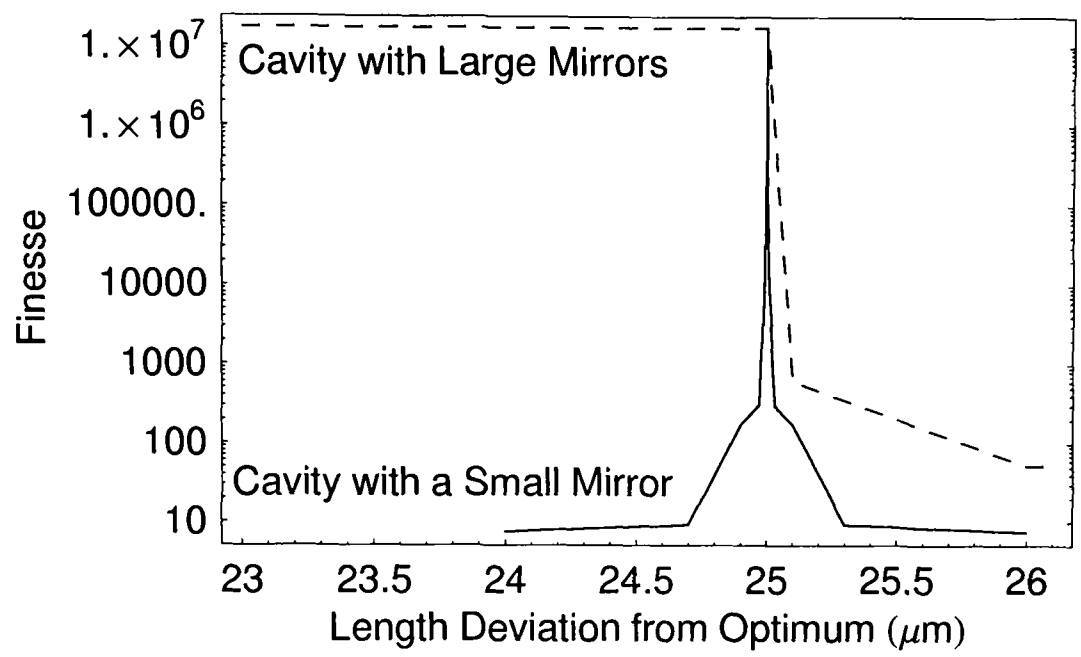

Figure 4.28: Finesse at different cavity lengths around the $R = L$ point ($R = 25$mm) for a cavity made of two large mirrors (dashed line) and the cavity made of the micro-mirror as the flat (solid line)

In Fig. 4.28 the calculated finesse is shown against the cavity length. Plotted are two hemispherical cavities one with a large-flat and the other with a 10μm radius flat. The cavity with the large flat has very high finesse when $L < R$. After that threshold the finesse tails off. In contrast the cavity with the tiny flat has a peak finesse length, deviations from which in either direction will result in a very sharp fall off of the finesse.

Coupling losses

This does not effect the finesse of the modes but alters the initial energy in them and the number of round-trips needed to reach the optimum field profile. The decay of the energy observed in CRD is a summation of exponential decays of different finesse modes in which one couples light. Higher finesse modes with low energy can be hidden by low finesse modes of high energy initially, but will always dominate at longer decay times. It is not possible to prepare the complicated cavity solution beam profile see in Fig. 4.23 but that mode has a $> 97\%$ intensity overlap with a Gaussian beam amplitude of the appropriate width and radius of curvature and so it suffices to consider the coupling of two Gaussian beams, when considering how to incouple to it.

The coupling coefficient K for the matching of two Gaussian beams a and b is given by the square of the

amplitude overlap of the two Gaussian beam profiles

$$\begin{aligned} K &= |c_{ab}|^2 \\ c_{ab} &= \int\int E_a^* E_b dS \\ &= < E_a | E_b > \\ &= < u_a | u_b > \\ &= \int\int u_a^*(r,\phi) u_b(r,\phi) r dr d\phi \end{aligned} \tag{4.32}$$

where u is the amplitude of the field E.

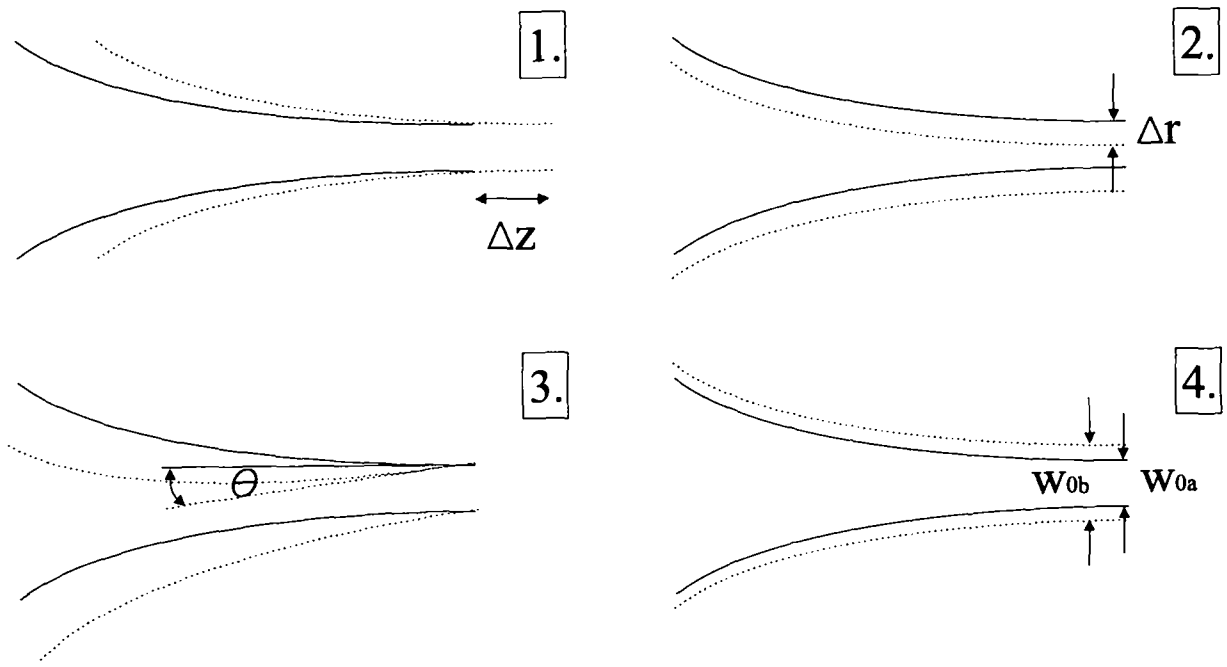

Figure 4.29: Beam offsets as described in the text.

There are four possible misalignments of the incoupling beam compared to the cavity solution mode, as illustrated in Fig. 4.29, they are

1. Separation of the waists by a displacement Δz.
2. A lateral displacement of the beams Δr.
3. An angular separation of the beams θ.
4. A ratio of waist sizes $\mathrm{w}_r = w_{0a}/w_{0b}$.

The K factors are given by [Goldsmith, 1998]:

$$K_{\Delta z, w_r} = \frac{4}{(w_r + 1/w_r)^2 + \chi^2 w_r^2} \tag{4.33}$$

$$K_\theta = e^{-2(\theta/\theta_t)^2} \tag{4.34}$$

$$K_{\Delta r} = e^{-2(\Delta r/\delta)^2} \tag{4.35}$$

where

$$\chi = \frac{\Delta z \lambda}{\pi w_{0a}^2} \tag{4.36}$$

$$\theta_t = \frac{\lambda}{\pi}\left(\frac{1}{w_{0a}^2} + \frac{1}{w_{0b}^2}\right) \tag{4.37}$$

$$\delta = \left(\frac{(w_{0a}^2+w_{0b}^2)^2+(\lambda\Delta z/\pi)^2}{w_{0a}^2+w_{0b}^2}\right)^{0.5}. \tag{4.38}$$

where subscript a refers to the cavity solution mode and b the incoupling beam, whose waist tends to be larger than ideal due to imperfect lenses. It is estimated that the cavity mount used here ensures that $\Delta z < 20\mu$m, $\Delta r < 2\mu$m, $w_r > 0.57$ and $\theta < 1$ degree. These values cause a total incoupling efficiency $> 50\%$ to the solution Gaussian mode which is considered sufficient for the current experimental purposes.

4.6 Ultra-fast Optical Switching of High Reflectivity Mirrors

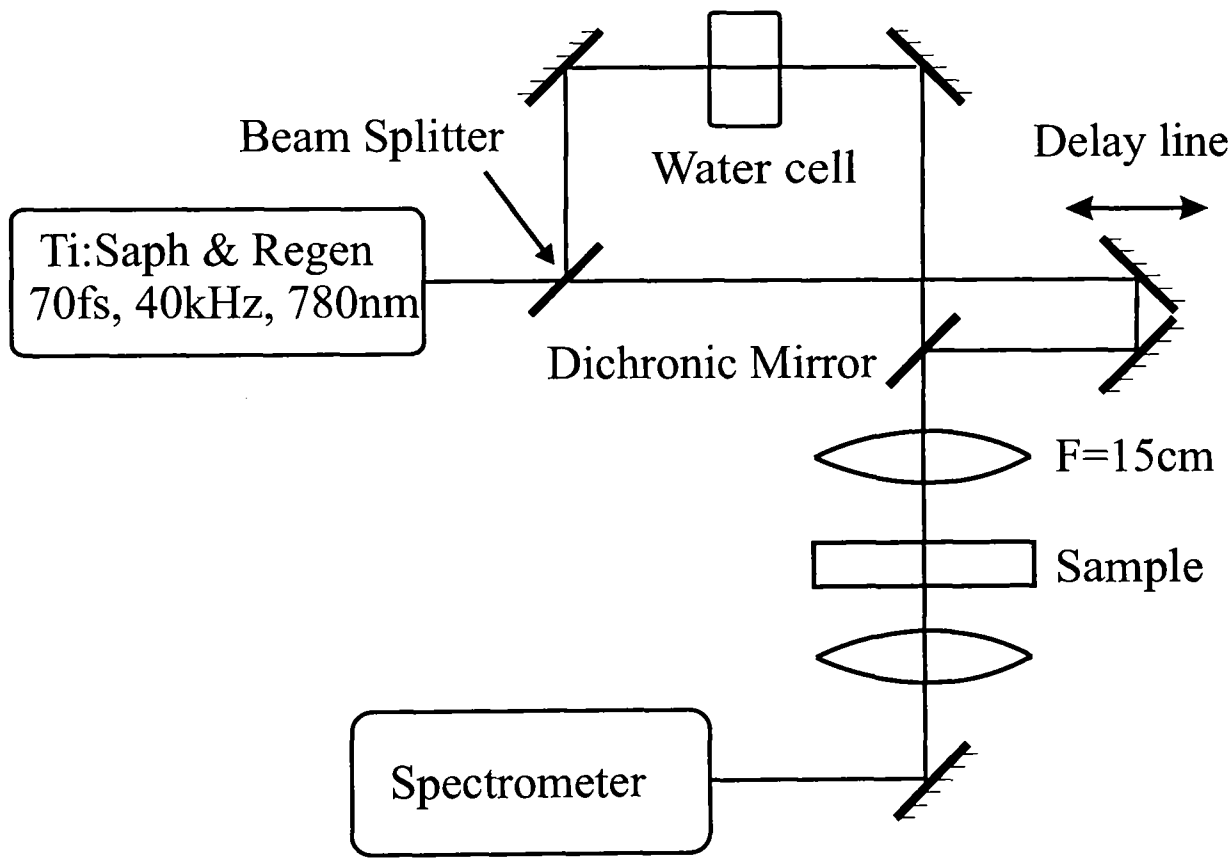

Figure 4.30: Schematic of a setup to measure the optical switching of high-reflectivity mirrors.

The principle of ultra-fast optical switching was described in §3.5. Here the first experimental results are reported. A DBR of 30 pairs of GaAs/AlAs with refractive indicies $n = 3.58$ and 2.97 respectively designed

for peak reflectivity at 910nm was deposited on a GaAs substrate by the EPSRC National Centre for III-V Technologies, at the University of Sheffield.

A scheme to measure the switching effect is shown in Fig. 4.30. A Ti:Sapphire with a regenerative amplifier gives a light source with a pulse width 70fs, a repetition rate of 40kHz and a mean power of up to 400mW. This is directed via an optical delay line on to the GaAs/AlAs mirror sample on which it is focussed to an area approximately 30μm diameter. Some of the light from the pulse is split off and passed through a water cell which results in an ultra short pulse white light source – the probe. This is co-aligned with the main pump beam onto the sample using a di-chronic mirror which reflects $<$ 800nm and transmits above. The light transmitted through the sample is sent to a spectrometer which can distinguish the probe from the pump light due to the difference in wavelength.

The delay line is scanned over the point of temporal overlap of the pump and probe on the sample. If the probe meets the sample before the pump then no switching is expected whereas maximum switching is expected at overlap which will result in a greater transmitted power of the probe beam (see §3.5). The pump power can be varied to study the effect.

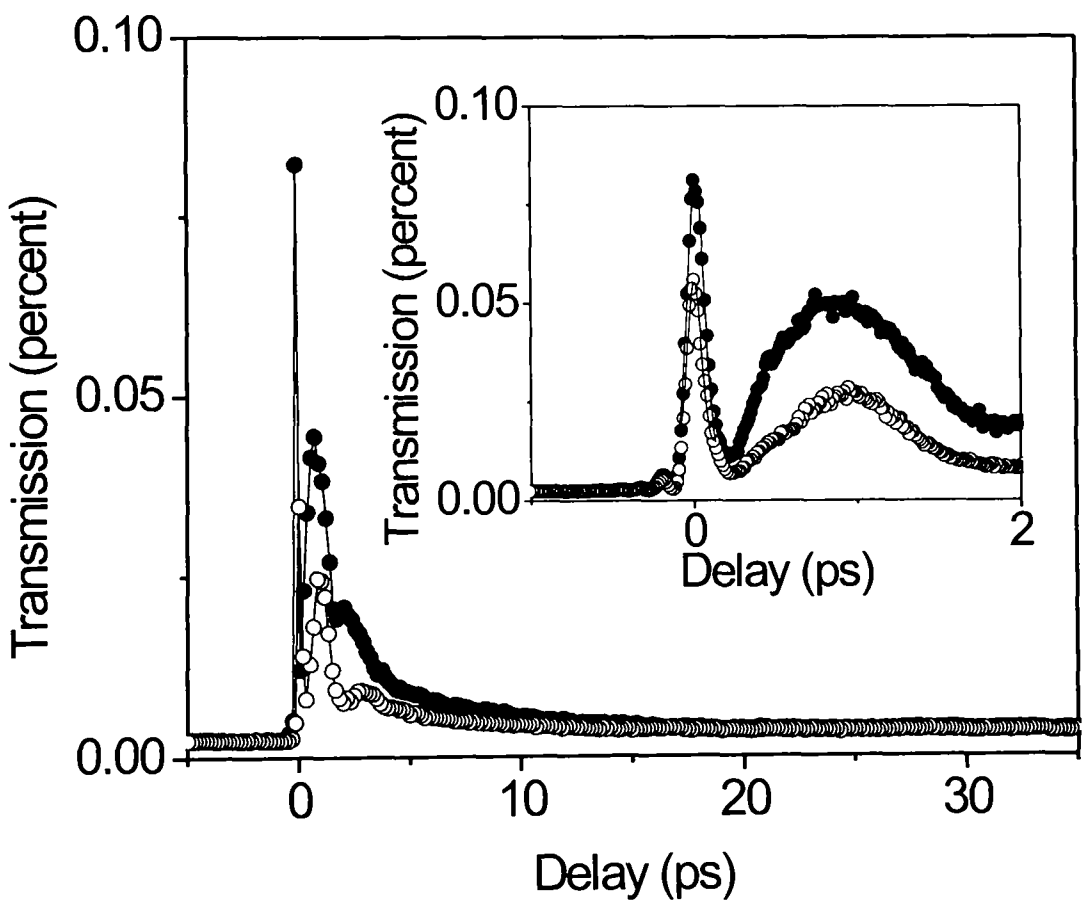

Figure 4.31: Results of initial switching measurements. The transmission of the probe beam through the mirror sample as a function of time after the pump pulse.

Transmission was observed as a function of delay between the pump and the probe at two powers of 8×10^{15}W/m^2 and 6.4×10^{15}W/m^2, not far below the damage threshold of GaAs. At negative delay the transmission is constant, as expected. At maximum pump probe overlap there is an initial fast response, due to the Kerr nonlinearity in GaAs and AlAs which changes the index of refraction of the GaAS and AlAs layers and therefore lowers the reflectivity of the mirror. For the higher power a switching by a factor of 27 from a transmission of 0.0024% to 0.065% was observed at 931nm [Hastings et al., 2004].

The second lower and longer-lived increase in transmission (which extends well beyond the pulse length) is due to the creation of free carriers in GaAs which also change the index of refraction in GaAs. A number of theoretical models for this fast change in index of refraction have been introduced such as Refs. [Kim, 1992, Spataru et al., 2001]. Because the pump energy is below the bandgap of AlAs, no free carriers are expected there.

From an average beam power of 30mW focussed on to an area of 30μm on the sample the intensity is 8×10^{15}W/m^2. This should result in $\Delta n = 3$ and thus a switching better than that shown on Fig. 3.6. The reason why it is so much less is that the pulse is being absorbed due to excitation of free carriers. The 1/e depth for the pump light at 780nm is just 11 pairs of layers and so most of the layers are not being significantly effected by the pulse. This is because the pulse is on the edge of the band-gap of GaAs: if it were to be pumped at 1000nm one would expect considerably less free carriers and thus switching of all 60 layers which is expected to lead to much greater switching effects. In addition, samples with a sharper band-gap edge could be designed and the experimental technique optimised further. Thus there is considerable scope for improvement of the mirror switching effect [Hastings et al., 2004].

Chapter 5

Conclusions and Way Forward

By coupling a photon in a superposition of two locations to a cantilevers motional state it is in principle possible to create a state involving two distinct locations of the cantilever. The analysis here shows how the experimental implementation of this basic idea seems just about feasible with current technology: it is possible for the photon to impart sufficient momentum that the cantilever is displaced by a separation greater than the ground state wavepacket; possible to maintain environmental decoherence sufficiently low on the experimental timescale, and; possible to keep sufficient interferometric stability for read out. The first experimental steps to this end are demonstrated here: (1) construction of a 10μm radius high reflectivity mirror onto a high mechanical quality micro-mechanical cantilever and (2) the incorporation of the micro-mirror/cantilever as one end of a long (relative to the small mirror) near-hemispherical cavity with moderate finesse ($F = 1000$). In addition, ultra-fast optical switchable mirrors were fabricated and showed a raise in transmission by a factor of 27 when pumped.

This really represents the beginning of the experimental effort since many developments of a challenging nature are to follow: (1) To achieve sufficient momentum transfer we require (a) improvement of the cavity finesse from 10^3 to 1.7×10^7. This will require greater alignment, the fabrication of higher reflectivity samples (23 pairs of layers instead of the current 16), (b) a lower mass cantilever ($< 5\times10^{-12}$ compared to 7×10^{-11} at present. (2) To meet the condition imposed by environmental induced decoherence one requires that (a) the setup shall have to be cooled to mK regime using a dilution refrigerator and (b) the vacuum will have to be improved from 10^{-4} Pa to 10^{12}atoms/m^3 $= 10^{-13}$Pa, (3) To allow interferometric read out, an increase of the stability of the cavity mirrors from 5×10^{-9}m/10ms to 6×10^{-15}m/min will be necessary through the use of a stack suspension system which isolates noise in the frequency regime around the cantilever frequency. This condition will be eased significantly by developments in either or both of (a) further cooling of the cantilever (e.g. via nuclear demagnetisation cooling) or (b) ultra fast switching of the cavity mirrors. The conditions achieved to date are compared to those required in Table 5. In addition, the middle column gives the values

which are known to be readily achievable.

	Measured Herein	**Within Reach**	**Required**
Cavity finesse	10^3	10^4	1.5×10^7
Cantilever Q, m, ω	2.2×10^4, 7×10^{-11}kg, 2π10kHz	10^5, $< 5 \times 10^{-12}$kg, 2π500Hz	10^5, $< 5 \times 10^{-12}$kg, 2π500Hz
Bath Temperature, T	300K	10mK	3mK
Mirror Mass, m	5×10^{-12}kg [5]	5×10^{-12}kg	5×10^{-12}kg
Vacuum	10^{-4}Pa ($= 10^{-6}$Torr)	10^{-10}Pa @mK	10^{12}atoms/m^3 $= 10^{-13}$Pa @mK
Stability	5×10^{-9}m/10ms [6]	5×10^{-10}m/10ms [6]	10^{-15}m/min

Table 5.1: Summary of the experimental demands versus those achieved experimentally herein.

There are several cross cutting issues: cooling helps (and is probably necessary) in order to achieve the required vacuum conditions. Stability increases are also necessary for achieving high finesse. Cooling may cause problems for the stability conditions since cooling mechanisms require contact to a refrigerating device and such contact is likely to lead to instabilities. A retractable cold finger may enable both. The key is that a simultaneous effort on several experimental fronts is necessary.

Meanwhile there are several theoretical tasks of interest: (1) an investigation of the behavior of the environmental decoherence for our specific system, (2) revision of the optimal experimental procedure in light of experimental progress and, (3) a more thorough investigation of the concrete predictions of various schemes suggesting a deviation from pure quantum mechanics. For example, the behaviour of the Penrose model of gravitational collapse as a function of the spatial separation of the two components of the quantum superposition, and predictions for the free constants of the Ghirardi, Rimini Weber model. Also, other methods of testing the superposition principle should be investigated further such as coupling of superposed states of currents in SQUIDs or molecules in atom interferometry to more massive systems (see [Leggett, 2002] and [Godun et al., 2001] for good review articles respectively).

Overall, although there remain many hurdles to achieve a massive superposition state none look insurmountable and this is a remarkable conclusion given that the proposed experiment would test the superposition principle in a mass regime some 9 orders of magnitude greater than experiments to date and as such would be of great fundamental interest in testing the reach of Quantum Mechanics. It also has the potential to probe the nature of decoherence (environmental and non-conventional schemes) and to shed light on the measurement problem.

Looking further ahead, in principle the proposed setup has the potential to test wave function reduction models. To test the gravitational decoherence model of Ref. [Penrose, 1996] it is estimated that the ratio Q/T needs to be improved by about five orders of magnitude from the values discussed in this paper ($Q = 10^5$ and $T = 2$mK) to make the predicted decoherence rate comparable to the environmental decoherence rate.

However, temperatures as low as 60 μK have been achieved with adiabatic demagnetization [Yao et al., 2000], while Q is known to increase with decreasing temperature [Mamin and Rugar, 2001] and through annealing [Yang et al., 2000]. Improvements in the cavity finesse or a shorter wavelength would result in a cascading effect easing all other experimental requirements.

The principle motivation derives from testing fundamental physics, however, there are a couple of technological developments contained in this approach which are of separate interest: specifically, active cooling of a macroscopic object and ultra-fast all-optical switching which both could have a variety of applications. The setup could also be of use for measuring very small forces.

It has been my task to perform a feasibility study for creating macroscopic quantum superpositions. At the start of my D.Phil it was unclear whether it would be realistic to perform such an experiment at all. After 18 months the details of a feasible, although extremely challenging, experiment emerged [Marshall et al., 2003a]. In the remaining PhD period significant experimental progress has been made [Marshall et al., 2004] and [Hastings et al., 2004]. As a result two new PhD students will continue the challenging project with well defined experimental milestones for the coming years: (1) the integration of the cavity into a vacuum chamber (under way), (2) further development of switchable mirrors (underway), (3) feedback optical cooling of the cantilever centre of mass motion from room temperature (under way), (4) testing of adiabatic nuclear demagnetisation of a cantilever (scheduled for early 2005), and (5) cryogenic cooling and further measures to improve the cavity finesse.

Appendix A

Cavity Mount Design

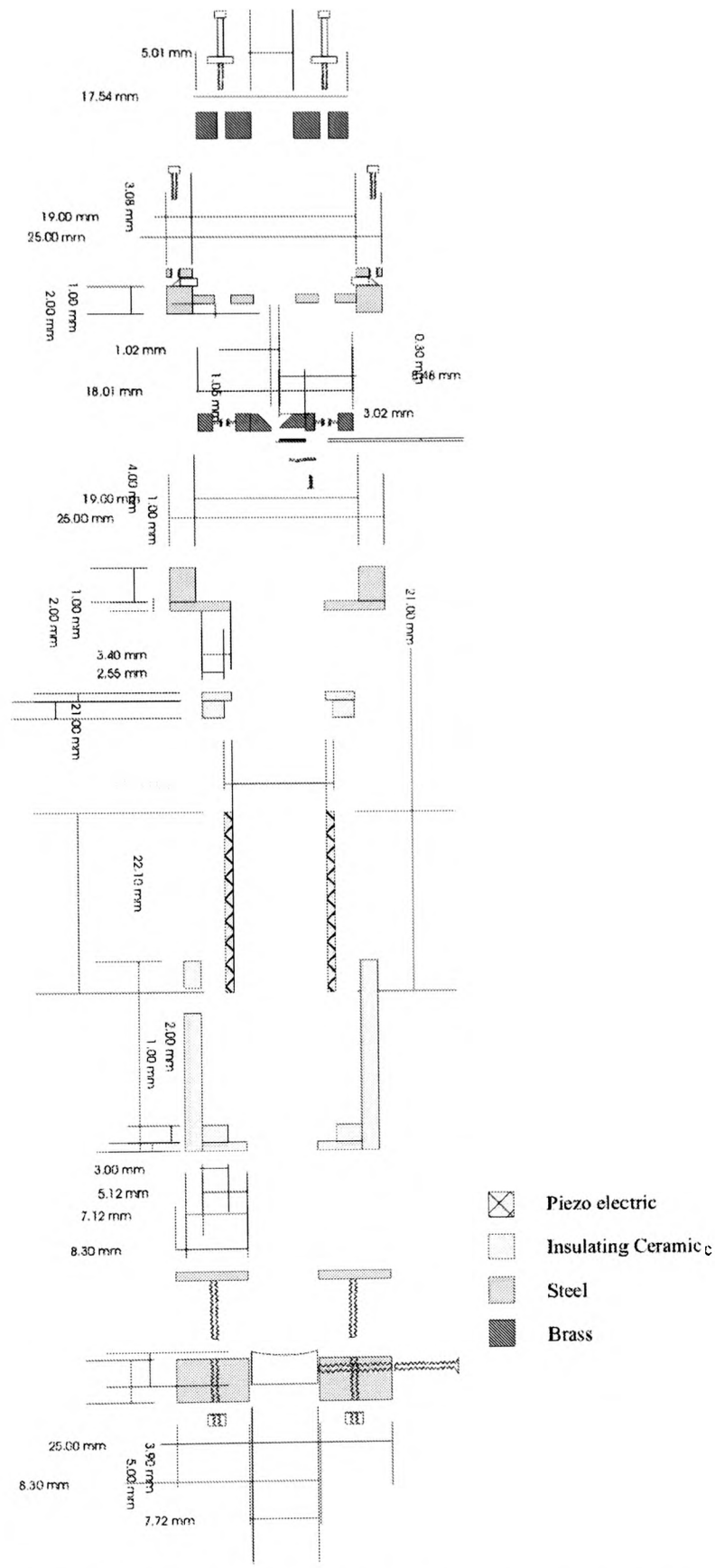

Figure A.1: Exploded diagram of the mount constucted to house the near-hemispherical cavity involving the micro-mirror on a cantilever.

Appendix B

Cavity Diffraction Loss Calculation

Diffraction Loss from a Hemispherical Cavity with a Small Flat Mirror

Will Marshall, 6.3.04

Importing relevant packages

```
In[1]:= << Graphics`Graphics`
        << Graphics`ImplicitPlot`
        $TextStyle = {FontFamily → "Arial", FontSize → 12};
```

Define Cavity

```
In[4]:= λ := 7.8 * 10^(-7) ;      (* Wavelength *)
        d := 0.0249996 ;          (* Length of cavity *)
        R := 0.025 ;              (* Radius of curvature *)
        w0 := 5 * 10^(-6) ;       (* Width of beam at small mirror *)
        a0 := 10^(-5) ;           (* Radius of small mirror *)
        a1 := 3 * 10^(-3) ;       (* Radius of large mirror *)
```

Cavity Propogation Kernels

Reflection from the small mirror and propagation to the large mirror :

```
In[5]:= Integrand0[r0_] :=
         Evaluate[u0[r0] * r0 * Exp[-I * Pi * r0^2 / (λ * d)] * BesselJ[0, 2 * Pi * r1 * r0 / (λ * d)]]
        Integral0[x0_] := Simplify[
          Evaluate[I * 2 * Pi / (λ * d) * Exp[-I * Pi * (1 - d / R) * r1^2 / (λ * d)] *
            NIntegrate[Integrand0[p] /. {r1 → x0}, {p, 0, a0}] /. {r1 → x0}]]
```

Reflection from the large mirror and propagation to the small mirror :

```
In[7]:= Integrand1[r1_] := Simplify[Evaluate[
           u1[r1] * r1 * Exp[-I * Pi * (1 - d / R) * r1^2 / (λ * d)] * BesselJ[0, 2 * Pi * r1 * r0 / (λ * d)]]]
        Integral1[x2_] := Simplify[Evaluate[I * 2 * Pi / (λ * d) * Exp[-I * Pi * r0^2 / (λ * d)] *
            NIntegrate[Integrand1[p] /. {r0 → x2}, {p, 0, a1}] /. {r0 → x2}]]
```

Propogation Loop

Defining field profile to evolve at each iteration of loop and defining initial input (Gaussian) field :

```
In[9]:= Profile[x_] := Exp[-x^2 / w0^2]   (*  Input Beam Profile (at small mirror) *)
        u0[x_] := Profile[x]
        u1[x1_] := ProfileAtHalftrip[x1]
```

Input number of round trips :

```
In[12]:= n = 100;
```

1. Two tables logging the field profile at each round trip,
and the power of the beam incident on the small mirror after each round trip relative to the beam after the previous round tripLoop which performs integration of propogation Kernels n times.
2. The initial field is input and the field after each round trip is inserted back in as the input field for the next loop.
3. The (a) Iteration number, (b) calculation time (s),
(c) Amplitude on the small mirror and (d) the power on the small mirror relative to the power on the previous round trip, are printed after each iteration of the loop :

```
In[13]:= ProfileTable = Table[0, {ii, 1, n}];
         PowerTable = Table[0, {11, 1, n}];
         For[s = 1, s < n, s++; T1 = TimeUsed[];
          ProfileList0 = Table[{x0, Abs[Integral0[x0]]}, {x0, 0, 2*a1, a1 / 100}];
          ProfileAtHalftrip = Interpolation[ProfileList0];
          ProfileList1 = Table[{x2, Abs[Integral1[x2]]}, {x2, 0, 2*a0, a0 / 100}];
          Profile = Interpolation[ProfileList1];
          ProfileTable[[s]] = Profile; T2 = TimeUsed[];
          PowerTable[[s]] = (Integrate[ProfileTable[[s]][x], {x, 0, a0}] /
              Integrate[ProfileTable[[s - 1]][x], {x, 0, a0}]) ^2; Print[s, "    |    ",
           T2 - T1, "      |      ", Integrate[ProfileTable[[s]][x], {x, 0, a0}],
           "       |      ", (Integrate[ProfileTable[[s]][x], {x, 0, a0}] /
              Integrate[ProfileTable[[s - 1]][x], {x, 0, a0}]) ^2;]
```

2 | 43.472 | 4.40339×10^{-6} | $\frac{1.93899\times10^{-11}}{\left(\int_0^{\frac{1}{100000}} 0[x]\,dx\right)^2}$

4 | 50.994 | 4.39104×10^{-6} | 0.997306

5 | 55.149 | 4.38572×10^{-6} | 0.997579

6 | 59.636 | 4.38098×10^{-6} | 0.997837

...

98 | 61.259 | 4.34842×10^{-6} | 0.999992

99 | 67.537 | 4.34841×10^{-6} | 0.999992

100 | 72.454 | 4.34839×10^{-6} | 0.999992

Results

Table of cumulative power of the beam in the cavity after successive round trips :

In[16]:=
```
UT := PowerTable[[3]]
```

In[17]:=
```
UTT = Table[0, {mm, 1, n}];
For[p = 4, p < n, p++; UTT[[p]] = UT; UT = UT * PowerTable[[p]];]
```

Plotting the power in the cavity as a function of round trip number :

In[18]:=
```
lossloglot = LogListPlot[UTT, PlotRange → {1.001, 0.97}, Frame → True,
  FrameLabel → {"Number of Round Trips", "Intensity in Cavity"}, FrameTicks → {Automatic, {0.92, 0.94, 0.96, 0.98, 1}},
  PlotStyle → PointSize[.015]];
```

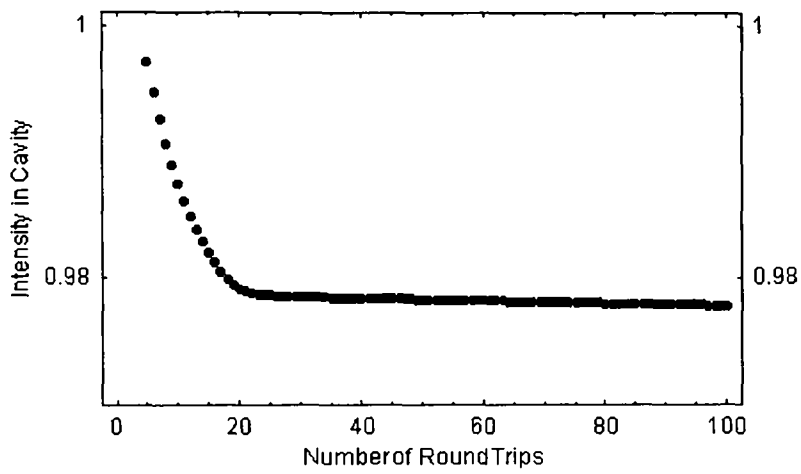

Plotting the beam profile inserted and the beam profile after n round trips :

In[26]:=
```
LogPlot[{Exp[-x^2 / w0^2], ProfileTable[[100]][x]}, {x, 0, 2 * a0}, Frame → True, FrameLabel → {"r (m)", "Amplitude"},
  PlotStyle → {Dashing[{0.03}], Automatic}, PlotRange → {0.00001, 1.1}];
```

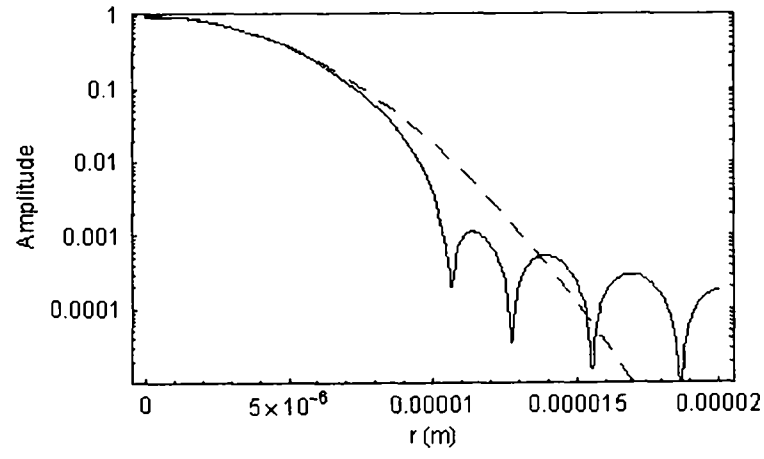

Exporting Data

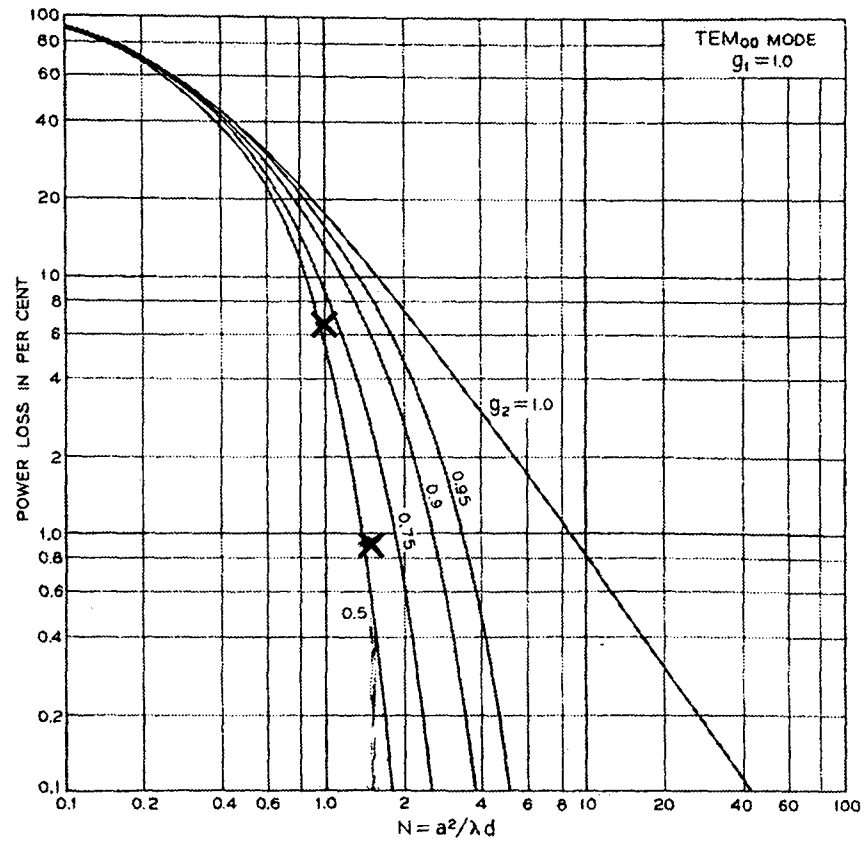

Fig. 9 — *Average* power loss per transit of the fundamental (TEM_{oo}) mode for the half-symmetric geometry.

Figure B.1: Comparison of diffraction loss calculations to the results of Fox and Li.

Appendix C

Relevant Papers by the Author

- William Marshall, Christoph Simon, Roger Penrose and Dik Bouwmeester, *Towards Quantum Superpositions of a Mirror*, Phys. Rev. Lett. **91**, 130401 (2003).
- William Marshall, Michiel de Dood, Hagai Eisenberg, Khodadad Nima Dinyari and Dik Bouwmeester, *A Macroscopic Cavity involving a Microscopic Mirror on a Cantilever.* [In preparation.]
- Sara Hastings, Michiel de Dood, William Marshall, Hagai Eisenberg, and Dik Bouwmeester, *Ultrafast Optical Response of a High Reflectivity GaAs/AlAs Bragg Mirror.* [Submitted to Appl. Phys. Lett..]

Towards Quantum Superpositions of a Mirror

William Marshall,[1,2] Christoph Simon,[1] Roger Penrose,[3,4] and Dik Bouwmeester[1,2]
[1]*Department of Physics, University of Oxford, Oxford OX1 3PU, United Kingdom*
[2]*Department of Physics, University of California, Santa Barbara, California 93106, USA*
[3]*Center for Gravitational Physics and Geometry, The Pennsylvania State University, University Park, Pennsylvania 16802, USA*
[4]*Department of Mathematics, University of Oxford, Oxford OX1 3LB, United Kingdom*
(Received 30 September 2002; published 23 September 2003; publisher error corrected 25 September 2003)

We propose an experiment for creating quantum superposition states involving of the order of 10^{14} atoms via the interaction of a single photon with a tiny mirror. This mirror, mounted on a high-quality mechanical oscillator, is part of a high-finesse optical cavity which forms one arm of a Michelson interferometer. By observing the interference of the photon only, one can study the creation and decoherence of superpositions involving the mirror. A detailed analysis of the requirements shows that the experiment is within reach using a combination of state-of-the-art technologies.

DOI: 10.1103/PhysRevLett.91.130401 PACS numbers: 03.65.Ta, 03.65.Yz, 42.50.Ct

Introduction.—In 1935 Schrödinger pointed out that according to quantum mechanics even macroscopic systems can be in superposition states [1]. The associated quantum interference effects are expected to be hard to detect due to environment induced decoherence [2]. Nevertheless, there have been proposals on how to create and observe macroscopic superpositions in various systems [3–7], as well as experiments demonstrating superposition states of superconducting devices [8] and large molecules [9]. One long-term motivation for this kind of experiment is the search for unconventional decoherence processes [5,10].

In several of the above proposals a small quantum system (e.g., a photon [4–6] or a superconducting island [7]) is reversibly coupled to a large system (e.g., a moveable mirror [4–6] or a cantilever [7]) in order to create a macroscopic superposition. The existence of the quantum superposition of the large system is verified by observing the disappearance and reappearance of interference for the small system, as the large system is driven into a superposition and then returns to its initial state. The challenge is to find a feasible implementation of this idea.

Our proposal develops on the ideas in Refs. [4,5]. We also use results from Ref. [6], which relies on coupling between atoms and photons in a microcavity to create and detect superposition states of a moveable mirror. In particular, the formalism used in Ref. [6], based on Refs. [11,12], is applicable to our case. The main purpose here is to show that our purely optical proposal has the potential to be performed with current technology.

Principle.—The proposed setup, shown in Fig. 1, consists of a Michelson interferometer which has a high-finesse cavity in each arm. The cavity in arm (A) contains a tiny mirror attached to a micromechanical oscillator, similar to the cantilevers in atomic force microscopes. The cavity is used to enhance the radiation pressure of the photon on the mirror. The initial superposition of the photon being in either arm causes the system to evolve into a superposition of states corresponding to two distinct locations of the mirror. The observed interference of the photon allows one to study the creation of coherent superposition states of the mirror.

The system can be described by a Hamiltonian [6,11]

$$H = \hbar\omega_c a^\dagger a + \hbar\omega_m b^\dagger b - \hbar G a^\dagger a(b + b^\dagger), \quad (1)$$

where ω_c and a are the frequency and creation operator for the photon in the cavity, ω_m and b are the frequency and phonon creation operator for the center of mass motion of the mirror, and $G = (\omega_c/L)\sqrt{(\hbar/2M\omega_m)}$ is the coupling constant, where L is the cavity length and M is the mass of the mirror.

Let us suppose that initially the photon is in a superposition of being in either arm A or B, and the mirror is in

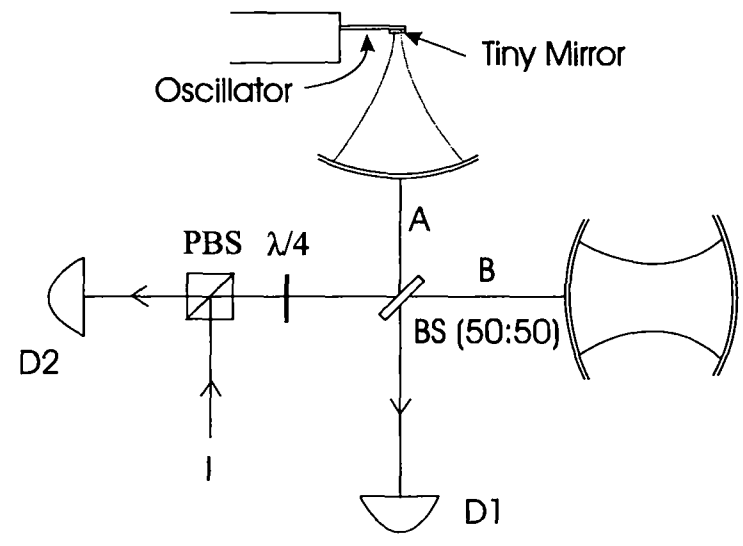

FIG. 1. The proposed setup: a Michelson interferometer for a single photon, where in each arm there is a high-finesse cavity. The cavity in arm A has a very small end mirror mounted on a micromechanical oscillator. The single photon comes in through I. If the photon is in arm A, the motion of the small mirror is affected by its radiation pressure. The photon later leaks out of either cavity and is detected at D1 or D2.

its ground state $|0\rangle_m$. Then the initial state is $|\psi(0)\rangle = (1/\sqrt{2})(|0\rangle_A|1\rangle_B + |1\rangle_A|0\rangle_B)|0\rangle_m$. After a time t the state of the system will be given by [6,12]

$$|\psi(t)\rangle = \frac{1}{\sqrt{2}} e^{-i\omega_c t}[|0\rangle_A|1\rangle_B|0\rangle_m + e^{i\kappa^2(\omega_m t - \sin\omega_m t)}|1\rangle_A|0\rangle_B \times |\kappa(1 - e^{-i\omega_m t})\rangle_m], \quad (2)$$

where $\kappa = G/\omega_m$, and $|\kappa(1 - e^{-i\omega_m t})\rangle_m$ denotes a coherent state with amplitude $\kappa(1 - e^{-i\omega_m t})$. In the second term on the right-hand side the mirror moves under the influence of the radiation pressure of the photon in cavity A. The mirror oscillates around a new equilibrium position determined by the driving force. The parameter κ quantifies the displacement of the mirror in units of the size of the ground state wave packet.

The maximum interference visibility for the photon is given by twice the modulus of the off-diagonal element of the photon's reduced density matrix. By tracing over the mirror one finds from Eq. (2) that the off-diagonal element has the form $\frac{1}{2} e^{-\kappa^2(1-\cos\omega_m t)} e^{i\kappa^2(\omega_m t - \sin\omega_m t)}$. The first factor is the modulus, reaching a minimum after half a period at $t = \pi/\omega_m$, when the mirror is at its maximum displacement. The second factor gives the phase, which is identical to that obtained classically due to the varying length of the cavity.

In the absence of decoherence, after a full period, the system is in the state $(1/\sqrt{2})(|0\rangle_A|1\rangle_B + e^{i\kappa^2 2\pi}|1\rangle_A|0\rangle_B) \times |0\rangle_m$, such that the mirror is again disentangled from the photon. Full interference can be observed if the photon is detected at this time, provided that the phase factor $e^{i\kappa^2 2\pi}$ is taken into account. This revival, shown in Fig. 2, demonstrates the coherence of the superposition state that exists at intermediate times. For $\kappa^2 \gtrsim 1$ the superposition involves two distinct mirror positions. If the environment of the mirror "remembers" that the mirror has moved, then, even after a full period, the photon will still be entangled with the mirror's environment, and thus the revival will not be complete. Therefore the setup can be used to measure the decoherence of the mirror.

Here we have assumed that the mirror starts out in its ground state. We will argue below that optical cooling close to the ground state should be possible. However, in Ref. [6] it was shown that this is not necessary for observing the revival, although for a thermal mirror state with an average phonon number $\bar{n} = 1/(e^{\hbar\omega_m/kT} - 1)$ the revival peak is narrowed by a factor of $\sqrt{\bar{n}}$, leading to stricter requirements on the stability; see Fig. 2 and the discussion below. We now discuss the experimental requirements for achieving a superposition of distinct mirror positions and for observing the revival at $t = 2\pi/\omega_m$.

Conditions for displacement by ground state size.—We require $\kappa^2 \gtrsim 1$, which implies the momentum imparted by the photon has to be larger than the initial quantum uncertainty of the mirror's momentum. Let N denote the number of round-trips of the photon in the cavity during one period of the mirror's motion, such that $2NL/c = 2\pi/\omega_m$. The condition $\kappa^2 \gtrsim 1$ can be written

$$\frac{2\hbar N^3 L}{\pi c M \lambda^2} \gtrsim 1, \quad (3)$$

where λ is the wavelength of the light. The factors entering Eq. (3) are not all independent. The achievable N, determined by the quality of the mirrors, and the minimum mirror size (and hence M) both depend on λ. The mirror's lateral dimension should be an order of magnitude larger than λ to limit diffraction losses. The thickness required in order to achieve sufficiently high reflectivity depends on λ as well.

Equation (3) allows one to compare the viability of different wavelength ranges. While the highest values for N are achievable for microwaves using superconducting mirrors (up to 10^{10}), this is counteracted by their longer wavelengths. On the other hand, there are no good mirrors for highly energetic photons. The optical regime is optimal, given current mirror technology. We propose an experiment with λ around 630 nm.

The cavity mode needs to have a sharp focus on the tiny mirror, which requires the other cavity end mirror to be large due to beam divergence. The maximum cavity length is therefore limited by the difficulty of making large high-quality mirrors. We propose a cavity length of 5 cm, and a small mirror size of $10 \times 10 \times 10$ μm, leading to a mass of order 5×10^{-12} kg.

Such a mirror on a mechanical oscillator can be fabricated by coating a silicon cantilever with alternating layers of SiO_2 and a metal oxide. The best current optical mirrors are made in this way. A larger silicon oscillator has been coated with SiO_2/Ta_2O_5 and used as part of a high-finesse cavity in Ref. [13].

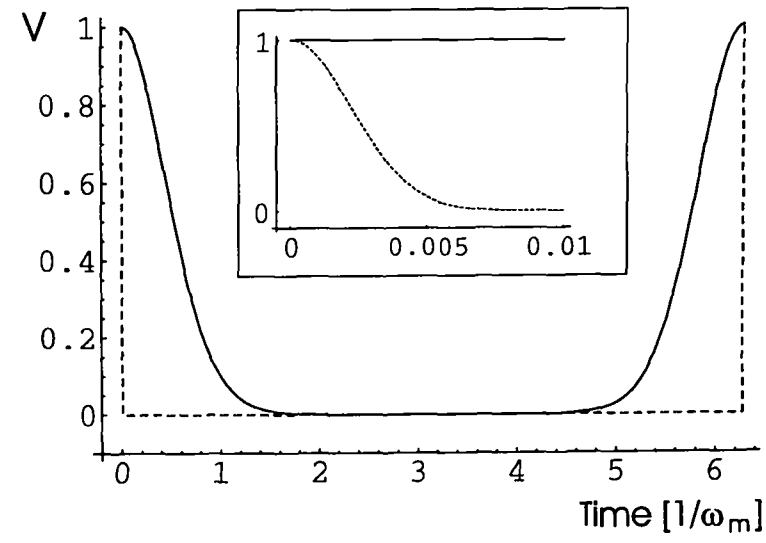

FIG. 2. Time evolution of the interference visibility V of the photon over one period of the mirror's motion for the case where the mirror has been optically cooled close to its ground state ($\bar{n} = 2$, solid line) and for $T = 2$ mK, which corresponds to $\bar{n} = 100\,000$ (dashed line—see also inset). The visibility decays after $t = 0$, but in the absence of decoherence there is a revival of the visibility after a full period. The width of the revival peak scales like $1/\sqrt{\bar{n}}$.

130401-2

For the above dimensions the condition Eq. (3) is satisfied for $N = 5.6 \times 10^6$. Correspondingly, photon loss per reflection must be smaller than 3×10^{-7}, about a factor of 4 below reported values for such mirrors [14] and for a transmission of 10^{-7}, consistent with a 10 μm mirror thickness. For these values, about 1% of the photons are still left in the cavity after a full period of the mirror. For the above values of N and L one obtains a frequency $\omega_m = 2\pi \times 500$ Hz. This corresponds to a spread of the mirror's ground state wave function of order 10^{-13} m.

The fact that a relatively large L is needed to satisfy Eq. (3) implies that the creation of superpositions following the microcavity based proposal of Ref. [6] imposes requirements beyond current technology. A large L is helpful because, for a given N, it allows a lower frequency ω_m, and thus a more weakly bound mirror that is easier to displace by the photon.

Decoherence.—The requirement of observing the revival puts a bound on the acceptable environmental decoherence. To estimate the expected decoherence we model the mirror's environment by an (Ohmic) bath of harmonic oscillators. The effect of this can approximately be described by a decoherence rate $\gamma_D = \gamma_m k T_E M(\Delta x)^2/\hbar^2$ governing the decay of off-diagonal elements between different mirror positions [2]. Here γ_m is the damping rate for the mechanical oscillator, T_E is the temperature of the environment, which is constituted mainly by the internal degrees of freedom of the mirror and cantilever, and Δx is the separation of two coherent states that are originally in a superposition. This approximation is strictly valid only for times much longer than $2\pi/\omega_m$ and for Δx large compared to the width of the individual wave packets. Here we assume that the order of magnitude of the decoherence is well captured by γ_D. If the experiment achieves $\kappa^2 \gtrsim 1$, i.e., a separation by the size of a coherent state wave packet, $\Delta x \sim \sqrt{(\hbar/M\omega_m)}$, the condition $\gamma_D \lesssim \omega_m$ can be cast in the form

$$Q \gtrsim \frac{kT_E}{\hbar\omega_m}, \tag{4}$$

where $Q = \omega_m/\gamma_m$ is the quality factor of the mechanical oscillator. For $Q \gtrsim 10^5$, which has been achieved [15] for silicon cantilevers of approximately the right dimensions and frequency, this implies that the temperature of the environment has to be of the order of 2 mK, which is achievable with state-of-the-art dilution refrigerators.

Optical cooling.—Cooling the mirror's center of mass motion significantly eases the stability requirements for the proposed experiment. A method for optical cooling of a mirror via feedback was first proposed in Ref. [16]. By observing the phase of the output field of a cavity, its length can be measured with high precision. This can be used to implement a feedback mechanism that cools the center of mass motion of the mirror far below the temperature of its environment. A variation of the original scheme was experimentally implemented in Ref. [17], where a vibrational mode of a macroscopic mirror was cooled using a feedback force proportional to the natural damping force, but larger by a gain factor g. The size of g determines the achievable final temperature for a given T_E. For a tiny mirror, large gain values are realistic using the radiation pressure of a second laser beam to implement the feedback force. To analyze cooling to the quantum regime, one has to take into account the fact that measurement and feedback introduce noise, Ref. [18].

For our proposed experiment the constant component of the feedback laser has to balance the force from the measurement field, since otherwise the mirror would start to oscillate when the light is turned off. Adapting Ref. [19], the final energy of the cooled mirror is given by

$$E_c = \frac{\hbar\omega_m}{2}\frac{1}{2(1+g)}\left[\frac{4k_B T_E}{\hbar\omega_m} + 2\zeta + \frac{g^2}{\eta\zeta}\right], \tag{5}$$

where T_E is the temperature of the mirror's environment, $\zeta = (64\pi c P/M\gamma_m\omega_m\lambda\gamma_c^2 L^2)$, with P the light intensity incident on the measurement cavity and γ_c the cavity decay rate, and η the detection efficiency. The first term in Eq. (5) comes from the original thermal fluctuations, which are suppressed by the feedback. The second term is the back action noise from the measurement and feedback light. It differs from the formula of Ref. [19] by a factor of 2 to include the noise from the feedback laser. The third term is the noise due to imperfect measurement. Increasing the light intensity in the cavity improves the measurement precision, but also increases the back action noise.

The energy of the mirror can be made very close to its ground state energy choosing realistic parameter values; $E_c = \hbar\omega_m$ can be achieved with $g = 6 \times 10^5$, $T_E = 2$ mK, $P = 10^{-8}$ W, $\gamma_c = 3 \times 10^7$ s^{-1}, $\lambda = 800$ nm, $\eta = 0.8$, $\gamma_m = 0.03$ s^{-1}, and M, ω_m, L as before. The necessary feedback force for such a high value of g can be achieved with a feedback laser intensity modulation of $\Delta P_{fb} = 10^{-6}$ W. To balance the measurement field, the constant component of the feedback laser should be $\bar{P}_{fb} = 4 \times 10^{-6}$ W. The relatively large value of γ_c can be achieved in the cavity used in the superposition experiment by working at a wavelength away from where the mirrors are optimal.

Once the mirror has been cooled close to its ground state, which is reached in a time of order $1/(\gamma_m g)$ [20], the measurement and feedback laser fields should be turned off simultaneously. Then the experiment proceeds as described above. Reheating of the mirror happens at a time scale of $1/\gamma_m$ [20] and thus is not a problem for a high-Q oscillator. After every run of the experiment, the mirror has to be reset to its initial state by the optical cooling procedure.

Stability.—The distance between the large cavity end mirror and the equilibrium position of the small mirror has to be stable to of order $\lambda/20N = 0.6 \times 10^{-14}$ m over

the whole measurement time, which is determined as follows. A single run of the experiment starts by sending a weak pulse into the interferometer, such that on average 0.1 photons go into either cavity. This probabilistically prepares a single-photon state as required to a good approximation. The two-photon contribution has to be kept low because it causes noise in the interferometer. Considering the required low value of ω_m and the fact that approximately 1% of the photons remain after a full period for the assumed loss, this implies a detection rate of approximately 10 photons per minute in the revival interval. Thus we demand stability to of order 10^{-14} m over a few minutes. Stability of order 10^{-13} m/min for an STM at 8 K was achieved with a rather simple suspension [21]. Gravitational wave observatories using interferometers also require very high stability in order to have a length sensitivity of 10^{-19} m over time scales of a ms or greater, for arm lengths of order 1 km [22]. If the mirror is in a thermal state, the revival peak is narrowed by a factor $\sqrt{\bar{n}}$ [6], leading to lower count rates in the revival interval and thus making the stability requirements stricter by the same factor, cf. Fig. 2.

The experiment also requires ultrahigh vacuum conditions in order to ensure that events where an atom hits the cantilever are sufficiently rare not to cause significant errors, which is at the level of about 5/s. Background gas particle densities of order $100/\text{cm}^3$ have been achieved [23] and are sufficient for our purposes.

Outlook and conclusions.—In principle the proposed setup has the potential to test wave function reduction models, in particular, the one of Ref. [5]. We estimate that the ratio Q/T needs to be improved by about 6 orders of magnitude from the values discussed in this Letter ($Q = 10^5$ and $T = 2$ mK) to make the predicted wave function decoherence rate comparable to the environmental decoherence rate. However, temperatures as low as 60 μK have been achieved with adiabatic demagnetization [24], while Q is known to increase with decreasing temperature [15] and through annealing [25].

We have performed a detailed study of the experimental requirements for the creation and observation of quantum superposition states of a mirror consisting of 10^{14} atoms, approximately 9 orders of magnitude more massive than any superposition observed to date. Our analysis shows that, while very demanding, this goal appears to be within reach of current technology.

This work was supported by the E.U. (IST-1999-10033). W. M. is supported by EPSRC (Contract No. 00309297). C. S. is supported by a Marie Curie Fund of the E.U. (No. HPMF-CT-2001-01205) and thanks the University of California Santa Barbara for its hospitality. R. P. thanks the NSF for support under Contract No. 00-90091 and the Leverhulme Foundation. We would like to thank S. Bose, M. Davies, M. de Dood, T. Knuuttila, R. Lalezari, A. Lamas-Linares, and J. Pethica for useful discussions.

[1] E. Schrödinger, Naturwissenschaften **23**, 807 (1935).
[2] E. Joos *et al.*, *Decoherence and the Appearance of a Classical World in Quantum Theory* (Springer, Berlin, 1996); W. H. Zurek, Phys. Today **44**, 36 (1991).
[3] J. Ruostekoski, M. J. Collett, R. Graham, and D. F. Walls, Phys. Rev. A **57**, 511 (1998); J. I. Cirac, M. Lewenstein, K. Molmer, and P. Zoller, Phys. Rev. A **57**, 1208 (1998).
[4] D. Bouwmeester, J. Schmiedmayer, H. Weinfurter, and A. Zeilinger, in *Gravitation and Relativity: At the Turn of the Millennium*, edited by N. Dadhich and J. Narlikar (IUCAA, Pune, 1998). This paper was based on discussions between J. Schmiedmayer, R. Penrose, D. Bouwmeester, J. Dapprich, H. Weinfurter, and A. Zeilinger (1997).
[5] R. Penrose, in *Mathematical Physics 2000*, edited by A. Fokas *et al.* (Imperial College, London, 2000).
[6] S. Bose, K. Jacobs, and P. L. Knight, Phys. Rev. A **59**, 3204 (1999).
[7] A. D. Armour, M. P. Blencowe, and K. C. Schwab, Phys. Rev. Lett. **88**, 148301 (2002).
[8] C. H. van der Wal *et al.*, Science **290**, 773 (2000); J. R. Friedman, V. Patel, W. Chen, S. K. Tolpygo, and J. E. Lukens, Nature (London) **406**, 43 (2000).
[9] M. Arndt *et al.*, Nature (London) **401**, 680 (1999); W. Schöllkopf and J. P. Toennies, Science **266**, 1345 (1994).
[10] G. C. Ghirardi, A. Rimini, and T. Weber, Phys. Rev. D **34**, 470 (1986); G. C. Ghirardi, P. Pearle, and A. Rimini, Phys. Rev. A **42**, 78 (1990); I. C. Percival, Proc. R. Soc. London A **447**, 189 (1994); D. I. Fivel, Phys. Rev. A **56**, 146 (1997); L. Diósi, Phys. Rev. A **40**, 1165 (1989).
[11] C. K. Law, Phys. Rev. A **51**, 2537 (1994); C. K. Law, Phys. Rev. A **49**, 433 (1993).
[12] S. Mancini, V. I. Man'ko, and P. Tombesi, Phys. Rev. A **55**, 3042 (1997).
[13] I. Tittonen *et al.*, Phys. Rev. A **59**, 1038 (1999).
[14] G. Rempe, R. J. Thompson, H. J. Kimble, and R. Lalezari, Opt. Lett. **17**, 363 (1992); C. J. Hood, H. J. Kimble, and J. Ye, Phys. Rev. A **64**, 033804 (2001).
[15] H. J. Mamin and D. Rugar, Appl. Phys. Lett. **79**, 3358 (2001).
[16] S. Mancini, D. Vitali, and P. Tombesi, Phys. Rev. Lett. **80**, 688 (1998).
[17] P. F. Cohadon, A. Heidmann, and M. Pinard, Phys. Rev. Lett. **83**, 3174 (1999).
[18] J.-M. Courty, A. Heidmann, and M. Pinard, Eur. Phys. J. D **17**, 399 (2001).
[19] D. Vitali, S. Mancini, L. Ribichini, and P. Tombesi, quant-ph/0211102.
[20] M. Pinard, P. F. Cohadon, T. Briant, and A. Heidmann, Phys. Rev. A **63**, 013808 (2000).
[21] B. C. Stipe, M. A. Rezaei, and W. Ho, Rev. Sci. Instrum. **70**, 137 (1999).
[22] S. Rowan and J. Hough, Living Rev. Relativity **3**, 2000 (2000).
[23] G. Gabrielse *et al.*, Phys. Rev. Lett. **65**, 1317 (1990).
[24] W. Yao *et al.*, J. Low Temp. Phys. **120**, 121 (2000).
[25] J. Yang, T. Ono, and M. Esashi, Appl. Phys. Lett. **77**, 3860 (2000).

In Preparation

A Macroscopic Cavity Involving a Microscopic Mirror on a Cantilever

William Marshall,[1,2] Michiel J. A. de Dood,[2] Hagai S. Eisenberg,[2] Khodadad Nima Dinyari,[2] and Dirk Bouwmeester[2]

[1]*Department of Physics, University of Oxford, Oxford OX1 3PU, UK*
[2]*Department of Physics, University of California Santa Barbara, CA 93106, Santa Barbara, USA*

(Dated: June 11, 2004)

We fabricate a 20μm diameter 30-layer SiO_2/Ta_2O_5 distributed Bragg reflector (DBR) mirror at 780nm and attach it to a silicon AFM-type cantilever. Measuring the Light Amplitude Ring-down Signal from an Optical Near-hemispherical resonator of length 2.5cm and which incorporates this tiny mirror/cantilever we demonstrate a finesse of $F > 1000$. Losses due to diffraction are calculated for this cavity geometry and this together with other limitations on the finesse are discussed. The set up meets the requirements needed for optical cooling of the cantilever and demonstrates preliminary technologies needed to demonstrate macroscopic superposition states involving the tiny mirror.

I. INTRODUCTION AND MOTIVATION

Coupling of photons to (micro)-mechanical systems, such as a cantilever, is of interest for accurate optical readout. The measurement accuracy ultimately depends on the intensity of the light field and could be increased by orders of magnitude if one could construct a high finesse cavity to read out the cantilever. This can be achieved by making a very high reflectivity cantilever or by simply attaching a dielectric mirror on the end of the cantilever. Although the measurement accuracy will benefit from higher light intensity, the light field also introduces feedback on the cantilever via the radiation pressure. This will displace the cantilever and puts a limit on the measurement accuracy Δx for an oscillator with mass m and frequency ω_0 , known as the "standard quantum limit": $\Delta x \geq \sqrt{\frac{\hbar}{2m\omega_0}}$.

On a more fundamental level, such a system is of interest to embark on a programme to study superpositions of larger mass systems in order to test quantum mechanics. To date there exist several proposals on how to create and observe superpositions in various macroscopic-mass systems [1, 2, 4? , 5]. Experimentally, quantum mechanics remains untested on mass scales $\gtrsim 10^{-25}$kg. The most massive superpostions demonstrated so far involve order 10^6 electrons in superconducting devices [6] and large ($\sim$ 100 atom) molecules in an atom interferometer [7].

In previous work [8], we discussed the technical feasibility of a scheme whose principle has been proposed in Ref. [2, 4?]. Here a photon is reversibly coupled via the radiation pressure to a mirror on a cantilever in order to create a macroscopic superposition involving two spatially distinct locations of the mirror. At the centre of the proposal lies a near-hemispherical cavity of $\sim$cm length, with a flat $\sim$ 10μm mirror as one of the end mirrors and an optical finesse $\sim 10^6$. A cavity of finesse 2×10^6 has been achieved for a cavity of mm length at optical wavelengths [11]. The $\sim$cm length of the cavity is dictated by the roundtrip time in the cavity that has to be long enough such that the cantilever has time to evolve into distinct spatial locations and then can be verified by monitoring the output of an interferometer over at least one oscillation period of the cantilever (typically in the milli-sec range) [8].

Conventional decoherence can be kept small by using low system temperatures and by using cantilevers of high mechanical quality $Q \geq 10^5$, which has been demonstrated for Si cantilevers, down to a thickness of $\sim$100 nm.

In this article we demonstrate the hemispherical cantilever-mirror cavity. To our knowledge we present the first demonstration of a macroscopic ($\sim$cm) cavity with a moveable micron-size mirror.

II. FABRICATION OF A MICROSCOPIC MIRROR ON A CANTILEVER

In the proposal of Ref. [8], the mirror mass was much larger than the cantilever mass. This can be achieved using state-of-the-art ultrathin cantilevers that also have a spring constant small enough such that the radiation pressure of a single photon in a high finesse ($> 10^6$) cavity is sufficient to displace the mirror. To facilitate the fabrication of the cavity and to allow initial studies to be done at room temperature use commercial atomic force microscope tips (Nanodevices Contact 10), that are an order of magnitude thicker than the ultrathin cantilevers. Ulitmately, we aim to fabricate a mirror of $\sim$ 10μm diameter and reflectivity $\sim$99.9997% and have this attached to the cantilever.

The high reflectivity of the mirror can be achieved by using dielectric mirrors with alternating high and low refractive index layers each of them $\lambda/4n$ thick, where n is the refractive index, such that the reflected intensities from each layer add constructively. In practice the best of such distributed Bragg reflectors (DBRs) at optical wavelengths are made using SiO_2 (n = 1.46) and Ta_2O_5 (n = 2.04) and have reflectivities of $\gtrsim$99.9997% at 780nm wavelength given $\gtrsim$ 37 layers and annealing [9]. Direct sputter deposition of such a mirror coating on a cantilever would yield a highly reflective cantilever. However, the strain build-up inherent to the deposition process results in significant bending of the cantilever due to strain. Therefore we developed an alternatively technique using a focused ion beam (FIB) to cut out a mirror that we glue on the cantilever.

Figure 1a shows scanning electron microscope (SEM) im-

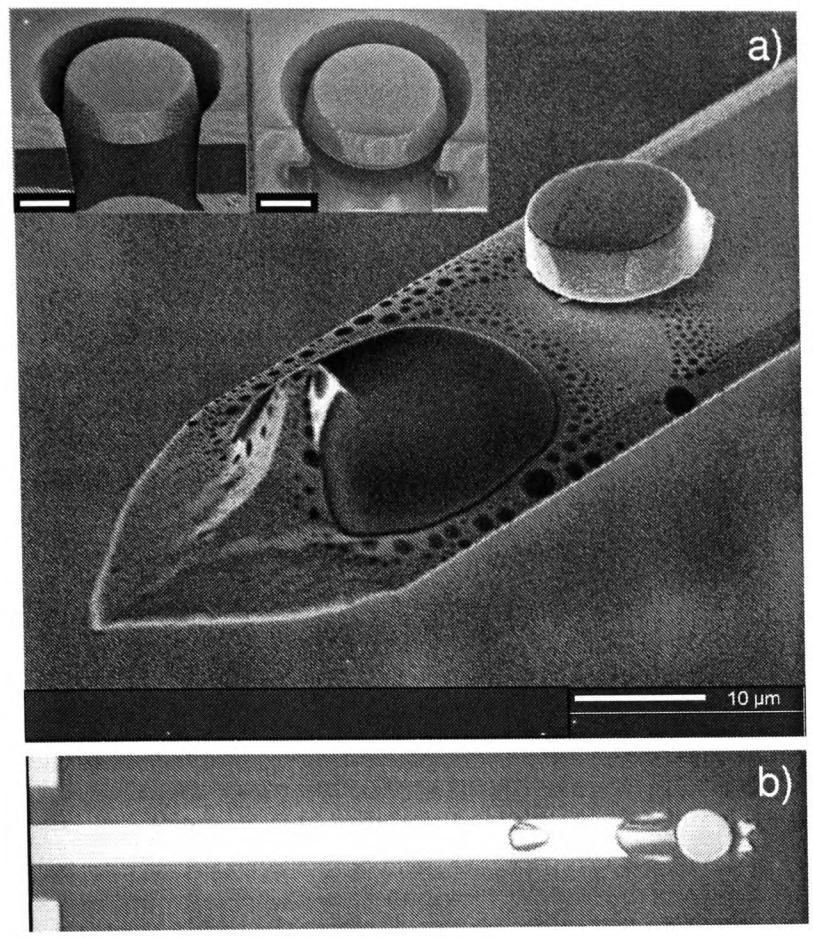

FIG. 1: SEM images of different steps in the fabrication process. (a) 10μm mirror glued on a commercial AFM tip. The insets show the same mirror after cutting from the top and the side repsectively, using a current of 7 nA in the FIB (scale bar is 5 μm). (b) Microscope image of a cantilever with 30μm diameter mirror.

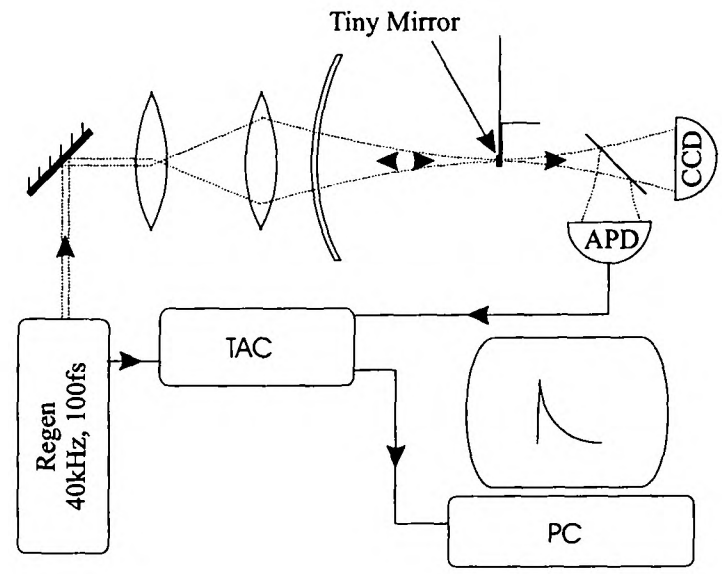

FIG. 2: A schematic of the experimental set up for cavity ring-down measurement. A Regenerative amplifier (Regen), with repetition rate 40kHz and pulse length 100fs, is incident on the cavity. An avalanche photo-diode (APD), capable of detecting individual photons and with timing information accurate to 0.5ns, detects the light transmitted through the cavity. A time-to-amplitude converter (TAC) measures the coincidence rate between the APD signal and the 40kHz trigger from the Regen. Every = 25μs, there should be a peak in coincidences corresponding to the laser pulse. After this pulse a decay curve is seen.

ages after subsequent steps the fabrication process. Our starting material consists of a a 30-layer SiO_2/Ta_2O_5 distributed Bragg reflector deposited on a conductive silicon substrate. The mirror has a designed peak reflectance of $R > 99.995\%$ [12] for 780nm wavelength. The FIB uses 30 keV Ga^+ ions that sputter away the mirror material so as to form a freestanding mirror. The first cut is made normal to the mirror surface, and at its edge, in the shape of a ring of inner diameter that of the intended mirror diameter (see the inset of Fig. 1a). We intentionally made this cut about $1 - 2\mu$m deeper than the thickness of the mirror layers. After rotating the sample by 90 degrees we made a second, rectangular, cut just below the mirror leaving the mirror almost completely free. To ensure that this cut is parallel to the mirror surface we needed to tilt the sample by an additional $\sim 6°$ to correct for the angle of the sidewalls of the cuts made by the FIB at the current of 7 nA used.

—

To transfer the mirror on the cantilever, we used a procedure reminescent of the procedure to transfer transmission electron microscope samples cut out with the FIB.

In the first step, we place a tiny droplet of glue on the cantilever using a glass fiber

The re-deposition places current practical limits on our ability to cut mirrors larger than 35μm.

Manipulating the mirror onto the cantilever is done in three steps, largely based on the procedure known for SEM tip making [13, 14]: (1) under a microscope, a sharp glass rod with a tip diameter of $3 - 5\mu$m mounted on a 3-axis micrometer translation stage, is manoeuvered to touch the mirror and snap it from its substrate. (2) Elecrostatic forces allow the mirror to be moved with the glass rod and placed on to an AFM cantilever with the rod. The cantilevers used were "Contact 10" single crystal silicon AFM cantilevers of dimension $450 \times 35 \times 4\mu$m, resonance frequency 10kHz, and typical spring constant 0.1N/m [15], which are known to have high quality factors once annealed [16] (3) A droplet of transparent epoxy glue of diameter $\sim 1 - 5\mu$m is placed on the cantilever and touching the mirror.

III. CAVITY RING-DOWN

A fixed cavity with a constant incident field contains a fixed field energy, and a fixed transmission intensity I_0. If the input is switched off then the energy of the cavity field decays exponentially and so does the transmission intensity as $I = I_0 e^{-t/\tau}$ where τ is related to the finesse F of the cavity by $\tau = \frac{LF}{2\pi c}$ where c is the speed of light and L is the cavity length.

Our set up to measure the decay is shown and described in fig.2. The limitations of the method are firstly that the time jitter of the APD of 0.5ns limits the finesses measurement to above $\gtrsim 5$ for the 2.5cm length cavity. Secondly, after detection of a photon the APD has a dead time of 20ns, thus for each pulse we typically have just one photon and the measurement curve only results from the average of decays from many

pulses over the period of integration, typically $1 - 100$s for a typical count rate of $5000/s$.

The system was tested up to a finesse of $F = 1.1 \times 10^6$ using a planar-concave cavity of similar length but with two large mirrors to ensure that we are not system limited.

To align the cavity one has to find the properties of the Gaussian beam which self-repeats after one round trip (the fundamental mode).

The solution for a planar-concave cavity has a complex beam parameter q given by $\frac{1}{q} = \frac{1}{R} - \frac{i\lambda}{\pi w^2}$ where w is the width of the beam and R is its radius of curvature, that must satisfy [23] $q = -d \pm d\sqrt{1 - R/d}$ where d is the mirror separation. The solution giving a real beam width shows that the beam width at the small mirror is

$$w_0^2 = \frac{\lambda}{2\pi}\sqrt{d(R-d)} \tag{1}$$

and that the beam width at the other mirror is inversely proportional to that, given by

$$w_0 = \frac{\lambda R}{\pi w_1}. \tag{2}$$

Both are determined by the cavity length to which they are very sensitive as $d \to R$. Such a cavity is stable so long as $d \leq R$. This cavity mode can be matched to by the incoupling beam through standard mode matching techniques. There are higher order modes solutions to the wave equation also, but for cavities in linear media always have lower finesse [25].

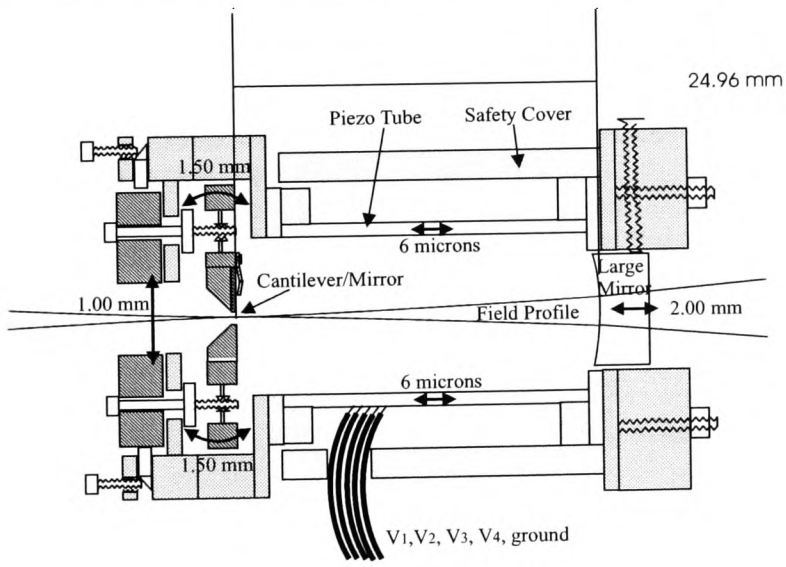

FIG. 3: The cavity mount.

The optimum cavity length is approximately given when the ratio of spot size to mirror aperture is equal at both ends since this minimizes power losses. For our cantilever mirror of radius 10μm and larger mirror radius 3mm this is the case for a focus radius at the tiny mirror of $w_0 = 4.55\mu$m, and radius $w_1 = 1.36$mm at the large mirror which corresponds to a cavity length $d = 24.99972$mm.

A specially designed cavity mount, shown in Fig.3, enabled 5 degrees of freedom of the cantilever, θ_x, θ_y, x, y and z,

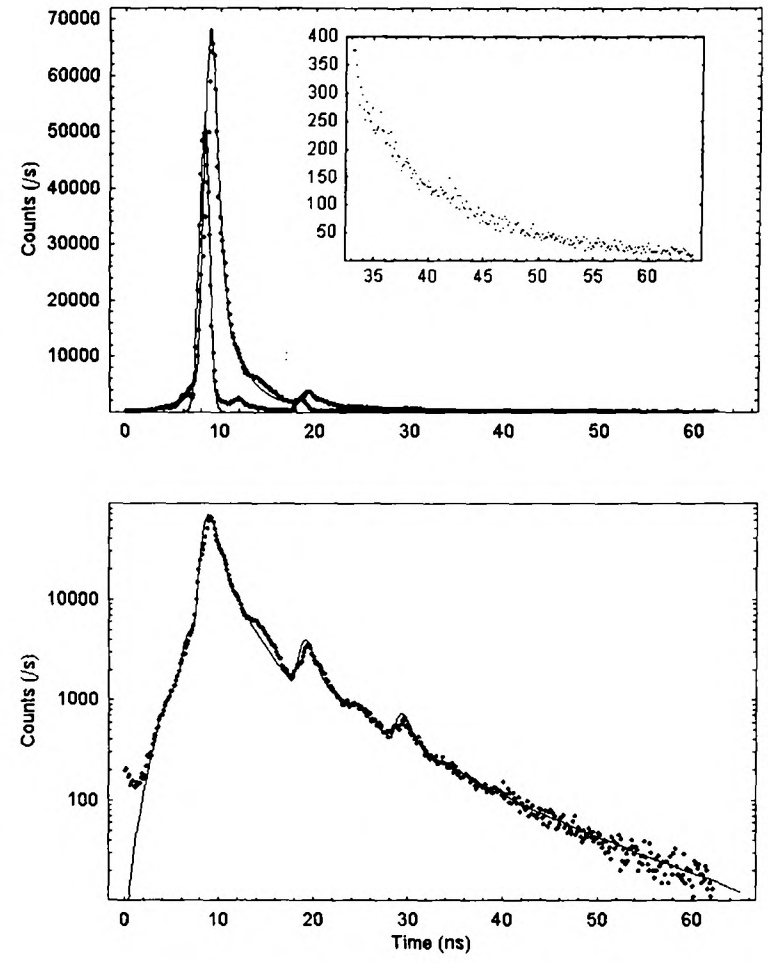

FIG. 4: CRD: (a) the field exiting the cavity is measured versus time after the pulse. The near-Gaussian peak is a misaligned cavity. The longer decay is that of the aligned cavity showing a finesse of F= 415 ± 30 at 12ns after the pulse (shown in the inset).(b) the same on a log plot showing a non-single exponential decay

where z is the optical axis, with respect to the other cavity mirror. The cantilever orientation and position with respect to the large mirror can be moved coursely using the 4 outer screws on the left hand side of the mount for movements in the plane x, y and 4 inner screws for z, θ_x, θ_y. This coarse adjustment allows a x,y,z range of $\sim$ 1mm and resolution of 0.01mm and θ_x, θ_y range of 10 degrees and resolution 0.3 degrees. The cantilever and large cavity mirror are held together with a piezo electric tube with 4 quandrant contacts on the outside and one on the inside allowing fine adjustment of z, (x, θ_x), (y, θ_y), where the brackets indicate coupling, of range 6μm, resolution $\sim$ 10nm, in translation and range 0.1^o and resolution 0.001^o in rotation.

Initial alignment was achieved by using a CCD camera to image the plane of the cantilever: the focussed beam was placed on the cantilever mirror and the first reflection spot from this used as a gauge with which to adjust the cavity length and alignment, such that this spot was focussed and also on top of the mirror. The incoupling optics were set to achieve a diffraction limited spot size of 3μm, but in practice was $5 - 6\mu$m.

CRD data was taken with the cavity aligned and misaligned fig.4. The data for the misaligned cavity is fit well by a Gaus-

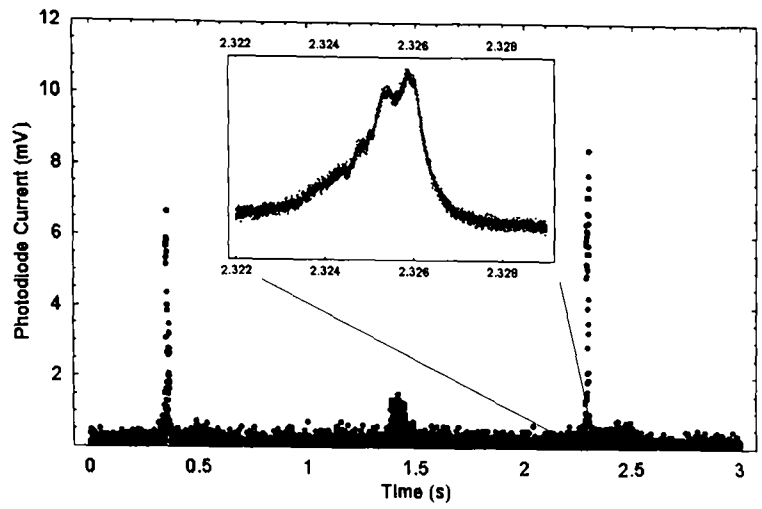

FIG. 5: Power transmitting through the cavity onto a photodiode is measured vs. time whilst the wavelength is scanned 0.05nm at 0.1Hz. The cavity Fabry-Perot peaks show a free spectral range of 2s, and a peak full width half maximum (see inset) of < 2ms

sian of width 0.34ns limited by time jitter of the APD. The longer decay curve associated with the aligned cavity shows a steep decay region immediately after the pulse which flattens to a shallower slope after $\sim 10 - 15$ns. This was fit with the convolution of the function generated by the interpolation of the misaligned cavity with two exponential decays with decay constants 0.9 ± 0.03 and 11 ± 1ns. This indicates that we are coupling to more than one mode and not perfectly to the high finesse one. This behaviour can be expected since the solution beam profile is non-Gaussian (see Sect. IV) and thus cannot be coupled to perfectly with a Gaussian beam. The longer ring down time corresponds to F$= 415 \pm 30$ and contains $6 \pm 1\%$ of the input power. The anomylous-looking peaks on the decay correspond to small power leakage of the regenerative amplifier, their separation in time corresponding to one cavity round trip time for that system.

By measuring the width and free spectral range of Fabry-Perot peaks seen through the cavity when illuminated by a continuous wave (external-cavity diode) laser source by scanning the wavelength over 0.05nm the finesse was confirmed to be > 1000, as shown in fig.5. The deviation from the CRD results can be attributed to alignment differences.

IV. LIMITATIONS

In practice the finesse F is limited by Mirror Reflectivity (F$_r$), Scattering and Absorption (F$_s$), Diffraction Losses (F$_d$), Geometric Losses (F$_g$) and Mechanical Stability (F$_m$), and is given by the following relation:

$$\frac{1}{F} = \frac{1}{F_r} + \frac{1}{F_s} + \frac{1}{F_d} + \frac{1}{F_g} + \frac{1}{F_m}. \qquad (3)$$

Each factor is discussed below, apart from F_s which is the limit on the finesse due to internal scattering and absorption in the cavity which we assume to be negligible (F$_s > 10^6$).

1. Mirror reflectivity $F_r \sim \frac{2\pi}{1-R_1R_2}$ where R_1 and R_2 are the reflectivities of the two mirrors: This is theoretically at most $F_r < 1.9 \times 10^5$ due to the designed DBR quality. However, cantilever mirror might not be as good as the designed DBR structure due to (a) spoiling of the mirror layers by the focussed ion beam which incorporates gallium ions and defects in the mirror at the edges a too high density of which would create a different refractive index or could cause absorption and thus ruin the mirror; (b) The mirror surface may be scratched by the 'picking' process. (c) The epoxy glue used to fasten the mirror to the cantilever may cause stress on the mirror layers causing deformation from flat, as can intrinsic stress.

2. Diffraction losses associated with finite sized mirrors causing the Finesse limitation F$_d$:

A first naive approach leads to the simple power loss of a Gaussian beam reflected by a finite mirror is given by

$$\frac{2}{\pi w^2}\int_{a_2}^{\infty} 2\pi r e^{-2r^2/w^2} dr = e^{-2a^2/w^2}. \qquad (4)$$

where a is the radius of the mirror and w is the beam radius at the mirror. From eqn(1) the losses per mirror reflection for the solution mode for the cavity with no apertures become $|\gamma|^2 = e^{-\frac{2\pi a_0 a_1}{\lambda R}}$. For our set up the losses are 3.4×10^{-4}.

More correctly we use the Huygen's integral to determine the field $u_2(r_2, \phi_2)$ at a distance d from a given aperture (or in our case finite mirror) given an arbitrary input field $u_1(r_1, \phi_1)$ which in cylindrical coordinates and given a circular aperture radius a is [27]:

$$u_1(r_2,\phi_2) = \frac{i}{2\lambda}\int_{r_1=0}^{a}\int_{\phi=0}^{2\pi} u_1(r_1,\phi_1)\frac{e^{-i2\pi\rho/\lambda}}{\rho}(cos\theta(r_1 r_2))r_1 d\phi_1$$

where θ is the angle between the element axis and the vector ρ which is the displacement between a point on the input aperture to any point of observation which for spherical mirrors of curvature R$_1$ and R$_2$ is

$$\rho = \sqrt{d^2 + g_1 r_1^2 + g_2 r_2^2 - 2r_1 r_2 cos(\phi_1 - \phi_2)}. \qquad (6)$$

where $g_1 = 1 - d/R_1$ and $g_2 = 1 - d/R_2$.

This is performed twice – once at each mirror aperture – to get the field profile after one round trip, relative to the input field. This is an eigenvalue equation for the propogator of the beam in the cavity. It has no known exact solution except in a few particular cases e.g. the confocal and parallel-plane geometries but for the near hemispherical resonator. It must be solved numerically. Fox and Li first performed such a numerical analysis using a method of successive approximations [25]. This is equivalent to propogating an initial arbitrary beam back and forth in the cavity until the field profile is self repeating except for a reduction in power $1 - |\gamma|^2$ per round trip. This is related to the finesse limitation F$_d = \frac{2\pi}{1-|\gamma|^2}$ This steady state solution is the normal mode of the cavity. Li also implemented this approach for the near-hemispherical

resonator [28] and Taché et al [26] gave an approximate expression for some of the results of ref.[28] but neither studies contain results directly relevant to our mirror sizes.

Under the Fresnel approximation $\rho \sim d + (r_1 + r_2 - 2r_1 r_2 cos(\phi_1 - \phi_2))/(2d)$ and noting the relation

$$e^{in(\pi/2-\beta)} J_n(xy) = \frac{1}{2\pi} \int_0^{2\pi} e^{ixycos(\alpha-\beta)-n\alpha} d\alpha \quad (7)$$

the eigenvalue integral equations reduce to

$$F_n^{(2)}(r_2) = \frac{\gamma_n^{(2)}}{\sqrt{r_2}} \int_0^{a_1} K_n(r_2, r_1) F_n^{(1)}(r_1) \sqrt{r_1} dr_1$$
$$F_n^{(1)}(r_1) = \frac{\gamma_n^{(1)}}{\sqrt{r_1}} \int_0^{a_2} K_n(r_2, r_1) F_n^{(2)}(r_2) \sqrt{r_2} dr_2 \quad (8)$$

where F is the componant of the field $u = F(r)e^{-i\phi}$ and the Huygen's kernel K for two circular mirrors, [28]

$$K_n(r_2, r_1) = \frac{i^{n+1} 2\pi}{\lambda d} J_n(\frac{2\pi r_1 r_2}{\lambda d}) \sqrt{r_1 r_2} e^{-\frac{i2\pi(g_1 r_1^2 + g_2 r_2^2)}{\lambda d}} \quad (9)$$

In our case the flat mirror has $g_1 = 1$, and the mode of interest is the TEM_{00} mode for which n= 0. The Fox and Li method was used to solve these. The beam profile converged in $15 - 1000$ round trips, depending on the exact cavity parameters computed. The routine was checked against results for a hemispherical cavity performed by Li[28].

For our set up the radius of the small flat mirror $a_0 = 10\mu$m and the large curved mirror has a radius $a_1 = 3$mm and a radius of curvature $R = 25mm$. We start with an input beam $u_1(r_1, \phi_1)$ which is Gaussian and an exact solution of this geometry assuming no edge effects, which is given by eqns.1,2. The solution where the mirror separation is such that the ratio of beam width to mirror width is identical at each ends is when the beam focus is $w_0 = 4.55\mu$m and the beam radius at the large mirror $w_1 = 1.36$mm, which dictates a cavity length of exactly 24.99972mm. This is expected to be close to the lowest loss mode for a cavity with finite mirrors.

Solving Eqs.8 for these parameters gives a power loss per round trip of the solution mode due to diffraction of $1 - |\gamma|^2 = 4 \times 10^{-7}$ corresponding to $F_d = 1.6 \times 10^7$. The shape of the solution beam that was converged to is shown in Fig.6 at the small mirror and also the initial Gaussian input beam. In addition the decay in power of the field as a function of number of round trips is shown, where it can be seen that the loss levels off to a constant after 38 round trips. This can be compared to fig.4 noting that 6 round trips corresponds to 1ns.

The loss expected from these considerations is a factor 430 less than the naive Gaussian loss calculation. This can be understood from the evolving beam profile which tends to "tuck in" the wings of the beam as seen in fig.6 where the solution mode profile sharply reduces in amplitude just before the mirror edge at 10μm.

Note on the validity of the Fresnel approximation: mathematically the approximation requires that $\frac{a^2}{\lambda d} << (\frac{a}{d})^2$ which

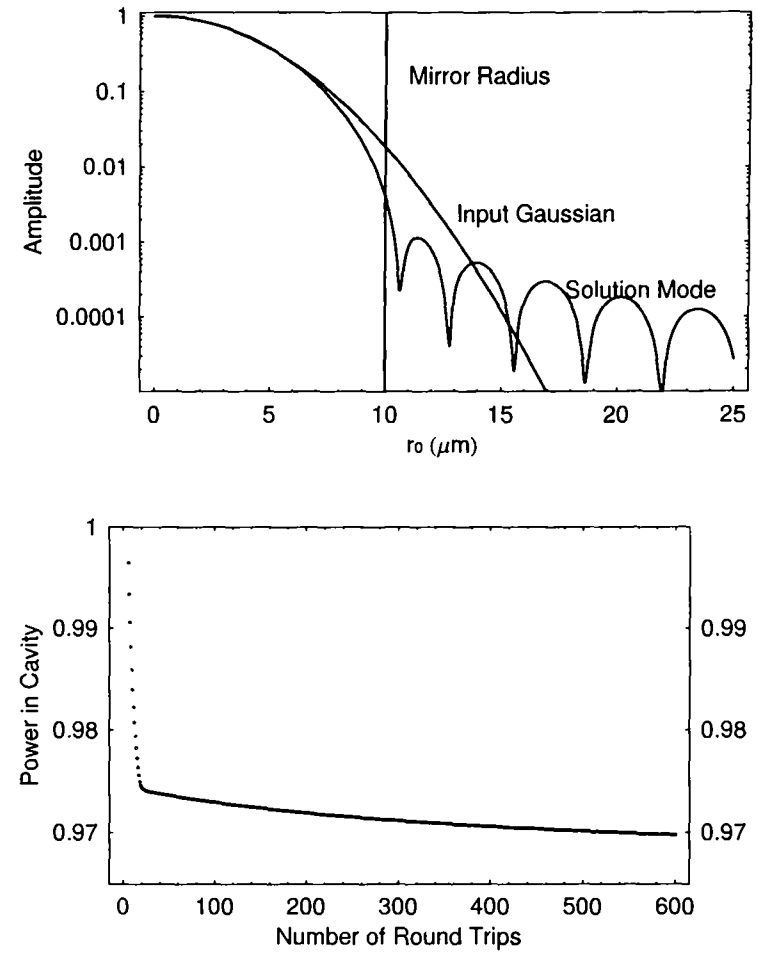

FIG. 6: Top: The solution mode for the cavity with diffraction loss (solid) compared to the input Gaussian profile (dashed). Bottom: The energy in the cavity as a function of number of round trips for ideal alignment (bold) and for the cavity length misaligned by 10μm. The loss rate settles to 0.99998 after 29 round trips for the former and to 0.99921 after 100 round trips for the latter

physically demands that the ratio of length of the cavity to the mirror diameter be large. This condition is not met in our geometry for the integral over the large mirror. However there is an inconsistency with this limitation since there is no such equivalent near-field limit for the paraxial approximation which is mathematically identical to the Fresnel approximation. It turns out that the Huygen's integral in the Fresnel approximation can be applied when the above condition is not met so long as the beam is truely paraxial [27]. The ratio of sizes of the terms in z to those in the x,y plane in the wave equation is given by $\theta^2/4$ and in our case of $\theta < 1/15$, the ratio is over 10^3 and thus the beam is truely paraxial.

3. Geometric losses causing a finesse limitation F_g, are effects due to non-perfect alignment: in a near-hemispherical cavity an angular misalignment of either mirror simply moves the element axis away from the centre of the curved mirror – a situation that is identical except for where the mirror edges are wrt the beam which, to a first approximation effectively reduces the mirror aperture, and thus acts to increase the diffraction losses.

We estimate that the relative angle of the elements axes of the two mirrors is < 1 degree. With a cavity length of 25mm,

this corresponds to 0.5mm offset of the beam on the large mirror. To a first approximation the losses in such a geometry would be the same as with the case of the big mirror reducing in radius by 0.5mm which from our diffraction loss calculations show increases loss by a factor 70 keeping all other factors equal. Double that angle would be a factor 2000.

Losses due to length misalignments are much more critical than angular misalignments and are computed directly by changing L in the diffraction calculation. For example a cavity length change of 1, 10 and 100μm from the optimum results in increased losses of a factor 50, 2000 and 10^5 respectively for increases and decreases in cavity length alike.

4. Mechanical Stability, F_m: Mechanical vibrations on the $<$ 1s measurement timescale can be from 3 sources: (a) shot noise from the laser, (b) thermal noise and (c) acoustic noise. The fabry-perot method of measuring the finesse is considerably more sensitive to vibrations than the cavity ring down since the transmission in the former method depends on the phase and hence the length $\Delta x < 2\pi\lambda/F$, which gives an upper limit of the vibrations at $<$ 5nm.

The motion due to shot noise is given by $\sqrt{\frac{N}{\omega}}\frac{Fh}{2\pi\lambda} = kx$ where ω is the frequency of interest and N is the number of photons per second in the beam. For 1mW power, and F= 1000 then x= 1.6×10^{-15}m and is thus not the limiting factor here.

The average motion $\langle x\rangle$ due to thermal energy in cantilever at a temperature T is given by $k_BT = k\langle x^2\rangle$, where k_B is Boltzmans constant. At room temperature we expect thermal vibrations to be of order x= 0.1nm for a cantilever such as the one used herein which has a force constant of 0.1Nm. This amplitude corresponds to $F_m = 5\times10^4$. The amplitude scales with the cantilever dimensions since $k \propto wt^3/L^2$, where w, t and L are the cantilever width, thickness and length respectively.

Acoustic noise intensity I at the resonance frequency or its harmonics results in a vibration amplitude x is given by $I = \frac{kx}{A}\frac{1}{2v\rho}$ where v is the velocity of sound in air and ρ is the density of air. To interfere with the cavity finesse at the best measured value an intensity of $I < 5\times10^{-7}W/m^2$ is required for a cantilever of dimensions used here – a sound level similar to that in our laboratory.

5. Coupling losses

This does not effect the finesse of the modes but alters the initial energy in them and the number of round trips needed to reach the optimum field profile. The decay of the energy observed in CRD is a summation of exponential decays of different finesse modes in which one couples light. Higher finesse modes with low energy can be hidden by low finesse modes of high energy initially, but will always dominate at longer decay times. It is not possible to prepare the complicated cavity solution beam profile see in fig.6 but that mode has a $>$ 97% overlap with a Gaussian beam amplitude so it suffices to consider the coupling of two Gaussian beams.

The coupling coefficients for the matching of two Gaussian beams given the four possible misalignments of (1) separation of the waists by a displacement Δz, (2) a lateral displacement of the beams Δr, (3) an angular separation of the beams θ and (4) a ratio of waist sizes $w_r = w_{0a}/w_{0b}$ is given in [29]. We estimate that our set up ensures that $\Delta z < 20\mu$m, $\Delta r < 2\mu$m, $w_r > 0.57$ for subscript a being the cavity solution mode and b being the incoupling beam (whose waist tends to be larger than ideal due to inperfect lenses) and $\theta <$ 1degree. From [29] these values cause a total incoupling efficiency $>$ 50%.

V. CONCLUSIONS

We have demonstrated a finesse of $F = 1000 \pm 30$ with a near-hemispherical cavity which has the flat DBR mirror of dimension 20μm mounted on a high-mechanical quality cantilever.

The limitations on finesse are dominated by accoustic vibrations. Thermal motion will become a significant loss if the finesse were to be increased by just 10 at this temperature.

The set up is useful for optical cooling of the cantilevers centre of mass motion as discussed in [8]. There is however problem of reheating and the overall scope is unclear as a result of large uncertainty in the thermal conductivity of silicon at very low temperatures.

The set up can be used to progress towards the capability to create macroscopic superposition states [8], which require an increase in finesse of 3-4 orders of magnitude than that shown here. Such an increase seems achievable by increasing the tiny mirror size to 12μm to offset diffraction losses, placing the set up in vacuum to aliviate accoustic vibrations by 3-4 orders (possibly with use of a simple suspension) and if the cantilver centre of mass motion is cooled to $\sim$ 50μK to offset thermal noise. The former of these requirements is simple to meet and the latter twho are in anycase needed for the achievement of verification of the superposition state since a number of other constraints need to be met which include the optical cooling of the cantilever motion to the ground state as above, the housing of the cantilever in a high vacuum ($<$ 100 atoms/cm^3), the cooling of the set up to mK temperatures and with high relative mechanical stability of the mirrors (10^{-14}m/min).

This work was supported by the National Science Foundation NIRT (number). W.M. is supported by EPSRC (award no. 00309297). We thank Doug Rehn of the UCSB Physics workshop for the construction of the cavity mount. We would like to thank Nano Devices Inc., Santa Barbara USA for the donation of test cantilevers and R. Lalezari of Advanced Thin Films, USA for the sputter deposition run and useful advice.

[1] J. Ruostekoski, M. J. Collett, R. Graham, and D. F. Walls, Phys. Rev. A **57**, 511 (1998); J. I. Cirac, M. Lewenstein, K. Molmer, and P. Zoller, Phys. Rev. A **57**, 1208 (1998).

[2] D. Bouwmeester, J. Schmiedmayer, H. Weinfurter, and A. Zeilinger, in N. Dadhich and J. Narlikar (Eds.), *Gravitation and Relativity: At the turn of the Millennium* (IUCAA, Pune, 1998).

[3] R. Penrose, in A. Fokas *et al.* (Eds.), *Mathematical Physics 2000* (Imperial College, London, 2000).
[4] S. Bose, K. Jacobs, and P.L. Knight, Phys. Rev. A **59**, 3204 (1999).
[5] A.D. Armour, M.P. Blencowe, and K.C. Schwab, Phys. Rev. Lett. **88**, 148301 (2002).
[6] C.H. van der Wal *et al.*, Science **290**, 773 (2000); J.R. Friedman, V. Patel, W. Chen, S.K. Tolpygo, and J.E. Lukens, Nature **406**, 43 (2000).
[7] M. Arndt *et al.*, Nature **401**, 680 (1999); W. Schöllkopf and J. P. Toennies, Science **266**, 1345 (1994).
[8] W. Marshall, C. Simon, R. Penrose and D. Bouwmeester, *Towards Quantum Superpositions of a Mirror*, Phys. Rev. Lett. **91**, 130401, (2003)
[9] Christina J. Hood, 'Real-time Measurement and Trapping of Single Atoms by Single Photons', Thesis, California Insitute of Technology; Hood, 'Characterisation of high-finesse mirrors: Loss, phase shifts, and mode structure in an optical cavity' PRA 64, 033804,
[10] E.C. Vail, G.S. Li, W. Yuen and C.J. Chang-Hasnain, "High performance micromechanical tunable vertical cavity surface emitting lasers" Electron. Lett. **32** 1888.. (1996); M.R. McDaniel, D.L. Huffaker and D.G. Deppe "Hybrid dielectric/metal reflector for low threshold vertical-cavity surface-emitting lasers" Electron. Lett. **33**, 1704, (1997); M.Y Li, W. Yuen and C.J. Chang-Hasnain, "Top-Emitting micromechanical VCSEL with 31.6-nm Tuning Range" IEEE Photonics. Tehc. Lett. **10**, 18 (1998)
[11] G. Rempe, R.J. Thompson, H.J. Kimble, and R. Lalezari, Opt. Lett. **17**, 363 (1992); C.J. Hood, H.J. Kimble, and J. Ye, Phys. Rev. A **64**, 033804 (2001).
[12] Personal Communication, Advanced Thin Films, Longmont, Colorado, USA
[13] Hansma P., Personal Communication, September 2003
[14] Digital Instruments, 'Attaching Particles to AFM Cantilevers', support note 226, Rev. A
[15] Contact 10 probes were obtained from Nano Devices, Santa Barbara, CA, *http* : *//www.nanodevices.com/pdf/Siliconspecsheetv*1*.pdf*
[16] Find Rougar paper
[17] I. Tittonen *et al.*, Phys. Rev. A **59**, 1038 (1999).
[23] H. Kogelnik and T. Li, "Laser Beams and Resonators", Proceedings of the IEEE vol. 54, pp. 1312, Oct. 1966.
[19] C.J. Hood, H.J. Kimble, and J. Ye, Phys. Rev. A **64**, 033804 (2001).
[20] Courty, 'Quantum limits of cold damping with optomechanical coupling' quant-ph/0107138, 27.7.01
[21] Tittonen, PRA 59, 1038 (1999) (high Q cavity) [31]
[22] Rempe, PRL 64, 2783 (1990) [32]
[23] H. Kogelnik and T. Li, 'Laser Beams and Resonators' Poc. IEEE, vol. 54, pp. 1312, Oct. 1966
[24] Fischer, P. et al. 'Feedback on the Motion of a Single Atom in an Optical Cavity' Phys. Rev. Lett. 88, 163002 (2002).
[25] A. Fox, T. Li, 'Computation of Optical Resonator Modes by the Method of Resonance Excitation', IEEE J. Quantum Electron. QE-4, 460
[26] J. P. Taché, 'Experimental determination of diffraction losses in a near-hemispherical resonator', Opt. Quantum Electron. **16** p71, 1984
[27] A. Siegman, 'Lasers' University Science Books, 1966, pg. 635
[28] Li, 'Diffraction loss and seletion of modes in maser reonators with circular mirrors', Bell Syst. Tech. J. **44** 917 (1965)
[29] P. F. Goldsmith, *Quasioptical Systems*, IEEE Press (1998).
[30] D. Vitali, S. Mancini, L. Ribichini, and P. Tombesi, quant-ph/0211102 (2002).

submitted to Appl. Phys. Lett.

Ultrafast Optical Response of a High Reflectivity GaAs/AlAs Bragg Mirror

Sara R. Hastings,[1] Michiel J. A. de Dood,[1,*] William Marshall,[2,1] Hagai S. Eisenberg,[1] and Dirk Bouwmeester[1]

[1] *Department of Physics, University of California at Santa Barbara, Santa Barbara, CA 93106*
[2] *Department of Physics, University of Oxford, Oxford OXI 3PU, United Kingdom*

The ultrafast response of a high reflectivity GaAs/AlAs Bragg mirror to optical pumping is investigated for all-optical switching applications. Both Kerr and free carrier nonlinearities are induced with 100 fs, 780 nm pulses with a fluence of 0.64 kJ/m^2 and 0.8 kJ/m^2. The absolute transmission of the mirror at 931 nm increases by a factor of 27 from 0.0024% to 0.065% on a picosecond timescale. These results demonstrate the potential for a high reflectivity ultrafast switchable mirror for quantum optics and optical communication applications. A design is proposed for a structure to be pumped below the bandgaps of the semiconductor mirror materials. Theoretical calculations on this structure show switching ratios up to 3,800 corresponding to switching from 0.012% to 45.6% transmission.

PACS numbers: 42.65.Pc 42.70.Nq 42.70.Qs

High finesse optical cavities are of interest in quantum optics experiments, in particular for cavity QED [1] and quantum state storage [2]. In many of these experiments it would be beneficial to be able to switch light in and out of a cavity on a fast timescale. Common Q-switching cavities use intracavity elements which unavoidably introduce additional cavity losses, limiting the finesse. In addition, switching elements such as acousto-optic modulators or Pockels cells are limited to timescales longer than tens of picoseconds.

Instead, we propose to switch the finesse of the cavity by switching one of the cavity end mirrors. The high reflectivity cavity mirrors are composed of alternating layers of two different dielectric materials. Ideally the layer thicknesses in this Bragg mirror are $\lambda/4n$, where n is the refractive index of each of the materials. If the index of refraction of at least one of the materials can be switched rapidly, the reflectivity of the mirror will change on the same time scale. The change in n alters the ideal $\lambda/4n$ length ratio in the layers and the index contrast between the two materials. This process can be used for ultrafast all optical switching of a Bragg mirror [3, 4].

Similarly, switching in two and three dimensional photonic crystals [5–7] and switching using other mechanisms, such as spin-polarization relaxation [8] and saturable absorption [9], has been studied.

This earlier work has focused primarily on switching by large absolute percentages. However, to build a high finesse switchable cavity a mirror with high initial reflectivity and a large switching ratio is required. In this letter we present time resolved pump-probe measurements of the change in transmission of a GaAs/AlAs Bragg mirror under intense optical pumping.

A switchable mirror with high initial reflectivity requires materials that have low absorption at the desired operation wavelength and a large contrast in index of refraction. At least one material must posses a large nonlinear index of refraction to allow effective all-optical switching. GaAs and AlAs meet these criteria and mirrors with ~30 layer pairs can be grown with reflectivities $> 99.99\%$. GaAs and AlAs have a Kerr nonlinearity and in addition, the nonlinearity in index of refraction related to free carriers in GaAs has previously been studied [10].

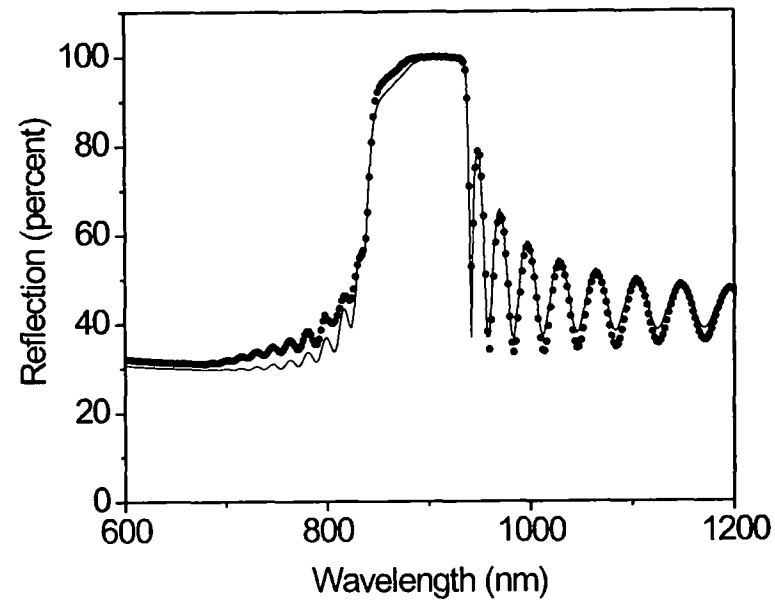

FIG. 1: Measured reflectivity (circles) and calculated reflectivity (solid line) of a 30 layer pair GaAs/AlAs Bragg mirror at 12.5° angle of incidence. The mirror is designed to have maximum reflectivity at 892nm for normal incidence.

The sample is a 30 pair GaAs/AlAs Bragg mirror on a GaAs substrate with a ~50 nm spacer layer of $Al_{0.4}Ga_{0.6}As$. The thicknesses of the GaAs and AlAs layers are 61.8 nm and 75.0 nm respectively, corresponding to $\lambda/4n$ for a wavelength of 892 nm. The measured reflectivity (circles) and calculated reflectivity (solid line) as a function of wavelength at a 12.5° angle of incidence is shown in figure 1.

The change in transmission through the sample as a function of the delay between pump and probe pulses is

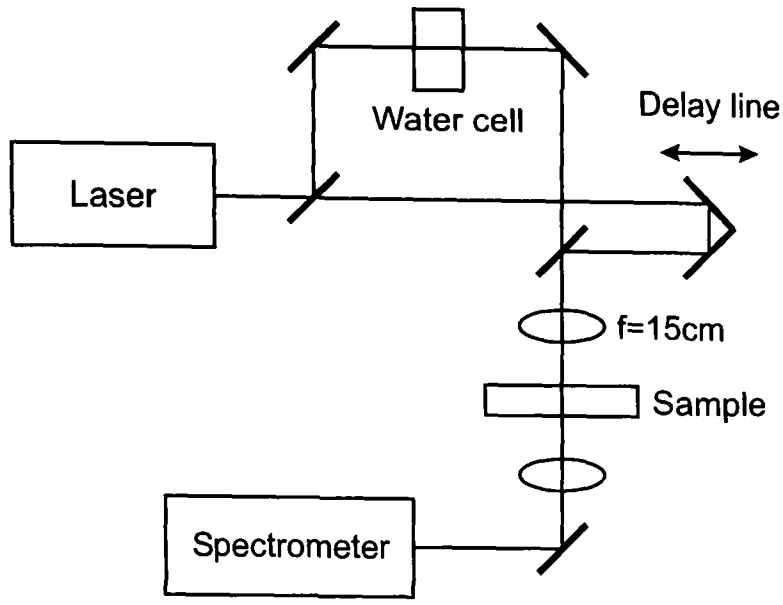

FIG. 2: Setup used to measure transmission through the mirror as a function of temporal pump-probe overlap. The probe is a broadband white light created by continuum generation with part of the pump light. The delay line in the pump path is scanned as transmission is measured in a spectrometer.

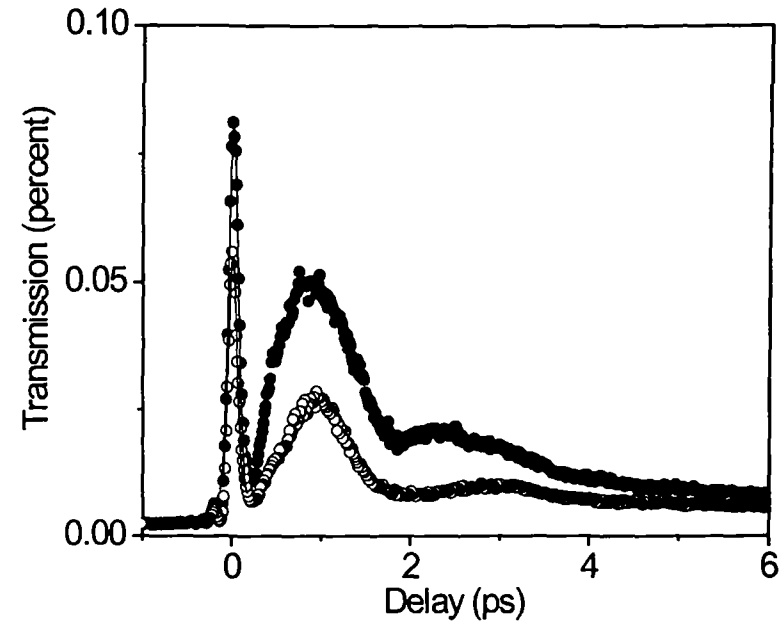

FIG. 3: Transmission at a wavelength of 931 nm as a function of probe delay for a pump fluence 0.8 kJ/m^2 (solid circles) and 0.64 kJ/m^2 (open circles).

studied using the setup shown in figure 2. The light from a regeneratively amplified Ti:Saph femtosecond mode locked laser at 780 nm with ~100 fs pulse width and 40 kHz repetition rate is used as the pump. A portion of the light is split off and focused into a cell of flowing water, generating ultrafast white light probe pulses [11]. The pump and probe are combined on a dichroic mirror that reflects the 780nm pump beam and transmits the white light probe for $\lambda > 820$ nm such that they propagate collinearly. The pump and probe are then focused to a 30 μm radius spot on the sample with a f=15 cm lens. The collinearity of the pump and probe ensure good overlap on the sample. The pump beam path has a delay line which is scanned and at each position a spectrum of the transmitted light is measured using a spectrometer with a cooled CCD camera. The pump light is absorbed in the sample, any residual pump light is at a different wavelength from the probe and does not interfere with the spectral measurement. A measurement of the transmission demonstrates the ability to switch the light out of a high finesse cavity, as this requires a mirror that has a increase in transmission under optical pumping.

The transmission through the GaAs/AlAs mirror at 931nm for a pump fluence of 0.8 kJ/m^2 (solid circles) and 0.64 kJ/m^2 (open circles) as a function of pump probe delay is shown in figure 3. These fluences correspond to 80% and 64% of the damage threshold for GaAs [10]. At negative delay the transmission is constant. The initial fast response, peaking at maximal pump probe overlap, is attributed to the Kerr nonlinearity in GaAs and AlAs which changes the index of refraction of both materials, leading to an increase in transmission of the mirror. At 931nm this change is a 27 time increase in transmission; from a transmission of 0.0024% to 0.065 %. The first peak is fit to a gaussian with a full width at half maximum of ~ 100 fs, consistent with the assumption that the switching is due to an instantaneous (Kerr) nonlinearity. The peak of the Gaussian corresponds to zero delay.

The second, lower but broader, peak is related to the presence of free carriers that induce a change the index of refraction in the and increase the transmission of the mirror. Because the pump energy is below the bandgap of AlAs, the free carriers are created predominantly in the GaAs. A number of theoretical models for this change in index of refraction have been introduced. For the intense pump pulses used in our experiment, electrostatic screening and many body effects from the large number of free carriers are responsible for the index change [12, 13].

Figure 4a shows the transmission as a function of wavelength for the unpumped mirror (solid triangles), the mirror at zero delay for a pump fluence of 0.8 kJ/m^2 (solid circles) and 0.64 kJ/m^2 (open circles). The ratio of the transmission in the pumped versus unpumped state is shown in figure 4b and is largest for the longer wavelengths and at a pump fluence of 0.8 kJ/m^2. The maximum ratio is a 27 time increase in transmission at a wavelength of 931 nm. The ratio of change is larger for the longer wavelengths, closer to the edge of the Bragg gap. There are two mechanisms that contribute to this effect. An overall change in the refractive index of the layers shifts the center wavelength of the Bragg mirror. In addition, a change in index contrast between the layers narrows the width of the Bragg gap.

The transmission at 0.95 ps delay, corresponding to the second peak in transmission, is shown in figure 4c. The overall switching ratio (figure 4d) is less than that at zero delay with a maximum ratio of 17 and an absolute

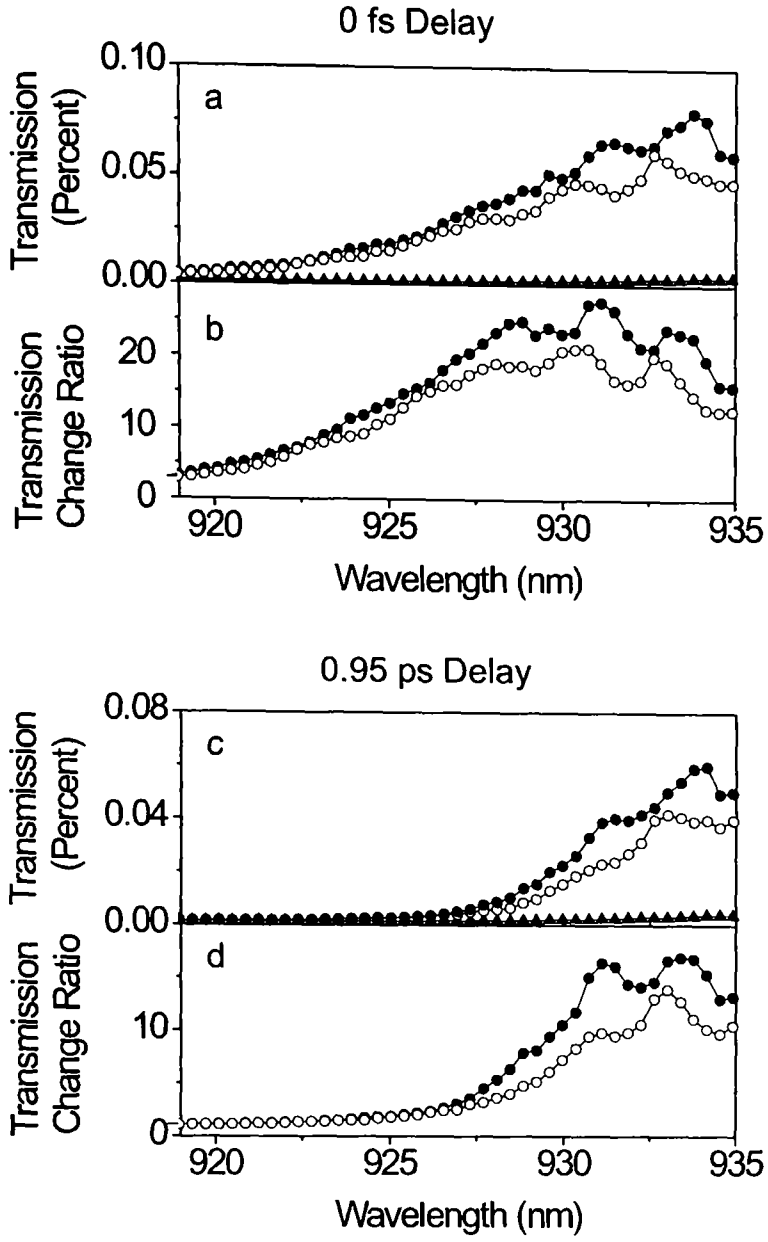

FIG. 4: Transmission spectrum for umpumped mirror (triangles) at maximal pump probe overlap (a) and at the second peak in transmission, a 0.95 fs delay (c) for pump fluence of 0.8 kJ/m^2 (solid circles) and 0.64 kJ/m^2 (open circles). The switching occurs over the whole wavelength range measured. The ratio of the pumped transmission to the umpumped transmission at zero delay (b) and 0.95 fs delay (d). At zero delay the largest change occurs for pump fluence of 0.8 kJ/m^2 at 931nm, a ratio of 27. At a 945 fs delay the largest change occurs for pump fluence of 0.8 kJ/m^2 at 933nm, a ratio of 17.

change from 0.0032% to 0.0544%.

The absorption of the pump in the sample is assumed to be linear in the GaAs layers and negligible in the AlAs. With an absorption coefficient of 1.5$\times$ 10^4 cm^{-1} at 780 nm the 1/e point for absorption of the pump is after $\sim$11 layer pairs. The different pump intensity in the different layers produces a different change in index of refraction for each layer, only switching the top layers of the mirror effectively. However, with lower absorption, the pump would propagate further into the mirror and the switching ratio would be much larger.

The observation of switching due to the Kerr nonlinearity in GaAs and AlAs demonstrates the potential to achieve a large switching ratio using a pump laser at an energy below the bandgap in GaAs. At this energy there is no linear absorption in the layers.

A 2x2 transfer matrix model for the transmission of a 30 layer pair GaAs/AlAs Bragg mirror with the substrate etched away is used to calculate the switching ratio for a pump at 1060 nm. A two photon absorption coefficient β = 26cm/GW and a nonlinear coefficient n_2 = -7.96 $\times$ 10^{-13} cm^2/W [14] in the GaAs layers is assumed. At 0.8 kJ/m^2 pump power, a switching ratio of 3,800 is calculated with transmission changing from 0.012% to 45.6% at 910nm. No data is available for the Kerr nonlinearity in AlAs, but the nonlinearity in AlAs below the bandgap is expected to be at least an order of magnitude smaller than that of GaAs according to the dependence of n_2 on the bandgap at pump energies below the bandgap [15, 16].

Using the Kerr nonlinearity to switch the mirror gives accurate control over switching times. Pump pulses in the range from tens of femtoseconds to tens of picoseconds could be used to achieve desired switching times.

In conclusion we have shown that the nonlinear index of refraction in GaAs and AlAs can be used to create a high reflectivity GaAs/AlAs all optically switchable mirror. Switching is demonstrated with a maximum change of 27 times in transmission from 0.0024% to 0.065% at 931 nm. With a larger switching ratio such a mirror would make an excellent optical switch as one end mirror of a high-Q cavity. A switching ratio of 3,800 is predicted for optical pumping at energies below the bandgap of the GaAs.

The authors thank W. Irvine and C. Simon for useful discussions. This work was supported by NSF grant PHY-0334970 here DARPA grant MDA972-01-1-0027. SH is supported by a NSF Graduate Fellowship.

---

* corresponding author: mdedood@physics.ucsb.edu

[1] G. Rempe, R. J. Thompson, R. J. Brecha, W. D. Lee, and H. J. Kimble, Phys. Rev. Lett. **67**, 1727 (1991).

[2] W. Marshall, C. Simon, R. Penrose, and D. Bouwmeester, Phys. Rev. Lett. **91** (2003).

[3] M. Scalora, J. P. Dowling, C. M. Bowden, and M. J. Bloemer, Phys. Rev. Lett. **73**, 1368 (1994).

[4] A. Hache and M. Bourgeois, Appl. Phys. Lett. **77**, 4089 (2000).

[5] S. W. Leonard, H. M. van Driel, J. Schilling, and R. B. Wehrspohn, Phys. Rev. B **66**, 161102 (2002).

[6] A. D. Bristow, J.-P. R. Wells, W. II. Fan, A. M. Fox, M. S. Skolnick, D. M. Whittaker, A. Tahraoui, T. F. Krauss, and J. S. Roberts, Appl. Phys. Lett. **83**, 851 (2003).

[7] D. A. Mazurenko, R. Kerst, J. I. Dijkhuis, A. V. Akimov, V. G. Golubev, D. A. Kurdyukov, A. B. Pevtsov, and

A. V. Sel'kin, Phys. Rev. Lett. **91**, 213903 (2003).
[8] Y. Nishikawa, A. Tackeuchi, S. Nakamura, S. Muto, and N. Yokoyama, Appl. Phys. Lett. **66**, 839 (1995).
[9] B. G. Kim, E. Garmire, S. G. Hummel, and P. D. Dapkus, Appl. Phys. Lett. **54**, 1095 (1989).
[10] L. Huang, J. P. Callan, E. N. Glezer, and E. Mazur, Phys. Rev. Lett. **80**, 185 (1998).
[11] R. L. Fork, C. V. Shank, C. Hirlimann, R. Yen, and W. J. Tomlinson, Opt. Lett. **8**, 1 (1983).
[12] D. H. Kim, H. Ehrenreich, and E. Runge, Solid State Communications **89**, 119 (1994).
[13] L. X. Benedict, Phys. Rev. B **63** (2001).
[14] A. A. Said, M. Sheik-Bahae, D. J. Hagan, T. H. Wei, J. Wang, J. Young, and E. W. Van Stryland, J. Opt. Soc. Am. B **9**, 405 (1992).
[15] M. Sheik-Bahae, D. J. Hagan, and E. W. Van Stryland, Phys. Rev. Lett. **65**, 96 (1990).
[16] J. S. Aitchison, D. C. Hutchings, J. U. Kang, G. I. Stegeman, and A. Villeneuve, IEEE J. Quant. Elec. **33**, 341 (1997).

Appendix D

Space Weapons: Actor Capabilities and a Qualitative Cost Benefit Analysis

Nationalism is an infantile disease. It is the measles of mankind.– Albert Einstein.

In this appendix 2 papers are presented regarding the possible deployment of space weapons:

1. J. Cowan, W. Marshall, G. Whitesides, R. Schingler, and R. Lawson *Space-Based Strike Weapons* in *Space Security 2003*, Department of Foreign Affairs, Canada (2004)

2. W. Marshall, G. Whitesides, R. Schingler, A. Nilsen and S.P. Worden *Space Weapons: The Immediate Debate* [In preparation]

Context

These articles, evidently unrelated to the core PhD research, were undertaken as a side research project with the kind support of my supervisors.

To give a brief perspective, I originally became interested in issues where science and technology impinge upon global security issues by (fortunately) becoming involved with the organisation Pugwash – which brings together, from around the world, influential scholars and public figures (and in particular physicists) concerned with reducing the danger of armed conflict. Pugwash helped galvanise my interest and increase my understanding of the relevant issues and I became aware early in my PhD of the issue of space weapons: I learnt about some of the crucial details which together force the realisation that the deployment of space weapons by the USA is fairly probable and that the timescale for this to occur is approximately 5-10 years from now. This circumstance struck a cord with both my feelings for responsible use of technology and my interest in space exploration from a purely scientific standpoint.

In the mid-twentieth century humanity developed the capability to consciously destroy itself (or at least civilisation) – and to our knowledge we are the first species to have done so. But we do not yet have the political or social institutions to adequately deal with such technological capabilities. Fundamentally, humanity needs to escape the continued building of more sophisticated arms and to instead seek to develop conflict resolution methodologies that avoid the endangerment of human lives through the development of international institutions and laws. The development of space weapons is in the opposite spirit here, setting off a new domain on the same path as old mistakes. Moreover, if the case of nuclear weapons is anything to go by then it is almost impossible to later remove such weapons from a nations arsenal since those weapons have been entangled into the political-strategic mind-set of the political institutions in the countries that possess them and moreover, no one actor would be willing to disarm first. My concern then with space weapons is that if they go ahead then future generations will have to carry the burden of them, to add to the already overwhelming ones at present.

Initially I wrote an opinion piece on this topic [Marshall et al., 2002] and attended two Pugwash working groups on this issue (whose reports can be found in [Marshall et al., 2003b] and [Schingler and Marshall, 2003]). Following this two research projects developed: (1) assisting a research project on "Space Security" being conducted by the Canadian Government's Foreign Ministry; and (2) researching and writing a paper with a US-Air Force General on the pros and cons of space weapons.

Project 1: Space Security 2003

I have been a consultant for the Canadian Government's Department of Foreign Affairs and International Trade (DFAIT) on a comprehensive study on space security. This aims to establish the trends in space developments and judge the effects of these on space security, which is defined as "secure and equitable access to space for all". The study undertakes to provide Canadian Government, and other Governments, with adequate facts with which to make decisions regarding the military uses of space. It shall be an annual project. My main contribution was in researching and drafting the chapter on "Space-Based Strike Weapons" which is included below.

Project 2: Space Weapons: The Immediate Debate

This is a research paper giving an overview of the space weapons debate. This was performed in collaboration with General Pete Worden, former Director of Operations, Air Force Space Command and Director of Transformation, Space and Missiles Systems Center, USAF. The aim of the paper was to help familiarise me with the real capabilities, motivations and intentions of the US military and together to write out the short and long term costs and gains of space weapons in as unbiased fashion as possible. The resultant article copied below is in preparation.

12 – Space-Based Strike Weapons

Introduction

This indicator assesses trends and developments related to the research, development, testing and deployment of space-based weapons. Space-based strike weapons (SBSW) are systems operating from orbit with the capability to inflict damage to terrestrial targets (land, sea or air), or to terrestrially-launched objects passing through space, via the projection of mass or energy.[163] This does not include the capabilities to strike against space-based targets, which are covered under the Space Negation indicator. Mass-to-target weapons cause damage by colliding with targets with the combined mass and velocity of the space-based weapon itself or by shooting targets with inert or explosive devices.

According to available evidence no such systems are currently deployed in space. Examples of such systems would include space-based ballistic missile interceptors such as the Brilliant Pebbles concept or inert hardened rods designed to be de-orbited to strike terrestrial objects with substantial energy. Energy-to-target weapons cause damage by transferring destructive energy through an energy beam focussed on a target for example, via lasers, microwaves or neutral particle beams. This includes concepts such as space-based lasers which would attempt to destroy ballistic missiles by heating the body of the missile and exploding the fuel within the missile. SBSW systems have the potential to affect space security in very direct ways. An actor with such capabilities would be able to prevent other actors from accessing and using space. Such capabilities would also provide an actor with the capability to threaten others from space.

This indicator assesses trends in the development of operational military doctrine related to SBSW, as well as trends related to the research, development, testing and deployment of SBSW. This includes key enabling technologies for such systems such as: space access and precision re-entry; precision attitude control and manoeuvrability; micro-satellites; high-energy laser and particle beam projection; and large deployable optics.

Background

A number of SBSW-related development programs were funded by the U.S. and U.S.S.R. during the Cold War.[164] In the 1960s, the U.S.S.R. developed a fractional orbital bombardment system (FOBS), designed to deliver from orbit a nuclear weapon onto an enemy target on Earth, while circumventing warning systems. Following 24 launches, of which 17 were successful, the system was declared operational in 1968. The U.S. also conducted research and development on FOBS system during the 1960s but this work was significantly reduced during the 1970s.

In the 1980s, the United States conducted research and testing of several SBSW systems under the Strategic Defense Initiative (SDI). This was to be a ballistic missile defense program, including active components that were space based, most notably (1) the space based interceptor (SBI) capable of disabling enemy missiles either by hit-to-kill or by delivery of conventional arms and (2) the space based laser (SBL) for use to destroy missiles in the launch and mid-course phases. The SBI program, from 1983 to the early 1990s, focused on the 'Brilliant Pebbles'

---

[163] Adapted from Bob Preston et al., *Space Weapons, Earth Wars*. p. xvi. (RAND: 2002). See also Michael Krepon and Christopher Clary, *Space Assurance or Space Dominance? The Case Against Weaponizing Space*, The Henry L. Stimson Center, 2003, p. 30. and Barry Watts, *The Military Use of Space: A Diagnostic Assessment, Center for Strategic and Budgetary Assessments*, February 2002, p. 86.

[164] Bob Preston, et al., *Space Weapons Earth War*, Ch.2 (RAND: 2002) and references therein; Michael Krepon and Christopher Cleary, *Space Assurance or Space Dominance?* Ch.1 (Stimson: 2002).

concept,[165] which envisioned an orbiting constellation of mini-SBI satellites each capable of autonomous interception of enemy missiles that travelled within its range. Ground testing of a Brilliant Pebble interceptor was conducted,[166] and the manufacturing and integration of a kinetic kill vehicle for flight-testing was completed.[167] This vehicle was not ultimately flight tested due to cancellation of the program by the Clinton administration. The U.S.S.R. reportedly orbited, but did not successfully test, a directed energy experiment included on a 100-ton satellite launched by an Energiya rocket in 1985, and flight tested particle beam technology during the planetary probe programs.[168]

The U.S. conducted an underground test of a nuclear-pumped X-ray laser in 1985[169] but this was not a fully integrated system. There was also laboratory research into nuclear pumped particle beams and free electron lasers.[170] The Relay Mirror Experiment was flight tested in 1990 successfully demonstrating ground-based laser re-directing and pointing.[171] While SDI encountered congressional concerns due to high costs and technology immaturity, these programs did establish a considerable technological base for these types of capabilities.

In the post-Cold War period, a number of key U.S. military doctrine and policy related documents made reference to the potential use of SBSW, including the 2001 Space Commission Report and the Air Force Space Command Strategic Master Plan, which emphasized the need for "space control" and called for the ability to "project power in, through and from space."[172] The US maintained an active SBSW research program within the framework of Ballistic Missile Defense, including work on the Space-Based Interceptor and Space-Based Laser. The Clementine mission flight-tested several components of the sensor hardware developed for Brilliant Pebbles.[173] Because executive and legislative opposition meant that SDI hardware would not be tested in LEO, Clementine was sent on a mission to test its sensors by exploring the Moon and an Earth-crossing asteroid. The SBL program was re-configured in the mid-1990s and was placed on a schedule for a flight test post 2010.[174] In the mid-1990s the US Air Force briefly studied the concept of uranium tipped tungsten rods approximately a few meters in length, which could be de-orbited for the purposes of a terrestrial strike.[175]

Although having not significantly increased capabilities since the end of the Cold War, Russia retained a number of key prerequisite SBSW technologies. There was little unclassified

---

[165] *Ibid,* and Ball Aerospace fact sheet on Brilliant Pebbles: http://www.ball.com/aerospace/bpebbles.html
[166] Philip Coyle, personal communication, Feb 3, 2004 & http://www.globalsecurity.org/wmd/facility/nts.htm
[167] *Ballistic Missile Defense (U) Budget Activity: 03, Program Element: 0603217C Project Number: 1214*, 1994 http://www.fas.org/spp/starwars/budget/peds_95/603217ca.htm; *Lawrence Livermore Timeline,* http://www.llnl.gov/timeline/80s.html , *Adapting to a Changing Weapons Program,* Lawrence Livermore, http://www.llnl.gov/str/January01/Batzel4.html
[168] "Space Based Laser," http://www.globalsecurity.org/space/systems/sbl.html.
[169] Robert Scheer, *Pssst. Want to Know a Secret? Just Ask Teller,* Los Angeles Times, 25 May 1999, http://www.robertscheer.com/1_natcolumn/99_columns/052599.htm; Joseph Nilsen, *Legacy of the X-ray Laser Program* Lawrence Livermore National Laboratory, 2004 http://www.llnl.gov/etr/pdfs/11_94.2.pdf.
[170] "Space Based Laser," http://www.globalsecurity.org/space/systems/sbl.htm.
[171] Ball Aerospace, *Relay Mirror Experiment,* http://www.ball.com/aerospace/rme.html.
[172] *Air Force Space Command Strategic Master Plan FY06 and Beyond,* http://www.peterson.af.mil/hqafspc/library/AFSPCPAOffice/Final%2006%20SMP--Signed!v1.pdf; *Report of the Commission to Assess United States National Security Space Management and Organization* http://www.defenselink.mil/pubs/spaceabout.html; *Joint Vision 2020*, http://www.dtic.mil/jointvision/jvpub2.htm .
[173] William Burrows in Air&Space Aug 1996 http://www.airspacemag.com/asm/Mag/Index/1996/AS/nmlm.html; Henry F. Cooper *Why Not Space-Based Missile Defense?,* Wall Street Journal/May 7, 2001 http://www.highfrontier.org/wsj_may7_01.htm.
[174] Worden, personal communication.
[175] Kelly, Jack. Possible space weapons of the Future. July 28 2003 Pittsburgh Post-Gazette.

evidence of Russian SBSW doctrine or R&D programs, and Russian officials repeatedly stated their concerns with U.S. SBSW related doctrine and R&D programs.[176] China developed some key prerequisite technologies for SBSW such as launchers and controlled re-entry, high-powered lasers, and precision guidance through its microsatellite program.[177] There was little unclassified evidence of Chinese SBSW doctrine or R&D programs. Chinese officials repeated expressed concern about U.S. space doctrine[178] and, with Russia, have continued to urge for a prohibition on space weapons in the Conference on Disarmament. There was little evidence of significant SBSW capabilities being developed by other actors.

2003 Developments

The U.S. Missile Defense Agency announced in December 2002 its intention to place in orbit a 'test-bed' for space-based ballistic missile boost-phase interceptors by the 2007/2008 timeframe,[179] but by July 2003 had delayed this projected date.[180] A total of US$14M was authorized by the US Congress in 2003 for FY2004 for R&D for this project.[181] In November 2003, the U.S. Air Force and the Defense Advanced Research Projects Agency (DARPA) announced the FALCON program[182] which supports the Air Force's development of the "Common Aero Vehicle" (CAV) a hypersonic, manoeuvrable glide vehicle for carrying a variety of payloads, including conventional weapons from space to earth-based targets. The Space Based Laser program office was closed due to immaturity of technology.[183]

Citing the programs of other actors, the Chief of the Indian Air Force announced that India had begun work on the "conceptualization" of weapon platforms in space,[184] though he later retracted this statement.[185] Both China and the US expressed concerns about each other's space programs. China expressed new flexibility within the Conference on Disarmament with respect to the possible mandate to address the issue of Preventing and Arms Race in Outer Space. While the Chinese Ambassador to the CD warned that the consequences, "if one country leads in ushering weapons into outer space," would be that "other states following suit."[186] U.S. officials stated that China's manned space program was directly linked to efforts to enhance their security interests and would "contribute to improved military space systems in the 2010-2020 timeframe."[187] The

---

[176] *Russia Statement to CD*, 28th June 2003 http://disarmament.un.org:8080/cd/cd-docs2002.html .
[177] Leonard David, "China's Space Ambitions Keep Western Experts Guessing." 8 July 2002. http://www.space.com/missionlaunches/storming_heaven_020708-1.html.
[178] Hu Xiaodi Ambassador for Disarmament Affairs, People's Republic of China, "Speech to the Conference on Disarmament," 7 February 2002, http://www.acronym.org.uk/docs/0202/doc05.htm.
[179] Missile Defense Agency, Fiscal Year (FY) 2004/FY 2005 Biennial Budget Estimates Submission, Press Release, January 2003, p. 16.
[180] Kerry Gildea, *Missile Defense Agency's Space-Based Boost Phase Program Put On Hold* Defense Daily, 1 August, 2003.
[181] *Missile Defense Test Fails, But Congress Approves FY04 Budget,* UCS Update, 27 June 2003 http://www.ucsusa.org/global_security/armsnet/page.cfm?pageID=1220 .
[182] DARPA, *Falcon Technology Demonstration Factsheet*, November 2003, http://www.darpa.mil/body/NewsItems/pdf/falcon_fs.pdf.
[183] Theresa Hitchens, *Developments in Military Space: Movement Towards Space Weapons?* presented to the workshop on "Outer Space and International Security: Options for the Future," October 29, 2003.
[184] *India Working on Space Weapons: IAF Chief*, Rediff.com, October 03, 2003. http://ushome.rediff.com/news/2003/oct/06iaf1.htm?zcc=ar.
[185] *Space will not be used for arms delivery,* The Hindu, Nov. 1, 2003 http://www.hindu.com/2003/11/01/stories/2003110102181200.htm.
[186] Statement by Ambassador Hu Xiaodi, Representative of the People's Republic of China to the First Committee of the 58th Session of the UN General Assembly on the Issue of Prevention of an Arms Race in Outer Space, October 21, 2003.
[187]United States Department of Defense, *Annual Report on the Military Power of the People's Republic of China*, 28 July 2003. p.37 http://www.defenselink.mil/pubs/20030730chinaex.pdf.

reactions of these actors highlighted the potential for negative action-reaction cycles that have, in the past, played a role in arms races.

Space Security 2003: Key Assessments

Space Security Survey (October 20 to November 14, 2003)		Space Security Working Group (November 24-25, 2003)	
Question: Taking into account your views on developments within doctrine, orbital bombardment and space-based missile defences) in the past year, how have overall changes in this area affected space security?		*Question: In your view, space security with respect to this indicator has been?*	
Enhanced:	1	Enhanced:	0
Somewhat enhanced:	7	Somewhat enhanced:	0
Little or no effect:	15	Little or no effect:	7
Somewhat reduced:	20	Somewhat reduced:	12
Reduced:	35	Reduced:	1

The SSWG assessed that, according to available information, no Space-Based Strike Weapons (SBSW) were deployed in space during 2003, and only a few states possessed any of the key capabilities required for SBSW systems. The SSWG assessed that while space actors continued to enjoy access to and use of space for a wide variety of important functions, the sustainability of this access and the degree to which states believed they will continue to enjoy freedom from space-based threats remained an issue of significant concern for many space security actors. U.S. Missile Defence Agency plans to develop and deploy a space-based interceptor test bed by 2012, although representing a delay from previous estimates, were frequently cited in relationship to these concerns. The apparent reaction to these developments by Chinese and Indian officials underscored the risk that some space security actors were beginning to assume that space would inevitably become weaponized, and were thus beginning long term planning on this assumption. This highlighted the potential for a negative action-reaction cycle similar to those which animated arms competitions during the Cold War. **As a result, while no space-based strike weapons were deployed in space in 2003, concern over possible future developments led to an overall assessment that space security had been somewhat reduced during 2003 with respect to this indicator.**

Space Weapons: The Immediate Debate

William Marshall[†], George Whitesides, André Nilsen and Simon P. Worden

The Urgent Debate

There is need for public discussion of the future military uses of space. This discussion is predicated on the confluence of four factors. First, the technology for developing and deploying basic weapon systems in space is already available in major space faring nations. Second, conflicts are beginning to arise over space-based assets, both for economic and security reasons. Third, there are few legal restrictions on the use of space weapons. Finally, a number of political and military leaders in some major powers have expressed their support for the deployment of space weapons. For all these reasons, deployment could be imminent. The stakes are high since once deployed, it may be difficult to eliminate space weapons, even if they prove unsuitable or destabilizing. However, given that deployment has not yet taken place, policymakers and the public have a unique opportunity to think through these issues now.

The challenge is to find a way of managing space that avoids the 'tragedy of the commons', whereby the pursuit of individual rationality by every state leads to a collectively worse outcome for everyone. The costs and gains of space weapons must therefore be addressed in a comprehensive and balanced debate. In synopsis, short term advantages from acquiring offensive space weapons must be weighed against the medium and long term consequences of deployment, most importantly the risk of a destabilizing arms race in space.

This paper is the result of collaboration among actors involved in the military, scientific, and commercial domains of space. It seeks to put the question of space weapons firmly on the current political agenda. To that end, and to encourage a considered public debate on the subject, we offer a framework of analysis that places the issue of space weapons in appropriate technological, economic, political, and strategic contexts.

CONTEXT

Diminishing Constraints, Growing Incentives

A decision to deploy certain space weapons faces few technological or legal constraints. After years of development, the technology required for space weapons is now feasible, albeit still expensive. Both the US and Russia have the capability to deploy advanced space weapons in a matter of years. Several other nations have the capability to launch lower technology space weapons in a similar timeframe. The last few US administrations funded, on the order of ten billion dollars, a variety of initiatives that laid the groundwork for contemporary space weapons systems. As a result, the development and deployment of certain space weapons is no longer a technological challenge, but a question of political will.

The legal framework governing space weapons is minimal. The most important document is the Outer Space Treaty, which explicitly prohibits treaty states from placing weapons of mass destruction in space orbit or weapons of any kind on celestial bodies. A prohibition against interference with verification satellites was established first in the now void ABM Treaty. The Strategic Arms Reduction Treaty (START I) prohibits the production, testing and deployment of "systems, including missiles, for placing

[†] Corresponding Author: wsm@physics.ox.ac.uk

nuclear weapons or any other kinds of weapons of mass destruction, into Earth orbit". The Conventional Forces in Europe (CFE) treaty establishes a multilateral agreement of non-interference with "national technical means," a phrase primarily focused on surveillance satellites. Among these agreements, there is no explicit prohibition against the myriad of other space or space-related weapons, including transit of nuclear ICBMs, space-based lasers or kinetic kill vehicles. Recently, a joint working paper on preventing space weapons was introduced by China and Russia in the UN Conference on Disarmament (UNCD), however little progress has been made on this issue. Therefore, present law is no serious obstacle to deploying non-nuclear space weapons.

As the technological and legal constraints on deployment are abating, incentives for deployment are growing. The critical role that space now plays in both civil and military activity has created the potential for future conflict. The US military is now dependent on space assets to wage its preferred tactics. Perhaps equally important, the economic benefits of the Global Positioning System (GPS) and other space based technologies gives the US and other countries a substantial interest in maintaining, protecting, and augmenting those assets – and an ability to affect other nations through control of access to this technology. Discord between peer competitors, such as the row sparked by Galileo, the European satellite navigation system, is seen by some as early seeds of greater conflict. Other conflicts have arisen due to differences over the distribution of reconnaissance data and radio spectra allocations. The effect of all these developments is that space policy is increasingly being influenced by security issues and framed as a core national interest.

Against the backdrop of waning constraints and rising tensions, it is no surprise that the political will to acquire space weapon systems is emerging. There have recently been prominent voices within the US military (US Space Command Master Plan 2001 and Air Force 2025) and political (Commission to Assess United States National Security Space Management and Operations, Rumsfeld, 2001) leadership in favor of considering the acquisition of space weapons. Most concretely, present plans for the US missile defense system include a space-based interceptor test bed by 2008. There have been small fiscal appropriations for the testing of such a system in FY2004. The decision on deployment could therefore be imminent.

Not Business as Usual

The decision on whether or not to deploy space weapons is unlike any other strategic choice. One reason is the asymmetric nature of offense and defense options before and after deployment. Historically, the introduction of new weapons systems has mostly been an irreversible path-dependent process. It is much easier not to deploy a new system than it is to withdraw it following deployment, even if it proves unsuitable or destabilizing. Nations will indefinitely be able to choose to deploy space weapons, but once deployed it may be difficult to return to a situation of no such weapons, as it has been for land mines and chemical weapons. This potential irreversibility of deployment suggests that careful consideration be put into this debate.

The relative peace characterizing the current international situation is a further reason why the decision on space weapons is different. Whereas the development of many new weapon systems, including weapons of mass destruction and many advances in aircraft and ships, have occurred during times of direct conflict or tense stand offs, particularly WWII and the Cold War, today we have the opportunity to analyze the case for space weapons in an environment of relative peace. This is a unique opportunity to consider the costs and benefits of space weapons in the long term, as well as the short and medium terms, prior to making a decision on their deployment.

A Brief History of Space and Defence

National interest in the access and utilization of space is not new. In addition to the economic potential of commercial exploitation of space and celestial bodies, space enjoys a unique military utility. Indeed, expenditure on space by the military has consistently outweighed civil spending. Even some scientific exploration missions have arguably been dominated by military objectives, such as the pursuit of technological supremacy during the Cold War which led both to the first satellite (Sputnik, 1957) and human (Yuri Gagarin, 1961) in space, culminating in the first and only manned lunar program (Apollo, 1963-72).

Historically, space-based military assets have been largely passive, concentrating on activities such as reconnaissance, communications, and navigation. To date, no publicly-acknowledged offensive space-based weapon has been deployed to orbit. The most serious related effort came during the parallel anti-satellite (ASAT) programs developed by the US and Soviet Union that were begun in the sixties. These programs primarily developed a variety of 'kinetic kill' vehicles, though initiatives for ground-based laser systems were also begun. Specifically these included initiatives such as nuclear pumped X-ray lasers, space-based optical lasers, radiation belt weapons, ground based reflected laser systems, and space based interceptors. Tests of such systems were periodically prohibited or left unfunded by the US Congress during the eighties and nineties. The US military also expressed its disinclination to use kinetic kill ASATs that tend to create large clouds of space debris. While many of these initiatives were not carried through, the technology base they developed now enables the near term deployment of space weapons.

Meanwhile, the broader international community has repeatedly stated its support for space to be used solely for peaceful purposes. This position was codified early in the space age by the 1967 Outer Space Treaty (OST), through which 102 states to date, including the US and former USSR, have recognized the common interest of all humankind in the exploration and use of outer space for "peaceful purposes". In 2001, the UN General Assembly approved by a 156-0 vote the basis for a treaty establishing a permanent prohibition on space-based weapons (Resolution 56/535), although the US abstained. What remains at issue is the meaning of "peaceful." The US and many other nations hold that peaceful does not mean non-military. Citing the U.N. Charter's acknowledgement of the inherent right of states to self-defense, the US and other states reserve the right to use military force, including weapons for "defensive" purposes. These states often maintain that the use of defensive weapons in outer space is thus not prohibited by any international agreement save the Outer Space Treaty prohibitions on weapons of mass destruction and military bases on the moon and other heavenly bodies.

Against this background, however, some elements have in recent years begun advocating the consideration of new space weapons with strike capabilities. This includes senior US politicians and perhaps more significantly, some elements of the US military who have advocated a strategy to include the deployment of space weapons within a matter of a few years. However, this position has not yet been adopted at the highest level. In fact, many military officers still regard space-based weapons with a dubious eye. The military focus on space, however, has been reaffirmed repeatedly in key documents such as Air Force Vision 2020 and other related strategic planning documents.

The Present Economic and Security Context

Against a background of inactivity and caution, new elements have in recent years begun advocating new space weapons with strike capabilities. In April 2003, for example, the US Congressman representing NASA's Florida base stated his support for weapons deployed in space, "We must adopt a doctrine that states that we as a nation will vigorously pursue the ability to project power to, through and from space against any aggressor." He also noted, "It would be inappropriate to deny ourselves this advantage

simply because of romantic notions of some that space is some type of sacred place." Voices within the present political leadership also favor considering the acquisition of space weapons (Commission to Assess US National Security Space Management and Operations, Rumsfeld, 2001).

Within the US military, the "US Space Command Master Plan 2001", "Air Force 2025", "Vision 2020" and other related strategic planning documents have repeatedly advocated a strategy to include the deployment of space weapons within a matter of a few years. In the US military document "Vision 2020", for instance, it is argued that the US should seek to operate freely within the domains of land, sea, air, space, and information. Moreover, it argues that the US should posses the capacity to deny space assets to others, if necessary. In light of such debate within the US administration, some believe that a decision the deployment of space weapons could be imminent.

Arguments over commercial and security, non-armament uses of space may have important effects on the issue of space weapons. Galileo, the European Union's embryonic satellite navigation system, to take one example, will provide rival navigational services to the American GPS. GPS data is used worldwide for anything from cellular telephones to farming equipment. In addition to Galileo's economic benefits, it makes the EU independent from US navigation data for modern warfare. These twin drivers of economics and security create a context of potential friction even between allies.

Friction also arises in the area of remote sensing surveillance satellites, and the specific issue of shutter control. Though the continuing proliferation of space-based high-resolution imaging has reduced the superpowers' exclusive hold on this strategic resource, this development has generally been seen as positive, increasing the stability of the global system. However, during 1991 Gulf War, these capabilities became a source of tension when SPOT, the French satellite imagery company, began receiving increasingly stern warnings from the US military about its data products over the Middle East. In the Afghanistan conflict the US instead decided to purchase the rights to all relevant commercial imaging data, thereby denying it to any adversary.

ANALYSIS

Definitions

To complicate the debate, there is no strict definition of a space weapon. The debate is shaped by whether or not to include both targets located in space and on the ground, direct and indirect applications of force, and temporary impairment as well as permanent destruction. Below, we characterize the generally agreed areas, as well as the increasing number of grey areas.

Activities in the white region of the chart are military applications that do not entail force application from assets stationed in space. The black region comprises technologies that fit the traditional definition of a space weapon. Weapons in the grey area are more difficult to classify, and can blur the line between space-based and space-transiting weapons; for example, temporarily emplaced weapons that orbit for days to weeks.

There is considerable controversy within the grey area discussed below. Opinion differs of over the height at which a weapon becomes a space weapon. There is also debate on when a dual-use technology can be considered an enabling component of a weapon. For example, the GPS precision targeting signal is critical to the guidance of some weapons; is the GPS considered a space-based weapons system? The

definition of 'peaceful purposes' is another area of intense debate that contributes to lack of progress in this discussion. Such discussions are likely to continue for some time.

Space Weapons *(Generally agreed as being a space weapon)*	Intermediate Systems	Military activities not involving Space Weapons *(Generally agreed to be "defensive")*
[Key Words: Degrade, Destroy, *Active*] ▪ WMD or radiological weapons ▪ Space-based directed energy weapons ▪ Space-based kinetic weapons ▪ Anti-satellite satellites (ASATs) that destroy or degrade other satellites	[Key words: Deny, Disrupt] ▪ Ground or air-based directed energy weapons (DEWs) used against space-borne targets ▪ Nuclear weapons for NEO defense ▪ Ground based interference, jamming, or cyber attack of GPS signals, satellite communications, or ground stations ▪ Suborbital mid-course intercept missile defense	[Key words: Facilitate, Assist, *Passive*,] ▪ Communication ▪ Navigation ▪ Reconnaissance (space based or high altitude platforms) ▪ Space monitoring networks ▪ Early warning systems ▪ ICBM with suborbital trajectory ▪ Suborbital delivery of troops or equipment

Table 2: The Spectrum of Military Space Activity: What is a Space Weapon?

Systems within the black area are not fully developed or deployed, but have been the subject of rigorous national and international discussion due to their potential to create instability in international affairs. Though debatably outside the traditional definition of space weapons, it may be the technologies within the grey area that deserve the most immediate attention. They are the most likely to be deployed in the short term, and could significantly increase the likelihood that other traditional space-based weapons will be deployed.

Space Strategy

Space strategy inherently rests on specific military technologies and capabilities; yet the true capabilities of actors are uncertain, and in any case change with time. What remains unchanged are two things; the characteristics of space as a medium, and the necessity for a defensive strategy. Both provide useful insights to the weapons debate.

The necessity for a defensive strategy has been discovered and rediscovered - the hard way - throughout history. Such a strategy need not involve weapons; hiding is one example. The military significance of space is inextricably linked to its resource value and utility for both civilian and military purposes. Like it or not, defensive needs now extend into space, as they did for airspace in the last century. A difference remains that weapons have not yet been placed in space and that there is an overall norm that space should be used for peaceful purposes and to benefit humankind.

The format of near-Earth space conflict will likely always be shaped by the fastest Low Earth Orbit (LEO) trajectory, which takes 90 minutes to circle the Earth once. With a rocket ascent to LEO taking 5-10 minutes, a flash conflict in or through LEO could occur in as little as minutes or hours, as it is does for the familiar scenario of an ICBM exchange. However, LEO weapons have a limited window of utility of only a few minutes as they transit over a point on the Earth, and it may several orbits to maneuver into the desired overhead position. Furthermore, space-based weapons occupying a more distant MEO orbit, for example lasers, enable the possessor a near-instant strike over a field of view occupying up to a third of the world's surface at any one time, but current technology limits any state's ability to perform meaningful offensive strikes from higher orbits. Such a capability is also presumably very expensive when it does become feasible.

Conflict in or through space could form one aspect of a ground-based war, could arise from disputes over resources in space, or uses of space that interfere with others. In the present US information-centric style of warfare, military dominance on land and air uses contributions from passive space-based systems in the form of battlefield intelligence, navigation, and communication. More than just a side benefit, these are perhaps a necessity for victory due to the increasing awareness of large scale collateral damage. In the future, space dominance could conceivably become a deciding factor as improvements in ground force capabilities stem from the use of space-related systems, leading to a tiered dominance with space at the top - 'the ultimate high ground'.

The reliance on passive space weapons to engage in a 21st century conflict and lack of defense for such systems is a major motivation for the weaponization of space. However, what will the effectiveness of these Anti-Satellites (ASATs) be? A large obstacle for the weaponization of space is the fear of the effectiveness of such weapons, their cost, and the reality of creating other vulnerable targets in space. Another tactical military concern is that objects in space can in principle be seen by all, though the capabilities of individual nations vary. For these reasons, temporary defense systems might be stowed on the ground and only deployed during periods of heightened risk.

Multiple Outcomes

The decision of whether or not to deploy space weapons cannot be reduced to a question of which individual nation possesses the required technological and economic capacities and the political will to do so, since outcomes emerge from strategic interactions between all the relevant actors. Whether or not a dominant state will enhance its comparative advantage or gain national security by acquiring new weapons therefore depends on how the other states are responding.

As In table 1 multiple outcomes with different degrees of likelihood as a final outcome are shown. The worst-case scenario, following the deployment of space weapons, could be an arms race in space (Outcome 4). Outcomes 2 and 3 are unlikely to be stable situations since one nation deploying space weapons is likely to cause others to. Other possible outcomes include an agreed no deployment regime, a competitive but stable system, or a unipolar stable system akin to the current US dominance of the high seas. Whether or not these latter situations are stable is arguable. Some would point out that no-deployment regimes can be unstable and could enable a covert "cheater" to amass a decisive advantage when used in a surprise attack.

	Other states do not deploy Space weapons	Other states deploy space weapons
Dominant state does not deploy space weapons	1: Moderately likely outcome	2: Unlikely outcome

Dominant state deploys space weapons	3: Very unlikely outcome	4: Likely outcome

Table 1: Strategic Analysis: Probabilities of Final Outcomes

In addition to the risk of triggering an arms race with space weapons, states should also consider the likelihood of spill-over effects into other strategic areas. The impact on nuclear strategy is particularly important to assess: some think that space weapons, along with information warfare, could eventually replace nuclear deterrence as a central strategic policy. This strategy could provide the post-nuclear deterrence paradigm for the US and other nations. Such a shift could be positive or negative on overall security: It could reduce the overall reliance on nuclear weapons by the dominant state – a positive effect, or, due to an increased military gap between the dominant state and other nations, the move could increase the likelihood of nuclear weapons being used as a last resort and decrease the threshold for using nuclear weapons in conflict.

Many Players

There is no shortage of potential actors that might respond to a first move by a state. While the US and Russia lead in capacity, the European Union, China, and India all have the requisite technical capability to produce certain space weapons systems.

Given a first move by another state, the US is likely to act quickly to ensure dominance in this domain. The Russian military still highly values its nuclear weapons capability, and could be expected to react quickly, as any deployment of space weapons would be a transition away from the nuclear deterrence paradigm and threaten a reduction in the utility of Russia's nuclear arsenal.

The European Union may move to compete as development of collective space defense infrastructure is initiated. A wish to reduce reliance on the US is demonstrated by the EUs pursuit of the Galileo navigation system. Explicitly addressing the connection between European Security and Space, European Research Commissioner Philippe Busquin has said that space-based observation, communication, and navigation systems represent exceptional tools for the construction and reinforcement of the EU, in particular with respect to European Security and Defense Policy.

China is also investing heavily in space and has publicly announced lunar exploration plans. It is unlikely to want to face foreign policy obstacles and has proposed a treaty banning space weapons in the UN Conference on Disarmament. However China's legal efforts in this respect are viewed with some skepticism in the USA, where an aggressive Chinese human spaceflight program is considered by some as a transparent attempt to gain a military or political space advantage. Although viewed with less suspicion in Washington policy-making circles, India's similar stated intention to engage in Lunar Missions could potentially become a source of unease.

Moreover, history contains many examples of small players combining forces to counterbalance the power of one strong player. Such behavior was in clear display by Germany, France, Russia, and China during the lead up to the war in Iraq. Such examples suggest that the dominant state should consider not only the chances of single nations countering their actions, but the risk of many nations combining initiatives.

Short Term Gains and Costs

The judgment of whether or not to deploy space weapons rests on a cost-benefit analysis that deals with repercussions for global stability and welfare in the short, medium, and long-term. The outcome of such an analysis is driven by ideological perceptions as well as the scientific facts. The following analysis outlines some key pros, cons, and common perceptions to consider within each timeframe.

In a short term perspective of less than a decade, several advantages of space weapons can be imagined:

1. **A superior weapon**: Space weapons are potentially a primary tool for information warfare, and thus may be a key to battlefield dominance in contemporary war. Space weapons enable an advantage in time and space over an adversary, enabling a state to acquire and maintain the initiative. [Table 1, Outcome 3]
2. **First Mover Advantage:** If the readiness for deployment of space weapons is low among other countries, the first state to deploy will enjoy a short-term advantage.
3. **Protection of space assets:** Assets in space are a critical part of modern communications, navigation and information gathering, important to the economy, vital to security and in demand in everyday life. Damage to these assets could seriously cripple a nation.
4. **Deterrence:** By bolstering the image of technological supremacy, space weapons could act as a deterrent to hostile action.
5. **Short-term industrial gains**: Military and commercial industry can be bolstered by gains from long-term (>5 years) research and development projects.

On the other hand, a range of short term disadvantages are possible:

1. **Ineffective and Expensive**: Space weapons could become the analogue of the 19th century Dreadnaught ships; very expensive to produce and deploy, with little tactical advantage and overstated performance. Worse, they could provide a false sense of superiority that justifies unwise actions.
2. **Vulnerability:** Space weapons aimed at Earth targets would need to be in Low-Earth Orbit (LEO) for a quicker response time and greater effectiveness. LEO-based weapons could run the risk of being orbital sitting ducks for any nation possessing ASAT capabilities.
3. **Provocation to Diplomatic and Arms Control Efforts**: Unilateral deployment of space weapons could spark an international backlash, poisoning other diplomatic efforts and removing the moral "high ground" from that state, making it more difficult to achieve other strategic goals. For example, It could be difficult for such a state to persuade others to forego weapons such as nuclear weapons while itself deploying space weapons to its unilateral advantage.
4. **Public Opposition:** The majority of public worldwide appears to oppose space weapons. There is a history of civil opposition concerning issues related to military uses of space or deployment of unconventional systems, such as nuclear powered spacecraft, in space. Similar opposition movements might accompany the deployment of space weapons, perceiving an opportunity for humanity to make a psychological leap in the way matters are solved by halting the spread of destructive weapons to the space frontier.
5. **Threat of Accident**: The Space Shuttle Colombia's break up on reentry highlights the hazard posed by even passive unarmed space systems. Space-based weapons systems, particularly those requiring large platforms, hazardous components (for example laser media), or high capacity power sources (for example nuclear electromagnetic pulse (EMP) generators), may pose a threat in the event of significant failure.
6. **Debris**: If space weapons are used on space-based targets, then it could considerably increase the already substantial problem of debris, degrading certain orbits, or even rendering them unusable.

Medium Term Gains and Costs

Looking between ten and twenty years ahead in time, there are advantages of space weapons:

1. **Stable Domination**: Cognizant of the arms race arguments against unilateral moves in space (see below), some argue that restraint on the part of a nation such as the US might dissuade other nations from moving ahead to their own advantage. Seizing the initiative, they argue, could enable the US to stop an arms race before it starts by establishing a globally dominant, stabilizing force in space.
2. **Global Stabilizing Effect on Earth**: The past half-decade has seen considerable instability and conflict throughout the world. Space offers not only the ability to detect certain kinds of threats globally on very short time scales, but some believe it may also offer the ability to counter those threats from space on similarly short time scales.
3. **Basis for new Multilateral Security Cooperation Regime**: While military use of space is still largely dominated by the US and to a lesser extent a handful of other major powers, its benefits for support of other military operations are manifest. Space-based weapons systems might enhance these benefits, motivating new cooperative security regimes in outer space. If placed at the service of global coalitions and following agreed "rules of the road", space arms might serve as a stabilizing influence

At the same time, there are potential disadvantages also in the medium term:

1. **Arms Race in Space**: The current global perception is that the US has a technical lead in the military use of space. This strategic advantage might spur other nations to accelerate their space security efforts, triggering an arms race. For example, the deployment of an ASAT could instigate the development and deployment of a "DSAT" to counter an ASAT. Such an arms race might also blur the distinction between conventional and mass destruction weapons in space. [Table 1: Outcome 4]
2. **Asymmetric Defense**: An economic or tactical asymmetry in the relationship between a weapons system and that system's countermeasure could lead to a situation in which an expensive weapon is rendered useless by a cheap defense. For example, a ton of gravel launched in an appropriate orbit could act as deliberate "space debris," destroying billions of dollars in both national security and commercial space assets.
3. **Moving away from conventional areas of strength:** Moving warfare into space may undermine a dominant nation's capabilities since it would sideline the conventional military superiority.

Long Term Gains and Costs

Some advantages of space weapons might only emerge in the long term, of at least twenty years:

1. **Outer Space "Naval" Paradigm**: The existence of weaponry in global "common" areas can be stable. The standard analogy of outer space is to the world's oceans, traversed by global, weaponized navies dominated by a single power (in the 19th Century Great Britain and in the 20th the US). If applicable to space, this regime could result in all nations operating free from interference based on an internationally recognized "Law of the Sea."
2. **Economic Impetus to Large Scale Space Exploitation**: Today much of the developmental spending on space, perhaps the majority of it, is spent on security-related expenditures. Indeed, the US Apollo program and associated "space race" was arguably motivated by security-related competition. Some argue that large-scale military space spending, particularly on weapons and even with (and maybe in light of) an arms race, would ignite rapid development of space technologies at a pace not seen since Apollo.
3. **NEO hazard mitigation:** Leading proponents of systems to protect the Earth against an asteroid impact (Near-Earth Object, NEO,) argue that key elements of such systems, including quite possibly weapon-like systems, may need to be deployed in Earth orbit to be accurate and effective enough. Not developing such systems could result in the remaining defenses being to slow to prevent some types of collision.

Notwithstanding, the long term disadvantages must also be taken into account:

1. **Long-term survival of the species/Threat to Long-term Peace**: Many believe that the choice for or against the deployment of space weapons is fundamentally linked to whether or not humans will have weapons in their long-term future. Deploying space weapons might threaten that future rather than enable it, proving impossible to fully eliminate, like land mines, and perpetuating a self-destructive precedent into the future as civilization expands into space.
2. **Proliferation of Weapons:** Perhaps the greatest threat to a dominant nation's security originates from the proliferation of weapons which it developed: Certainly the greatest threat to the US has been the potential use of nuclear weapons on US home soil. By analogy, the first state to deploy space weapons may find itself faced all-too-soon with these same weapons as they proliferate.
3. **The Unique Environment of Space:** Some argue that space has a unique identity beyond a traditional arena of classical balance of power politics. Space is humanity's shared resource and future, its common heritage (phrase used in Moon treaty) or 'common province' according to OST. The question of whether or not weapons should be deployed in space is therefore an issue beyond the interests of any one country or generation and could be seen as a moral decision, not a strategic one.
4. **Orbital Planetary Defense Elements may be a Pandora's Box:** Opponents of space-based planetary protection systems (see gains point 3 above) are concerned that the costs and dangers of developing such systems may far outweigh the advantages. Indeed, current planned space-based weapons could prove too weak for NEO defense, yet open a back-door to the weaponization of space.

The Way Ahead

Three main options are available for the future:

Fairly comprehensive prohibition: A ban of space weapons might halt the potential for an arms race, but may constrain states if a situation arises and a state decides to abrogate a ban. A legal regime could be negotiated in an international forum such as the United Nations Conference on Disarmament, an ad-hoc gathering, or a treaty conference for interested nations hosted by a country that supports the prohibition of space weapons. Challenges, however, would be to establish effective sanctions against treaty violations and independent compliance monitoring and verification.

An intermediate legal regime: An international agreement on space weapons analogous to the International Law of Sea could be created. This could lead to a stable situation that avoids the earlier pitfalls. It could require an international regime backed up by global, real-time monitoring. The downside is that it is not concrete and might be overtaken by events.

No regime: In this current state of uncertainty, the global security in the mid-term future is unclear. This situation could enable a dominant power, such as the US to establish its own vision of a peaceful and stable world order. But such an attempt also holds the potential for an arms race in space. Without establishing the rules of the road, even the lead nations are subject to consequences, especially in a domain as potentially asymmetric as space.

Bibliography

1. B. Preston et al. "Space Weapons Earth Wars", RAND publication http://www.rand.org/publications/MR/MR1209/
2. M. Krepon, C. Clary, "Space Assurance or Space Dominance? The Case Against Weaponizing Space", Stimson Center publication http://www.stimson.org/pubs.cfm?ID=81
3. United Nations Treaties and Principles on Space Law

http://www.oosa.unvienna.org/SpaceLaw/treaties.html
4. Jane's Space Directory, http://jsd.janes.com/
5. Report of Working Group 2 on "Missile Defenses and the Uses of Space", at the 52nd Pugwash Conference in La Jolla, USA, http://www.pugwash.org/reports/pac/52/52_reports_wg2.htm
6. White, Preserving Space for Peaceful Use: A Case for a New Space Treaty, Centre for Peace Studies, University of Auckland *
7. Commission to Assess United Space National Security Space Management and Organisation, Chaired by Donald Rumsfeld, 2000
8. Arms Control Association: Arms Control Today, Boese, W., "December Missile Defense Tests Yield One Success, One Failure", http://www.armscontrol.org/act/2002_01-02/misdeftestjanfeb02.asp (Last accessed: 02 Sept. 2002)
9. Canadian Position on Space Weapons http://www.dfait-maeci.gc.ca/arms/outer-en.asp ; "Non-Weaponization of Outer Space," Hon. Bill Graham, Minister of Foreign Affairs, Statement in the House of Commons, Ottawa, Ontario, 27 February 2002.
10. Space Preservation Treaty http://www.peaceinspace.com/L3-legislation-treaty.shtml
11. S. Worden, M. France, Towards an Evolving Deterrence Strategy: Space and Information Dominance
12. S.M.Walt, "Rigor or Rigor Mortis? Rational Choice and Security Studies" http://mitpress.mit.edu/journals/pdf/isec_23_04_5_0.pdf
13. Air Force 2025, Air University Press, Maxwell AFB, USA, 1996. http://www.au.af.mil/au/2025/
14. R. Garwin, "Space Weapons or Space Arms Control", Pugwash workshop on space weapons, May 2003

Bibliography

[A. Cleland, 2003] A. Cleland, M. G. (2003). Superconducting qubit storage and entanglement with nanomechanical resonators. *Preprint cond-mat/0311007*.

[Advanced Thin Films, 2002] Advanced Thin Films, Longmont, C. U. (2002). Personal communication.

[Anglin and Zurek, 1996] Anglin, J. R. and Zurek, W. H. (1996). Decoherence of quantum fields: Pointer states and predictability. *Phys. Rev. D*, 53(7327).

[Armour and Blencowe, 2001] Armour, A. and Blencowe, M. (2001). Possibility of an electromechanical which-path interferometer. *Phys. Rev. B*, 64(035311).

[Armour et al., 2002] Armour, A., Blencowe, M., and Schwab, K. (2002). Entanglement and decoherence of a micromechanical resonator via coupling to a cooper-pair box. *Phys. Rev. Lett.*, 88(148301).

[Arndt et al., 1999] Arndt, M., Nairz, ., Vos-Andreae, J., Keller, C., van der Zouw, G., and Zeilinger, A. (1999). Waveparticle duality of c60 molecules. *Nature*, 401(680).

[Asheghi et al., 2004] Asheghi, M., Leung, Y. K., Wong, S. S., and Goodson, K. E. (2004). Phonon-boundary scattering in thin silicon layers. *Appl. Phys. Lett.*, 71(1798).

[Bassi et al., 2004] Bassi, A., Ippoliti, E., and Adler, S. (2004). Towards quantum superpositions of a mirror: Stocastic collapse analysis. *Preprint quant-ph/0406108*.

[Bell, 2004] Bell, J. S. (2004). *Speakable and unspeakable in Quantum Mechanics*. Cambridge University Press (2nd Ed.).

[Blakemore, 1985] Blakemore, J. S. (1985). *Solid State Physics*. Cambridge University Press (2nd Ed.).

[Bose et al., 1999] Bose, S., Jacobs, K., and Knight, P. (1999). Scheme to probe the decoherence of a macroscopic object. *Phys. Rev. A*, 59(3204).

[Bouwmeester et al., 1998] Bouwmeester, D., Schmiedmayer, J., Weinfurter, H., and Zeilinger, A. (1998). *Gravitation and Relativity: At the turn of the Millennium*. IUCAA, Pune.

[Bradinsky and Khalili, 1996] Bradinsky, V. B. and Khalili, F. Y. (1996). Quantum nondemolition measurements: the route from toys to tools. *Rev. Mod. Phys.*, 68(1).

[Bradinsky et al., 1995] Bradinsky, V. B., Khalili, F. Y., and Thorne, K. (1995). *Quantum Measurement.* Cambridge University Press.

[Bristow et al., 2003] Bristow, A. D., Wells, J.-P. R., Fan, W. H., Fox, A. M., Skolnick, M. S., Whittaker, D. M., Tahraoui, A., Krauss, T. F., and Roberts, J. S. (2003). Ultrafast all-optical switching in a silicon-based crystal. *Appl. Phys. Lett.*, 83(851).

[Brune et al., 1996] Brune, M., Hagley, E., Dreyer, J., Matre, X., Maali, A., Wunderlich, C., Raimond, J. M., and Haroche, S. (1996). Observing the progressive decoherence of the "meter" in a quantum measurement. *Phys. Rev. Lett.*, 77(4887).

[Caldeira and Leggett, 1983] Caldeira, A. O. and Leggett, A. J. (1983). Path integral approach to quantum brownian motion. *Physica*, 121A(587).

[Chan et al., 1999] Chan, H., Long, J., and Price, J. (1999). Taber vibration isolator for vacuum and cryogenic applications. *Rev. Sci. Inst.*, 70(2742).

[Cirac et al., 1998] Cirac, J. I., Lewenstein, M., Molmer, K., and Zoller, P. (1998). Decoherence and the transition from quantum to classical. *Phys. Rev. A*, 57(1208).

[Cleland, 2004] Cleland, A. (2004). *Personal Communication.*

[Cohadon et al., 1999] Cohadon, P., Heidmann, A., and Pinard, M. (1999). Cooling of a mirror by radiation pressure. *Phys. Rev. Lett.*, 83(3174).

[Collett et al., 1994] Collett, B., Pearle, P., Avignone, F., and Nussinov, S. (1994). Constraint on collapse models by limit on spontaneous x-ray emission in ge. *Preprint.*

[Courty et al., 2001] Courty, J.-M., Heidmann, A., and Pinard, M. (2001). Quantum limits of cold damping with optomechanical coupling. *Eur. Phys. J. D*, 17(399).

[D.Home and R.Chattopadhyaya, 1996] D.Home and R.Chattopadhyaya (1996). Dna molecular cousin of schrdinger's cat: A curious example of quantum measurement. *Phys. Rev. Lett.*, 76(2836).

[Digital Instruments,] Digital Instruments, I.

[Diòsi, 1989] Diòsi, L. (1989). Models for universal reduction of macroscopic quantum fluctuations. *Phys. Rev. A*, 40(1165).

[Dmitriev et al., 1999] Dmitriev, V., Gurzadyan, G., and Nikogosyan, D. (1999). *Handbook of Nonlinear Optical Crystals.* Springer, Berlin (3rd Ed.).

[Eisberg and Resnick, 1985] Eisberg, R. and Resnick, R. (1985). *Quantum Physics of Atoms, Molecules, Solids, Nuclei, and Particles*. 2nd ed. New York: Wiley.

[Elshabini-Riad and Barlow, 1997] Elshabini-Riad, A. and Barlow, F. (1997). *Thin Film Technology Handbook*. McGraw-Hill Professional Publishing.

[Everett, 1973] Everett, H. (1973). *The Theory of the Universal Wave Function*. in DeWitt and Graham.

[Feynman and Vernon, 1963] Feynman, R. P. and Vernon, F. (1963). *Ann. Phys. (N.Y.)*, 24(118).

[Fox and Li, 1968] Fox, A. and Li, T. (1968). Computation of optical resonator modes by the method of resonance excitation. *IEEE J. Quantum Electron.*, QE-4(460).

[Friedman, 2000] Friedman (2000). Quantum superposition of distinct macroscopic states. *Nature*, 406(43).

[Gabrielse et al., 1990] Gabrielse, G., X. Fei, L. A. O., Tjoelker, R. L., Haas, J., Kalinowsky, H., Trainor, T. A., and Kells, W. (1990). Thousandfold improvement in the measured antiproton mass. *Phys. Rev. Lett.*, 65(1317).

[Ghirardi, 1990] Ghirardi, G. (1990). Continuous-spontaneous reduction model involving gravity. *Phys. Rev. A*, 42(1057).

[Ghirardi et al., 1990] Ghirardi, G., Pearle, P., and Rimini, A. (1990). Continuous-spontaneous-reduction model involving gravity. *Phys. Rev. A*, 42(1057).

[Ghirardi et al., 1986] Ghirardi, G., Rimini, A., and Weber, T. (1986). Unified dynamics for microscopic and macroscopic systems. *Phys. Rev. D*, 34(470).

[Godun et al., 2001] Godun, R., M.B.d'Arcy, Summy, G., and Burnett, K. (2001). Prospects for atom interferometry. *Contemporary Physics*, 42(77).

[Goldsmith, 1998] Goldsmith, P. F. (1998). *Quasioptical Systems*. IEEE Press.

[Grosso and Parravicini, 2000] Grosso, G. and Parravicini, G. P. (2000). *Solid State Physics*. Academic Press.

[Günter, 1997] Günter, P. (1997). *Non-linear optical effects and materials*. Springer, Berlin.

[Hache and Bourgeois, 2000] Hache, A. and Bourgeois, M. (2000). Ultrafast all-optical switching in a silicon-based crystal. *Appl. Phys. Lett.*, 77(4089).

[Hackermüller et al., 2004] Hackermüller, L., Hornberger, K., Brezger, B., Zeilinger, A., and Arndt, M. (2004). Decoherence of matter waves by thermal emission of radiation. *Nature*, 427(711).

[Hansma, 2003] Hansma, P. (2003). Personal communication.

[Harris et al., 1999] Harris, J. G. E., Awschalom, D. D., Matsukura, F., Ohno, H., Maranowski, K. D., and Gossard, A. C. (1999). Integrated micromechanical cantilever magnetometry of $ga_{1-X}mn_Xas$. *Appl. Phys. Lett.*, 75(1140).

[Hastings et al., 2004] Hastings, S., de Dood, M., Marshall, W., and Bouwmeester, D. (2004). Ultrafast optical switching of a high quality gaas/alas bragg mirror. *[Submitted to Appl. Phys. Lett.]*.

[Hecht, 2002] Hecht, E. (2002). *Optics*. Addison Wesley 4th Ed.

[Hood, 2000] Hood, C. (2000). Real-time measurement and trapping of single atoms by single photons. *Ph.D. Thesis, California Insitute of Technology*.

[Hood et al., 2001] Hood, C., Kimble, H., and Ye, J. (2001). Characterization of high-finesse mirrors: Loss, phase shifts, and mode structure in an optical cavity. *Phys. Rev. A*, 64(033804).

[Huang et al., 1998] Huang, L., Callan, J., Clezer, E., and Mazur, E. (1998). *Phys. Rev. Lett.*, 80.

[Huang et al., 2003] Huang, X., Zorman, C., Mehregany, M., and Roukes, M. (2003). Nanodevice motion at microwave frequencies. *Nature*, 421(496).

[Joos et al., 1996] Joos, E., Zeh, H. D., Kiefer, C., Giulini, D., Kupsch, J., and Stamatescu, I. O. (1996). *Decoherencess and the Appearance of a Classical World in Quantum Theory*. Springer, Berlin.

[Károlyházy et al., 1982] Károlyházy, Frenkel, A., and Lukács, B. (1982). *On the Possibility of Observing the Eventual Breakdown of the Superposition Principle*. MIT Press.

[Károlyházy et al., 1986] Károlyházy, Frenkel, A., and Lukács, B. (1986). *On the possible role of Gravity in the Reduction of the Wave Function*. Oxford University Press.

[Kenyon, 1990] Kenyon, I. (1990). *General Relativity*. Oxford University Press.

[Kim, 1992] Kim, M. (1992). Decay of quantum coherences under the influence of a thermal heatbath: Schrödinger cat states at finite temperature. *J. Mod. Opt.*, 39(1602).

[Knobel and Cleland, 2003] Knobel, R. and Cleland, A. (2003). Nanometre-scale displacement sensing using a single electron transistor. *Nature*, 424(291).

[Knuuttila, 2000] Knuuttila, T. A. (2000). Nuclear magnetism and superconductivity in rhodium. *Ph.D. Thesis, Helsinki University of Technology*.

[LaHaye et al., 2004] LaHaye, M., Buu, O., Camarota, B., and Schwab, K. (2004). Approaching the quantum limit of a nanomechanical resonator. *Science*, 304(74).

[Law, 1993] Law, C. K. (1993). Effective hamiltonian for the radiation in a cavity with a moving mirror and a time-varying dielectric medium. *Phys. Rev. A*, 49(433).

[Law, 1994] Law, C. K. (1994). Interaction between a moving mirror and radiation pressure: A hamiltonian formulation. *Phys. Rev. A*, 51(2537).

[Leggett, 1984] Leggett, A. (1984). *Contemporary Physics*, 54(583).

[Leggett, 2002] Leggett, A. (2002). *Qubits, Cbits, Decoherence, Quantum Measurement and Environment.* Springer.

[Leonard et al., 2002] Leonard, S., van Driel, H., Schilling, J., and Wehrspohn, R. B. (2002). Ultrafast all-optical switching in a silicon-based crystal. *Phys. Rev. B.*, 66(161102).

[Li et al., 1998] Li, M., Yuen, W., and Chang-Hasnain, C. (1998). Top-emitting micromechanical vcsel with 31.6-nm tuning range. *IEEE Photonics. Tehc. Lett.*, 10(18).

[Li, 1965] Li, T. (1965). Diffraction loss and seletion of modes in maser reonators with circular mirrors. *Bell Syst. Tech. J.*, 44(917).

[Mamin and Rugar, 2001] Mamin, H. and Rugar, D. (2001). Universality of decoherence for macroscopic quantum superpositions. *Appl. Phys. Lett.*, 79(3358).

[Mancini et al., 1997] Mancini, S., Man'ko, V., and Tombesi, P. (1997). Ponderomotive control of quantum macroscopic coherence. *Phys. Rev. A*, 55(3042).

[Mancini and Tombesi, 1994] Mancini, S. and Tombesi, P. (1994). Quantum noise reduction by radiation pressure. *Phys. Rev. A*, 49(4055).

[Mancini et al., 1998] Mancini, S., Vitali, D., and Tombesi, P. (1998). Optomechanical cooling of a macroscopic oscillator by homodyne feedback. *Phys. Rev. Lett.*, 80(688).

[Marshall et al., 2004] Marshall, W., de Dood, M., Eisenberg, H., Dinyari, K., and Bouwmeester, D. (2004). A macroscopic cavity involving a microscopic mirror on a cantilever. *[In Preparation].*

[Marshall et al., 2003a] Marshall, W., Simon, C., Penrose, R., and Bouwmeester, D. (2003a). Towards quantum superpositions of a mirror. *Phys. Rev. Lett.*, 91(130401).

[Marshall et al., 2002] Marshall, W., Whitesides, G. T., de Angelis, I., Takaya, Y., Schingler, R., Reilly, P., and Lupisella, M. (2002). The weaponisation of space. *Pugwash Newsletter*, 39(102).

[Marshall et al., 2003b] Marshall, W., Whitesides, G. T., and Schingler, R. (2003b). Report on working group 2, weaponisation of space and missile defence. *Proc. of 53rd Pugwash Conf. on Science & World Affairs*, (http: //www.pugwash.org/reports/pac/53/wg2.htm).

[Mazurenko et al., 2003] Mazurenko, D. A., Kerst, R., Dijkhuis, J. I., Akimov, A. V., Golubev, V. G., Kurdyukov, D. A., Pevtsov, A. B., and Sel'kin, A. V. (2003). Ultrafast optical switching in three-dimensional photonic crystals. *Phys. Rev. Lett.*, 91(213903).

[Miller and Mlynek, 1982] Miller, D. A. B. and Mlynek, J. (1982). Large room-temperature optical nonlinearity in gaas/ga1x alxas multiple quantum well structures. *Appl. Phys. Lett.*, 41(679).

[Monroe et al., 1996] Monroe, C., Meekhof, D. M., King, B. E., and Wineland, D. J. (1996). A "schrdinger cat" superposition state of an atom. *Science*, 272(1131).

[Nakamura et al., 1999] Nakamura, Y., Paskin, Y., and Tsai, J. (1999). Coherent control of macroscopic quantum states in a single-cooper-pair box. *Nature*, 398(786).

[Nanodevices,] Nanodevices, I.

[Oja and Lounasmaa, 1997] Oja, A. S. and Lounasmaa, O. V. (1997). Nuclear magnetic ordering in simple metals atpositive and negative nanokelvin temperatures. *Rev. Mod. Phys.*, 69(1).

[Palik, 1997] Palik, E. D. (1997). *Handbook of Optical Constants of Solids*. Academic Press.

[Pearle, 1999] Pearle, P. (1999). Collapse models. *Preprint, quant-ph/9901077*.

[Penrose, 1996] Penrose, R. (1996). On gravity's role in quantum state reduction. *Gen. Rel. Grav.*, 28(581).

[Penrose, 1999] Penrose, R. (1999). A proposed space experiment: is quantum state reduction a gravitational phenomenon? *IAF 1999 Proceedings, Amsterdam.*

[Penrose, 2000] Penrose, R. (2000). *Wavefunction Collapse as a real Gravitational Effect, in Mathematical Physics 2000.* GR-15 Proceedings, IUCAA, Imperial College, London.

[Penrose, 2004] Penrose, R. (2004). *The Road to Reality.*

[Pinard et al., 2000] Pinard, M., Cohadon, P., Briant, T., and Heidmann, A. (2000). Full mechanical characterization of a cold damped mirror. *Phys. Rev. A*, 63(013808).

[Preskill, 1998] Preskill, J. (1998). *Lecture Notes for Physics 229: Quantum Information and Computation.* Caltech.

[Raimond and Haroche, 1999] Raimond, J. and Haroche, S. (1999). *Atoms and cavities: the birth of a Schrdinger cat of the radiation field.* Springer Verlag.

[Rau et al., 2003] Rau, A. V., Dunningham, J. A., and Burnett, K. (2003). Measurement-induced relative-position locatization through entanglement. *Science*, 301(1081).

[Rempe et al., 1992] Rempe, G., Thompson, R., Kimble, H., and Lalezari, R. (1992). Measurement of ultralow losses in an optical interferometer. *Opt. Lett.*, 17(363).

[Rohde et al., 2002] Rohde, H., Eschner, J., Schmidt-Kaler, F., and Blatt, R. (2002). Optical decay from a fabry-perot cavity faster than the decay time. *J. Opt. Soc. Am. B*, 19(1425).

[Rowan and Hough, 2000] Rowan, S. and Hough, J. (2000). Gravitational wave detection by interferometry (ground and space). *Living Review in Relativity*, 3(2000-3).

[Ruostekoski et al., 1998] Ruostekoski, J., Collett, M. J., Graham, R., and Walls, D. F. (1998). Decoherence and the transition from quantum to classical. *Phys. Rev. A*, 57(511).

[Sacher, 2003] Sacher, G. L. (2003). Tec−500 - littman laser systems. *http: //www.sacher.de.*

[Said et al., 1992] Said, A. A., Sheik-Bahae, M., Hagan, D. J., Wei, T. H., Wang, J., Young, J., and Stryland, E. W. V. (1992). Determination of bound-electronic and free-carrier nonlinearities in znse, gaas, cdte, and znte. *Opt. Soc. Am.*, B9(405).

[Sakurai, 1994] Sakurai, J. J. (1994). *Modern Quantum Mechanics.* Addison-Wesley Publishing, Revised Ed.

[Scalora et al., 1994] Scalora, M., Dowling, J. P., Bowden, C. M., and Bloemer, M. J. (1994). Optical limiting and switching of ultrashort pulses in nonlinear photonic band gap materials. *Phys. Rev. Lett.*, 73(1368).

[Schingler and Marshall, 2003] Schingler, R. and Marshall, W. (2003). Report of the pugwash workshop on preserving the non-weaponization of space. (http: //www.pugwash.org/reports/sc/may2003/space2003-report.htm).

[Schrödinger, 1935] Schrödinger (1935). Die gegenwärtige situaton in der quantenmechanik. *Naturwissenschaften*, 23:807.

[Sidles et al., 1995] Sidles, J. A., Garbini, J. L., Bruland, K. J., Rugar, D., Zger, O., Hoen, S., and Yannoni, C. S. (1995). Magnetic resonance force microscopy. *Rev. Mod. Phys.*, 67(249).

[Siegman, 1966] Siegman, A. (1966). *Lasers.* University Science Books.

[Spataru et al., 2001] Spataru, C. D., Benedict, L. X., and Louie, S. G. (2001). Ab initio calculation of band-gap renormalization in highly excited gaas. *Phys. Rev. B*, 63(205204).

[Stipe et al., 1999] Stipe, B., Rezaei, M., and Ho, W. (1999). A variable-temperature scanning tunneling microscope capable of single-molecule vibrational spectroscopy. *Rev. Sci. Inst.*, 70(137).

[Strunz and Haake, 2003] Strunz, W. and Haake, F. (2003). Decoherence scenarios from microscopic to macroscopic superpositions. *Phys. Rev. A*, 67(022102).

[Strunz et al., 2003] Strunz, W. T., Haake, F., and Braun, D. (2003). Universality of decoherence for macroscopic quantum superpositions. *Phys. Rev. A*, 67(022101).

[Taché, 1984] Taché, J. P. (1984). Experimental determination of diffraction losses in a near-hemispherical resonator. *Opt. Quantum Electron.*, 16(71).

[Tittonen et al., 1999] Tittonen, I., Breitenbach, G., Kalkbrenner, T., Müller, T., Conradt, R., Schiller, S., Steinsland, E., Blanc, N., and de Rooij, N. F. (1999). Interferometric measurements of the position of a macroscopic body: Towards observation of quantum limits. *Phys. Rev. A*, 59(1038).

[Tuoriniemi and Knuuttila, 2000] Tuoriniemi, J. T. and Knuuttila, T. A. (2000). Nuclear cooling and spin properties of rhodium down to picokelvin temperatures. *Physica B*, 280(474).

[Unruh and Zurek, 1989] Unruh, W. and Zurek, W. (1989). Reduction of a wave packet in quantum brownian motion. *Phys. Rev. D*, 40(1071).

[Vail et al., 1996] Vail, E., Li, G., Yuen, W., and Chang-Hasnain, C. (1996). High performance micromechanical tunable vertical cavity surface emitting lasers. *Electron. Lett.*, 32(1888).

[van der Wal et al., 2000] van der Wal, C., ter Haar, A. C. J., Wilhelm, F. K., Schouten, R. N., Harmans, C. J. P. M., Orlando, T. P., Lloyd, S., and Mooij, J. E. (2000). Quantum superposition of macroscopic persistent-current states. *Science*, 290(773).

[Venugopalan, 1999] Venugopalan, A. (1999). Pointer states via decoherence in a quantum measurement. *Phys. Rev. A*, 61(012102).

[Virwani et al., 2003] Virwani, K. R., Malshe, A. P., Schmidt, W. F., and Sood, D. K. (2003). Young's modulus measurements of silicon nanostructures using a scanning probe system: a non-destructive evaluation approach. *Smart Mater. Struct.*, 12(1028).

[Vitali et al., 2002] Vitali, D., Mancini, S., Ribichini, L., and Tombesi, P. (2002). Quantum limits of cold damping with optomechanical coupling. *Preprint quant-ph/0211102.*

[Walls and Milburn, 1985] Walls, D. F. and Milburn, G. J. (1985). Effect of dissipation on quantum coherence. *Phys. Rev. A*, 31(2403).

[Y. Stockman, 1997] Y. Stockman, J-P. Collette, J. P. T. D. d. C. P. G. (1997). Optical testing of xmm flight model mirror module i and ii at the vertical euv/x facility. *Proc. SPIE*, 3114(566).

[Yang et al., 2000] Yang, J., Ono, T., and Esashi, M. (2000). Surface effects and high quality factors in ultrathin single-crystal silicon cantilevers. *Appl. Phys. Lett.*, 77(3860).

[Yao et al., 2000] Yao, W., Knuuttila, T. A., Nummila, K. K., Martikainen, J. E., Oja, A. S., and Lounasmaa, O. V. (2000). A versatile nuclear demagnetization cryostat for ultralow temperature research. *J. Low Temp. Phys.*, 120(121).

[Yasumara et al., 2000] Yasumara, K. Y., Stowe, T. D., Chow, E. M., Pfafman, T., Kenny, T., Stipe, B., and Rugar, D. (2000). Quality factors in micron- and submicron-thick cantilevers. *J. of Microelectromechanical Systems*, 9(117).

[Zeh, 1970] Zeh, H. D. (1970). On the interpretation of measurement in quantum theory. *Found. Phys.*, 1(69).

[Zurek, 1991] Zurek, W. H. (1991). Decoherence and the transition from quantum to classical. *Physics Today*, 44(36).